AN INVESTIGATION OF FLEXURE IN REINFORCED MASONRY BEAMS

A Thesis Presented to

The Faculty of Graduate Studies

The University of Manitoba

In Partial Fulfillment

of the Requirements for the Degree

Master of Science

in

Civil Engineering

by

Fouad Mohammed Khalaf

May 1981

بسم الله الرحمن الرحيم

إهداء

أهدي هذه الرسالة إلى والدتي الحبيبة

وإلى ذكرى والدي

الغالية

This thesis

is dedicated with love

to my Mother and the memory of my

Father

AN INVESTIGATION OF FLEXURE IN REINFORCED MASONRY BEAMS

BY

FOUAD MOHAMMED KHALAF

A thesis submitted to the Faculty of Graduate Studies of the University of Manitoba in partial fulfillment of the requirements of the degree of

MASTER OF SCIENCE

ACKNOWLEDGEMENTS

The author wishes to express his sincere appreciation and thanks to Professor J.I. Glanville for his valuable guidance and advice, both during the experimental stages and the later preparation of this thesis.

The author also wishes to express appreciation to Professor S. Rizkalla for his advice and interest in the theoretical and experimental stages of this investigation. The author would also like to acknowledge the assistance of the Civil Engineering Laboratory staff, E. Lemke, M. McVey, D. Wiebe, W. Wiles and B. Turnbull, during the experimental part of this thesis. Thanks to Chi-Man Yam, a fellow researcher and friend, for his invaluable help in the construction and testing of the specimens. Special thanks to D. Bagby for cooperation and help during the preparation and typing of this thesis.

The author gratefully acknowledges the financial support given by the University of Technology in Baghdad for his studies at the University of Manitoba.

Finally, the author expresses his gratitude to his family for their interest and support during his studies.

ABSTRACT

An experimental investigation into the behaviour in flexure of concrete block masonry beams reinforced with a range of steel ratios has been undertaken; a series of masonry specimens representing the compression zone in beams has been tested for their strength and strain performance; and a Finite Element Analysis has been performed to study the mode of failure of beams and prisms, and to evaluate the test results. Eight concrete block masonry beams with different amounts of reinforcement and twenty-one concrete block prisms were tested.

The experimental performance of all beams was compared with calculated predictions using the Ultimate Strength Design Theory for reinforced concrete, with modifications to suit various aspects of masonry. The thesis presents the results of the experimental and analytical investigation; and recommends appropriate compressive strengths, ultimate strain values, and realistic limits on steel ratios for use in a strength design.

TABLE OF CONTENTS

Page

ACKNOWLEDGEMENTS i

ABSTRACT ii

TABLE OF CONTENTS iii

LIST OF TABLES vii

LIST OF FIGURES ix

LIST OF PLATES xv

CHAPTER

1 INTRODUCTION 1

1.1 History of Masonry Construction 1
1.2 The Present Situation 2
1.3 Experimental Background 4
1.4 Object and Scope of the Present Investigation 5

2 TESTING PROGRAM 9

2.1 Selection of Samples 9
2.1.1 Reinforced Concrete Masonry Beams 9
2.1.2 Two-Block Prisms 14

2.2 Material Properties 17
2.2.1 Material Properties of the Masonry Beams 17
2.2.1.1 Concrete Blocks 17
2.2.1.2 Grout 17
2.2.1.3 Mortar 23
2.2.1.4 Reinforcement 23
2.2.2 Material Properties of the Concrete Block Prisms 29
2.2.2.1 Concrete Blocks 29
2.2.2.2 Grout 29
2.2.2.3 Mortar 35

Page

2.3 Construction of Specimens 40
2.3.1 Construction of Masonry Beams . . 40
2.3.2 Comparison of Beam Construction Techniques 45
2.3.3 Construction of the Two-Block Prisms 46

2.4 Specimen Testing Arrangement and Procedure 48
2.4.1 Beam Testing Arrangement and Procedure 48
2.4.2 Two-Block Prisms Testing Arrangement and Procedure 51

3 FINITE ELEMENT ANALYSIS 54

3.1 Introduction 54
3.2 The Finite Element Method 54

3.3 Two-Dimensional Analysis 55
3.3.1 Plane Stress Idealization 58
3.3.2 The Two-Dimensional Finite Element Computer Model and Analysis Results 61

3.4 Three-Dimensional Analysis 65
3.4.1 Linear Constitutive Equations . . 66
3.4.2 Three-Dimensional Finite Element Computer Model and Analysis Results 71

4 TEST RESULTS 73

4.1 General 73

4.2 Masonry Beams 73
4.2.1 General Modes of Failure 73
4.2.2 Individual Behaviour of the Beams 75
4.2.2.1 Beam #1 75
4.2.2.2 Beam #2 77
4.2.2.3 Beam #3 82
4.2.2.4 Beam #4 87
4.2.2.5 Beam #5 93
4.2.2.6 Beam #6 103
4.2.2.7 Beam #7 103
4.2.2.8 Beam #8 113

Page

4.3 Two-Block Prisms 114
4.3.1 Behaviour and Mode of Failure of the Two-Block Prisms 114
4.3.1.1 Unfilled Two-Block Prisms Axially Loaded with PIN/FIX End Conditions 114
4.3.1.2 Partially Filled Two-Block Prisms Axially Loaded with PIN/FIX End Conditions 119
4.3.1.3 Partially Filled Two-Block Prisms Eccentrically Loaded with PIN/FIX End Conditions 123
4.3.1.4 Partially Filled Two-Block Prisms Eccentrically Loaded with PIN/PIN End Conditions 138
4.3.1.5 Completely Filled Two-Block Prisms Axially Loaded with PIN/FIX End Conditions 138

5 TEST RESULTS AND COMPUTER ANALYSIS EVALUATION 158

5.1 General 158

5.2 Single-Block Specimens 159
5.2.1 Unfilled Single-Block Specimens . 159
5.2.2 Partially Filled Single-Block Specimens 161
5.2.3 Completely Filled Single-Block Specimens 163

5.3 Two-Block Prisms 165
5.3.1 Unfilled Two-Block Prisms 165
5.3.2 Partially Filled Two-Block Prisms 167
5.3.3 Partially Filled Two-Block Prisms Eccentrically Loaded with PIN/PIN End Conditions 171
5.3.4 Completely Filled Two-Block Prisms 173

5.4 Masonry Beams 177

Page

6 CONCLUSIONS AND RECOMMENDATIONS 196

6.1 Conclusions 196
6.2 Recommendations and Suggested Future Research 199

BIBLIOGRAPHY 201

APPENDIX

A F.E.M. Analysis Results 203

B Strain Readings 235

C Design and Analysis 255

LIST OF TABLES

Table		Page
2.1	Beam reinforcing details	13
2.2	Two-block prism details	16
2.3	Concrete block compression test data	20
2.4	Grout prisms compressive strength test data for the grout used to fill the beams	24
2.5	Mortar cubes compressive strength test data for the mortar used to build the beams	26
2.6	Sieve analysis of mortar sand	27
2.7	Physical properties of the reinforcement	30
2.8	Compression strength test data for half-block prisms	32
2.9	Grout prisms compressive strength test data for the grout used to fill the two-block prisms	36
2.10	Mortar cubes compressive strength test data for the mortar used to build the two-block prisms	38
3.1	Material properties used in the F.E.M analysis	56
4.1	Summary of the material properties and test data for the two-block prisms	157
5.1	Test and analysis results for the single-block specimens	164
5.2	Test and analysis results for the two-block prisms using the two-dimensional F.E.M. analysis	175
5.3	Test and analysis results for the two-block prisms using the three-dimensional F.E.M. analysis	176

Table		Page
5.4	Summary of compressive strengths and material properties for the single and the two-block specimens	179
5.5	Summary of beam properties	180
5.6	Summary of beam results	181
5.7	Beam cross-section properties and modulus of rupture calculation	186
5.8	Z quantity calculation for long term cracking control	188
5.9	Calculation of beam deflections	193
B.1	Beam #1, Strain readings for side "A" . . .	236
B.2	Beam #1, Strain readings for side "B". . . .	237
B.3	Beam #1, Longitudinal steel strain readings	238
B.4	Beam #2, Strain readings for side "A" . . .	239
B.5	Beam #2, Strain readings for side "B" . . .	240
B.6	Beam #2, Longitudinal steel strain readings	241
B.7	Beam #3, Strain readings for side "A" . . .	242
B.8	Beam #3, Strain readings for side "B" . . .	243
B.9	Beam #3, Longitudinal steel strain readings	244
B.10	Beam #4, Strain readings for side "A" . . .	245
B.11	Beam #4, Strain readings for side "B" . . .	246
B.12	Beam #5, Strain readings for side "A" . . .	247
B.13	Beam #5, Strain readings for side "B" . . .	248
B.14	Beam #6, Strain readings for side "A" . . .	249
B.15	Beam #6, Strain readings for side "B" . . .	250
B.16	Beam #7, Strain readings for side "A" . . .	251
B.17	Beam #7, Strain readings for side "B" . . .	252
B.18	Beam #8, Strain readings for side "A" . . .	253
B.19	Beam #8, Strain readings for side "B" . . .	254

LIST OF FIGURES

Figure		Page
2.1	Unfilled voids between filled standard blocks	12
2.2	Details of typical masonry beam	12
2.3	Typical partially filled two-block prism under axial load	15
2.4	Block details	18
2.5	Axially loaded single-block specimens. (A) Unfilled block (B) Partially filled block	19
2.6	Load-strain curve for the axially loaded unfilled single-block specimens	21
2.7	Load-strain curve for the axially loaded partially filled single-block specimens	21
2.8	Sieve analysis of mortar sand	28
2.9	Prefabricated horizontal joint reinforcement	31
2.10	Stress-strain curve for masonry concrete	33
2.11	Vertical strain - horizontal strain curve for masonry concrete	33
2.12	Stress-strain curve for concrete fill	37
2.13	Vertical strain - horizontal strain curve for concrete fill	37
2.14	Stress-strain curve for mortar	39
2.15	Vertical strain - horizontal strain for mortar	39
2.16	Location for "Demec" points in Series I beams (upper diagram) and Series II beams (lower diagram)	44
2.17	Location of "Demec" points in axially and eccentrically loaded partially filled two-block prisms	47

Figure		Page
2.18	The test set-up for beams	49
2.19	Beam loading, shear force, and bending moment diagrams	50
2.20	Clamping process of two-block prisms	52
2.21	Set-up of the axially and eccentrically loaded two-block prisms	53
3.1	Stress-strain curves for mortar, concrete fill, and masonry concrete	57
3.2	Two-dimensional finite element mesh	62
3.3	Three-dimensional finite element mesh . . .	72
4.1	Diagram of modified bending moment due to applied load	76
4.2	Load-deflection curves for Beam #1	78
4.3	Beam #1, Side A, average strain readings . .	79
4.4	Beam #1, Side B, average strain readings . .	79
4.5	Beam #1, average of strain readings for both sides	80
4.6	Load-deflection curves for Beam #2	83
4.7	Beam #2, Side A, average strain readings . .	84
4.8	Beam #2, Side B, average strain readings . .	84
4.9	Beam #2, average of strain readings for both sides	85
4.10	Load-deflection curves for Beam #3	88
4.11	Beam #3, Side A, average strain readings . .	89
4.12	Beam #3, Side B, average strain readings . .	89
4.13	Beam #3, average of strain readings for both sides	90
4.14	Load-deflection curves for Beam #4	94
4.15	Beam #4, Side A, average strain readings . .	95

Figure		Page
4.16	Beam #4, Side B, average strain readings . .	95
4.17	Beam #4, average of strain readings for both sides	96
4.18	Load-deflection curves for Beam #5	99
4.19	Beam #5, Side A, average strain readings . .	100
4.20	Beam #5, Side B, average strain readings . .	100
4.21	Beam #5, average of strain readings for both sides	101
4.22	Load-deflection curves for Beam #6	104
4.23	Beam #6, Side A, average strain readings . .	105
4.24	Beam #6, Side B, average strain readings . .	105
4.25	Beam #6, average of strain readings for both sides	106
4.26	Load-deflection curves for Beam #7	109
4.27	Beam #7, Side A, average strain readings . .	110
4.28	Beam #7, Side B, average strain readings . .	110
4.29	Beam #7, average of strain readings for both sides	111
4.30	Load-deflection curves for Beam #8	115
4.31	Beam #8, Side A, average strain readings . .	116
4.32	Beam #8, Side B, average strain readings . .	116
4.33	Beam #8, average of strain readings for both sides	117
4.34	Load-strain curve for Sample #14, Side A . .	120
4.35	Load-strain curve for Sample #14, Side B . .	120
4.36	Load-strain curve for Sample #14, Side C . .	121
4.37	Load-strain curve for Sample #14, Side D . .	121
4.38	Load-strain curve for Samples #3 and #4 . .	124
4.39	Load-strain curve for Sample #18, Side A . .	125

Figure		Page
4.40	Load-strain curve for Sample #18, Side C . .	126
4.41	Load-strain curve for Sample #11, Side A . .	127
4.42	Load-strain curve for Sample #11, Side B . .	128
4.43	Load-strain curve for Sample #11, Side C . .	129
4.44	Load-strain curve for Sample #11, Side D . .	130
4.45	Load-strain curve for Sample #12, Side A . .	131
4.46	Load-strain curve for Sample #12, Side B . .	132
4.47	Load-strain curve for Sample #12, Side C . .	133
4.48	Load-strain curve for Sample #12, Side D . .	134
4.49	Load-strain curve for Sample #17, Side A . .	139
4.50	Load-strain curve for Sample #17, Side B . .	140
4.51	Load-strain curve for Sample #17, Side C . .	141
4.52	Load-strain curve for Sample #17, Side D . .	142
4.53	Load-strain curve for Sample #13, Side A . .	143
4.54	Load-strain curve for Sample #13, Side B . .	144
4.55	Load-strain curve for Sample #13, Side C . .	145
4.56	Load-strain curve for Sample #13, Side D . .	146
4.57	Load-strain curve for Sample #19, Side A . .	149
4.58	Load-strain curve for Sample #19, Side B . .	149
4.59	Load-strain curve for Sample #19, Side C . .	150
4.60	Load-strain curve for Sample #19, Side D . .	151
4.61	Load-strain curve for Sample #22, Side A . .	152
4.62	Load-strain curve for Sample #22, Side B . .	153
4.63	Load-strain curve for Sample #22, Side C . .	154
4.64	Load-strain curve for Sample #22, Side D . .	155
5.1	Average strain profile across the mortar joint for the axially loaded partially filled two-block prism with PIN/FIX end conditions	170

Figure		Page
5.2	$\frac{M}{bd^2}$ - strain curves (a) Beams 1,2,3,4 and 5 (b) Beams 6,7 and 8 . .	184
5.3	Three cross-section cases for tested masonry beams (a) and (b) partially filled sections (c) completely filled section	185
5.4	Load-deflection curves for the tested masonry beams	191
5.5	Load-deflection curves for concrete beams .	192
A.1	Direct vertical stresses for the unfilled single-block specimen with PIN/FIX end conditions	204
A.2	Direct vertical stresses for the unfilled single-block specimen with PIN/PIN end conditions	205
A.3	Stresses for the partially filled single-block specimen with PIN/FIX end conditions (a) Direct vertical stresses (b) Direct horizontal stresses (c) Direct shear stresses	206
A.4	Stresses for the partially filled single-block specimen with PIN/PIN end conditions (a) Direct vertical stresses (b) Direct horizontal stresses (c) Direct shear stresses	208
A.5	Stresses for the partially filled single-block specimen with PIN/FIX end conditions and $f_G' = 500$ p.s.i. (a) Direct vertical stresses (b) Direct horizontal stresses (c) Direct shear stresses	210
A.6	Direct vertical stresses for the completely filled single-block specimen with PIN/FIX end conditions	212
A.7	Magnified lateral deflection for the unfilled two-block prism	213
A.8	Direct vertical stresses for the unfilled two-block prism with PIN/FIX end conditions	214
A.9	Direct vertical stresses for the unfilled two-block prism with PIN/PIN end conditions	215

Figure		Page
A.10	Magnified lateral deflection for the partially filled two-block prism	216
A.11	Stresses for the partially filled two-block prism with PIN/FIX end conditions (a) Direct vertical stresses (b) Direct horizontal stresses (c) Shear stresses	217
A.12	Stresses for the partially filled two-block prism with PIN/PIN end conditions (a) Direct vertical stresses (b) Direct horizontal stresses (c) Shear stresses	219
A.13	Stresses for the partially filled two-block prism with PIN/FIX end conditions and f_G' = 500 p.s.i. (a) Direct vertical stresses (b) Direct horizontal stresses (c) Shear stresses	221
A.14	Stresses for the partially filled two-block prism with PIN/FIX end conditions and f_M' = 500 p.s.i. (a) Direct vertical stresses (b) Direct horizontal stresses (c) Shear stresses	223
A.15	Direct vertical stresses for the completely filled two-block prism with PIN/FIX end conditions	225
A.16	Direct vertical stresses at six different sections for the partially filled two-block prism eccentrically loaded with PIN/PIN end conditions	226
A.17	Direct horizontal stresses at six different sections for the partially filled two-block prism eccentrically loaded with PIN/PIN end conditions	229
A.18	Direct horizontal stresses at six different sections for the partially filled two-block prism eccentrically loaded with PIN/PIN end conditions	232
C.1	Typical beam cross-section	256

LIST OF PLATES

Plate		Page
2.1	(a) Tested unfilled block (b) Tested partially filled block	22
2.2	Grout prisms (a) Preparation (b) During testing (c) After testing	25
2.3	Compression tests of the half-block specimens (a) Before testing (b) After testing	34
2.4	The construction of the beams	42
2.5	(a) The horizontal and (b) the vertical reinforcement in place	43
2.6	The holding procedure for the two-block prisms	52
4.1	Two sheets of Teflon were used instead of rollers in the end-bearing supports for Series II beams	76
4.2	Flexural failure in Beam #1 looking at Side B	81
4.3	Flexural failure in Beam #1 looking at Side A	81
4.4	Cracking and final flexural failure of Beam #2	86
4.5	Cracking of Beam #2	86
4.6	Cracking and final flexural failure of Beam #3 (Side A)	91
4.7	Cracking and flexural failure of Beam #3 (Side B)	91
4.8 & 4.9	Beam #3 failed by longitudinal splitting in the concrete followed by severe crushing of the block legs	92
4.10	Cracking and final flexural failure of Beam #4 (Side A)	97
4.11	Cracking and final flexural failure of Beam #4 (Side B)	97

Plate		Page
4.12	Close-up of concrete crushing in the compression zone	102
4.13	Cracking and final flexural failure of Beam #5 (Side B)	102
4.14	Cracking and final flexural failure of Beam #6 (Side A)	107
4.15	Close-up of the compression zone	107
4.16	Cracking and final flexural failure of Beam #7 (Side A)	112
4.17	Beam #7 showing a flexural failure (Side B)	112
4.18	Cracking and final flexural failure of Beam #8 (Side B)	118
4.19	Cracking and final flexural failure of Beam #8 (Side B)	118
4.20	Typical mode of failure for the unfilled two-block prism axially loaded with PIN/FIX end conditions	122
4.21	Typical Mode I failure by mortar crushing of the partially filled two-block prism axially loaded with PIN/FIX end conditions	135
4.22	Typical Mode II failure by splitting and leg crushing of the partially filled two-block prism axially loaded with PIN/FIX end conditions	136
4.23	Typical mode of failure for the partially filled two-block prism eccentrically loaded with PIN/FIX end conditions	137
4.24	Typical mode of failure for the partially filled two-block prism eccentrically loaded with PIN/PIN end conditions	147
4.25	Typical mode of failure for the completely filled two-block prism axially loaded with PIN/FIX end conditions	156

CHAPTER 1

INTRODUCTION

1.1 HISTORY OF MASONRY CONSTRUCTION

Long before the advent of recorded history, masonry was used as a material of convenience and necessity. Other than wood, man had no choice but to work with the materials of earth, stone and clay.

Many of the ancient masonry structures are still standing today. The craftsmanship and ingenuity of the ancient Egyptians, for example, as demonstrated in the pyramids, were truly wonders in themselves. Another example is the "Pharoah of Alexandria", the lighthouse that stood watch over navigators of the Mediterranean sea.

At about the same time that the Egyptians were constructing their monuments in stone, fired bricks were being used in Mesopotamia with a bonding agent of asphalt. By the sixth century B.C., brick construction in Babylon was well-developed. The Tower of Babel had walls eighty feet high and wide enough at the top to accommodate chariot races. It is doubtful if any place has equalled this level of use of brick.

Through the Minoan, Mycenaean, Greek and Roman periods, further developments in masonry are observed. The Romans, in particular, elaborated on the use of the arch and produced such impressive structures as the Coliseum

and the aqueducts. Their use of mortar and concrete was unsurpassed until the nineteenth century.

The Dark Ages of Western Civilization through the Renaissance until the last century saw great developments in stone masonry, as can be seen from the bridges, castles, churches and magnificent cathedrals. The use of the arch, dome and flying buttress showed great structural ingenuity.

Advances in the Theory of Elasticity and the development of structural steel shapes and reinforced concrete contributed to a general decline in the use of masonry, to the point where brick, concrete block and stone were used primarily as architectural infill and veneer. It is only during the last few decades that the load-carrying potential of masonry has been appreciated.

1.2 THE PRESENT SITUATION

In recent years great advances have taken place in the use of masonry in buildings. Buildings have increased in height from a few stories to fifteen or twenty, while at the same time wall thicknesses have decreased from several feet to several inches.

An important factor in the development of masonry construction was the introduction of concrete block in the early 1900's. The inherent economy, strength, safety, fire resistance, sound insulation and weather resistance of clay and concrete masonry offer appealing benefits to the owner, architect, engineer and contractor.

A significant development was the introduction of reinforced masonry, wherein masonry walls are reinforced in much the same way as reinforced concrete. This enables masonry to sustain not only axial forces but significant bending also. A reinforced masonry structure is better able to resist cracking due to the lateral dynamic forces of wind and earthquake. Using the shear wall technique, structures have been designed and built with concrete-filled reinforced block walls without other structural framing. With the increase in ductility resulting from the use of reinforcement, masonry shear wall structures up to twelve stories in height are common in seismic zones.

In spite of the enhanced resistance to bending produced by reinforcing, the use of masonry beams in the construction industry has been largely limited to lintels over door and window openings. Loads and spans are usually small, larger openings being spanned for the most part by reinforced concrete which in turn supports the masonry above. The result is a more expensive structure with a less pleasing appearance. The main advantage of reinforced and concrete-filled masonry lies in the fact that there is no need for formwork.

The main reason for the reluctance on the part of engineers to design longer-span masonry beams lies in the almost total absence of adequate information regarding the fundamental behaviour of reinforced masonry in flexure, and

an apparent lack of communication between engineers who work in masonry. The recently published bibliography of masonry [17] reveals little that throws light on the behaviour of masonry beams. Current codes [6] and handbooks [2] advocate the use of working stress design, based on elastic theory, with no guide being given to ultimate strength design principles. There is a clear need for further relevant information on the behaviour of masonry beams.

1.3 EXPERIMENTAL BACKGROUND

Although much experimental research has been done on masonry, it appears to be related mainly to the behaviour of masonry walls. Reference to the "Masonry Bibliography 1900 - 1977" [17] reveals that little published work exists on the experimental determination of the behaviour of masonry beams.

In general, experimental work with masonry beams has examined flexure and has attempted to prove similarity of behaviour with reinforced concrete, especially in relation to Ultimate Strength Design. Edgehill [9] concluded, after testing a series of reinforced and concrete-filled concrete block masonry beams, that masonry beams behave in a manner similar to reinforced concrete beams and can be designed in accordance with the American Concrete Institute 318-71 "Building Code Requirements for Reinforced Concrete". [1]

Baydack [4] tested another series of reinforced concrete masonry beams, some completely filled with concrete

and some with vertical cores filled with concrete at regular intervals. Baydack concluded that the behaviour of reinforced masonry beams in flexure and shear can be predicted safely by the Ultimate Strength Theory for reinforced concrete.

While Edgehill and Baydack tested multi-course beams, Rathbone [18] tested one course beams and arrived at similar conclusions.

Although these researchers state their conclusions emphatically, the scope of their work was rather limited. A number of problems encountered in masonry, such as discontinuities in the concrete fill and poor bond between concrete fill and block, and the effect of these stress-raisers on the behaviour of masonry, was not considered in detail. These early investigations, although incomplete, provide a useful background to a more thorough examination into masonry beam behaviour.

1.4 OBJECT AND SCOPE OF THE PRESENT INVESTIGATION

Previous work on masonry beams [4] [9] carried out at the University of Manitoba indicated that in some instances Ultimate Strength Design principles similar to those of reinforced concrete can be applied to reinforced masonry. However, as the masonry beam is a four-component element (concrete block, mortar, concrete-fill and steel reinforcement) the reinforced concrete theory cannot be applied universally to all conditions of masonry.

The question of continuity of material arises in concrete masonry beams where standard hollow block is used for all courses, except the lowest course. The advantage of using the standard hollow block for the top course of a masonry beam rather than the "U" or lintel block is evident when one considers the problem of filling the masonry beam with concrete. However, this method of construction leads inevitably to incompletely filled voids between individual blocks. This inadequacy of construction leads to stress concentrations in zones of high compression, and may lead to a premature failure if the beam has been analysed by Ultimate Strength theory assuming a completely-filled beam. [5]

This present investigation deals with the behaviour of reinforced concrete block masonry beams. In particular, the investigation addresses the problem of what value of f'_m (ultimate compressive strength of concrete block masonry) to use in the application of an Ultimate Strength theory of flexure similar to that used for reinforced concrete.

Emphasis has been placed on the behaviour of the material at the location of the void between individual blocks which, in the top course of beams tested, was left purposely unfilled.

The purpose of the study was:

1. To compare the load carrying capacity of reinforced concrete masonry beams obtained from testing with that predicted from standard Ultimate Strength Design theory for reinforced concrete.

2. To determine a suitable guide for the determination of a suitable value of f_m' to be used in the design of masonry beams.

3. To test prisms representative of the compression zone in a masonry beam and to compare the behaviour with that predicted from a Finite Element analysis.

4. To examine whether the assumption that sections plane before bending remain plane after bending can be applied to reinforced masonry.

5. To determine the appropriate ultimate strain values, masonry modulus of elasticity E_m , masonry modulus of rupture f_{mr}, and realistic limits on steel ratios.

6. To observe the cracking pattern, behaviour and ductility of reinforced concrete masonry beams under load.

The scope of the experimental work is limited to axially-loaded and eccentrically-loaded compression prisms, and to concrete masonry beams. A total of 17 axially-loaded prisms, 5 eccentrically-loaded, and 8 concrete masonry beams were tested to failure. Data acquired during testing included load, deflection and strains obtained by mechanical extensometers and electrical resistance strain gauges.

CHAPTER 2

TESTING PROGRAM

2.1 SELECTION OF SAMPLES

As the present research is an investigation into flexure, the testing program included specimens of beams, prism specimens representative of isolated portions of beams for closer inspection, and specimens tested to determine the fundamental engineering properties of the materials used. Data acquired were load, strain by electrical resistance gauges and by mechanical "Demec" gauges, and beam deflections.

2.1.1 REINFORCED CONCRETE MASONRY BEAMS

Two series of reinforced concrete masonry beams, representing a total of eight beams, were built, each with a different percentage of tensile steel reinforcement. The dimensions were chosen on the basis that the experimental models would be representative of full-size practical beams, and also on the basis of the handling and testing facilities of the laboratory.

All beams were constructed such that the bottom course consisted of "U", or lintel, blocks, the remaining courses being standard concrete blocks. Each beam, after placement of reinforcement, was filled with concrete, care being taken to ensure that, for the top course at least, the

voids between the individual blocks were left unfilled by concrete (see Figure 2.1). The voids between blocks were left unfilled for the following reasons:

1. The voids are too small (approximately 2" x 4") to fill completely.
2. As the concrete fill is poured after the masonry work is completed, it is unlikely that these voids in lower courses will be filled with concrete, even with mechanical vibration.
3. Field practice is such that these voids will almost certainly be left unfilled.

All courses were laid in running bond, requiring half blocks at the ends of alternate courses, and horizontal joint-reinforcement (9 gauge) was placed between each course. The longitudinal tensile reinforcement and vertical shear steel were placed after the masonry work was finished.

In order to ensure flexure failure, all beams were designed to have an excess of shear resistance through a suitable number of vertical stirrups placed in the block cores.

All beams were constructed sixteen feet long to be tested over a simply-supported span of fifteen feet with one-third span point loads to give a section of almost

constant moment five feet long at the centre. A typical beam is shown in Figure 2.2. (Note the unfilled voids between blocks.)

Series I consisted of five beams of 8" standard hollow concrete block four courses high (i.e. 7 5/8" x 31 5/8" in cross-section). Each beam was provided with a different tensile steel ratio, this ratio varying from approximately minimum ρ to balanced ρ. The minimum value used was $80/f_y$ as prescribed by CSA Standard S304 [6] while the reference balanced value use was as defined in the A.C.I. Code 318 [1] and in CAN3 A23.3 [5].

Series II consisted of three beams of 8" standard hollow block three courses high (i.e. 7 5/8" x 23 5/8") with steel percentages of approximately fifty, seventy-five, and one hundred percent of balanced reinforcement. The effective compressive strength of the masonry (f_m') used as a replacement for the compressive strength of concrete (f_c') in establishing balanced ρ by reinforced concrete theory was initially assumed to be a value of 1806 p.s.i. on the gross width of the section (see Section 2.2.1.1 and Table 2.3).

A detailed summary of the beams and their reinforcement is shown in Table 2.1. As can be seen, tension steel ratios of 14, 37, 52, 54, 79, 88, 1.13 and 1.26 percent of balanced ρ were used.

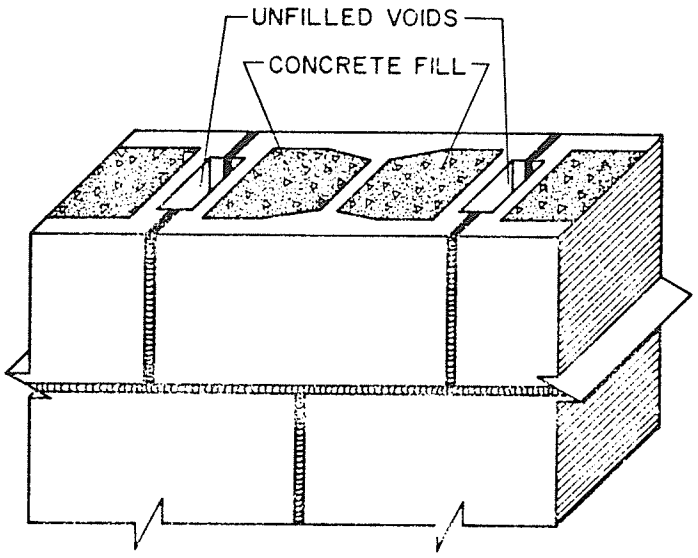

Figure 2.1 Unfilled voids between filled standard blocks.

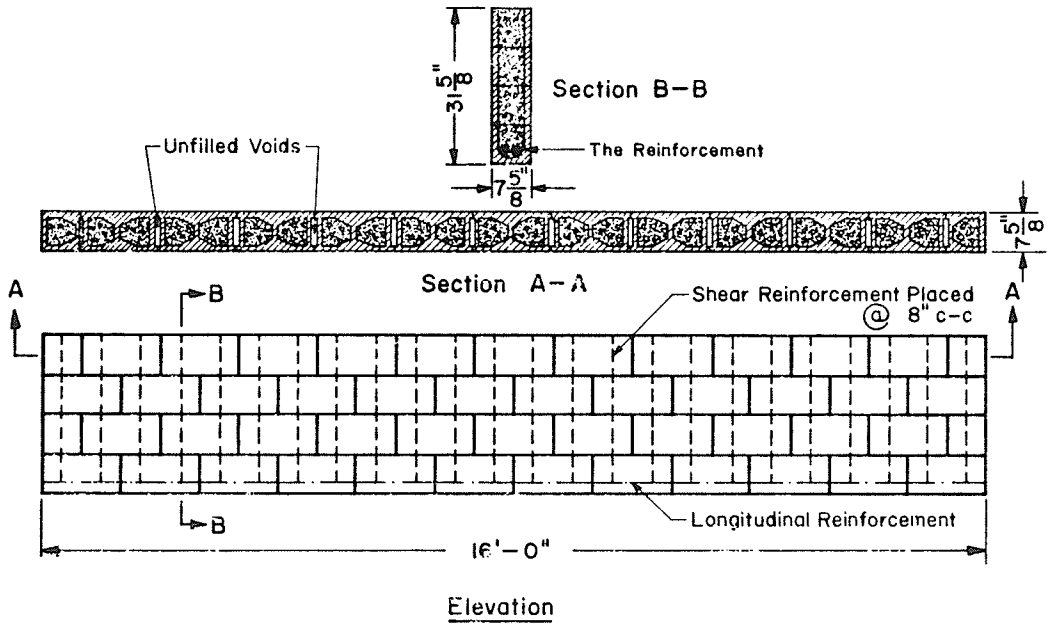

Figure 2.2 Details of typical masonry beam.

Table 2.1 Beam reinforcing details

SERIES	BEAM NO.	TENSION REINFORCEMENT	EFFECTIVE DEPTH (INCHES)	STEEL RATIO $\rho = A_s/bd$	$\rho/\rho_{bal.}$	SHEAR REINFORCEMENT
	1	1 - 15M	28.75	.00141	.14	10M @ 8" c/c
	2	1 - 25M	29.00	.00350	.37	10M @ 8" c/c
I						
8" x 32"	3	2 - 25M	27.25	.00746	.79	10M @ 8" c/c
NOMINAL						
	4	3 - 25M	26.75	.0114	1.26	10M @ 8" c/c
	5	1 - 25M 1 - 30M	27.75	.00879	.88	10M @ 8" c/c
	6	1 - 25M	20.00	.00508	.54	10M @ 8" c/c
II						
8" x 24"	7	2 - 20M	20.00	.00610	.52	10M @ 8" c/c
NOMINAL						
	8	2 - 25M	19.25	.01056	1.13	10M @ 8" c/c

2.1.2 TWO-BLOCK PRISMS

As a main point for investigation is the effect of the unfilled voids between blocks, a testing program of three series of two-block prisms was undertaken. These specimens, nominally 8" x 8" x 32" high (7 5/8" x 7 5/8" x 31 5/8" actual dimensions), were orientated and tested as shown in Figure 2.3 to simulate the compression zone in a beam.

Prisms were built unfilled by concrete, concrete-filled except for the void between blocks, and completely filled (including the void between blocks). The prisms were tested under axial load, eccentric load, and with varying end conditions. The series were designed to provide data for a comparative study of factors affecting the strength of the compressive zone in a beam. Pertinent details of the prisms are shown in Table 2.2.

The end conditions designated to the specimens related to the nature of the testing machine which included an upper spherical loading head (PIN) and a lower horizontal plate (FIX). The PIN/PIN end condition was obtained by providing a rigid plate and roller at the base.

The prisms were constructed in a horizontal orientation, as would be the case in practice. The blocks were carefully clamped together to prevent joint-cracking during lifting and placing in the testing machine. The clamping rig was carefully removed prior to testing.

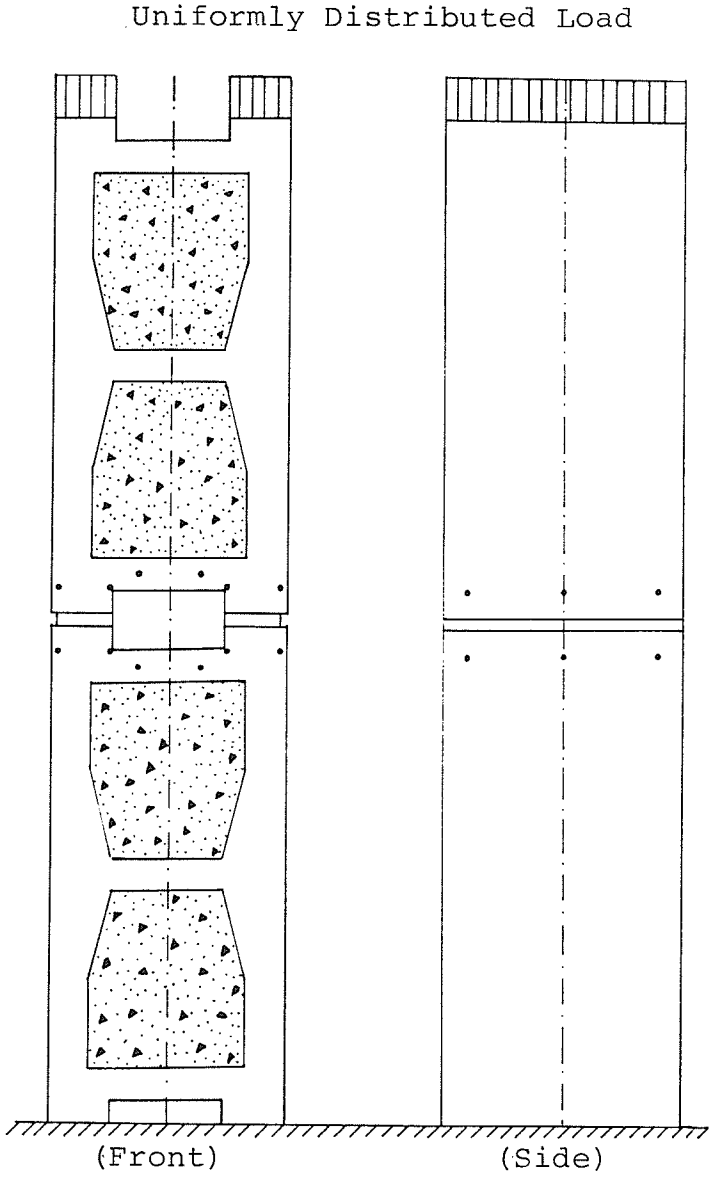

Figure 2.3 Typical partially filled two-block prism under axial load.

Table 2.2 Two-block prism details

SERIES	CONCRETE FILL*	NUMBER OF SPECIMENS	LOADING ECCENTRICITY	END CONDITIONS
I	UNFILLED	2	e = 0	PIN/FIX
II	PARTIAL FILL	12	e = 0	PIN/FIX
		4	e = d/6	PIN/PIN
		1	e = d/6	PIN/FIX
III	COMPLETE FILL	3	e = 0	PIN/FIX

* Unfilled - i.e., no concrete fill.
Partial fill - i.e., concrete filled, except for void between blocks.
Complete fill - i.e., fully concrete filled, including the void between blocks.

2.2 MATERIAL PROPERTIES

In order to evaluate the data obtained from the beam prism tests, it is necessary to know the appropriate properties of the component parts.

2.2.1 MATERIAL PROPERTIES OF THE MASONRY BEAMS

2.2.1.1 CONCRETE BLOCKS

The basic units used to build the concrete masonry beams were lintel blocks, standard blocks, end and half blocks. These were tested to determine strength and deformation properties. Block dimensions and details are shown in Figure 2.4. Figure 2.5 shows the different types of samples tested to determine the physical properties of the unfilled and filled block units. Table 2.3 lists the test results for all the different samples tested. The load-strain curves for unfilled and partially-filled single-block specimens are shown in Figures 2.6 and 2.7. Plate 2.1 shows a typical mode of failure for unfilled and partially-filled block.

2.2.1.2 GROUT

The concrete grout used to fill Series I beams was mixed in the concrete laboratory by a horizontal drum mixer. Each mix contained 197 lb. of 3/8" maximum coarse aggregate, 170 lb. of fine aggregate, 39 lb. of high-early strength cement (Type 20), and 32 lb. of water. A 7-day compressive

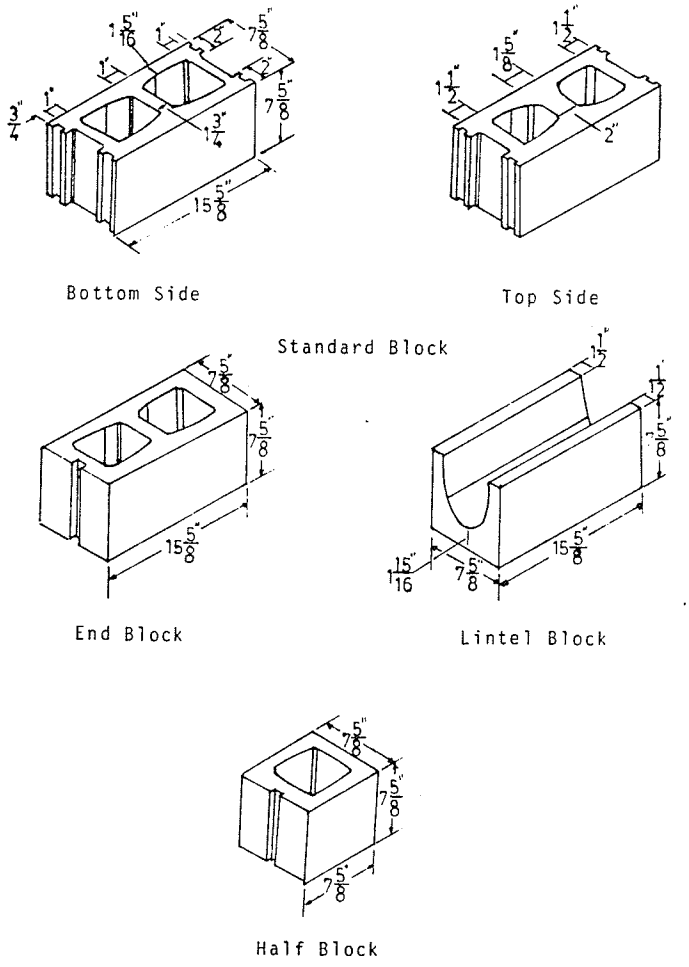

Figure 2.4 Block details.

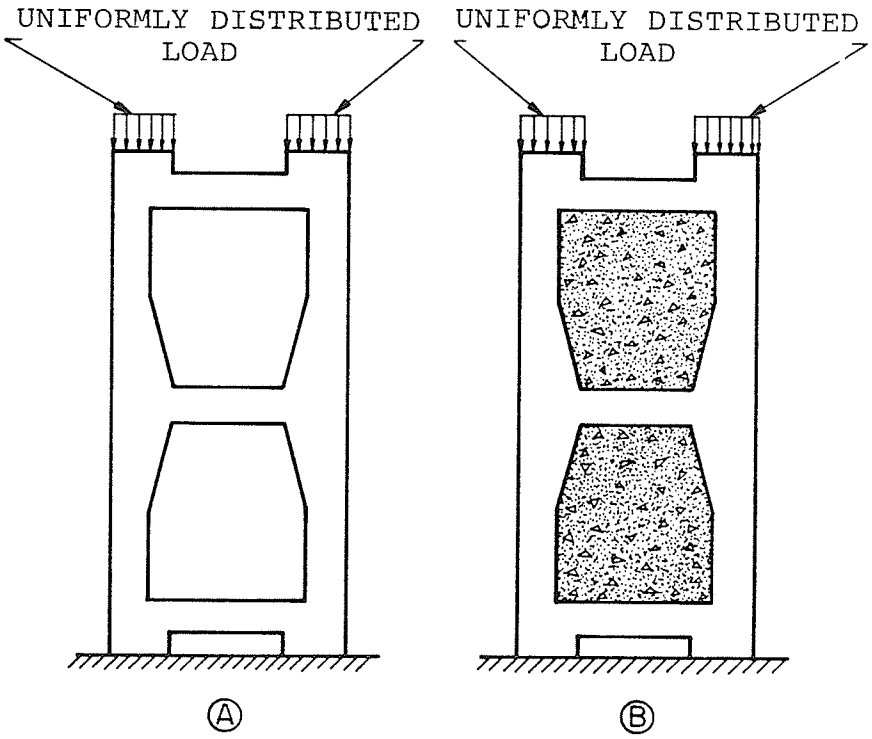

Figure 2.5 Axially loaded single-block specimens. (A) Unfilled block. (B) Partially filled block.

Table 2.3 Concrete block compression test data

TYPE OF BLOCK	TOTAL LOAD (POUNDS)	COMPRESSIVE STRENGTH (p.s.i) BASED ON NET AREA	AVERAGE	f_m'* (p.s.i)
STANDARD UNFILLED BLOCK	60230	3009	3353	1806
	71630	3579		
	58780	2937		
	72960	3645		
	72000	3597		

TYPE OF BLOCK	TOTAL LOAD (POUNDS)	BASED ON GROSS AREA	BASED ON NET AREA	BASED ON GROSS AREA	BASED ON NET AREA	f_m'* (p.s.i)
STANDARD PARTIALLY FILLED CONCRETE BLOCK	88000	1514	2885	1521	2898	——
	103000	1772	3377			
	84000	1445	2754			
	72000	1238	2361			
	95000	1634	3115			

* Refer to CSA Standard S304 - 1977 for type "S" mortar and unit strength shown.

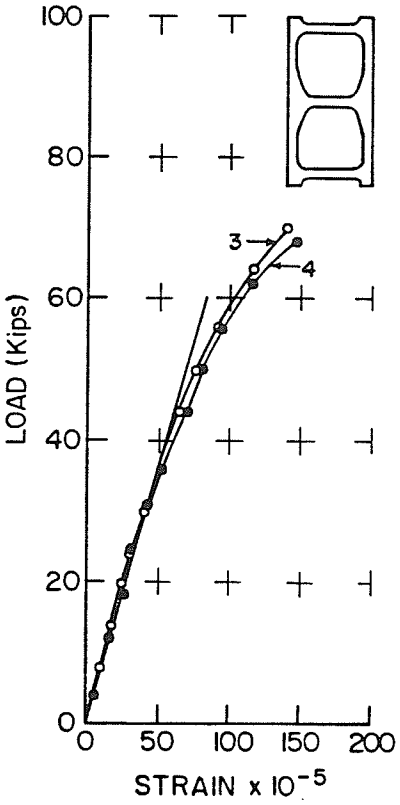

Figure 2.6 Load-strain curve for the axially loaded, unfilled single-block specimens.

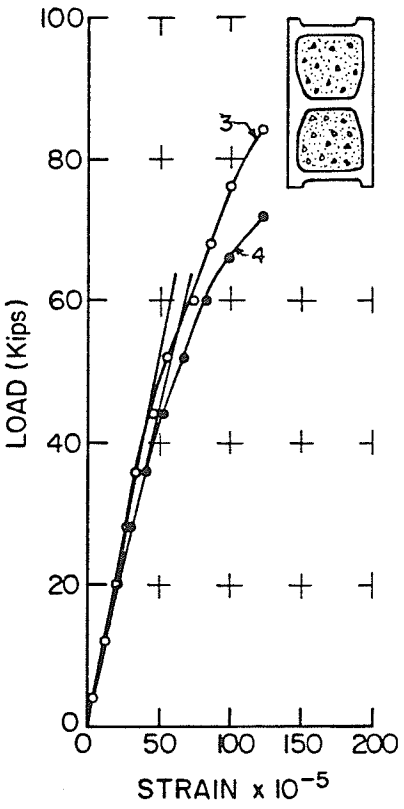

Figure 2.7 Load-strain curve for the axially loaded, partially filled single-block specimens.

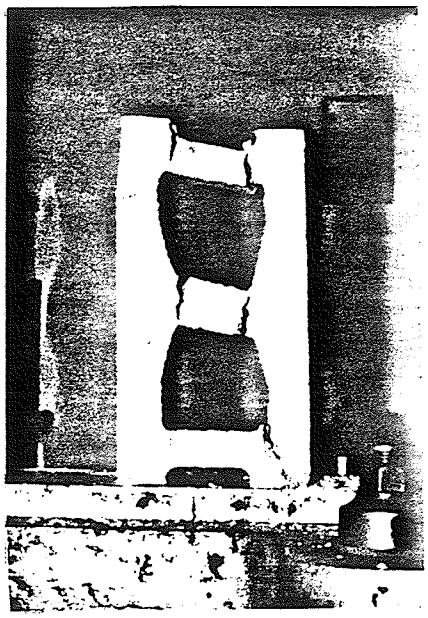

(a)

Plate 2.1 (a) Failed unfilled block
(b) Failed partially filled block

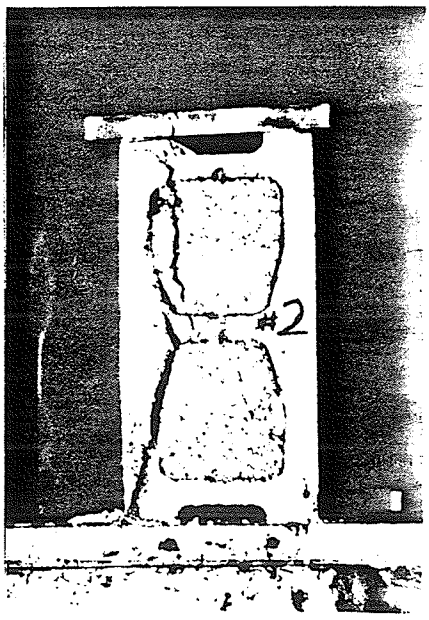

(b)

strength of at least 3000 p.s.i. was expected. The concrete grout used for the Series II beams was supplied by a local manufacturer with a specified strength of 3000 p.s.i. and a 6-inch slump. The maximum size of the coarse aggregate was ½ inch. For each pour, three grout test prisms, 3" x 3" x 6", were prepared in accordance with CSA Standard A 179 - 1975 [7]. The results of the compression tests for the grout prisms are shown in Table 2.4 and details of the prism preparations and testing are shown in Plate 2.2.

2.2.1.3 MORTAR

The mortar used was type "S" mortar, prepared in accordance with the requirements of CSA Standard A179 - 1975 [7]. Three 2" x 2" x 2" mortar cubes were prepared. The results for the cube compression tests are listed in Table 2.5. The sieve analysis of the mortar sand is shown in Table 2.6, and the size distribution is shown graphically in Figure 2.8.

2.2.1.4 REINFORCEMENT

The deformed bars used were 15M, 20M, 25M and 30M for longitudinal reinforcement, while a 10M deformed bar was used for web reinforcement. For tensile tests, two 18-inch samples were cut from each bar to evaluate the yield point, ultimate tensile strength, and the percentage of elongation

Table 2.4 Grout prisms compressive strength test data for the grout used to fill the beams.

BEAM NO.	TEST NO.	TOTAL LOAD (IBS.)	f'_G COMP. STRESS (P.S.I)	f'_G AVERAGE (P.S.I)	AGE* (DAYS)
	1	29875	3319		
1	2	30000	3333	3113	9
	3	24175	2686		
	1	33600	3733		
2	2	27200	3022	3344	13
	3	29500	3277		
	1	38000	4222		
3	2	46100	5122	4807	14
	3	45700	5077		
	1	36300	4033		
4	2	33500	3722	3641	7
	3	28500	3167		
	1	34000	3778		
5	2	41200	4578	3982	11
	3	32300	3589		
	1	38350	4261		
6	2	43805	4867	4646	8
	3	43300	4811		
	1	43900	4878		
7	2	46600	5178	4789	11
	3	38800	4311		
	1	41200	4578		
8	2	43800	4867	4678	12
	3	41300	4589		

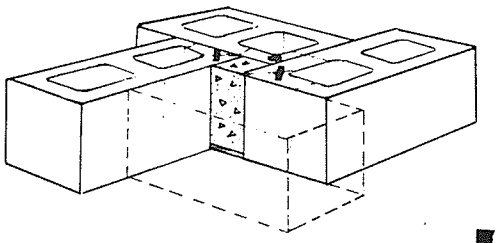

(a)

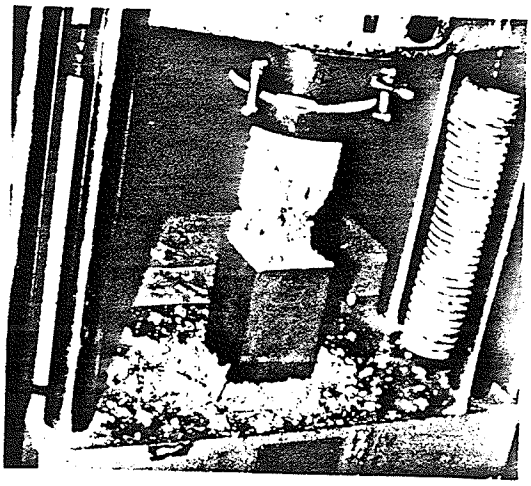

(b)

(c)

Plate 2.2 Grout prisms.
(a) Preparation
(b) During testing
(c) After testing

Table 2.5 Mortar cubes compressive strength test data for the mortar used to build the beams.

BEAM NO.	TEST NO.	TOTAL LOAD (IBS.)	f_M' COMP. STRESS (P.S.I)	f_M' AVERAGE (P.S.I)	AGE (DAYS)
-	1	15050	3763		
1	2	18200	4650	4117	17
	3	15750	3938		
	1	15100	3775		
2	2	16850	4213	4057	22
	3	16750	4188		
	1	16050	4013		
3	2	16850	4214	4192	30
	3	17400	4350		
	1	15630	3908		
4	2	16200	4050	3895	28
	3	14910	3728		
	1	17400	4350		
5	2	17700	4425	4417	22
	3	17900	4475		
	1	14900	3725		
6	2	11700	2925	3554	13
	3	16050	4013		
	1	15400	3850		
7	2	16200	4050	4054	16
	3	17050	4263		
	1	16875	4219		
8	2	15675	3919	4025	17
	3	15750	3938		

Table 2.6 Sieve analysis of mortar sand.

SIEVE NO.	PERCENT PASSING %
4	100
8	98.9
16	94.5
30	76.0
50	17.5
100	2.2
REMAIN	0

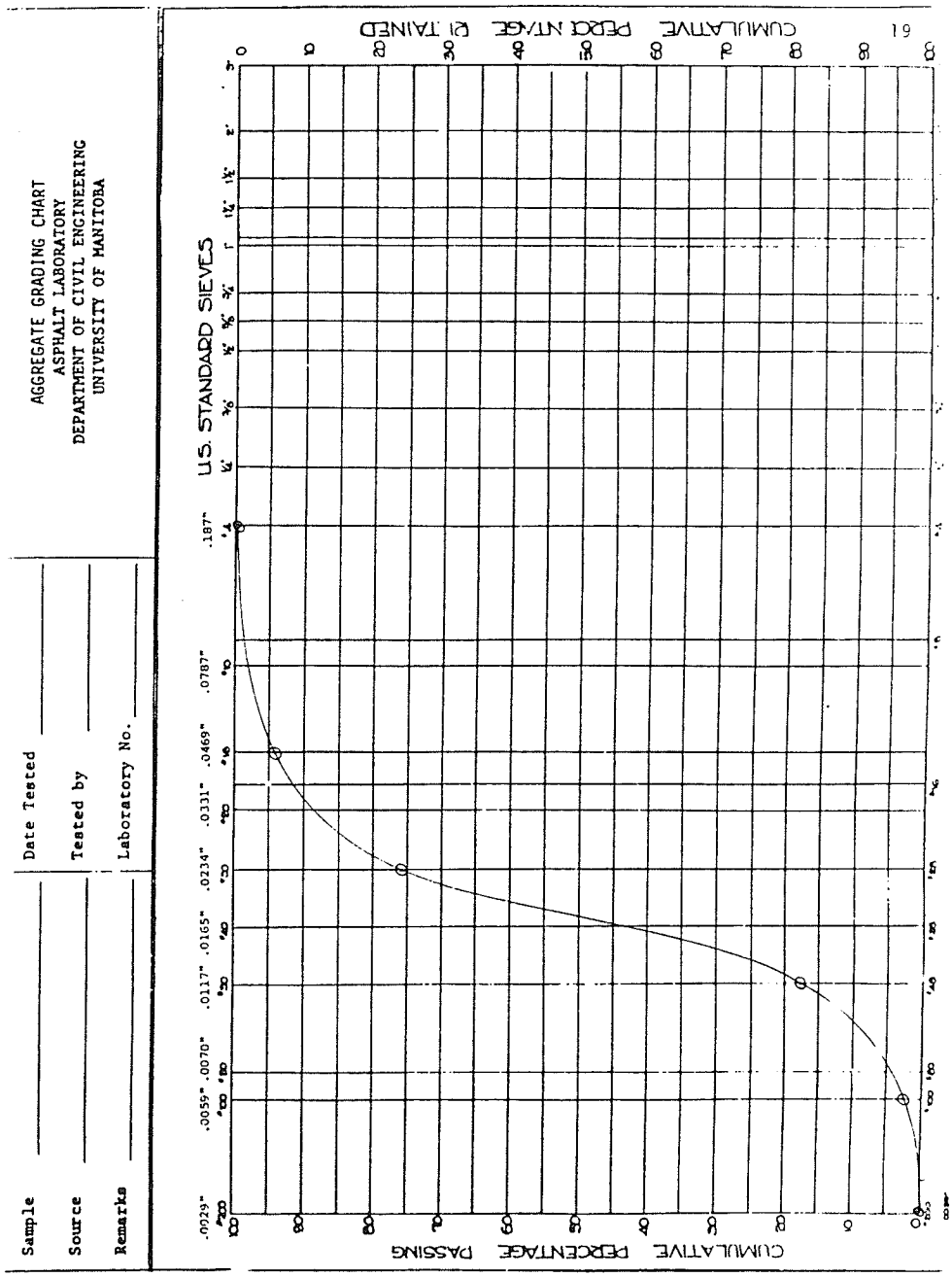

Figure 2.8 Sieve analysis of mortar sand.

over an 8-inch length. The testing results are shown in Table 2.7. The joint-reinforcement used in the beams has the dimensions shown in Figure 2.9. Strength tests on joint reinforcement were not conducted.

2.2.2 MATERIAL PROPERTIES OF THE CONCRETE BLOCK PRISMS

2.2.2.1 CONCRETE BLOCKS

Two half block samples were tested in compression to establish the physical properties (i.e. compressive strength, stress-strain relationship, Modulus of Elasticity and Possion's Ratio) of the concrete used to manufacture the concrete blocks. Each test specimen was three blocks high with Plaster of Paris joints between the half blocks. Electrical strain gauges and "Demec" points were used to establish the vertical and horizontal strains on two sides of each sample. The test results for the two samples are given in Table 2.8. Figure 2.10 shows the average stress-strain curve for sample nos. 1 and 2. Figure 2.11 shows the average strain-strain curve for sample nos. 1 and 2. Plate 2.3 (a,b,) shows the sample before and after testing.

2.2.2.2 GROUT

The concrete grout used to fill the two-block prisms was mixed so it would be the same as that used to fill the Series I beams. Most of the grout specimens, (3" x 3" x 6") were prepared in accordance with CSA Standard A 179 - 1975 [7].

Table 2.7 Physical properties of the reinforcement

Beams Sampled	Type of Bar	Sectional Area (sq.ins.)	Test No.	Yield Point Load (pounds)	Yield Point Stress (p.s.i)	Yield Point Avg. Stress (p.s.i)	Ultimate Load (lbs)	Ultimate Stress (p.s.i)	Ultimate Avg. Stress (p.s.i)	Average elong. in 8 inches (percent)
1	15M	0.31	1	21,700	70,000	70,163	34,250	110,484	111,129	15
			2	21,800	70,326		34,650	111,774		
	10M	0.155	1	7,925	51,129	51,855	11,750	75,806	77,419	20
			2	8,150	52,580		12,250	79,032		
2	25M	0.775	1	58,600	75,613	74,451	83,250	101,419	109,999	15
			2	56,800	73,290		87,250	112,580		
	10M	0.155	1	7,365	47,516	49,435	12,050	77,742	76,225	18
			2	7,960	51,355		11,580	74,709		
3	25M	0.775	1	57,420	74,090	74,271	85,480	110,296	110,861	13
			2	57,610	74,336		86,000	110,968		
			3	57,510	74,206		85,670	110,542		
			4	57,700	74,451		86,520	111,639		
	10M	0.155	1	8,550	55,161	54,678	12,750	82,258	81,936	19
			2	8,400	54,194		12,650	81,613		
4	25M	0.775	1	58,350	75,290	76,489	85,990	110,839	111,336	13
			2	62,110	80,142		87,030	112,297		
			3	59,460	76,726		86,150	111,161		
			4	58,510	75,497		86,280	111,329		
			5	58,880	75,974		86,480	111,587		
			6	58,360	75,303		85,870	110,800		
	10M	0.155	1	8,450	54,516	54,678	12,100	78,064	79,999	20
			2	8,500	54,839		12,700	81,935		
5	30M	1.085	1	74,850	68,986	69,216	122,970	113,336	113,502	13
			2	75,350	69,447		123,330	113,668		
	25M	0.775	1	57,350	74,000	74,051	86,010	110,980	111,341	13
			2	57,430	74,103		86,570	111,703		
	10M	0.155	1	8,500	54,839	54,678	12,650	81,613	81,452	20
			2	8,450	54,516		12,600	81,290		
6	25M	0.775	1	57,480	74,168	74,871	84.980	109,651	111,097	13
			2	58,570	75,574		87,220	112,542		
	10M	0.155	1	8,250	53,225	53,613	12,300	79,355	79,436	20
			2	8,370	54,000		12,325	79,516		
7	20M	0.465	1	29,800	64,086	64,247	49,100	105,591	105,429	13
			2	29,900	64,301		49,000	105,376		
			3	29,900	64,301		48,900	105,161		
			4	29,900	64,301		49,100	105,591		
	10M	0.155	1	7,925	51,129	51,855	11,875	76,613	77,823	22
			2	8,150	52,581		12,250	79,033		
8	25M	0.775	1	58,150	75,032	74,845	86,470	111,574	111,387	13
			2	58,210	75,110		86,610	111,754		
			3	57,670	74,413		86,010	110,981		
			4	57,990	74,826		86,210	111,239		
	10M	0.155	1	8,175	52,742	52,984	12,050	77,742	78,307	20
			2	8,250	53,226		12,225	78,871		

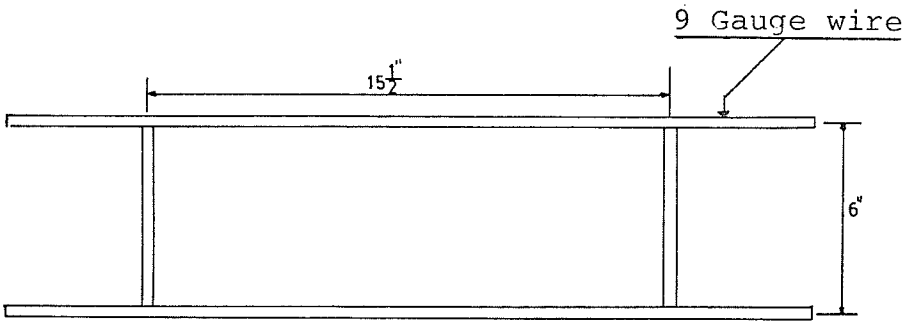

Figure 2.9 Prefabricated horizontal joint reinforcement.

Table 2.8 Compression strength test data for half-block prisms.

SAMPLE NO.	TOTAL LOAD (IBS.)	NET AREA (IN^2)	f_B' BLOCK COMPRESSIVE STRENGTH (P.S.I)	f_B' (AVG.) (P.S.I)	$E_{SEC.}$ SECANT MODULUS OF ELASTICITY (P.S.I)	$E_{SEC.}$ (AVG.) (P.S.I)	ν POISSON'S RATIO	ν (AVG.)
1	165300	37.9	4365	4411	4.5×10^6	4.4×10^6	0.18	0.17
2	168600	37.8	4458		4.3×10^6		0.16	

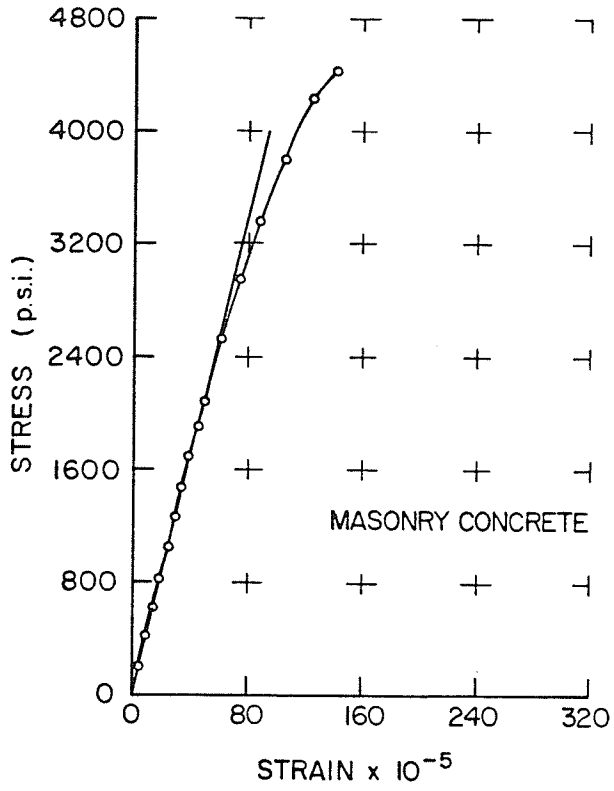

Figure 2.10 Stress-strain curve for masonry concrete.

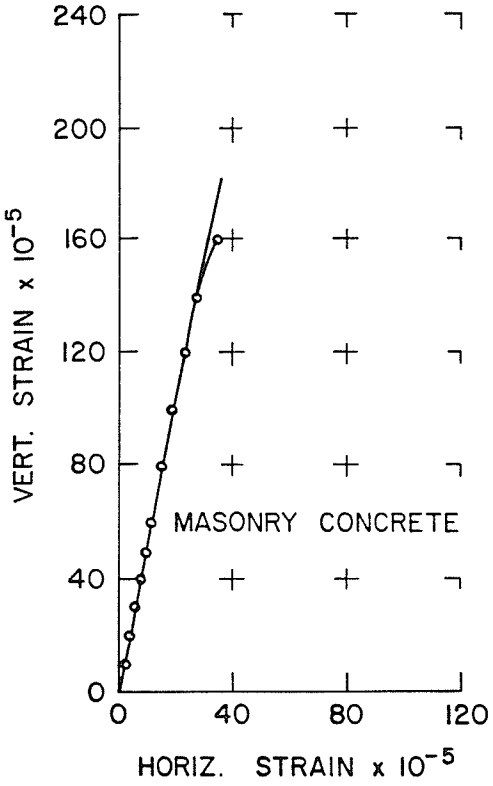

Figure 2.11 Vertical strain - horizontal strain curve for masonry concrete.

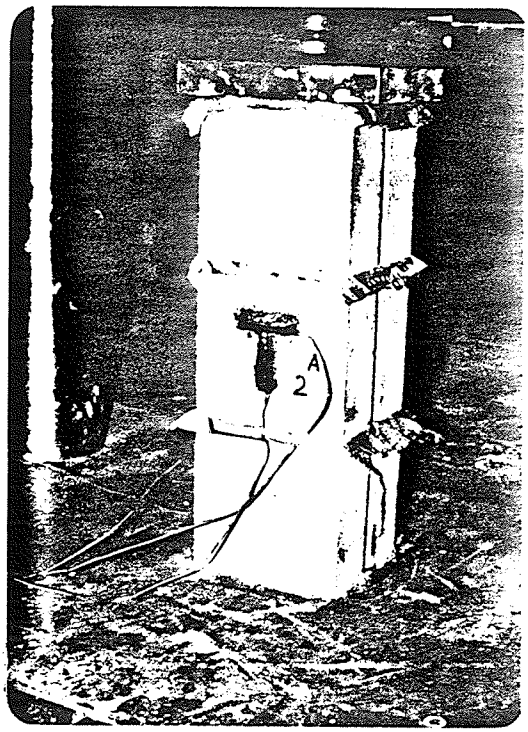

(a)

Plate 2.3 Compression tests of the half-block specimens.
(a) Before testing
(b) After testing

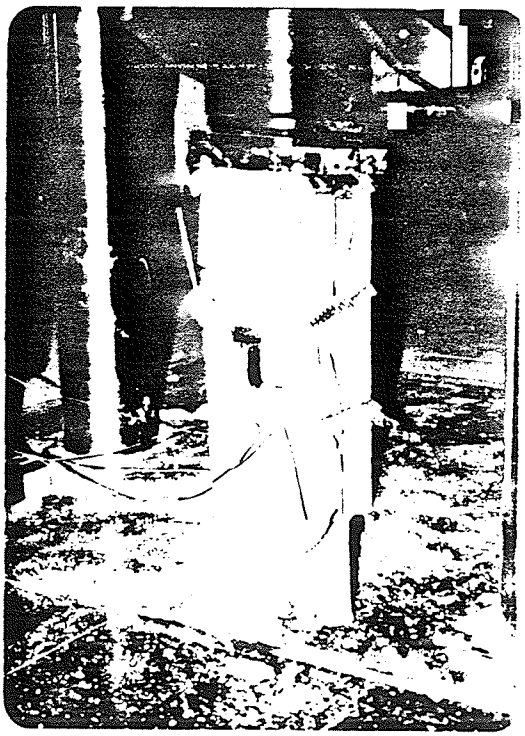

(b)

Some of the specimens were prepared with different dimensions, 4" x 4" x 8". The first dimensions were chosen to simplify the sampling process. The results of the compression tests for the grout prisms are given in Table 2.9. Figures 2.12 and 2.13 show the stress-strain and the strain-strain curves respectively for the tested grout prisms.

2.2.2.3 MORTAR

Type "S" mortar was used and mixed in accordance with CSA Standard A 179 - 1975 [7]. The proportion is exactly similar to the mortar used for building the beams. The results for the mortar cube tests are listed in Table 2.10. Figures 2.14 and 2.15 show the stress-strain and the strain-strain curves respectively for the tested mortar cubes.

Table 2.9 Grout prisms compressive strength test data for the grout used to fill the two-block prisms.

TWO-BLOCK PRISM NO.	TEST NO.	TOTAL LOAD (IBS.)	f_G' GROUT COMPRESSIVE STRENGTH (P.S.I)	f_G' AVERAGE (P.S.I)	$E_{SEC.}$ SECANT MODULUS OF ELASTICITY (P.S.I)	ν POISSON'S RATIO
1,2,3,4	1	42000	2545	2643	3.0×10^6	0.168
	2	49900	2973			
	3	40400	2411			
5,6,7,8,9	1	70000	4107	4117	3.1×10^6	0.166
	2	76300	4552			
	3	60100	3691			
10,11,12,13,15,16,17,18	1	75400	4713	4761	3.2×10^6	0.164
	2	76100	4757			
	3	77028	4814			
19,21,22	1	34800	3867	3996	3.1×10^6	0.166
	2	34200	3800			
	3	38900				

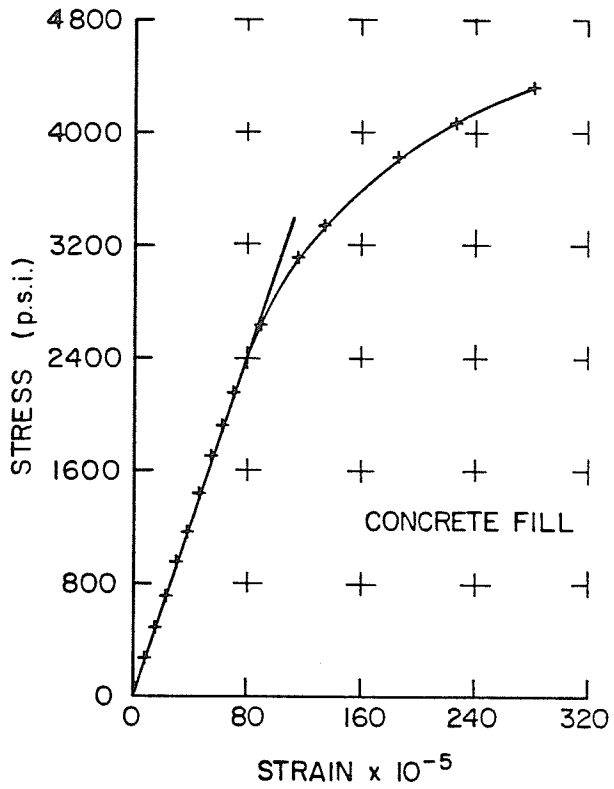

Figure 2.12 Stress-strain curve for concrete fill.

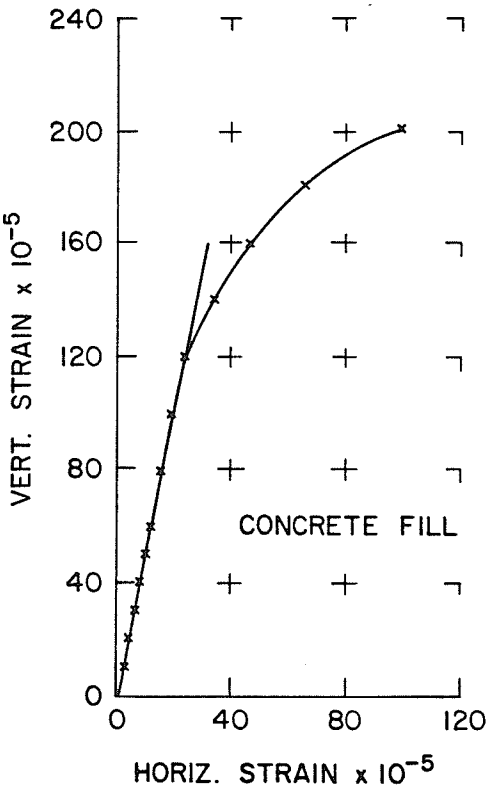

Figure 2.13 Vertical strain - horizontal strain curve for concrete fill.

Table 2.10 Mortar cubes compressive strength test data for the mortar used to build the two-block prisms.

TWO-BLOCK PRISM NO.	TEST NO.	TOTAL LOAD (IBS.)	f_M' MORTAR COMPRESSIVE STRENGTH (P.S.I)	f_M' AVERAGE (P.S.I)	$E_{SEC.}$ SECANT MODULUS OF ELASTICITY (P.S.I)	ν POISSON'S RATIO
1,2,3,4	1	15250	3812	3527	2.1×10^6	0.175
	2	13225	3306			
	3	13850	3462			
7	1	11300	2825	2954	2.0×10^6	0.170
	2	12400	3100			
	3	12300	3075			
5,6,8,9	1	10020	2550	2584	——	——
	2	10920	2730			
	3	9562	2391			
14	1	13750	3437	3407	——	——
	2	13506	3376			
	3	13627	3407			
10,13,16, 17,18	1	13100	3275	3286	2.2×10^6	0.177
	2	13460	3350			
	3	12932	3223			
11,12,15	1	13125	3281	3320	——	——
	2	12865	3216			
	3	13850	3463			
19,20,21, 22	1	22476	5619	4773	2.1×10^6	0.178
	2	16700	4175			
	3	18100	4525			

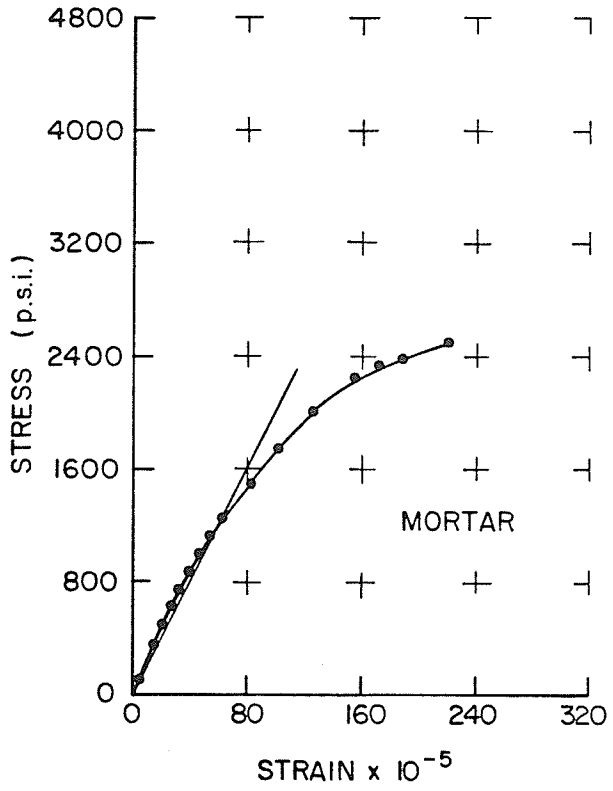

Figure 2.14 Stress-strain curve for mortar.

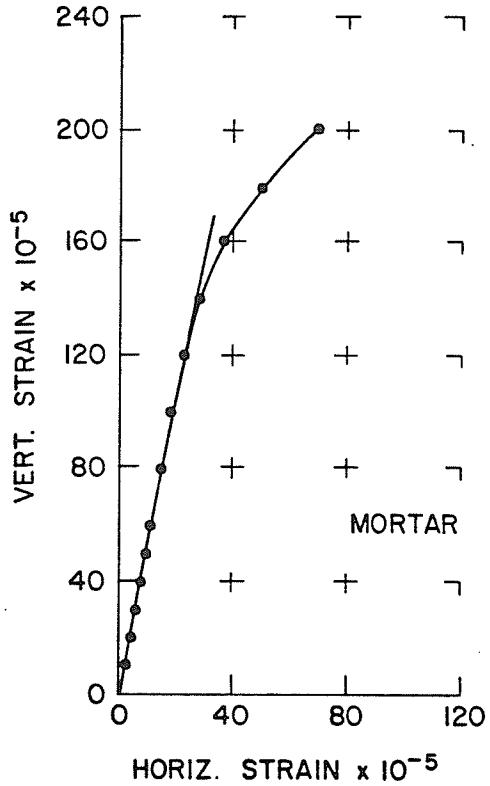

Figure 2.15 Vertical strain - horizontal strain curve for mortar.

2.3 CONSTRUCTION OF SPECIMENS

The beam specimens were built in two series and two stages. The first stage involved the construction of the permanent form with concrete blocks and placing the reinforcement bars. The second stage consisted of filling the masonry beams with concrete grout.

The prism specimens were built in three series in two stages. The first stage consisted of mortaring two blocks together. The second stage involved filling the cores of the two blocks with concrete grout. This was done only for the partially and completely filled prisms.

2.3.1 CONSTRUCTION OF MASONRY BEAMS

The construction technique was similar for all beams. First the bottom course of lintel blocks was mortared together on a level floor using ordinary construction methods and workmanship. The remainder of the courses were laid in running bond with horizontal joint reinforcement being laid between courses. All horizontal and vertical mortar joints were approximately 3/8 inch thick. After the last course was laid, the mortar joints were tooled in order to compact the mortar and force it tightly against the masonry. Three days after the beams were built, stirrups and horizontal reinforcing bars were placed in position with stirrups being placed in every core and hooked under the horizontal reinforcing bars. After that the concrete

grout was poured. The cores were filled with concrete to mid-height and compaction achieved with an electric vibrator. The cores were then filled to the top and the grout was again vibrated. The top course was then finished by trowelling the concrete. Care was taken to leave the voids between the blocks unfilled (See Figure 2.1 and Section 2.3.2).

Three grout test specimens for each beam were prepared in accordance with the requirements of CSA Standard A 179 - 1975 [7]. After the beams were filled, the exposed surfaces of the beams and the specimens were covered with wet burlap and a layer of polyethlylene film. The beams and specimens were cured at room temperature under wet burlap. In preparation for testing, the beams were allowed to air dry for 24 hours. After the beams were dry, four columns of "Demec" points were placed 8 inches apart on the middle section of the beams on both sides. The beams were then painted with white plaster to aid in the detection of cracks during testing.

The beam construction technique is shown in Plate 2.4 (a,b,c). Plate 2.5 (a,b) shows the stirrups and the horizontal reinforcement in place. Figure 2.16 (a,b) shows the location of the "Demec" points on the middle section of the beams.

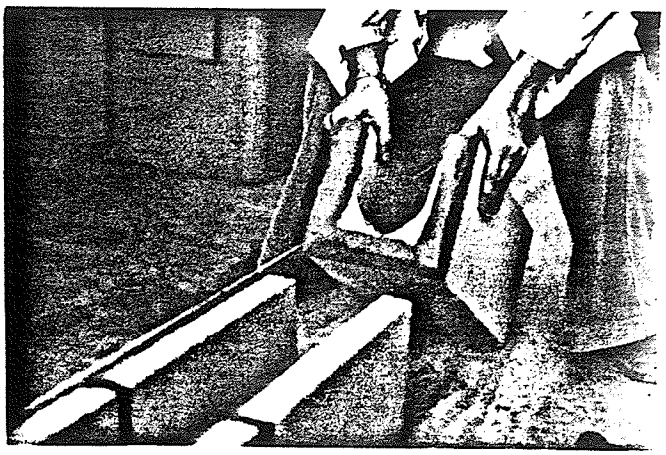

(a)

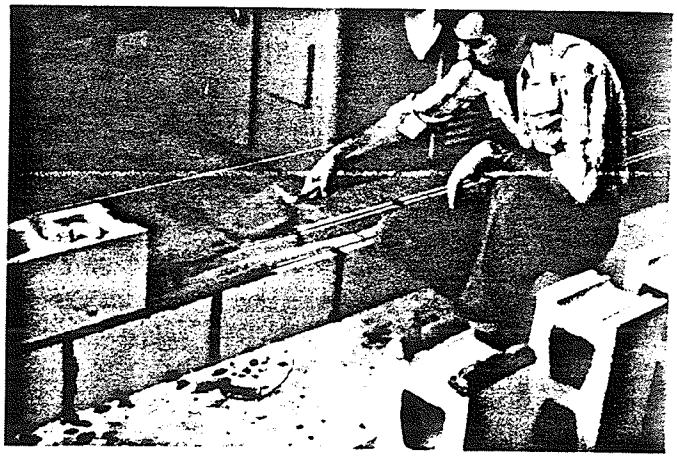

(b)

Plate 2.4 The construction of the beams.

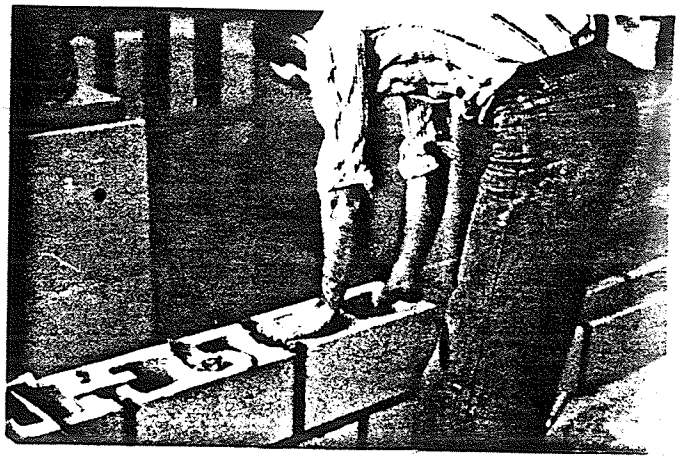

(c)

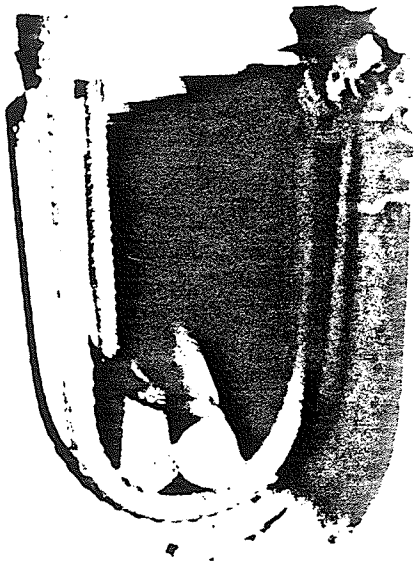

(a)

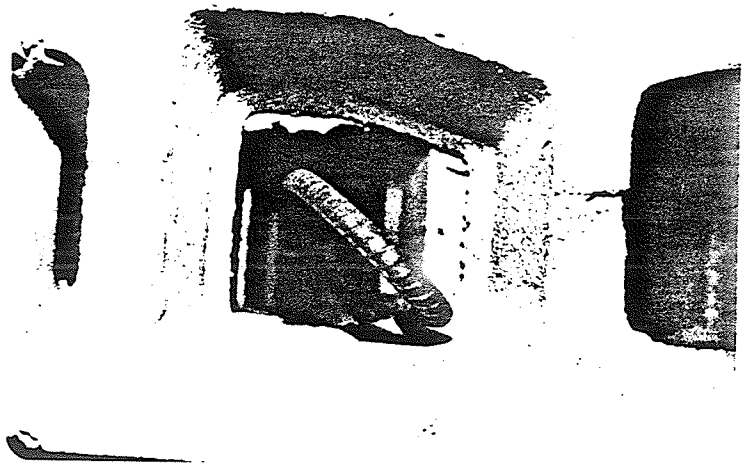

(b)

Plate 2.5 (a) The horizontal and (b) the vertical reinforcement in place.

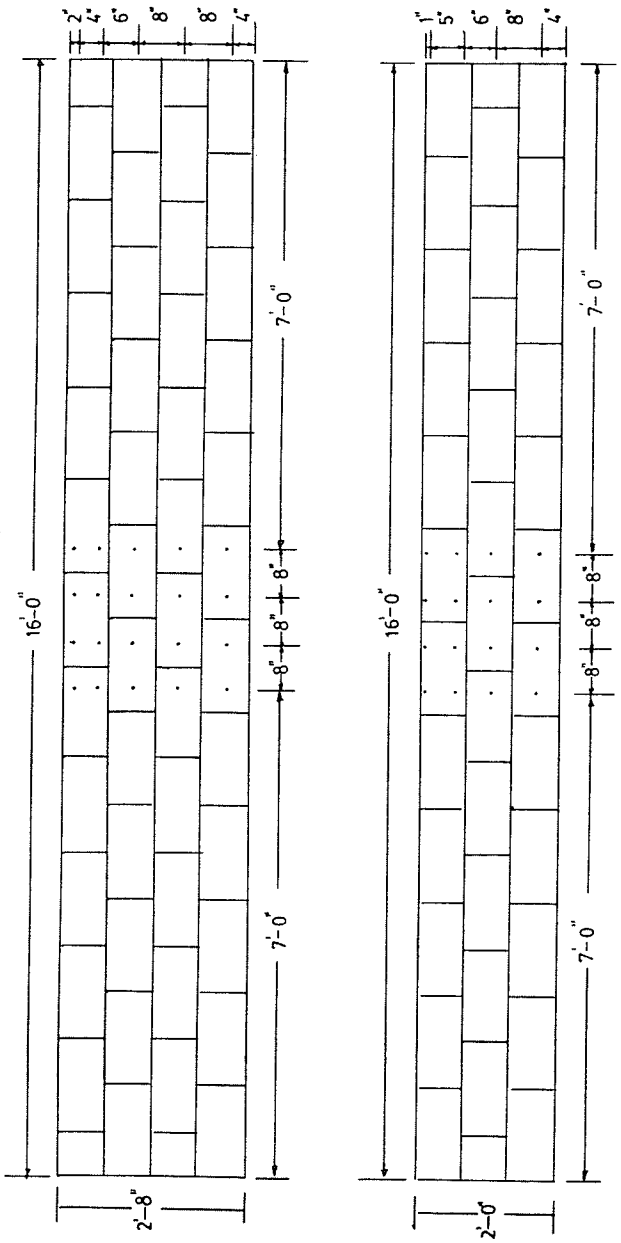

Figure 2.16 Location for "Demec" points in Series I beams (upper diagram) and Series II beams (lower diagram).

2.3.2 COMPARISON OF BEAM CONSTRUCTION TECHNIQUES

There are different types of construction and filling techniques for masonry beams. For filled masonry beams, the block frame is constructed as described in the previous section. However, the top course can be constructed with either "U" blocks or standard hollow blocks. The common practice is to favour the latter because it facilitates filling the beam with concrete. Even if the top steel is used in the beam, the webs can be partially removed to enable the steel to be placed with appropriate cover.

The main problem associated with using standard hollow blocks for the top course is that the voids between blocks are rarely filled with concrete (See Figure 2.1) because filling these small voids properly would require a compacting technique different from that used for the cores. This discontinuity represents a stress-raiser in regions of high compressive stress. As this situation is common practice, and has not been considered in previous investigations, the situation was duplicated in the present study by taking care to ensure that the voids between blocks were left unfilled.

2.3.3 CONSTRUCTION OF THE TWO-BLOCK PRISMS

The two-block prisms were built on the horizontal in a manner to duplicate the construction of the beams, and on a bed designed to permit clamping the blocks together for handling. The concrete grout was placed three days after the prisms were assembled. Grout was placed in two lifts, each lift being rodded 25 times for compaction and the top trowelled level.

Three grout test specimens for every five prisms were prepared in accordance with the requirements of CSA Standard A 179 - 1975 [7]. Prisms and grout specimens were cured under wet burlap, and subsequently, in preparation for testing, were air-dried for twenty-four hours. After drying, the prisms were clamped to prevent mortar joint-cracking during lifting and placing in the testing machine. "Demec" points and electrical strain gauges were placed across the mortar joint and in selected locations on the prisms. Figure 2.17 shows the locations of the "Demec" points in the partially filled two-block prisms.

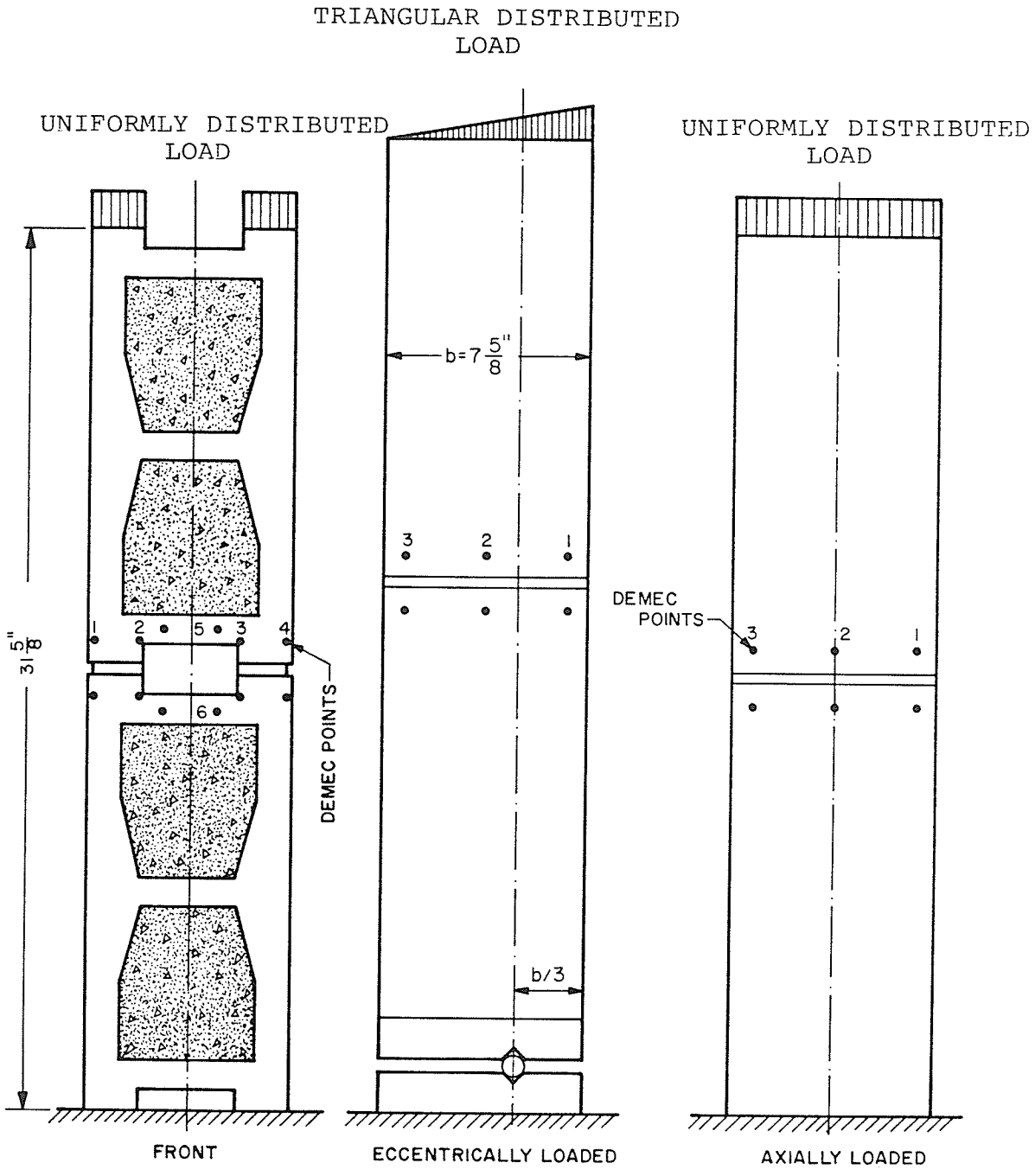

Figure 2.17 Location of "Demec" points in axially and eccentrically loaded partially filled two-block prisms.

2.4 SPECIMEN TESTING ARRANGEMENT AND PROCEDURE

All beams and block prisms were tested to failure in a 600 Kip Universal Testing machine with strains and loads being recorded at appropriate load increments.

2.4.1 BEAM TESTING ARRANGEMENT AND PROCEDURE

All beams were tested on a W 24 x 100 steel beam which was mounted in the 600 Kip Universal Testing machine. The beams were simply supported over a fifteen foot span and loaded at the one-third points. The beams were PIN-supported at one end, PIN-roller supported at the other end, and PIN-rollers were provided at the loading points. This arrangement was used to eliminate external horizontal forces from being applied to the beams. All support and loading plates were laid in plaster to minimize beam twisting and stress concentrations. The test arrangement is shown in Figure 2.18.

The loading arrangement and the resulting shear and bending moment diagrams for the tested beams are shown in Figure 2.19. Dial gauges were placed under the mid-span as well as under both loading points to measure deflections. After the initial strain and dial gauge readings were taken, the loads were applied in increments of 1 Kip to 5 Kip depending on the capacity of the beams. Following each load increment, the machine was held in strain control until the strain and dial gauge readings were taken. Beams 1, 2

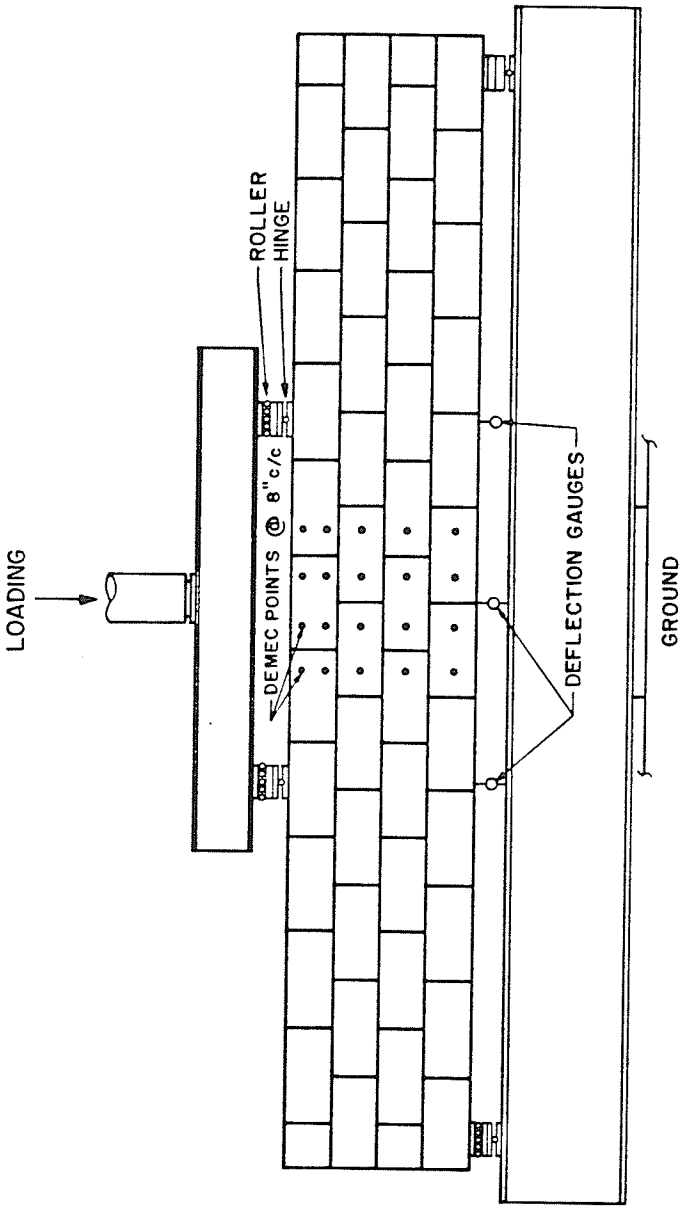

Figure 2.18 The test set up for beams.

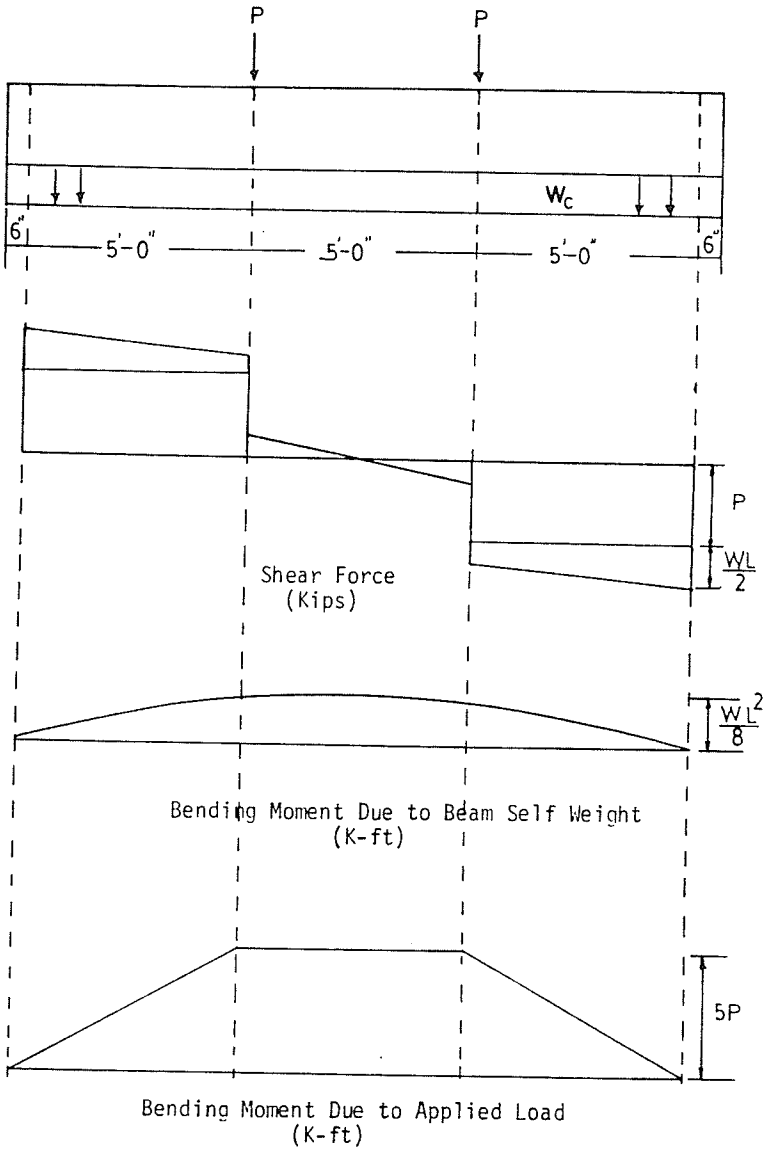

Figure 2.19 Beam loading, shear force, and bending moment diagrams.

and 3 also had strain gauges mounted on the reinforcing steel. Cracks were traced and corresponding loads were marked with ink on both sides of the beams.

2.4.2 TWO-BLOCK PRISMS TESTING ARRANGEMENT AND PROCEDURE

The prisms were carefully clamped and lifted into the testing position. The prisms were tested with two types of end conditions: PIN/FIX and PIN/PIN. All the axially loaded specimens had the PIN/FIX end conditions. The platform of the testing machine was the "fixed" end and the spherical head was the "pinned" end. The remainder of the eccentrically loaded prisms had PIN/PIN end conditions, with a hinge being used at the base and the spherical head of the machine at the top of the specimens. Steel base and cap plates were applied by means of a plaster layer to minimize stress concentrations. The loads were applied in increments of 3 Kip to 5 Kip depending on the type and capacity of each prism. After each load increment, the machine was held in strain control until the electrical resistance gauge readings and the "Demec" gauge readings were taken.

Figure 2.20 and Plate 2.6 show the clamping and the holding process of the two-block prisms. Figure 2.21 shows the test arrangement of the axially and eccentrically loaded two-block prisms.

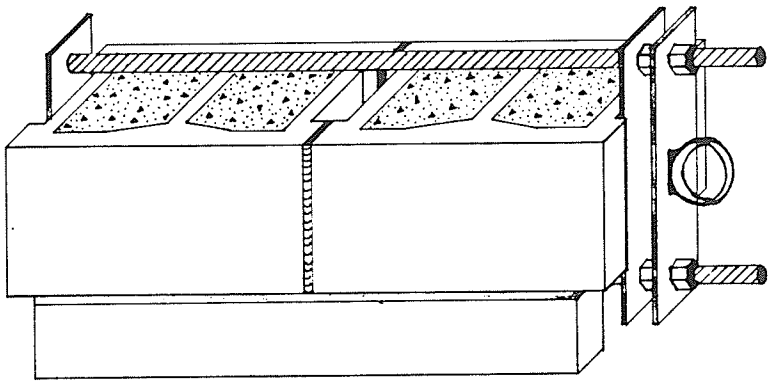

Figure 2.20 Clamping process of two-block prisms.

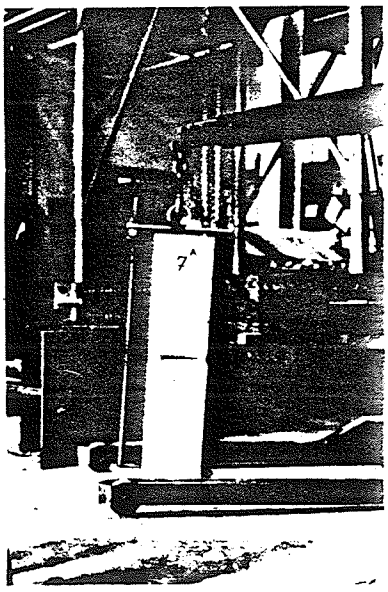

Plate 2.6 The holding procedure for the two-block prisms.

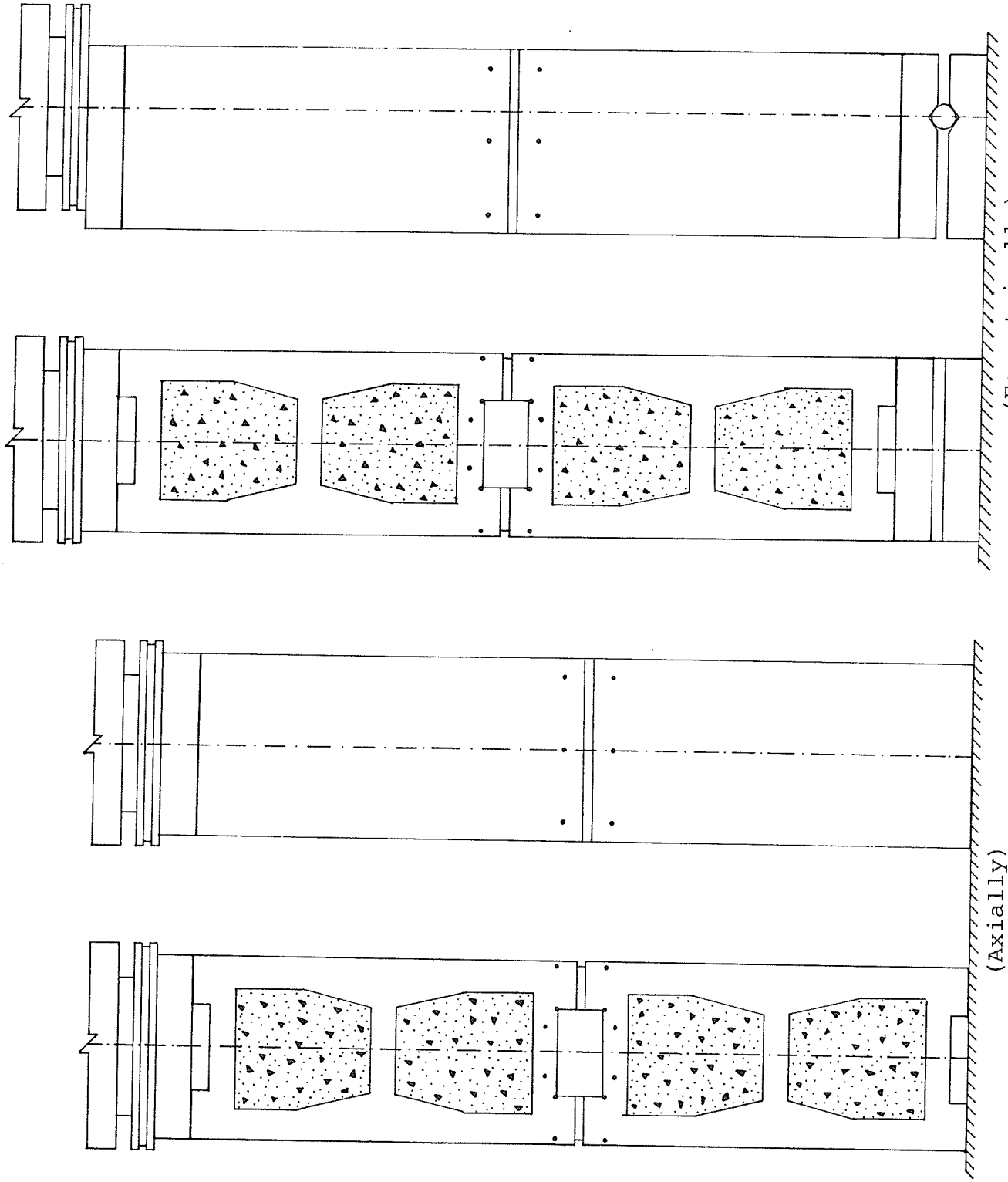

Figure 2.21 Set up of the axially and eccentrically loaded two-block prisms.

CHAPTER 3

FINITE ELEMENT ANALYSIS

3.1 INTRODUCTION

Planar and three dimensional stress analyses[8][3] were performed for the different types of single-block specimens and two-block prisms using the finite element analysis technique. The elastic properties for the masonry concrete, grout and mortar were used to determine all the stresses in the analyzed prisms.* The finite element method was used to find and study the vertical, horizontal, shear and principal stresses at any point in the single-block specimens and the two-block prisms; and to predict the initiation of cracking and the mode of failures. The method was also used to compare the results of the prism tests with the analysis of the actual isolated portion of the beam compression zone. The effects on the stress and strain distribution caused by changing material properties were also investigated.

3.2 THE FINITE ELEMENT METHOD

The finite element method is a very powerful technique for solving different kinds of continuum mechanics problems including planar and three dimensional stress analysis, plate and shell analysis, seepage through porous media, heat conduction, dynamic problems, etc. The method, which

---

* The material properties used in the present F.E.M. analyses were obtained from testing and are given in Table 3.1 .

originated with an engineering group at Boeing Aircraft Corporation in about 1952, depends on the use of the digital computer. The finite element method involves subdividing the continuum into a series of elements or units (various shapes of elements: triangles; rectangles; quadrelaterals; tetrahedrons; hexahedrons; etc.). These elements are considered interconnected at joints or nodal points. Simple functions are chosen to approximate the distribution or variation of the actual displacements over each finite element. Hence, the final solution will give the approximate displacements at discrete locations in the body, the nodal points. The polynomials and trigonometric functions are various simple forms of a displacement model. The polynomials offer easier mathematical manipulations, and have been used commonly in finite element applications. The two dimension and the three-dimension finite element analysis were used to analyze the single-block samples and the two-block prisms. The two methods used elastic material properties in the analysis. Table 3.1 gives these material properties. The mortar, concrete fill and masonry concrete stress-strain curves are shown in Figure 3.1.

3.3 TWO-DIMENSIONAL ANALYSIS

The finite element method selected for this analysis can be used to determine displacements and stresses within axisymmetric and plane solids.[8] This method may be

Table 3.1 Material properties used in the F.E.M. analysis

MATERIAL	COMPRESSIVE STRENGTH (P.S.I)	SECANT MODULUS OF ELASTICITY (P.S.I)	SHEAR MODULUS OF ELASTICITY (P.S.I)	POISSON'S RATIO
MORTAR	2600	2.1×10^6	8.9×10^5	0.175
CONCRETE FILL	4500	3.1×10^6	1.3×10^6	0.166
MASONRY CONCRETE	4411	4.4×10^6	1.9×10^6	0.170

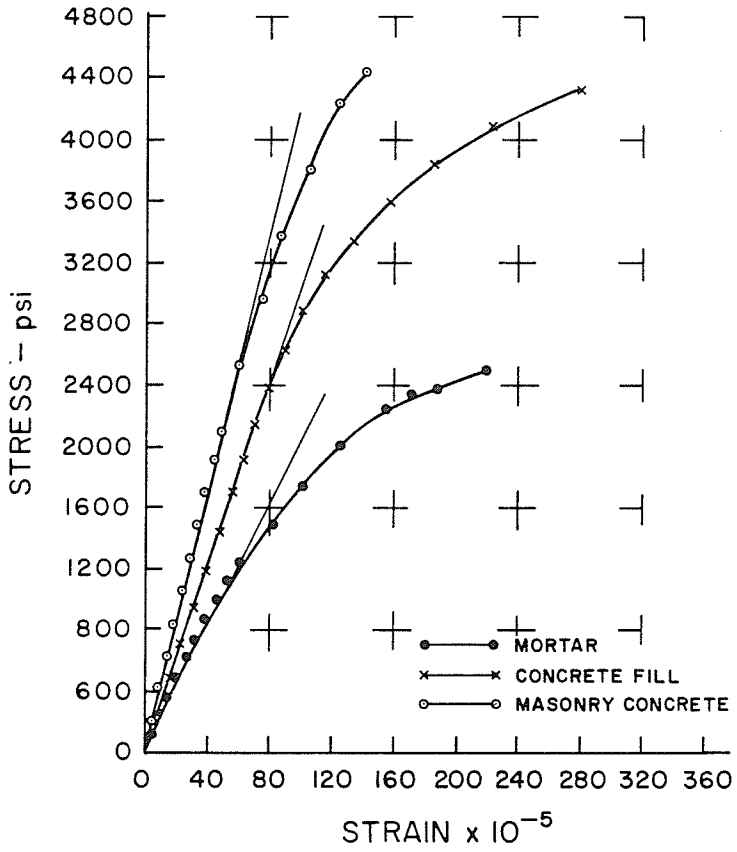

Figure 3.1 Stress - strain curves for mortar, concrete fill, and masonry concrete.

applied to structures composed of many different materials and structures with complex geometry. In most cases the element used is based on a linear displacement field which gives a constant strain variation within each element. The use of a higher order displacement function (a quadratic displacement field) yields to linear strain variations within the element. Consequently fewer elements are required to model the structural response. The nodal point and element data generation options allow the program to be readily used. The method is general with respect to geometry and elastic material properties. Displacement or stress boundary conditions can be specified at any point within the finite element system. Arbitrary thermal, mechanical, and accelerational loads are possible in this method. Any desired degree of accuracy can be obtained by changing the number of elements in the continuum.

3.3.1 PLANE STRESS IDEALIZATION

The loads are applied in the plane of the body or the structure, that is the x - y plane. The thickness is small compared to the x - y dimensions of the body. Such loadings are often referred to as in-plane or membrane loadings. It is assumed that out of the six components of stresses in a three-dimensional body; three components, σ_z, τ_{zx}, and τ_{yz} can be ignored in comparison to the remaining three, σ_x, σ_y, and τ_{xy}. This idealization is called plane

stress and involves only the following nonzero stress components.

$$\{\sigma\} = \begin{pmatrix} \sigma_x \\ \sigma_y \\ \tau_{xy} \end{pmatrix} \tag{3.1}$$

which are functions of the coordinates x,y only. The corresponding components of strains are

$$\{\varepsilon\} = \begin{pmatrix} \varepsilon_x \\ \varepsilon_y \\ \gamma_{xy} \end{pmatrix} \tag{3.2}$$

where σ and ε = components of direct stress and strain respectively

τ and γ = components of shear stress and strain respectively.

The vectors of stress and strain components are

$$\{\sigma\}^T = | \sigma_x \quad \sigma_y \quad \tau_{xy} | \text{ and } \{\varepsilon\}^T = | \varepsilon_x \quad \varepsilon_y \quad \varepsilon_{xy} | .$$

In view of the plane stress assumption, two components of displacements need to be considered at a point, U and V, in the x and y directions respectively. If we restrict ourselves to linear, elastic, and isotropic materials, the material behaviour can be expressed by using the generalized Hooke's Law. Thus,

$$\sigma_x = \frac{E}{1-\nu^2}\varepsilon_x + \frac{\nu E}{1-\nu^2}\varepsilon_y,$$

$$\sigma_y = \frac{\nu E}{1-\nu^2}\varepsilon_x + \frac{E}{1-\nu^2}\varepsilon_y, \qquad (3.3a)$$

$$\tau_{xy} = \frac{E}{2(1+\nu)}\gamma_{xy}$$

or in matrix notation

$$\{\sigma\} = |C|\{\varepsilon\} = \frac{E}{1-\nu^2}\begin{vmatrix} 1 & \nu & 0 \\ \nu & 1 & 0 \\ 0 & 0 & \frac{1-\nu}{2} \end{vmatrix}\{\varepsilon\} \qquad (3.3b)$$

where $|C|$ = stress - strain or constitutive matrix.

E = Young's modulus.

ν = Poisson's ratio.

3.3.2 THE TWO-DIMENSIONAL FINITE ELEMENT COMPUTER MODEL AND ANALYSIS RESULTS

The computer finite element model (see Figure 3.2) was built up by taking into consideration the following factors:

1. The advantages of symmetry.
2. The elastic material properties were the same for all specimens, only if stated otherwise. (See Table 3.1 and Figure 3.1)
3. The elements were numbered in such a way that the same model can be used for single and two-block, unfilled, partially filled and completely filled axially loaded specimens. This model can be used for the grooved and nongrooved prisms (i.e. tooled and untooled joints).

The nodal points and elements were numbered sequentially starting with one in a counterclockwise direction around the element center. It was found that these points should be numbered sequentially in the shortest model dimension (the width of the model) to minimize solution time and to prevent singularity and reduce band width in the stiffness matrix. The nodal points which fall on the axis of symmetry were fixed against horizontal movement and were free to move vertically to represent the boundary conditions due to symmetry. Figure 3.2 shows the finite element mesh used for the two-dimensional analysis.

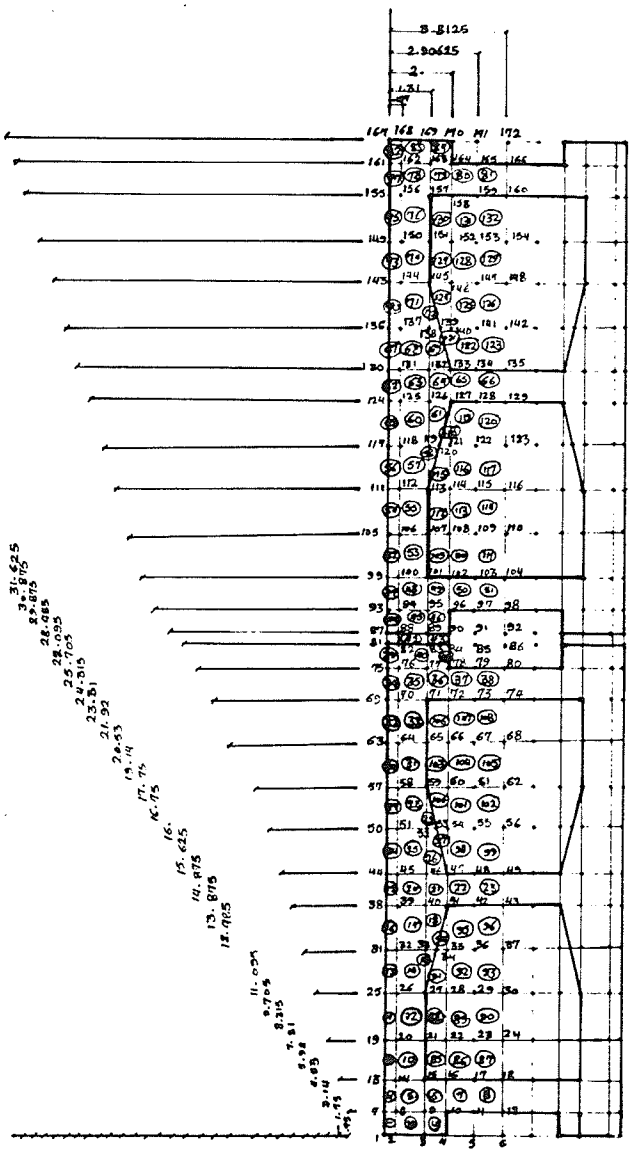

Figure 3.2 Two-dimensional finite element mesh.

The results for axially-loaded single and two-block specimens analyzed were:

1. Unfilled single-block.*
   (a) PIN/FIX end conditions (see Figure A.1)**
   (b) PIN/PIN end conditions (see Figure A.2)**

2. Partially filled single-block.
   (a) PIN/FIX end conditions (see Figure A.3 a,b,c)
   (b) PIN/PIN end conditions (see Figure A.4 a,b,c)
   (c) f_G' = 500 p.s.i. (see Figure A.5 a,b,c)

3. Completely filled single-block (see Figure A.6)

4. Unfilled two-block prism. (note the magnified lateral deflection for the unfilled two-block prism in Figure A.7)
   (a) PIN/FIX end conditions (see Figure A.8)
   (b) PIN/PIN end conditions (see Figure A.9)

---

*Note: (1) The word block in this chapter represents the standard hollow block.
(2) The material elastic properties are the same for all models only if specified otherwise.
(3) The end conditions are PIN/FIX for all the models only if specified otherwise.
(4) The two-block prism models are grooved only if specified otherwise.

**All figures are found in Appendix A.

5. Partially filled two-block prism. (note the magnified lateral deflection for the partially filled two-block prism in Figure A.10)

   (a) PIN/FIX end conditions (see Figure A.11 a,b,c)

   (b) PIN/PIN end conditions (see Figure A.12 a,b,c)

   (c) f_G' = 500 (p.s.i.) (see Figure A.13 a,b,c)

   (d) f_M' = 500 (p.s.i.) (see Figure A.14 a,b,c)

6. Completely filled two-block prism. (see Figure A.15 a,b,c)

3.4 THREE-DIMENSIONAL ANALYSIS

The finite element method selected for this analysis was the SAP IV three-dimensional finite element analysis.[3] The program is a general analysis tool for the linear static and dynamic analysis of complex structures. The nodal point input data is read and generated by the program. With the coordinate of all nodal points known and the equation numbers of the degrees of freedom having been established, the stiffness mass and stress-displacement transformation matrices for each structural element in the system are generated and placed on tape storage. These basic steps are independent of the element type used and are the same for either a static or dynamic analysis. There is no restriction on the number of elements used, the number of load cases or the order and band width of the stiffness matrix. Each nodal point in the system can have zero to six displacement degrees of freedom. The nodal point equilibrium equation for a linear system can be written in the following form:

$$M\ddot{U} + C\dot{U} + KU = R \qquad (3.4)$$

where M = mass matrix

C = damping matrix

K = stiffness matrix

U = nodal displacements

$\dot{U}$ = velocities

$\ddot{U}$ = accelerations

R = generalized loads

The structure matrices are formed by direct addition of the element matrices, for example,

$$K = \Sigma K_m$$

where

K_m = stiffness matrix of the m'th element.

A static analysis involves the solution of the equilibrium equation

$$KU = R \qquad (3.5)$$

followed by the calculation of element stresses.

The solution of the equations is obtained by using a Gauss elimination subroutine. After the nodal point displacements have been evaluated sequentially, the element stress - displacement matrices are read from storage and the element stresses are calculated.

3.4.1 LINEAR CONSTITUTIVE EQUATIONS

Hooke's law for uniaxial deformation states that the deformation (strain) is proportional to the force (stress). In the more general case of three-dimensional bodies, six components of stress and strain will be present. As a natural extension of Hooke's law, each of the six stress

components may be expressed as a linear function of the six components of strain, and vice versa. Such relations constitute the generalized Hooke's law:

$$\begin{pmatrix} \sigma_x \\ \sigma_y \\ \sigma_z \\ \tau_{xy} \\ \tau_{zx} \end{pmatrix} = \begin{vmatrix} C_{11} & C_{12} & \cdot & \cdot & \cdot & C_{16} \\ C_{21} & C_{22} & \cdot & \cdot & \cdot & C_{26} \\ \cdot & & & & & \cdot \\ \cdot & & & & & \cdot \\ C_{61} & C_{62} & \cdot & \cdot & \cdot & C_{66} \end{vmatrix} \begin{pmatrix} \varepsilon_x \\ \varepsilon_y \\ \varepsilon_z \\ \gamma_{xy} \\ \gamma_{zx} \end{pmatrix} \qquad (3.6a)$$

or

$$\{ \sigma \} = |C| \{ \varepsilon \} \qquad (3.6b)$$

and

$$\begin{pmatrix} \varepsilon_x \\ \varepsilon_y \\ \varepsilon_z \\ \gamma_{xy} \\ \gamma_{yz} \\ \gamma_{zx} \end{pmatrix} = \begin{vmatrix} D_{11} & D_{12} & \cdot & \cdot & \cdot & D_{16} \\ D_{21} & D_{22} & \cdot & \cdot & \cdot & D_{26} \\ \cdot & & & & & \cdot \\ \cdot & & & & & \cdot \\ \cdot & & & & & \cdot \\ D_{61} & D_{62} & \cdot & \cdot & \cdot & D_{66} \end{vmatrix} \begin{pmatrix} \sigma_x \\ \sigma_y \\ \sigma_z \\ \tau_{xy} \\ \tau_{yz} \\ \tau_{zx} \end{pmatrix} \qquad (3.6c)$$

or

$$\{ \varepsilon \} = |D| \{ \sigma \} \qquad (3.6d)$$

where σ and ε = components of direct stress and strain respectively.

τ and γ = components of shear stress and strain respectively.

Equations (3.6a) or (3.6c) represent the constitutive law for a linear, elastic, anistropic, and homogeneous material. The matrices $|C|$ and $|D|$ are symmetric; hence, a complete constitutive description of a general anistropic solid necessitates experimental evaluation of 21 elastic constants.

Certain materials exhibit symmetry with respect to planes within the body, so the number of material constants will be reduced from 21 required in the anistropic case. That means orthotropic material is expressed in terms of nine constants:

$$\begin{Bmatrix} \sigma_x \\ \sigma_y \\ \sigma_z \\ \tau_{xy} \\ \tau_{yz} \\ \tau_{zx} \end{Bmatrix} = \begin{vmatrix} C_{11} & C_{12} & C_{13} & 0 & 0 & 0 \\ & C_{22} & C_{23} & 0 & 0 & 0 \\ & & C_{33} & 0 & 0 & 0 \\ & & & C_{44} & 0 & 0 \\ & \text{symmetrical} & & & C_{55} & 0 \\ & & & & & C_{66} \end{vmatrix} \begin{Bmatrix} \varepsilon_x \\ \varepsilon_y \\ \varepsilon_z \\ \gamma_{xy} \\ \gamma_{yz} \\ \gamma_{zx} \end{Bmatrix} \qquad (3.7a)$$

The strain - stress equations for orthotropic materials may be written in terms of the Young's moduli and Poisson's ratios as follows:

$$\varepsilon_x = \frac{\sigma_x}{E_x} - \frac{\nu_{yx}}{E_y} \sigma_y - \frac{\nu_{zx}}{E_z} \sigma_z$$

$$\varepsilon_y = -\frac{\nu_{xy}}{E_x} \sigma_x + \frac{\sigma_y}{E_y} - \frac{\nu_{zy}}{E_z} \sigma_z$$

$$\varepsilon_z = -\frac{\nu_{xz}}{E_x} \sigma_x - \frac{\nu_{yz}}{E_y} \sigma_y + \frac{\sigma_z}{E_z} \qquad (3.7b)$$

$$\gamma_{xy} = \frac{\tau_{xy}}{G_{xy}}, \quad \gamma_{yz} = \frac{\tau_{yz}}{G_{yz}}, \quad \gamma_{zx} = \frac{\tau_{zx}}{G_{zx}}$$

These equations may be inverted to obtain the values of the elements of $|C|$ in equations (3.7a). There are twelve material parameters in equations (3.7b); however, only nine of these are independent because the following must be true:

$$\frac{E_x}{\nu_{xy}} = \frac{E_y}{\nu_{yx}}, \quad \frac{E_y}{\nu_{yz}} = \frac{E_z}{\nu_{zy}}, \quad \frac{E_z}{\nu_{zx}} = \frac{E_x}{\nu_{xz}} \qquad (3.7c)$$

The simplest specialization of the generalized Hooke's law is the case in which the material is assumed to be linear, isotropic, and elastic. An isotropic material is one that has point symmetry. It can be shown that only two independent elastic constants are necessary to represent the behaviour in the case of such symmetry. Hence equation (3.6c) in terms of E and ν becomes

$$\begin{Bmatrix} \varepsilon_x \\ \varepsilon_y \\ \varepsilon_z \\ \gamma_{xy} \\ \gamma_{yz} \\ \gamma_{zx} \end{Bmatrix} = \begin{vmatrix} 1/E & -\nu/E & -\nu/E & 0 & 0 & 0 \\ & 1/E & -\nu/E & 0 & 0 & 0 \\ & & 1/E & 0 & 0 & 0 \\ & & & \frac{2(1+\nu)}{E} & 0 & 0 \\ & \text{symmetrical} & & & \frac{2(1+\nu)}{E} & 0 \\ & & & & & \frac{2(1+\nu)}{E} \end{vmatrix} \begin{Bmatrix} \sigma_x \\ \sigma_y \\ \sigma_z \\ \tau_{xy} \\ \tau_{yz} \\ \tau_{zx} \end{Bmatrix} \quad (3.6e)$$

or in terms of stress components, equation (3.6a) becomes

$$\begin{Bmatrix} \sigma_x \\ \sigma_y \\ \sigma_z \\ \tau_{xy} \\ \tau_{yz} \\ \tau_{zx} \end{Bmatrix} = \frac{E}{(1+\nu)(1-2\nu)} \begin{vmatrix} 1-\nu & \nu & \nu & 0 & 0 & 0 \\ & 1-\nu & \nu & 0 & 0 & 0 \\ & & 1-\nu & 0 & 0 & 0 \\ & & & \frac{1-2\nu}{2} & 0 & 0 \\ & \text{symmetrical} & & & \frac{1-2\nu}{2} & 0 \\ & & & & & \frac{1-2\nu}{2} \end{vmatrix} \begin{Bmatrix} \varepsilon_x \\ \varepsilon_y \\ \varepsilon_z \\ \gamma_{xy} \\ \gamma_{yz} \\ \gamma_{zx} \end{Bmatrix} \quad (3.6f)$$

3.4.2 THREE-DIMENSIONAL FINITE ELEMENT COMPUTER MODEL AND ANALYSIS RESULTS

The total number of elements and nodal points used in this model were (670) elements and (1056) nodal points (see Figure 3.3).

The need for the three-dimensional analysis arose from the eccentric load case. The case was analyzed by applying an equal 1000 p.s.i. reference triangular distributed load on both sides of the partially filled two-block model. This type of loading represents the PIN/PIN end conditions for the tested prisms.

The model represents the test specimens by having a groove in the mortar joint which results from joint tooling in these specimens.

The material properties used for the three-dimensional finite element analysis are the same as the ones used for two-dimensional finite element analysis. (see Table 3.1 and Figure 3.1) Figure 3.3 shows the three-dimensional finite element computer model.

The finite element analysis results for the analyzed partially filled two-block prism, eccentrically loaded, PIN/PIN end conditions, are shown in the following Figures:*

Figure A.16(a,b,c) shows direct vertical stresses across the width of the specimen.

Figure A.17(a,b,c) shows direct horizontal stresses in the x- direction, and Figure A.18(a,b,c) shows direct horizontal stresses in the y- direction.

---

* See Appendix A

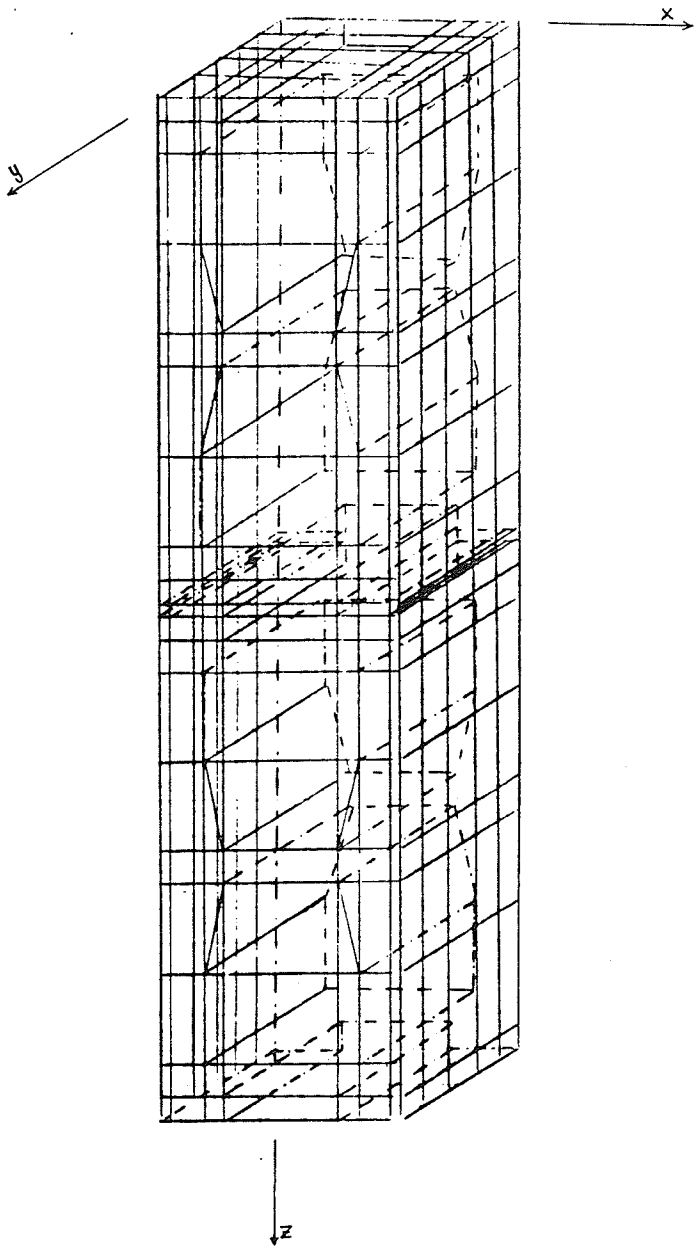

Figure 3.3 Three-dimensional finite element mesh.

CHAPTER 4

TEST RESULTS

4.1 GENERAL

The behaviour, modes of failure and the test results for the masonry beams and the two-block prisms are presented in this chapter. The results are summarized with the help of the tables, curves and photographs.

4.2 MASONRY BEAMS

The general modes of failure behaviour and test results for all the beams are presented and discussed in the following subsections.

4.2.1 GENERAL MODES OF FAILURE

The mode of failure for all the tested beams was essentially by flexure. The load-deflection curves for all the tested beams were linear, initially. The curve changed slope after the formation of flexural cracks which became visible as the loads were increased to between 15 and 30 percent of the ultimate loads. The cracks started at a vertical mortar joint in the lower course at low loads. As the loads were further increased, these cracks widened and began to extend upward towards the compression zone. Some of the cracks cut right through the blocks while others moved along the mortar joints with some portions

cutting through the blocks. At loads greater than approximately 60 percent of the ultimate load, very few new cracks formed and there was little additional crack extension. The load-deflection curves start to flatten as the steel yields. Failure was by flexure either in primary tension or in primary compression, depending on the amount of flexural reinforcement. With the exception of beams 4,5 and 8, all beams failed in the primary tension mode characteristic of "under-reinforced" sections. The yield of the steel took place well in advance of the crushing of masonry and varying ductility was observed in the load-deflection curves. Beams 4,5 and 8, on the other hand, having steel ratios approximately in the vicinity of balanced design defined for reinforced concrete, behaved in a different manner than over-reinforced concrete beams. There was more ductility than expected following the crushing of masonry legs or mortar joints as the load carrying capacity of the beams was reached. In all cases, final failure was by crushing and lateral deflection of the masonry shell in the pure flexural zone of the beam's top course.

The loading arrangement shown in Figure 2.18 was used for the first five beams. It was suspected that some horizontal resistance was encountered at one or more of the loading or support points. Furthermore, a shift in the relative position of these points led to a minor modification of the moment diagram, as shown in Figure 4.1.

The remainder of the beams were tested using "Teflon" bearing pads as shown in Plate 4.1. The reason for this change was to allow both ends of the beams freedom to move freely and evenly, thereby eliminating horizontal constraining forces. The load-deflection curves were plotted by the x-y plotter and from dial gauge readings under the mid-span points and under the two applied loads. The strain readings at various levels in the cross section were also plotted to check whether the plane-section assumption is valid. Plates of the beams after testing are also shown.

4.2.2 INDIVIDUAL BEHAVIOUR OF THE BEAMS

The behaviour of the beams during the tests are described with the help of tables, curves and photographs.

4.2.2.1 BEAM #1

The steel ratio for Beam #1 was approximately 14% of its $\rho_{balance}$ (see Section 2.1.1 and Table 2.1). The first flexural cracks were visible at the mortar joints at mid-span as well as in the shear span close to the loading points. The first cracks became visible at a load of 6 Kips. As the load increased more cracks became visible. The old cracks widened and propogated toward the compression zone, reaching a height of about 7 inches from the beam top at a load of 15 Kips. Further increments of load only resulted in a very small extension of the cracks.

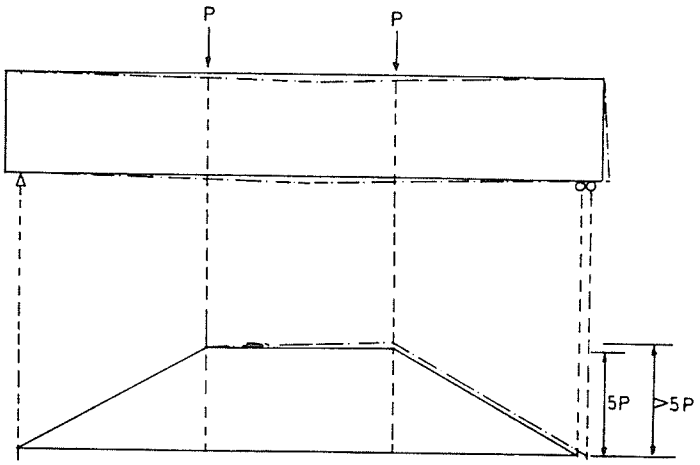

——— Idealized

— — — After load applied

Figure 4.1 Diagram of modified bending moment due to applied load.

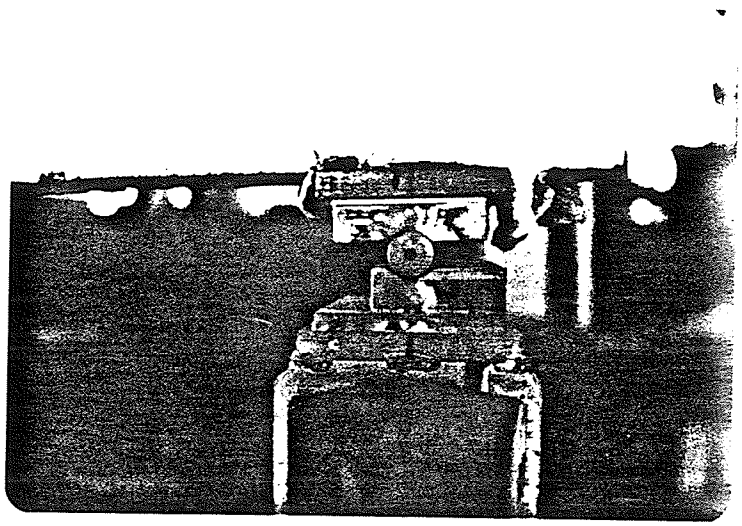

Plate 4.1 Two sheets of Teflon were used instead of rollers in the end-bearing supports for Series II beams.

The steel started to yield at a load of approximately 18.6 Kips. At the same time, a flexural crack under one of the loading points became inclined, widened rapidly and extended further towards the mortar joint region just beside the loading point, reaching a height of 4 inches from the beam top at a load of 20 Kips. Although showing considerable deflection, the beam continued to carry more load. The beam finally failed by crushing and lateral deflection of the block shell at the mortar joint when the load was 21.6 Kips and the deflection was 1.6 inches.

Load-deflection curves are shown in Figure 4.2. Strain readings for the beam are shown in Table B.1 and B.2. Strain readings for longitudinal reinforcement are given in Table B.3. Figures 4.3 to 4.5 present the strain profile diagrams. Plates 4.2 and 4.3 illustrate the beam failure mode.

4.2.2.2 BEAM #2

The steel ratio for Beam #2 was approximately 37% of its $\rho_{balance}$ (see section 2.1.1 and Table 2.1). The first flexural cracks were observed at the mortar joints in both the mid-span and the shear span regions at a load of 8 Kips. As the load increased, the flexural cracks extended toward the compression zone and new cracks became visible in the mortar joints and in the concrete blocks along the bottom course. At a load of approximately 30 Kips,

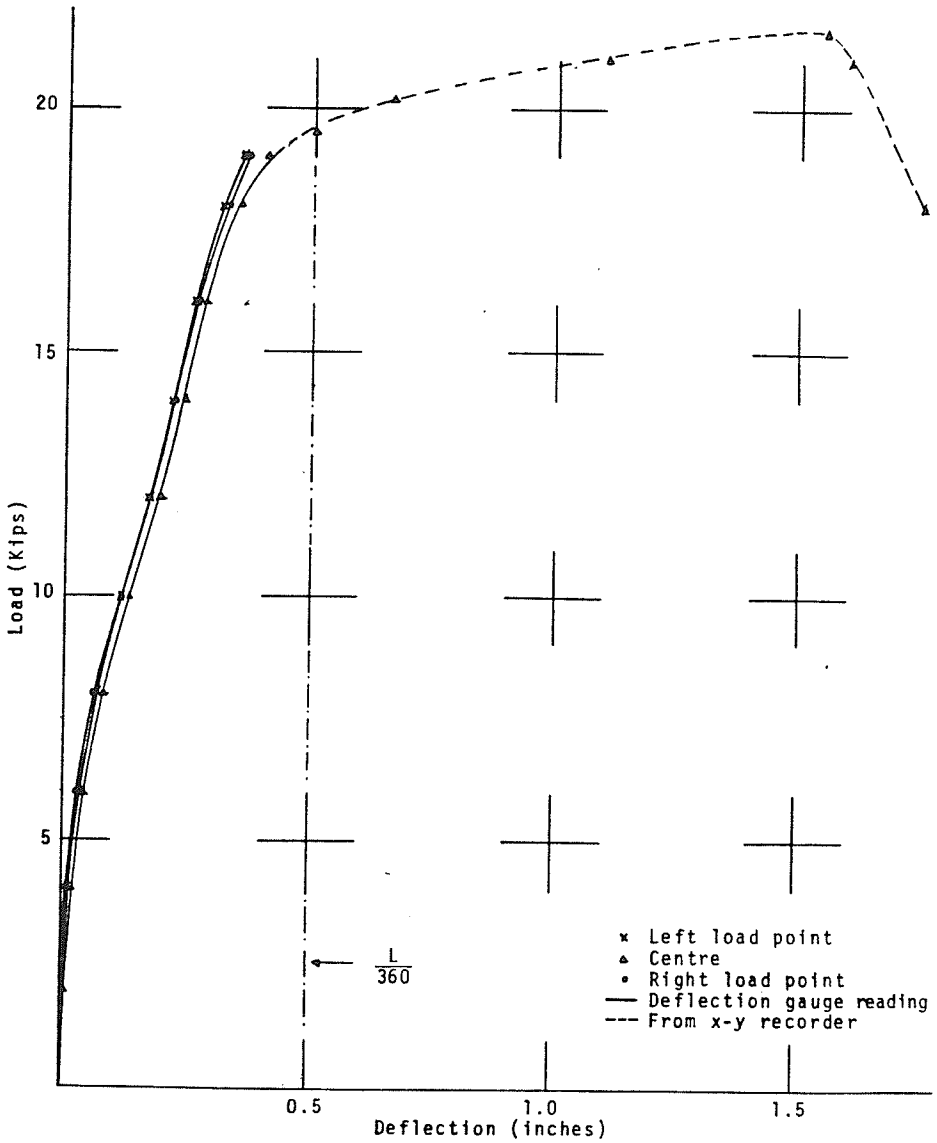

Figure 4.2 Load - deflection curves for Beam #1.

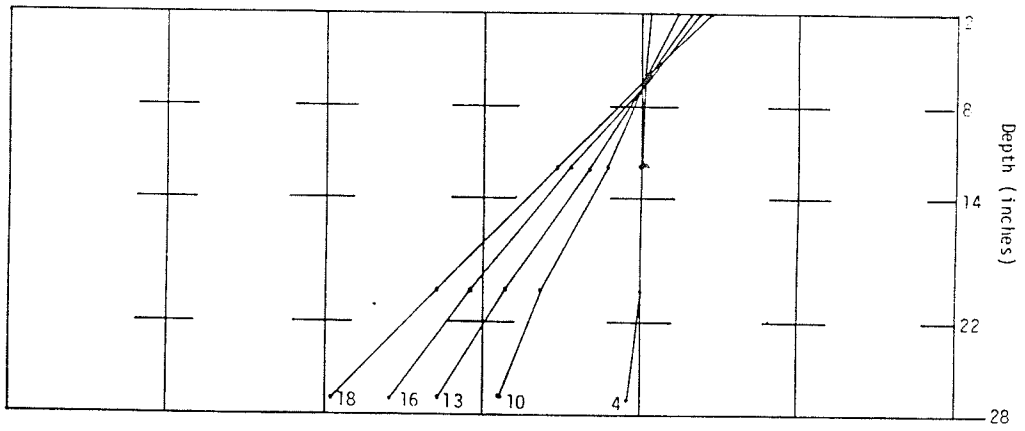

Figure 4.3 Beam #1, Side A, average strain readings.

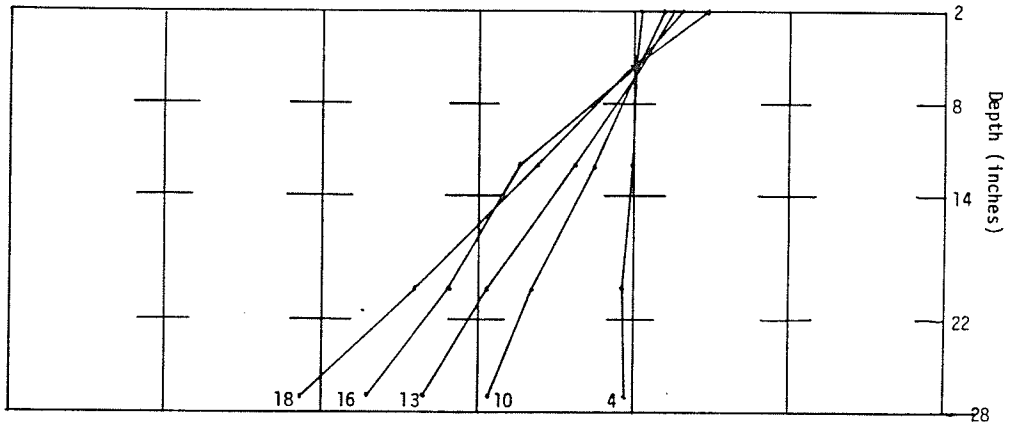

Figure 4.4 Beam #1, Side B, average strain readings.

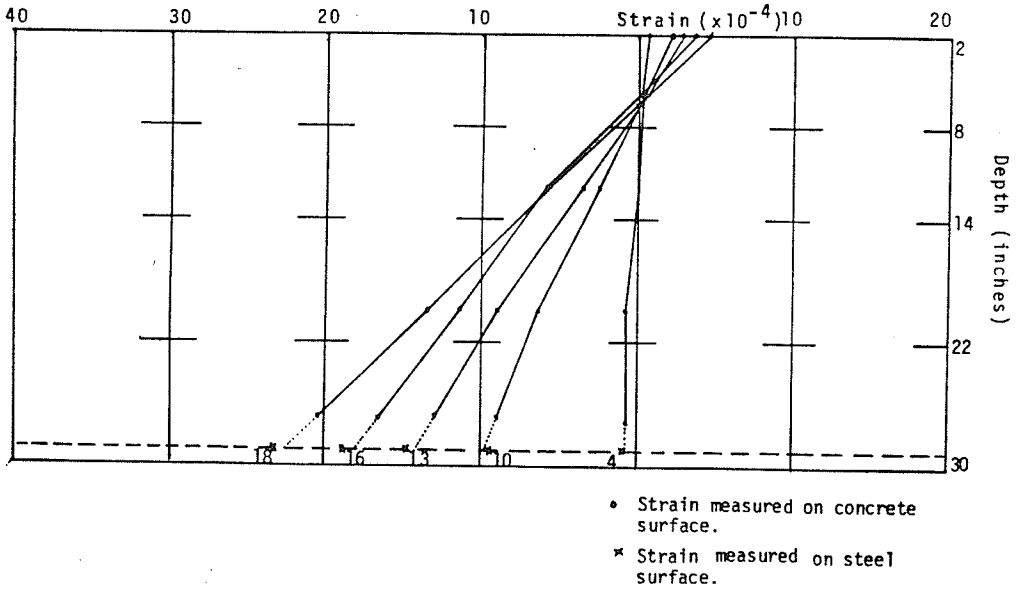

Figure 4.5 Beam #1, average of strain readings for both sides.

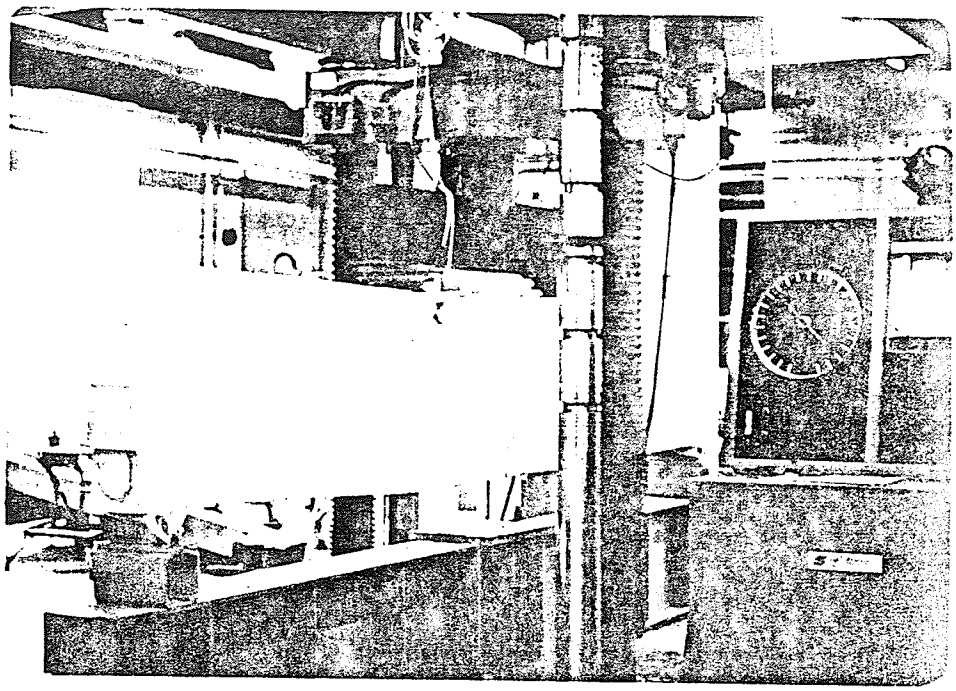

Plate 4.2 Flexural failure in Beam #1 looking at Side B.

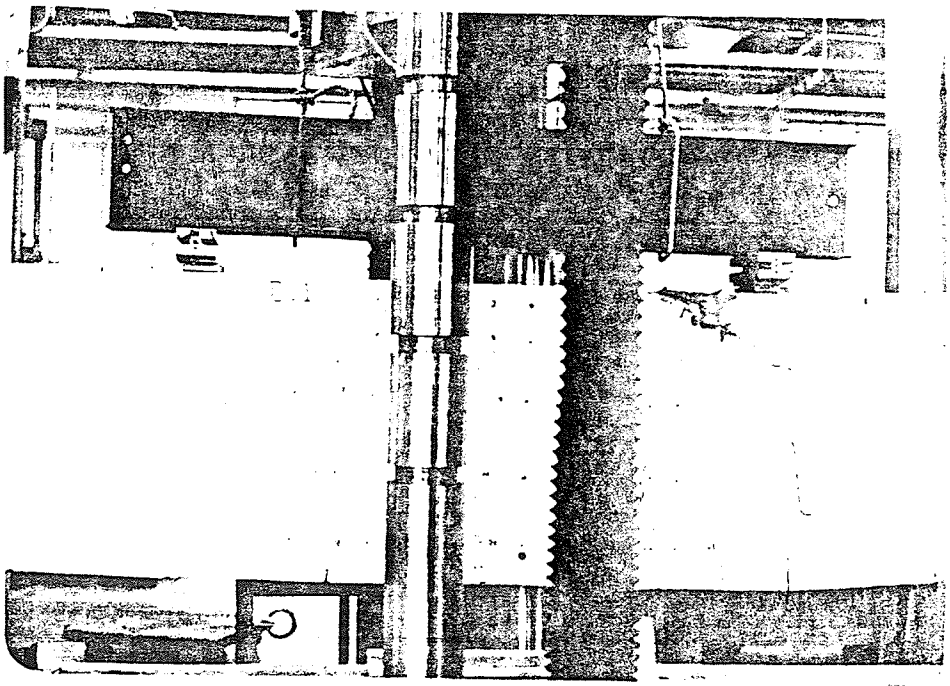

Plate 4.3 Flexural failure in Beam #1 looking at Side A.

a few cracks in the shear span became inclined and extended towards the loading points. As the load increased, the cracks slowly progressed. At a load of 40 Kips, the cracks reached a height of about 6 inches from the top of the beam. More loads were applied and at 46 Kips, the steel started to yield and a fair amount of deflection was observed. A flexural failure resulted in crushing and lateral deflection of the block shell at the mortar joint. The failure load of 51 Kips with a deflection of 0.9 inches was recorded.

Load-deflection curves are shown in Figure 4.6. Strain readings for the beam are given in Table B.4 and B.5. Table B.6 gives the strain readings for the longitudinal reinforcement. The strain profile diagrams are shown in Figures 4.1 to 4.9. The tested beam is shown in Plates 4.4 and 4.5.

4.2.2.3 BEAM #3

The steel ratio for Beam #3 was approximately 79% of its $\rho_{balance}$ (see Section 2.1.1 and Table 2.1) The first flexural cracks were observed at the mortar joints in the mid-span region at 10 Kips and in the shear span at 15 Kips. As the load was increased, more flexural cracks were observed developing in the concrete block along the bottom course. With increased loads, the flexural cracks progressed slowly and reached a maximum height of about

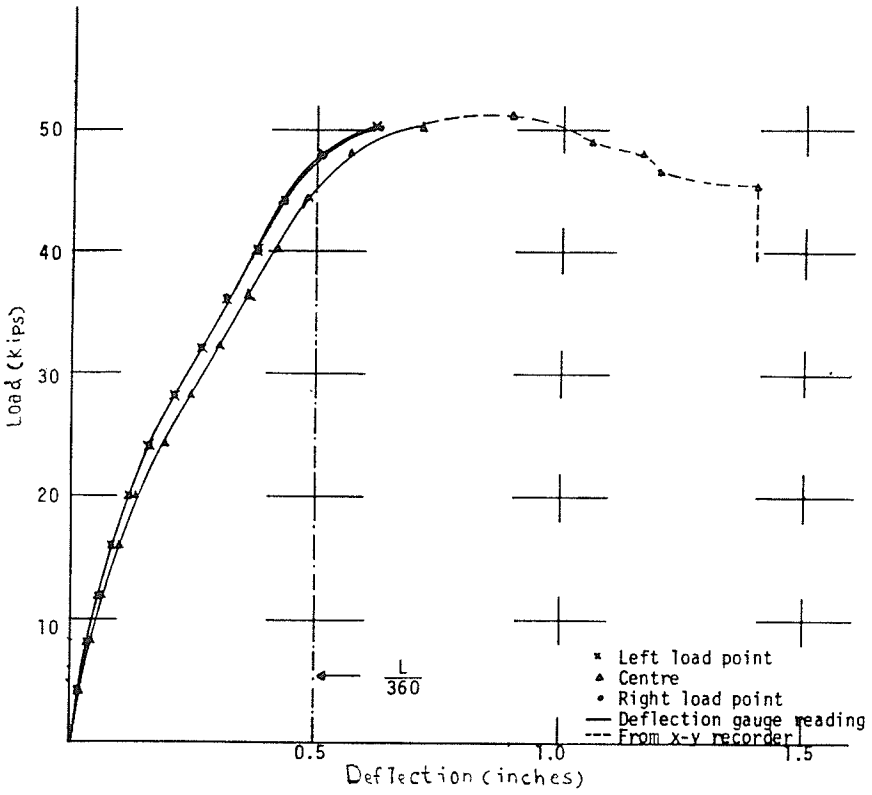

Figure 4.6 Load - deflection curves for Beam #2.

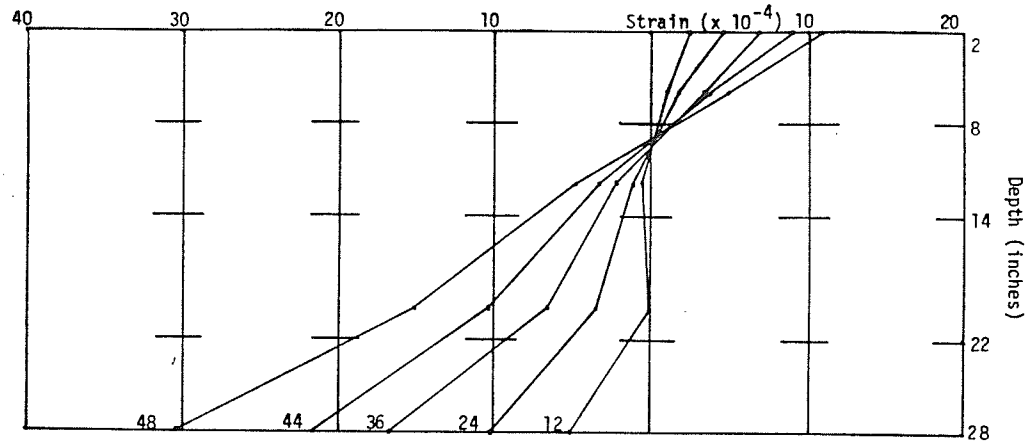

Figure 4.7 Beam #2, Side A, average strain readings.

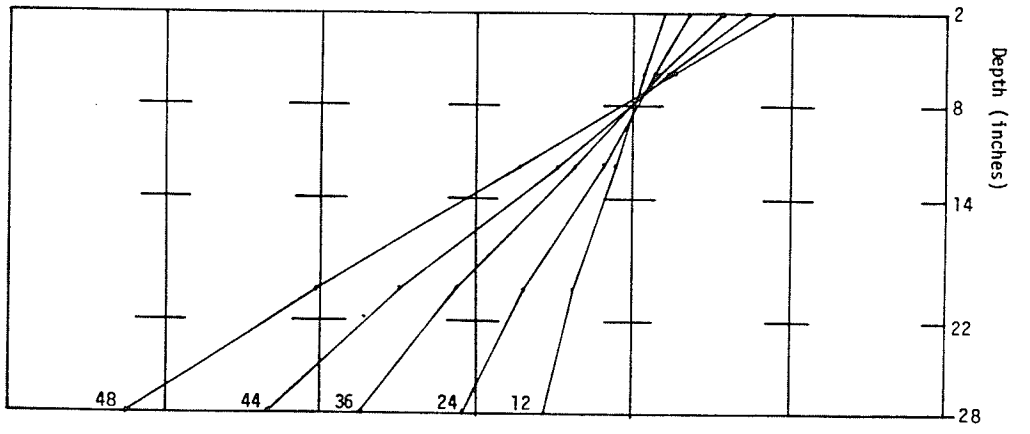

Figure 4.8 Beam #2, Side B, average strain readings.

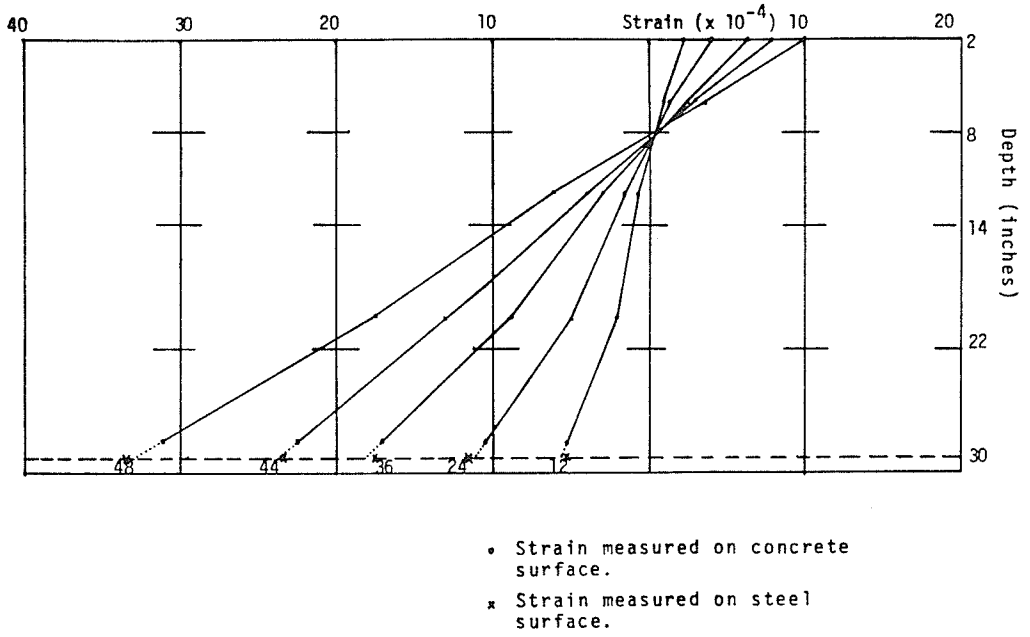

Figure 4.9 Beam #2, average of strain readings for both sides.

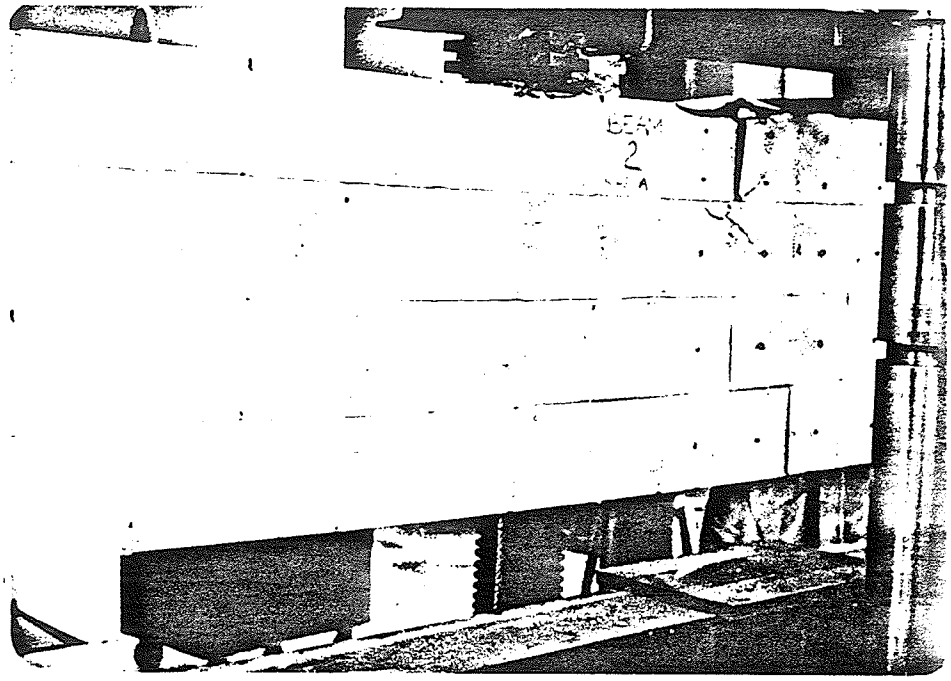

Plate 4.4 Cracking and final flexural failure of Beam #2.

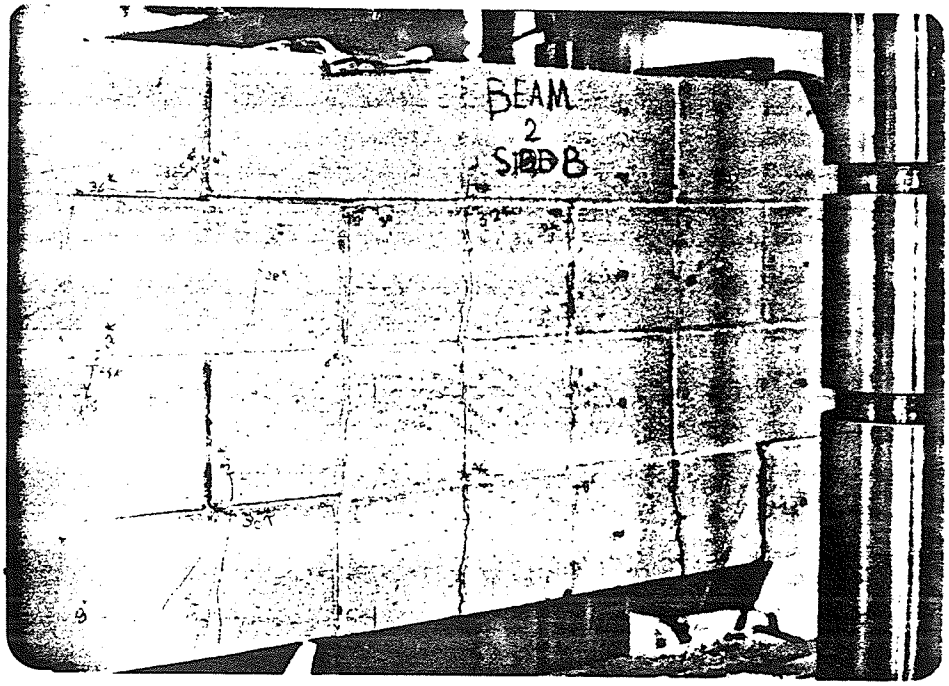

Plate 4.5 Cracking of Beam #2.

10 inches from the beam top at a load of 50 Kips.

Diagonal cracks were first observed in the shear span at a load of 15 Kips and they progressed slowly as the loads increased. At a load of 60 Kips, some diagonal cracks reached a height of 8 inches from the top and started traveling horizontally along the mortar joint towards the loading points. Yielding of the steel started at 83 Kips. After that, the load-deflection curve levelled off. The load remained constant at 83 Kips while the deflection increased by about 0.4 inches. The beam failed suddenly by a longitudinal split in the center of the top course, followed by severe crushing and lateral deflection of the block shell (see Plates 4.8 and 4.9). A maximum load of 83 Kips with a deflection of 1.16 inches was recorded.

Load-deflection curves are shown in Figure 4.10. Strain readings for the beam are shown in Tables B.7 and B.8. Strain readings for the longitudinal reinforcement are given in Table B.9 Figures 4.11 to 4.13 show strain profile diagrams. The tested beam is shown in Plates 4.6 to 4.9.

4.2.2.4 BEAM #4

The steel ratio for Beam #4 was approximately 126% of its $\rho_{balance}$ (see Section 2.1.1 and Table 2.1). The first flexural cracks appeared at the mortar joints in both the mid-span and the shear span at 10 Kips. Signifi-

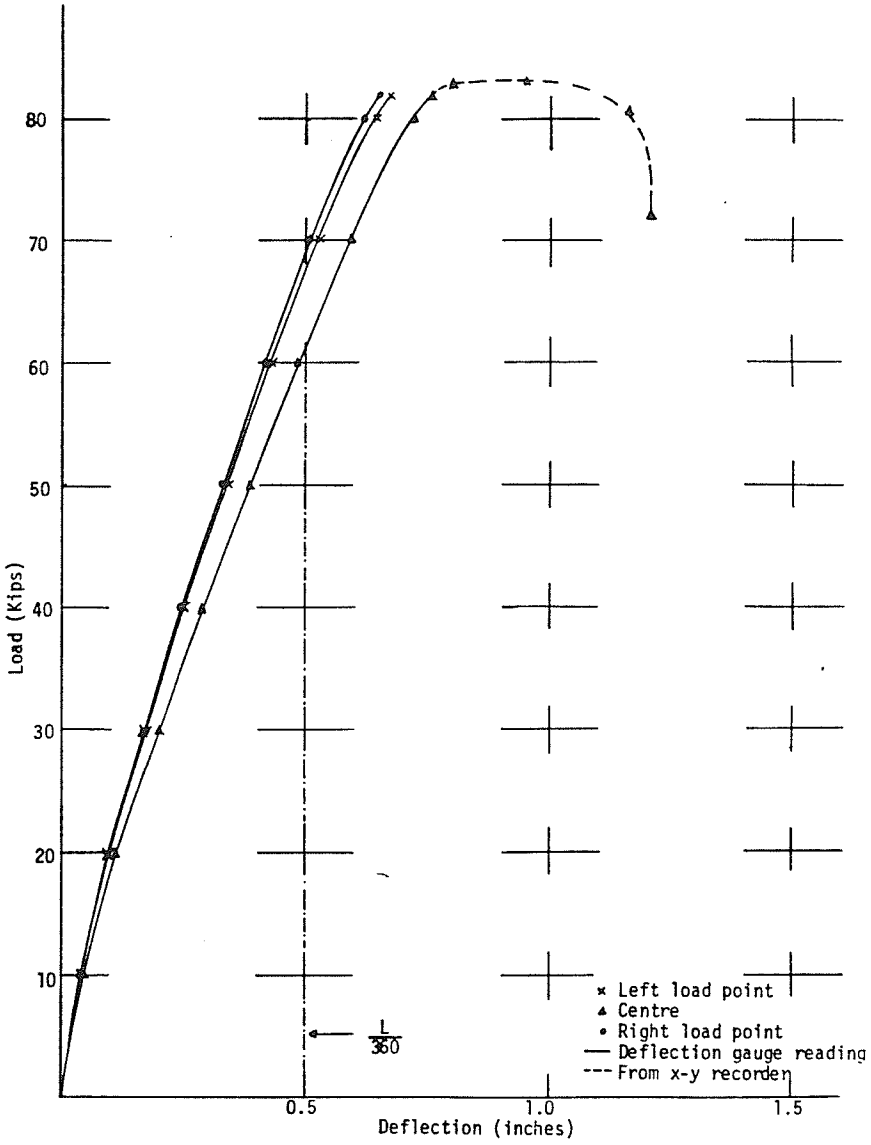

Figure 4.10 Load - deflection curves for Beam #3.

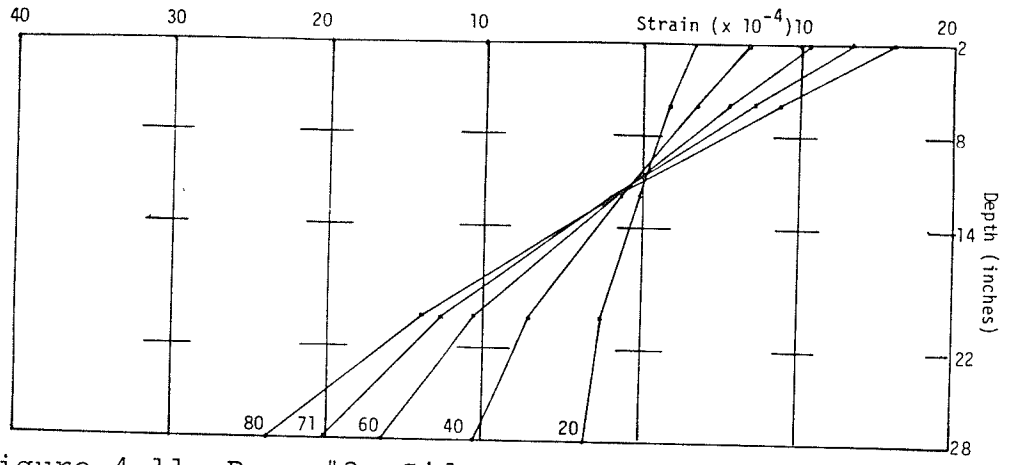

Figure 4.11 Beam #3, Side A, average strain readings.

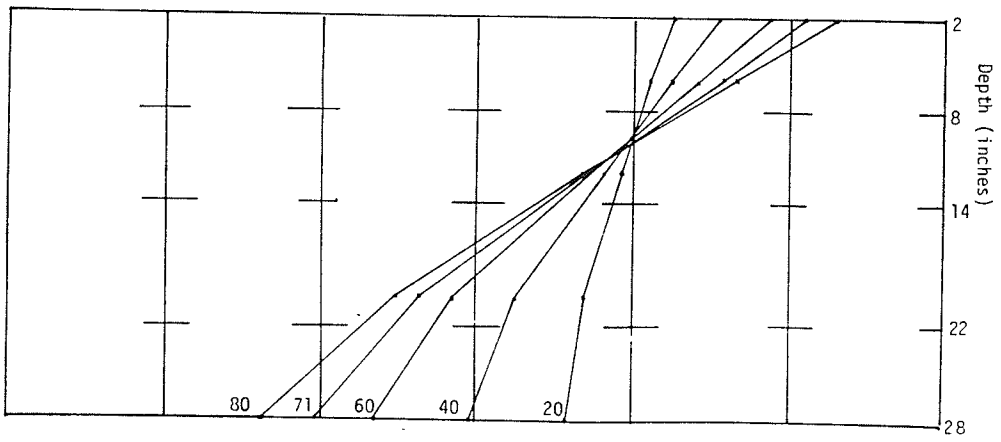

Figure 4.12 Beam #3, Side B, average strain readings.

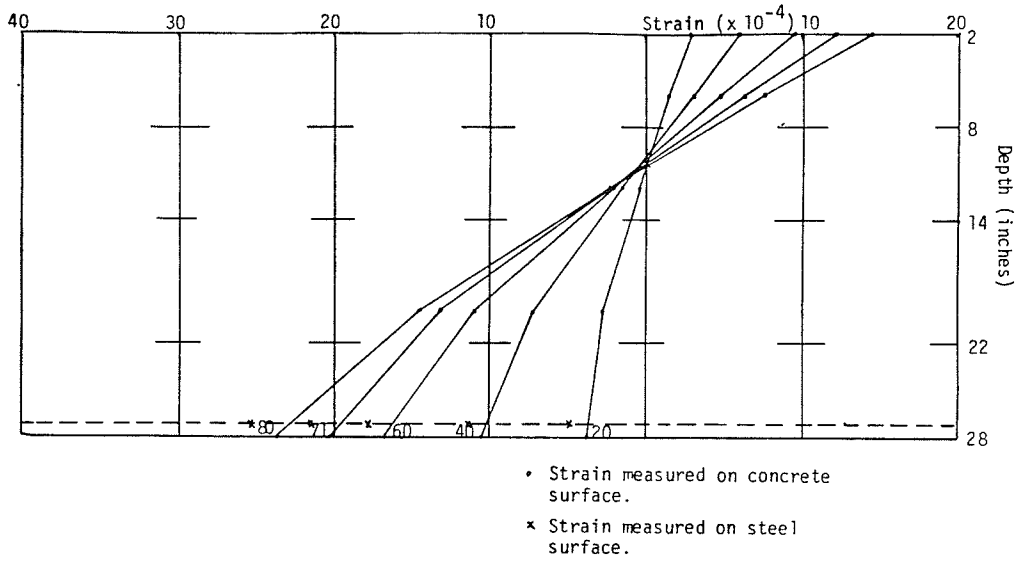

Figure 4.13 Beam #3, average of strain readings for both sides.

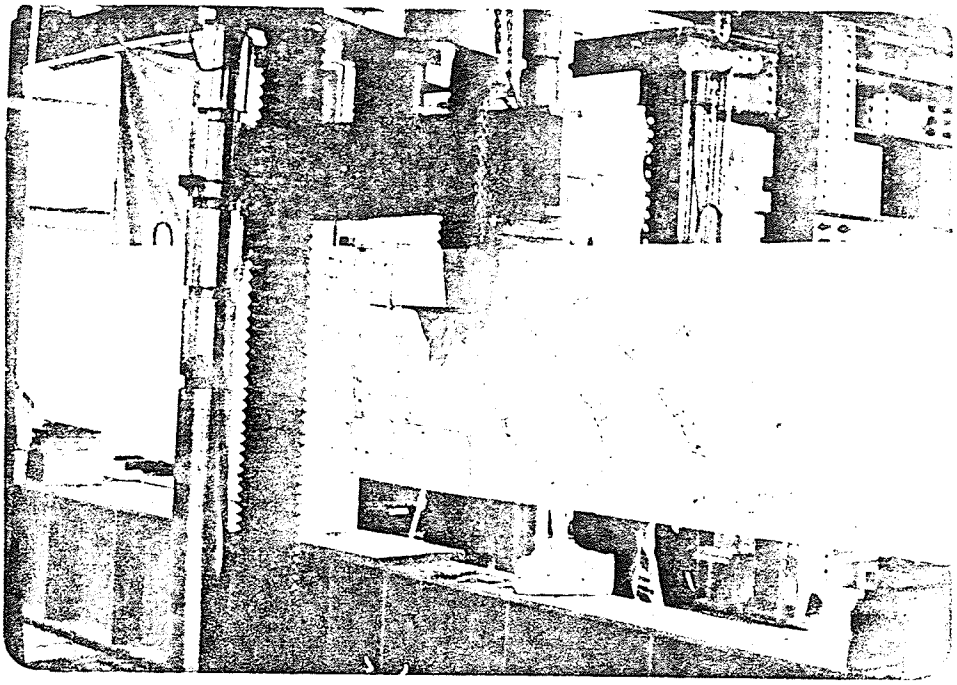

Plate 4.6 Cracking and final flexural failure of Beam #3(Side A).

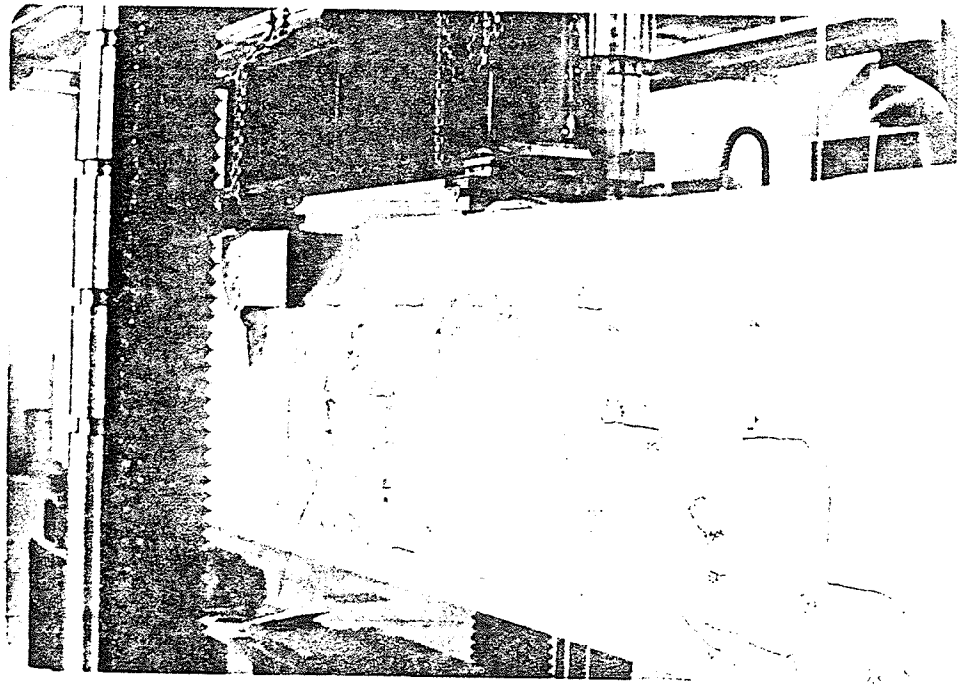

Plate 4.7 Cracking and flexural failure of Beam #3(Side B).

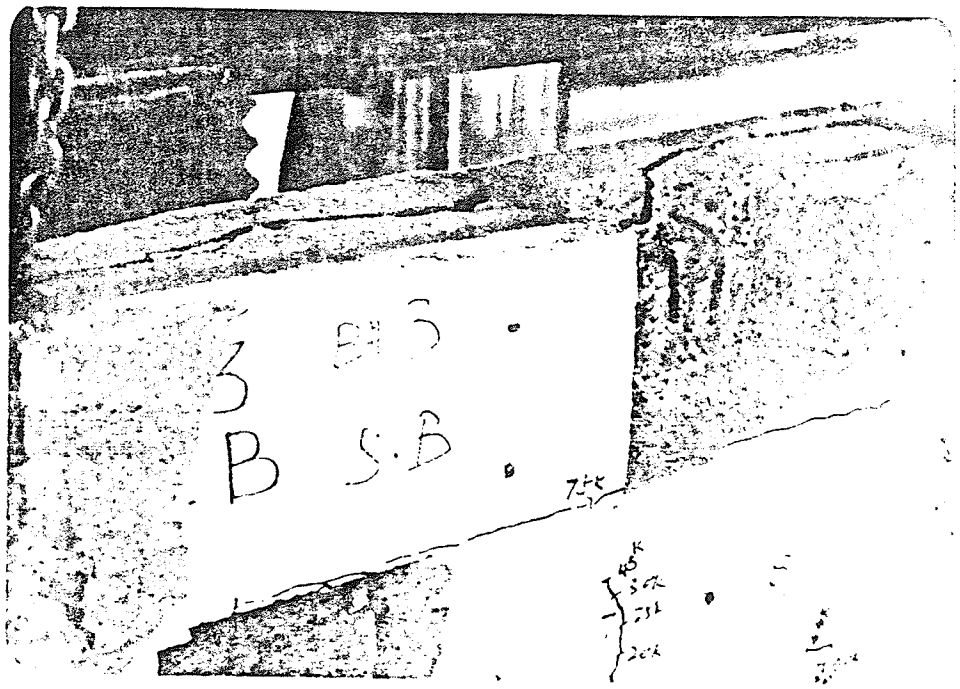

Plates 4.8 & 4.9 Beam #3 failed by longitudinal splitting in the concrete followed by severe crushing of the block legs.

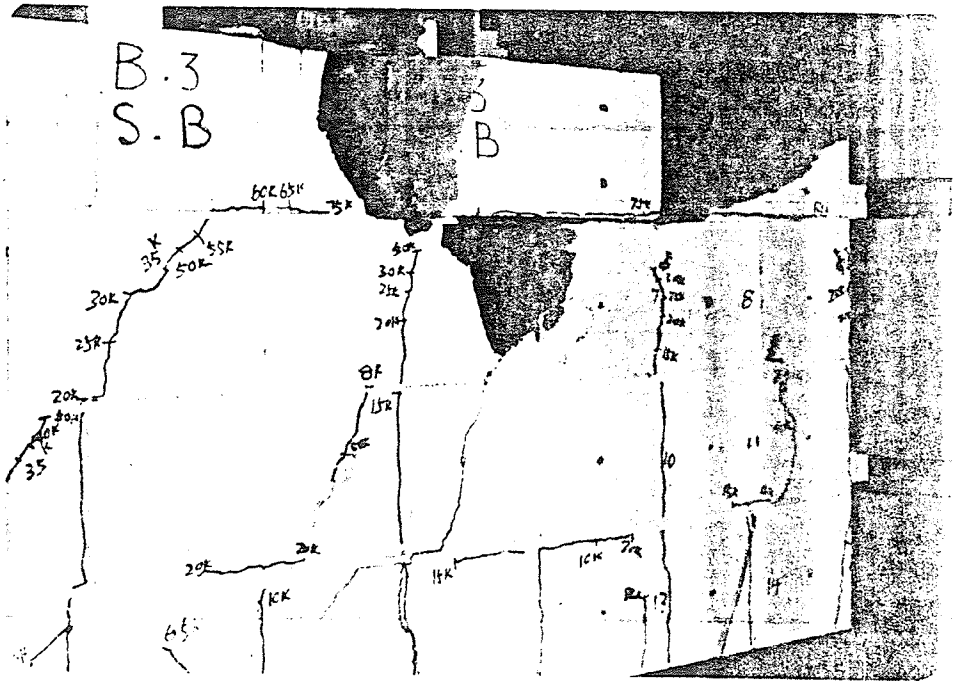

cant diagonal cracks developed in the shear span from 30 Kips onward. Propagation of the flexural cracks in the mid-span became insignificant after reaching a height of about 15 inches from the beam top at 60 Kips while the diagonal cracks reached a height of 8 inches from the top at a load of 90 Kips. A drop of almost 8 Kips in the load-deflection curve was observed while the recordings were being made at the load of 100 Kips. This might have been an indication of imminent failure. When the increased load reached 105.5 Kips, sudden failure was introduced with severe crushing and lateral deflection of the block shell at the mortar joint in the compression zone. A maximum load of 105.5 Kips with a deflection of 0.98 inches was recorded.

Load-deflection curves are shown in Figure 4.14. Strain readings for the beam are given in Tables B.10 and B.11. Strain profile diagrams are shown in Figures 4.15 to 4.17. The tested beam is shown in Plates 4.10 to 4.11.

4.2.2.5 BEAM #5

The steel ratio for Beam #5 was approximately 88% of its $\rho_{balance}$ (see Section 2.1.1 and Table 2.1). The test behaviour of this beam was similar to that of Beam #4 except at failure. The first flexural cracks were found in both the mid-span and shear span at a load of 10 Kips. As the load was increased, the flexural cracks in the mid-span progressed vertically upward and stayed at a height

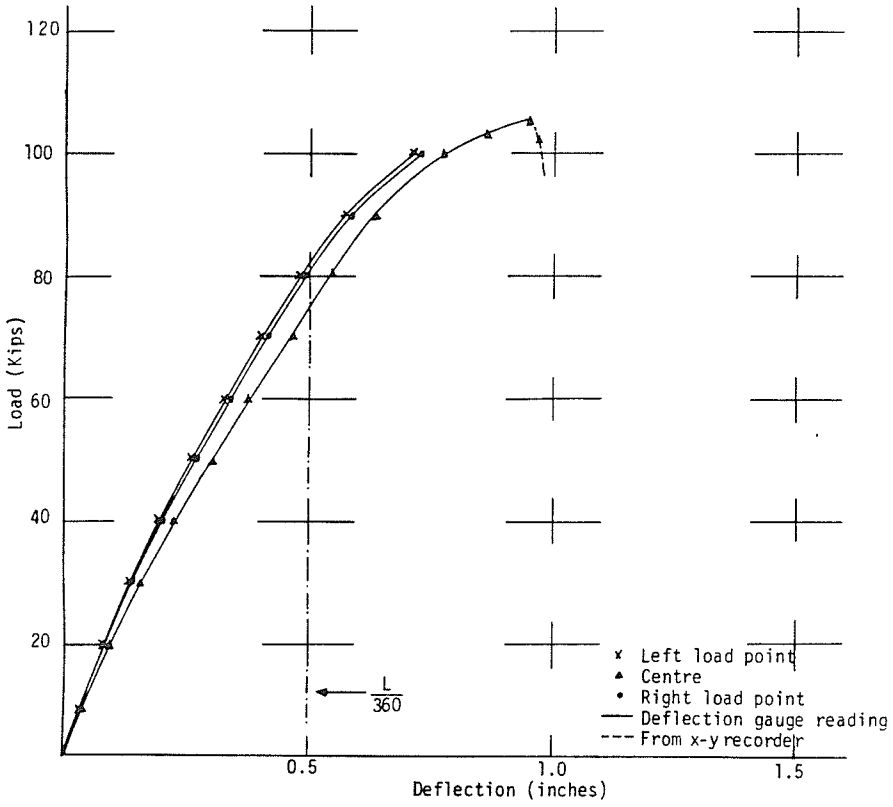

Figure 4.14 Load - deflection curves for Beam #4

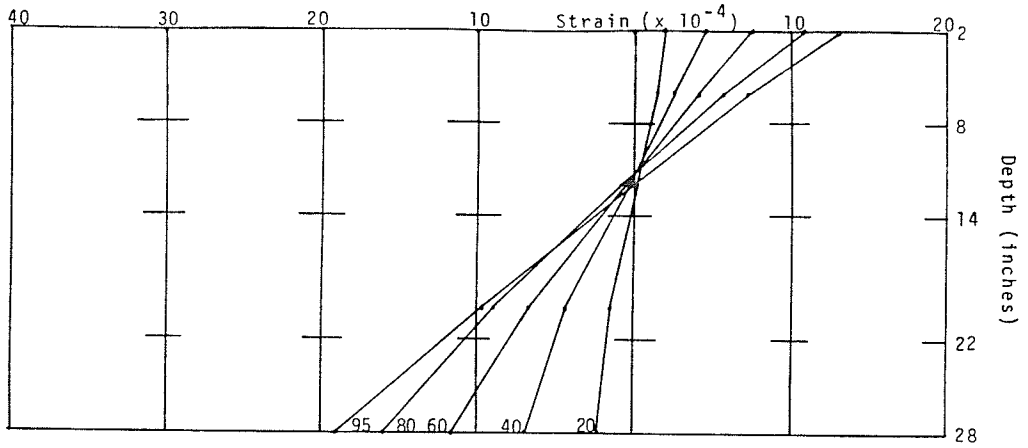

Figure 4.15 Beam #4, Side A, average strain readings.

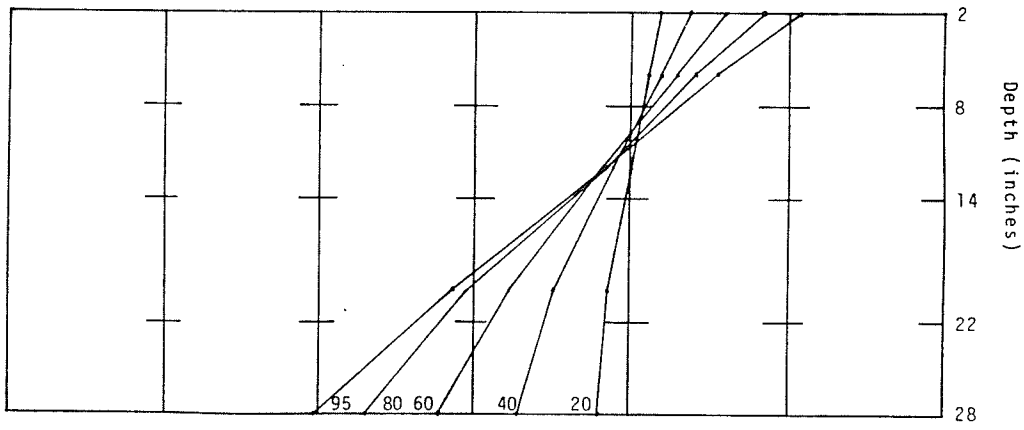

Figure 4.16 Beam #4, Side B, average strain readings.

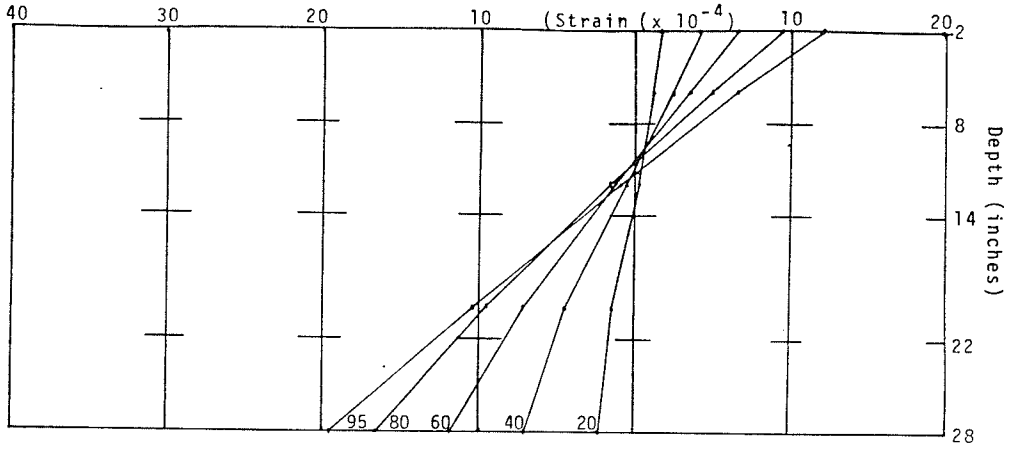

Figure 4.17 Beam #4, average of strain readings for both sides.

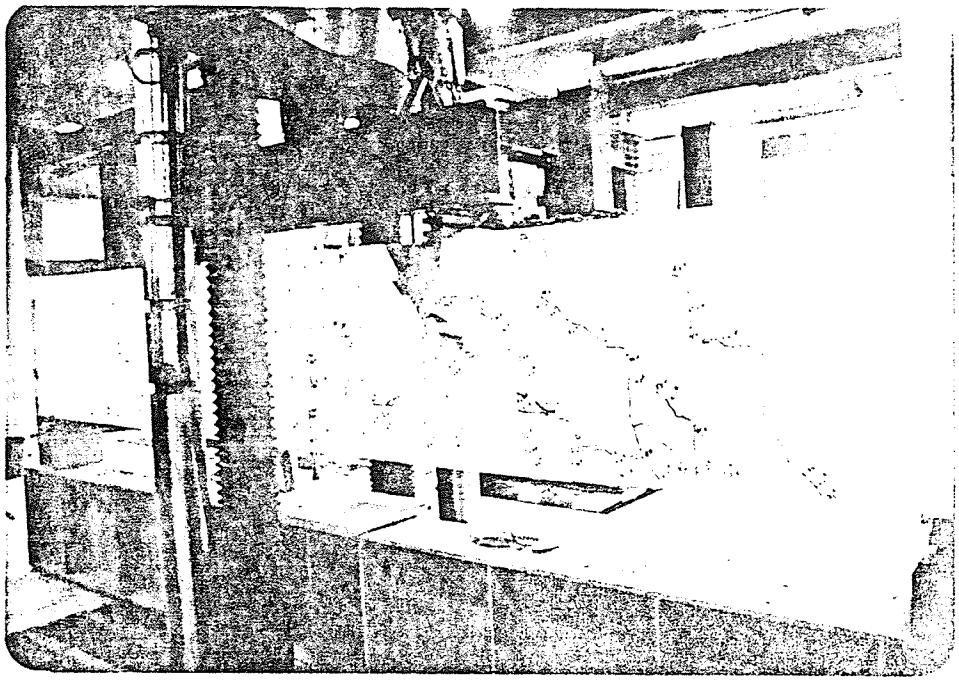

Plate 4.10 Cracking and final flexural failure of Beam #4 (Side A).

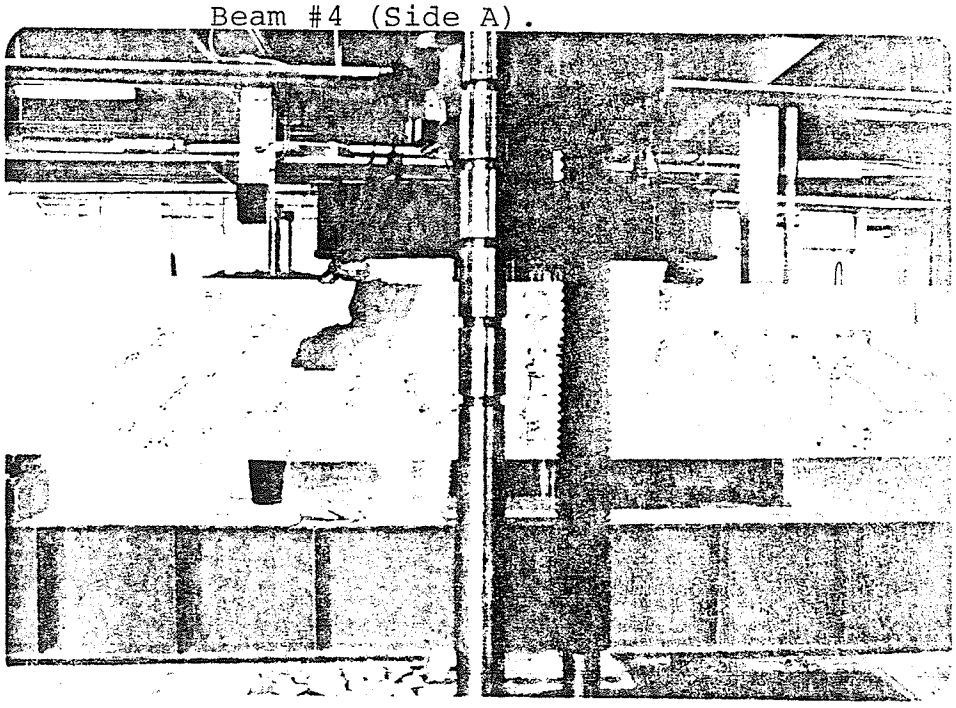

Plate 4.11 Cracking and final flexural failure of Beam #4 (Side B).

of about 5 inches from the top at 55 Kips while the diagonal cracks progressed further as more load was applied. The diagonal cracks reached a maximum height of 8 inches from the beam top at a load of 85 Kips. Further increase in load resulted in only a slight increase in the crack widths. When a load of 102 Kips was reached, crushing and lateral deflection of the block shell at the mortar joint near one of the loads occurred and the beam was expected to fail. Surprisingly, the load only dropped to 96 Kips and then slowly rose to 102 Kips with a considerable amount of deflection. This unusual failure might be due to the high compressive strength of the concrete fill (see Table 2.4). The beam first failed by crushing and lateral deflection of the block shell at the mortar joint. This caused a transfer of the stresses to the second course, and therefore the second course failed by crushing, too. Then the voids in the first course closed forming a new compression area. All of that caused a localized re-distribution of internal forces, permitting in this case a further load-carrying performance from the beam. The first failure load was recorded as the "true" failure. Thus, Beam #5 failed at 102 Kips with a mid-span deflection of 0.73 inches.

Load-deflection curves are shown in Figure 4.18. Strain readings for the beam are given in Tables B.12 and B.13. Strain profile diagrams are shown in Figures 4.19 to 4.21. The tested beam is shown in Plates 4.12 and 4.13.

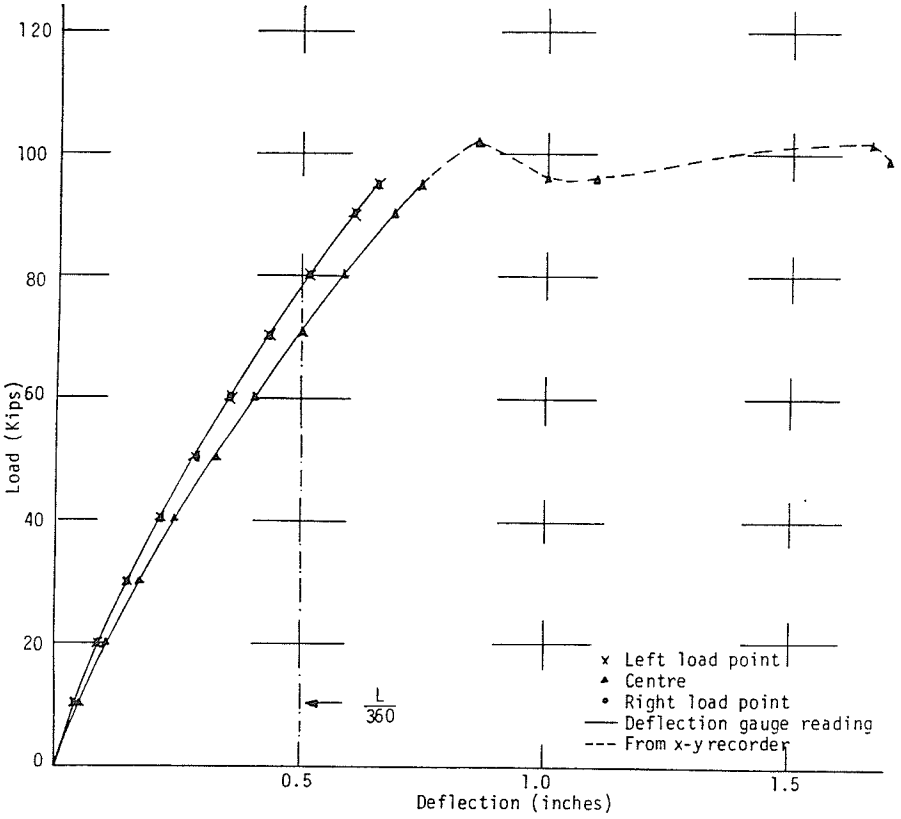

Figure 4.18 Load - deflection curves for Beam #5.

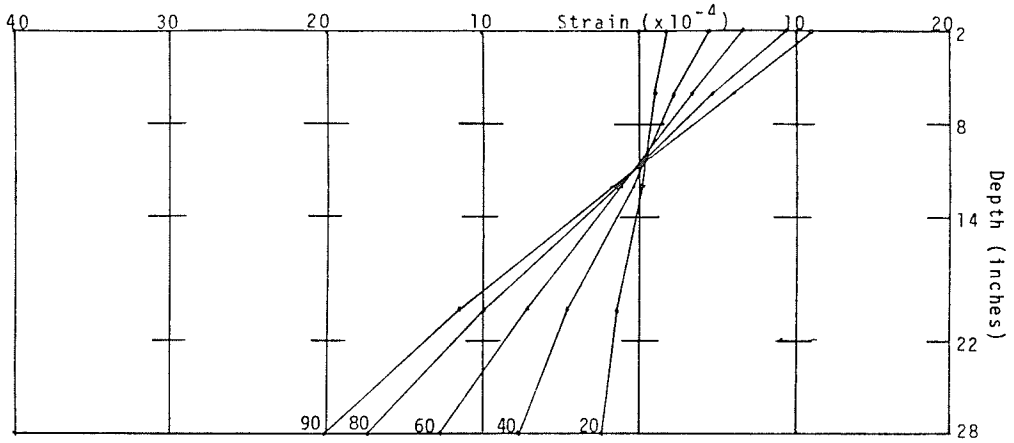

Figure 4.19 Beam #5, Side A, average strain readings.

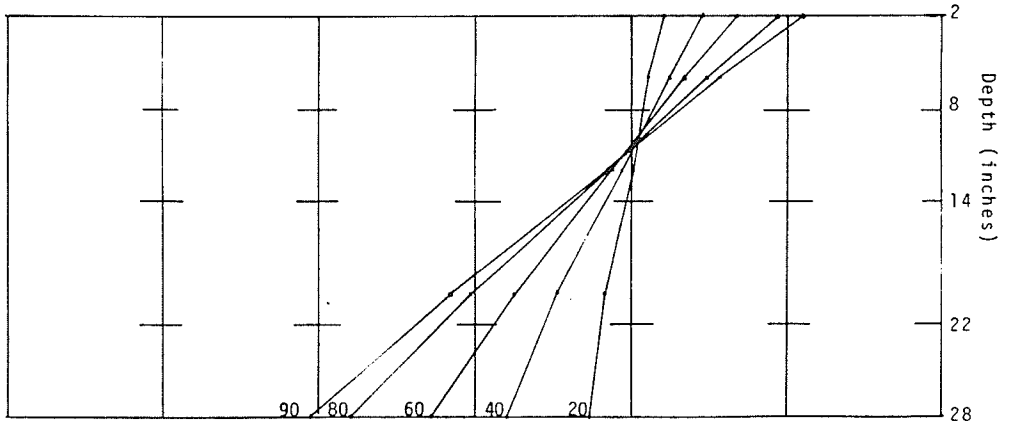

Figure 4.20 Beam #5, Side B, average strain readings.

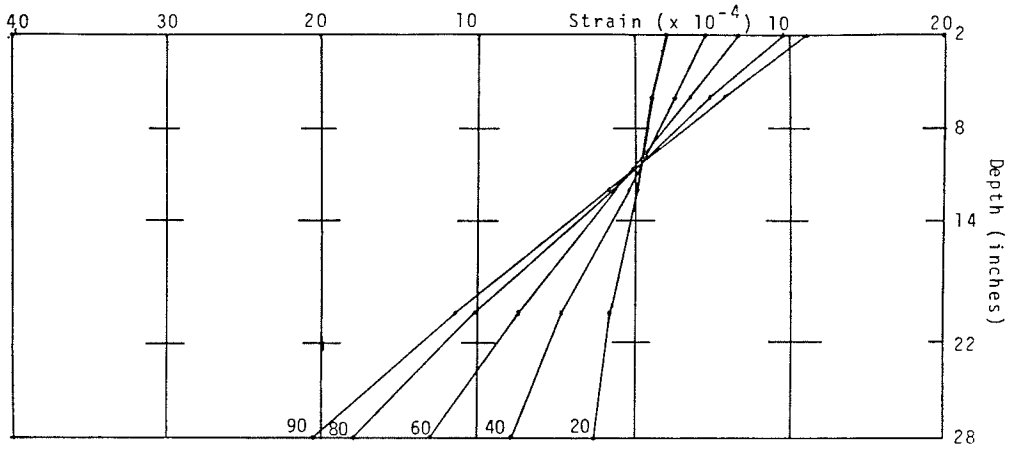

Figure 4.21 Beam #5, average of strain readings for both sides.

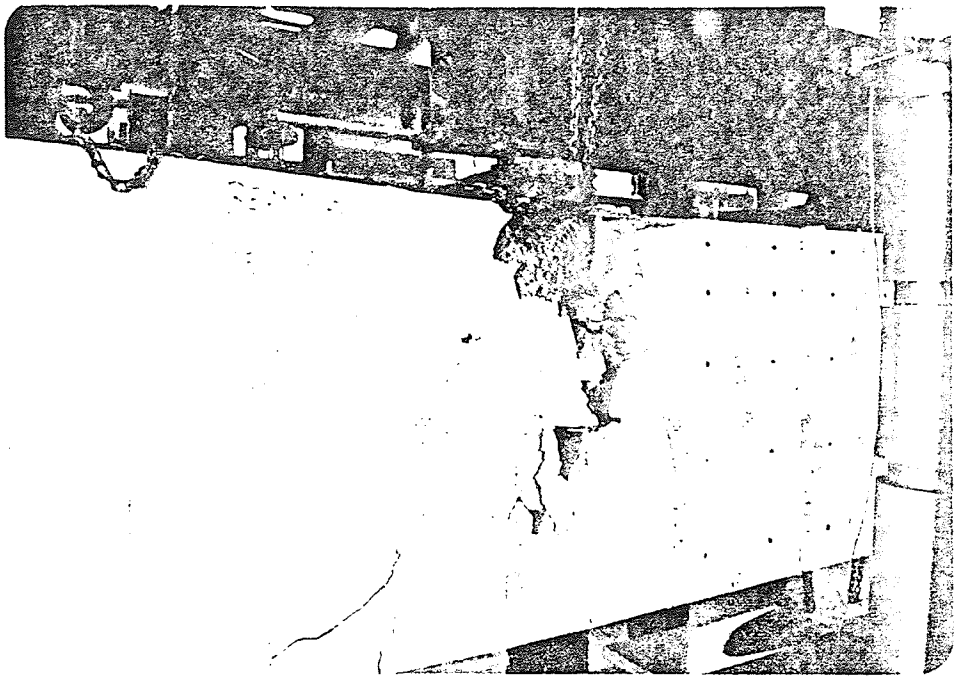

Plate 4.12 Close-up of concrete crushing in the compression zone.

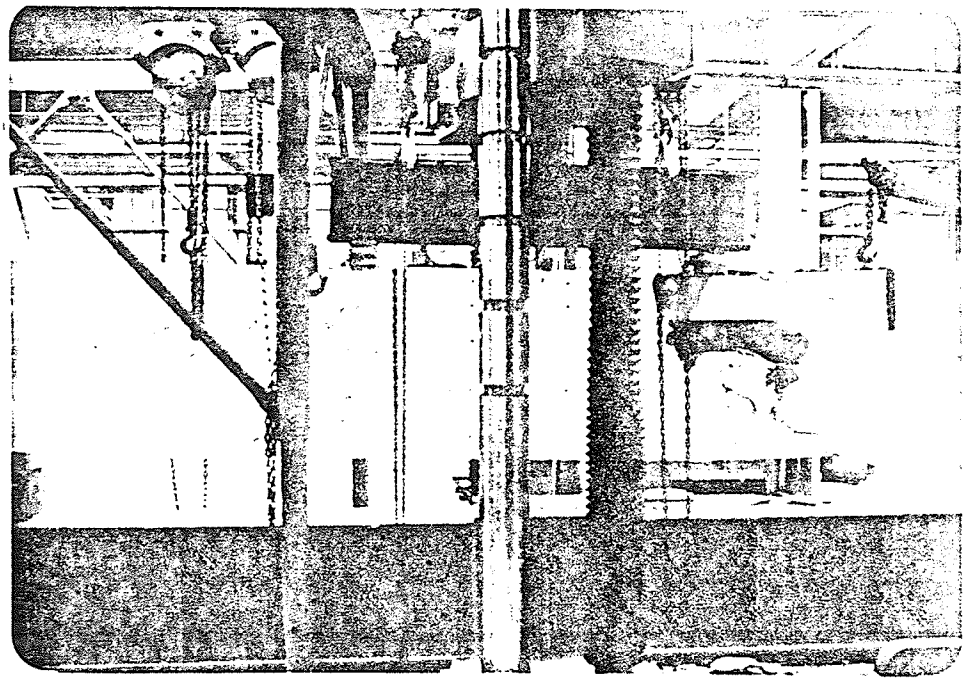

Plate 4.13 Cracking and final flexural failure of Beam #5 (Side B).

4.2.2.6 BEAM #6

The steel ratio for Beam #6 was approximately 54% of its $\rho_{balance}$ (see Section 2.1.1 and Table 2.1). The first flexural cracks appeared in the mortar joints in both the mid-span and the shear span at 6 Kips. The cracks progressed vertically upward in the mid-span while a few cracks in the shear span became inclined at and above a load of 24 Kips. Both flexural and diagonal cracks finally stabilized at a height of about 8" from the beam top at a load of 24 Kips and 26 Kips respectively. As the load was further increased, the cracks became wider and when a load of 33 Kips with a deflection of 0.76 inches was reached, the steel started to yield. The beam finally failed by crushing and lateral deflection of the block shell at a mortar joint and a large increase in deflection was recorded. The beam failed at 34.8 Kips with a mid-span deflection of 1.36 inches.

Load-deflection curves are shown in Figure 4.22. Strain readings for the beam are listed in Tables B.14 and B.15. Strain profile diagrams are shown in Figures 4.23 to 4.25. The tested beam is shown in Plates 4.14 and 4.15.

4.2.2.7 BEAM #7

The steel ratio for Beam #7 was approximately 52% of its $\rho_{balance}$ (see Section 2.1.1 and Table 2.1). The test behaviour for Beam #6 and Beam #7 was almost identical

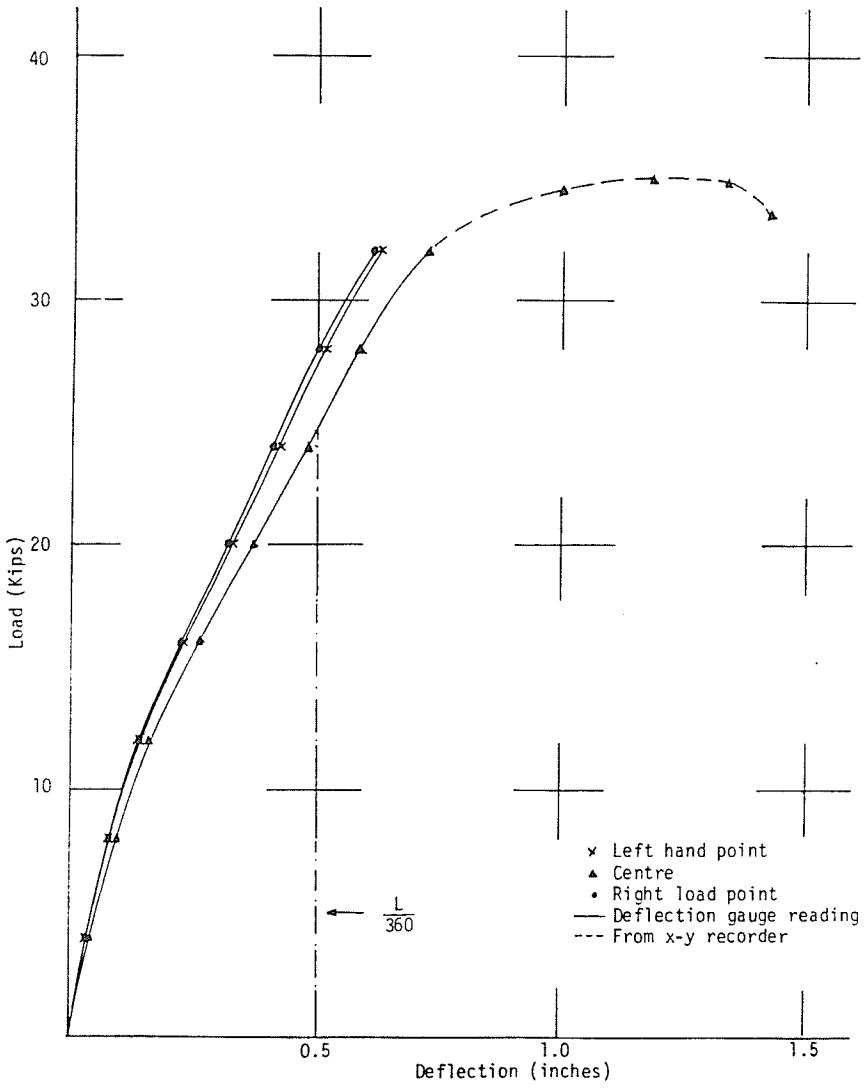

Figure 4.22 Load - deflection curves for Beam #6.

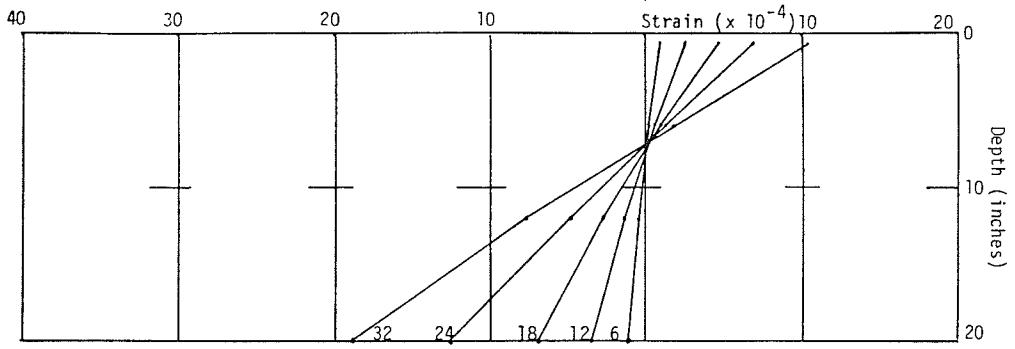

Figure 4.23 Beam #6, Side A, average strain readings.

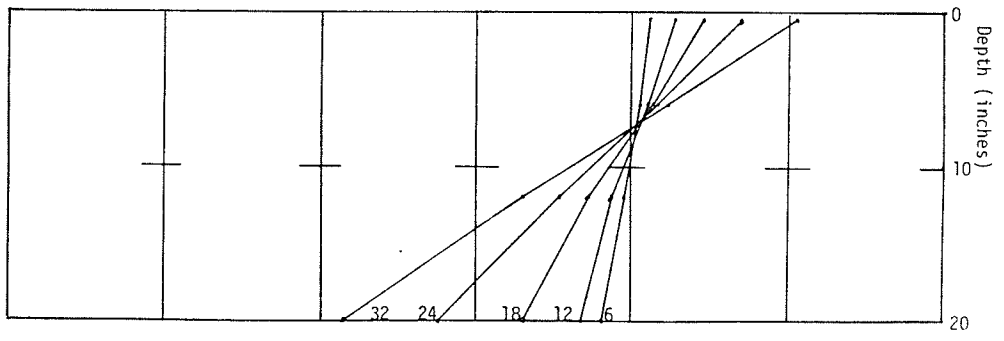

Figure 4.24 Beam #6, Side B, average strain readings.

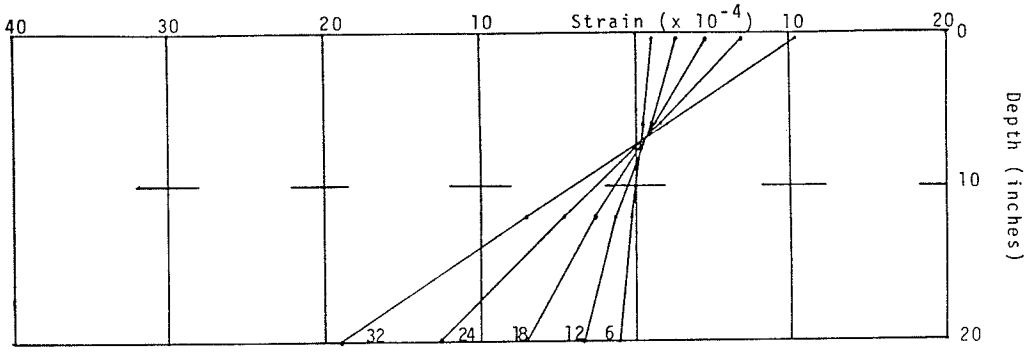

Figure 4.25 Beam #6, average of strain readings for both sides.

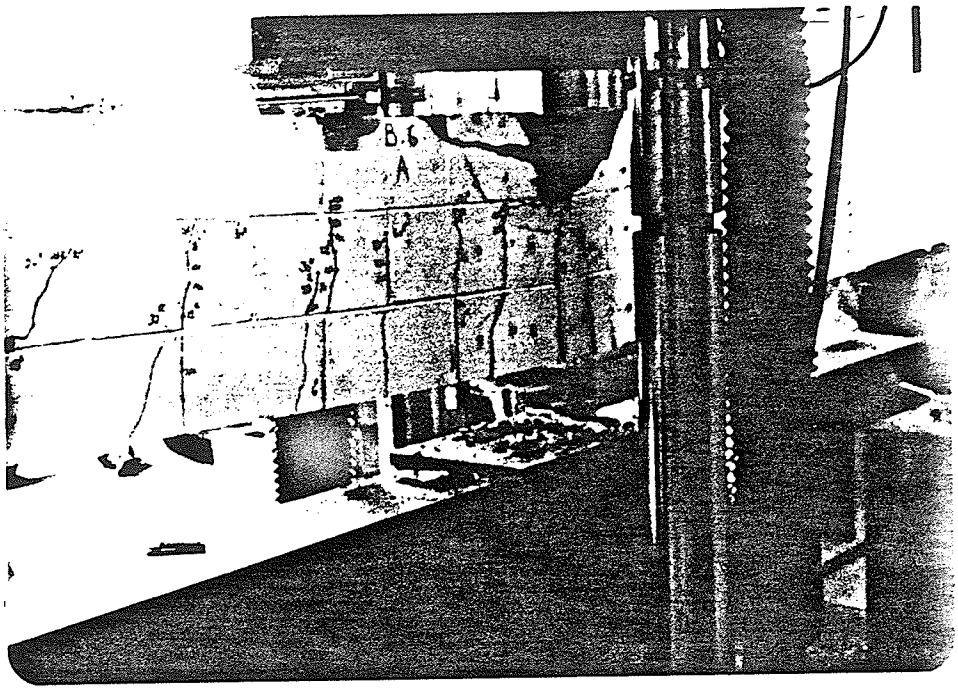

Plate 4.14 Cracking and final flexural failure of Beam #6 (Side A).

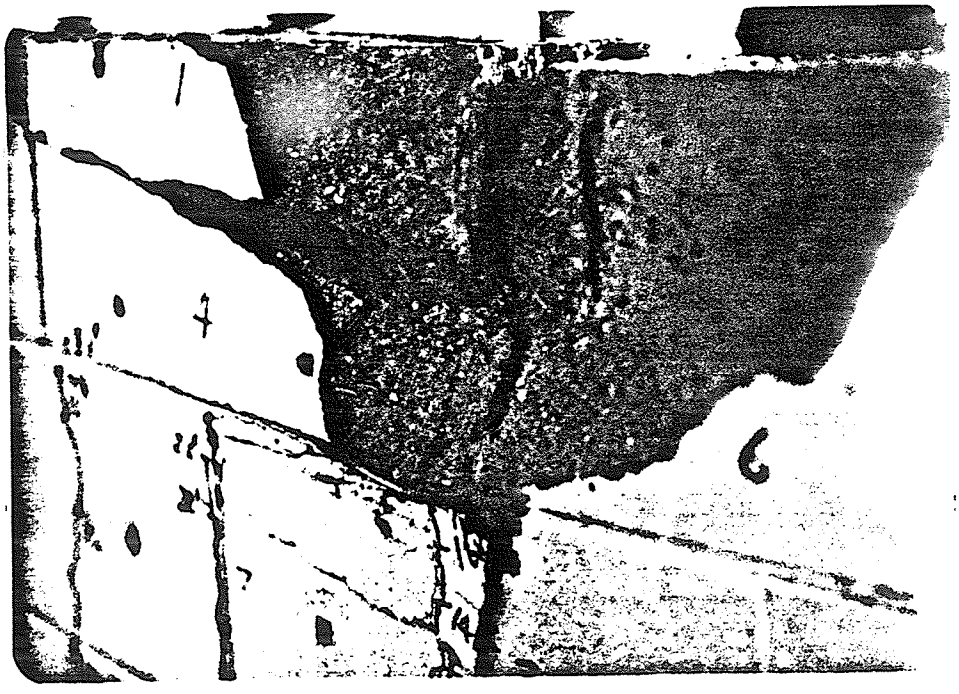

Plate 4.15 Close-up of the compression zone.

since the load-carrying capacity of these two beams was calculated to be almost the same. The original idea behind the design of these two beams was that Beam #6 and Beam #7 would have a percentage of steel equal to 50% and 75% of the balance steel area respectively. However, the test results have shown that the yield strength of the steel used in Beam #7 was unexpectedly low (see Table 2.7) and the total strength of the two 20 M bars used for Beam #7 could only give the same strength as the single 25 M bar used for Beam #6. Nevertheless, it afforded the opportunity to check if there would be any difference in the test behaviour of the two almost identical beams.

The test behaviour for Beam #7 was almost identical to Beam #6 except that the diagonal cracks in Beam #7 were relatively more pronounced than in Beam #6. Both flexural and diagonal cracks went up to almost the same height (8 inches from the beam top) at almost the same loads. As the load increased to 32.5 Kips with a corresponding deflection of 0.72 inches, the steel started to yield and the beam finally failed at 34.9 Kips by crushing and lateral deflection of the block shell at a mortar joint with a deflection of 1.38 inches.

Load-deflection curves are shown in Figure 4.26. Strain readings for the beam are given in Tables B.16 and B.17. Strain profile diagrams are shown in Figures 4.27 to 4.29. The test beam is shown in Plates 4.16 and 4.17.

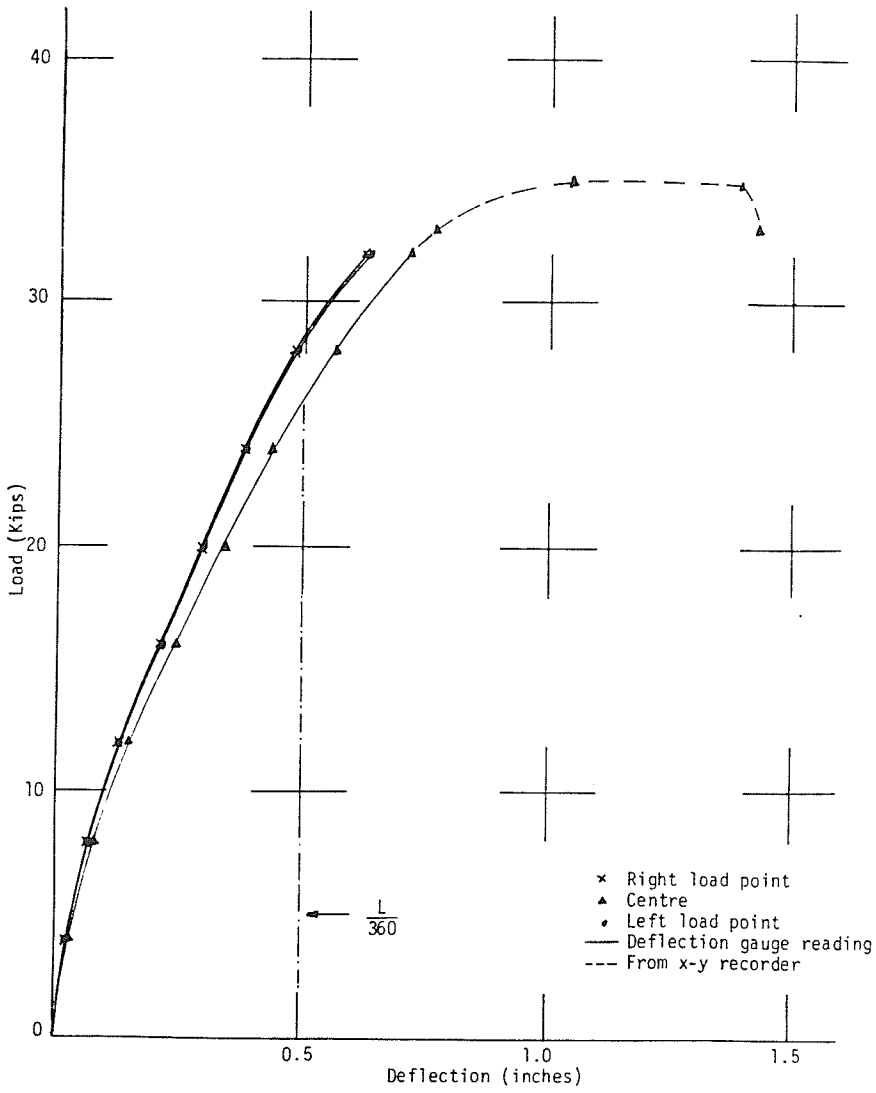

Figure 4.26 Load - deflection curves for Beam #7.

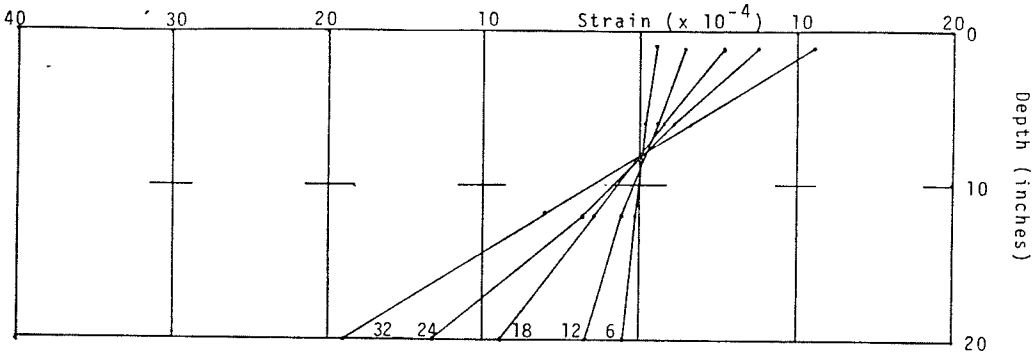

Figure 4.27 Beam #7, Side A, average strain readings.

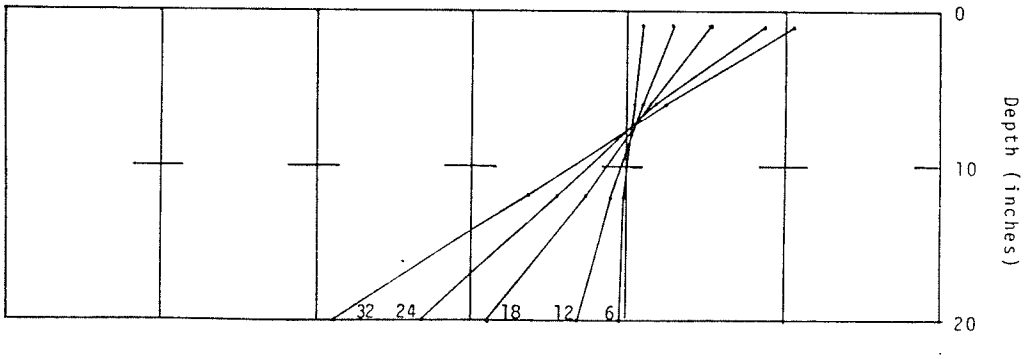

Figure 4.28 Beam #7, Side B, average strain readings.

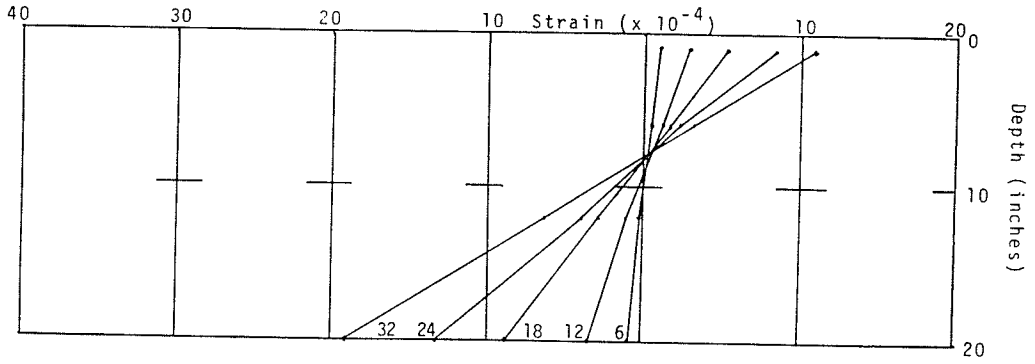

Figure 4.29 Beam #7, average of strain readings for both sides.

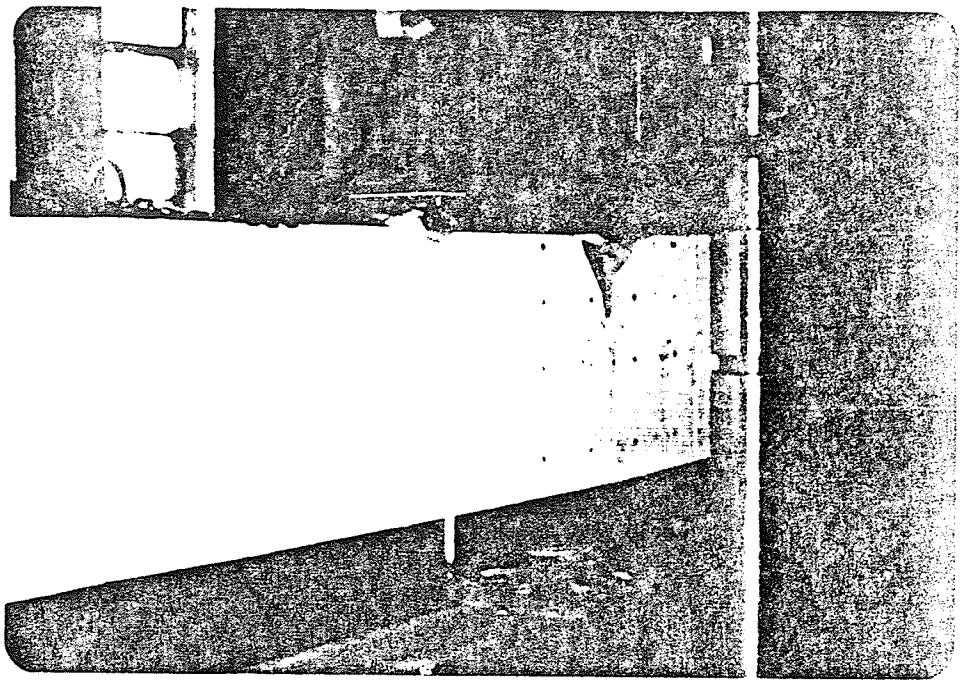

Plate 4.16 Cracking and final flexural failure of Beam #7 (Side A).

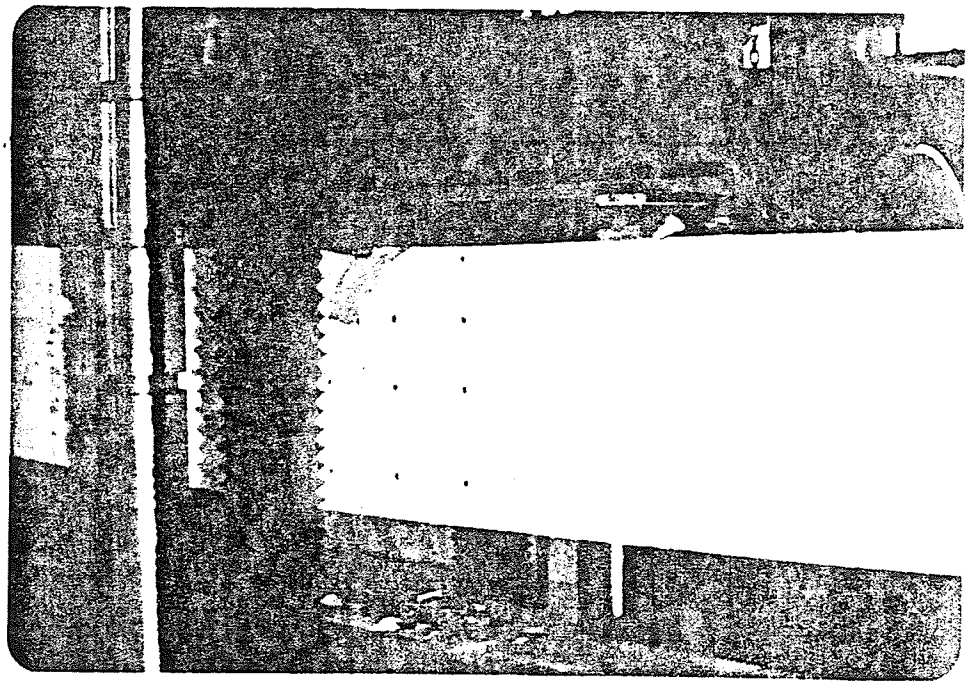

Plate 4.17 Beam #7 showing a flexural failure (Side B).

4.2.2.8 BEAM #8

The steel ratio for Beam #8 was approximately 113% of its $\rho_{balance}$ (see Section 2.1.1 and Table 2.1). The first flexural cracks were observed at the mortar joints in both the mid-span and shear span at a load of 10 Kips. Flexural cracks in the mid-span widened and progressed upward as the load increased, with little extension after reaching a height of 9 inches from the beam top at a load of 35 Kips. Diagonal cracks were first observed in the shear span at a load of 25 Kips and more developed as the load was increased. The diagonal cracks finally reached a maximum height of 7 inches from the top at 50 Kips. As more load was applied, the beam failed suddenly by crushing and lateral deflection of the block shell at a mortar joint with an immediate drop of load. However, the strength did not drop away completely as usually expected for an over-reinforced beam. The load dropped to about 48 Kips and remained steady for almost ten seconds before failure occurred. This unusual failure was again suspected to be due to the relatively high compressive strength of the concrete fill (see Table 2.4) as in Beam #5. Only this time, the concrete crushed before the steel yielded and hence not much ductility was regained when the load was sustained at 48 Kips.

Beam #8 actually failed at 57.6 Kips with a mid-span deflection of 1.08 inches. Load-deflection curves are

shown in Figure 4.30. Strain readings for the beam are listed in Tables B.18 and B.19. Strain profile diagrams are shown in Figures 4.31 to 4.33. The tested beam is shown in Plates 4.18 and 4.19.

4.3 TWO-BLOCK PRISMS

Two-block prisms, simulating the compression zone in a beam, were tested in three types (unfilled, partially-filled, and completely filled) and under two kinds of applied loads (axial and eccentric). The behaviour, modes of failure, and the test results for all the prisms are presented and discussed in the following sub-sections.

4.3.1 BEHAVIOUR AND MODE OF FAILURE OF THE TWO-BLOCK PRISMS

Three different types of specimen were tested under axial and eccentric loads. The behaviour, mode of failure, and test results for each type of specimen (unfilled, partially filled and completely filled) are outlined below.

4.3.1.1 UNFILLED TWO-BLOCK PRISMS AXIALLY LOADED WITH PIN/FIX END CONDITIONS

Two specimens were tested under axial load. The mode of failure of the two specimens was essentially by a local crushing to the outer face of the mortar joint followed by complete disintegration of the top standard hollow block. The failure was very brittle since there were no signs of

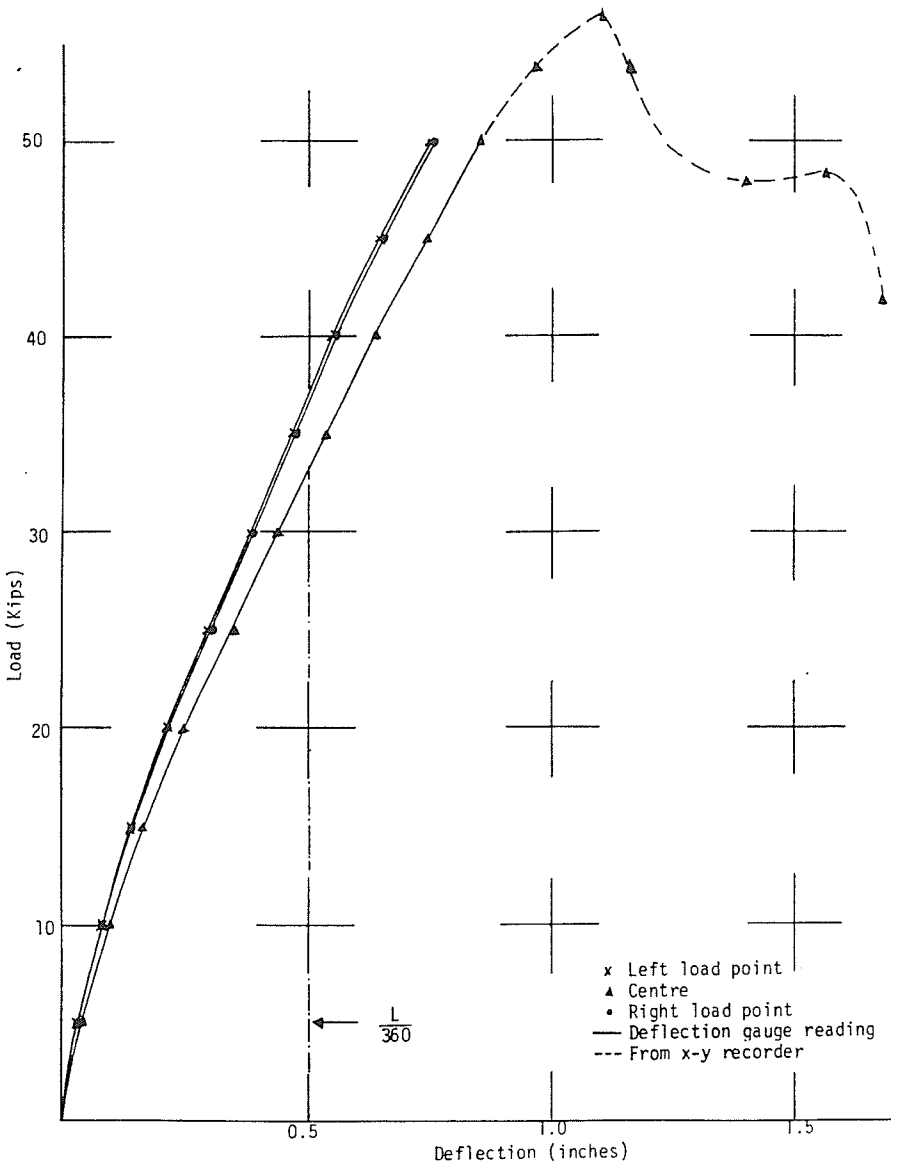

Figure 4.30 Load - deflection curves for Beam #8.

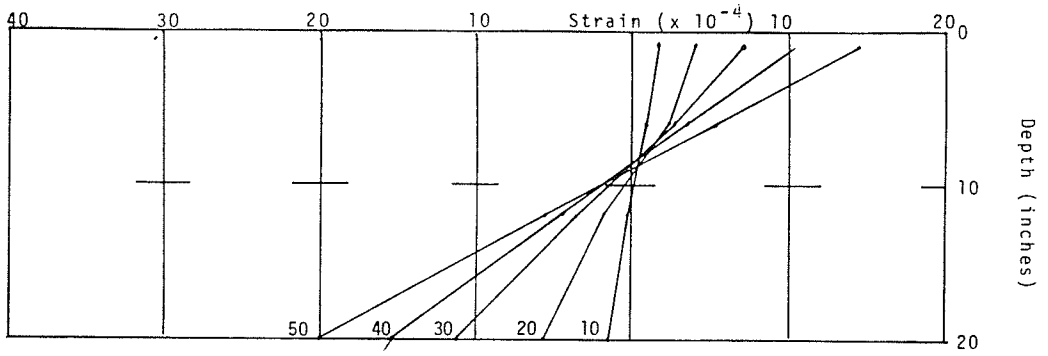

Figure 4.31 Beam #8, Side A, average strain readings.

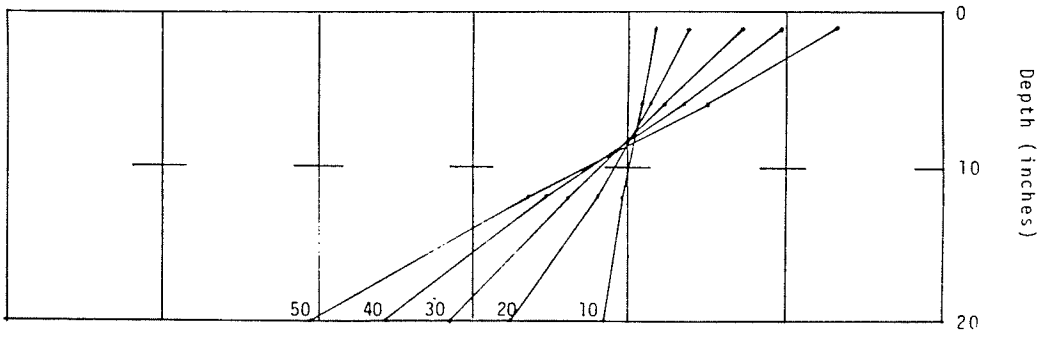

Figure 4.32 Beam #8, Side B, average strain readings.

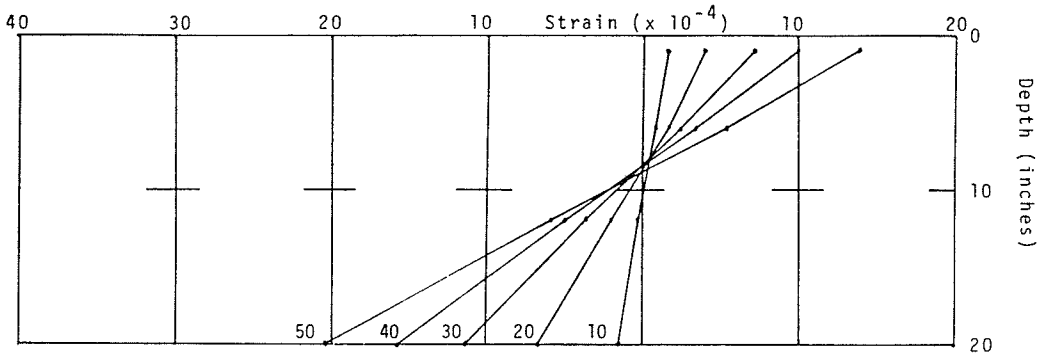

Figure 4.33 Beam #8, average of strain readings for both sides.

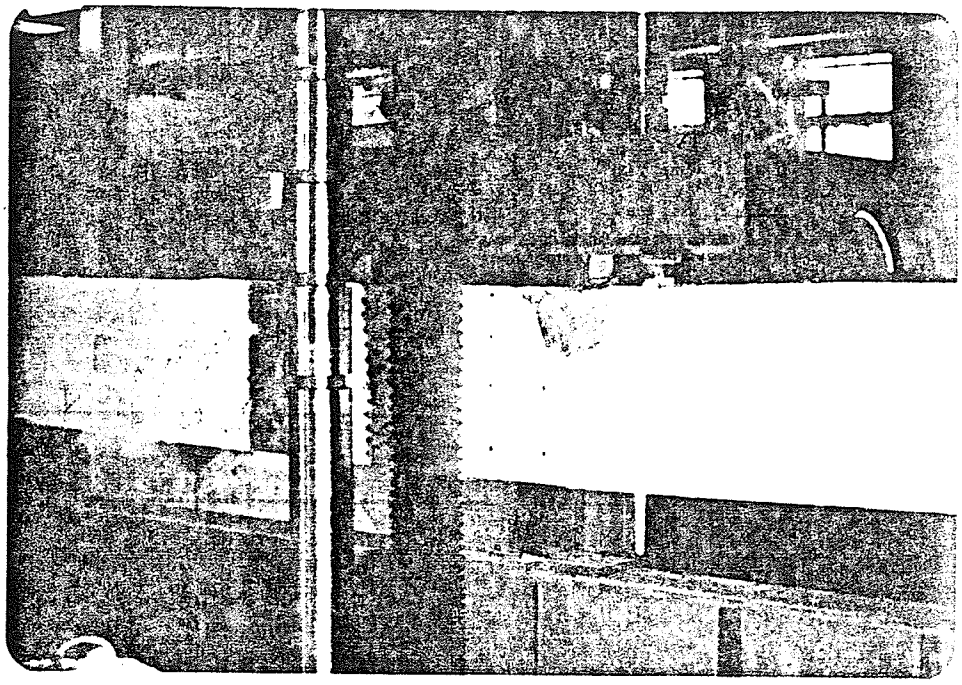

Plate 4.18 Cracking and final flexural failure of Beam #8 (Side B).

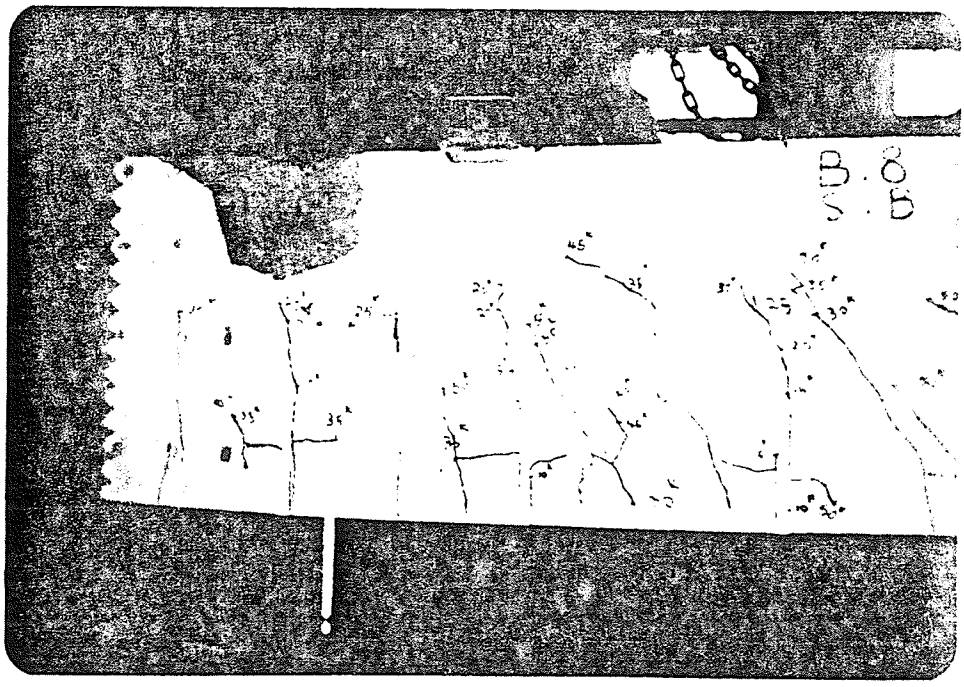

Plate 4.19 Cracking and final flexural failure of Beam #8 (Side B).

any major cracks during the loading process until failure. A summary of the prisms' properties, failure loads, and stresses are shown in Table 4.1.

The load-strain curves for prism #14 are shown in Figures 4.34 to 4.37. (See Figure 2.17 for positions of "Demec" points.) Plate 4.20 shows the typical mode of failure for unfilled two-block prisms.

4.3.1.2 PARTIALLY FILLED TWO-BLOCK PRISMS AXIALLY LOADED WITH PIN/FIX END CONDITIONS

Twelve specimens were tested under axial load. Two modes of failure were observed. The first mode was essentially by crushing of the mortar joint followed by crushing and lateral deflection of the block shell at the mortar joint. There was no evidence of any tensile cracks at the center of the webs near the mortar joints (see Plate 4.21).

The second mode was simply by crushing and lateral deflection of the block shell at the mortar joint (see Plate 4.22). There were serious tensile cracks at the center of the webs near the mortar joints.

The particular mode of failure depends on the relative compressive strength of the mortar and the partially filled single-block specimen. The first mode will occur if the mortar compressive strength is lower than the new compressive strength of the partially filled single-block specimen. The second mode will occur if the mortar compressive

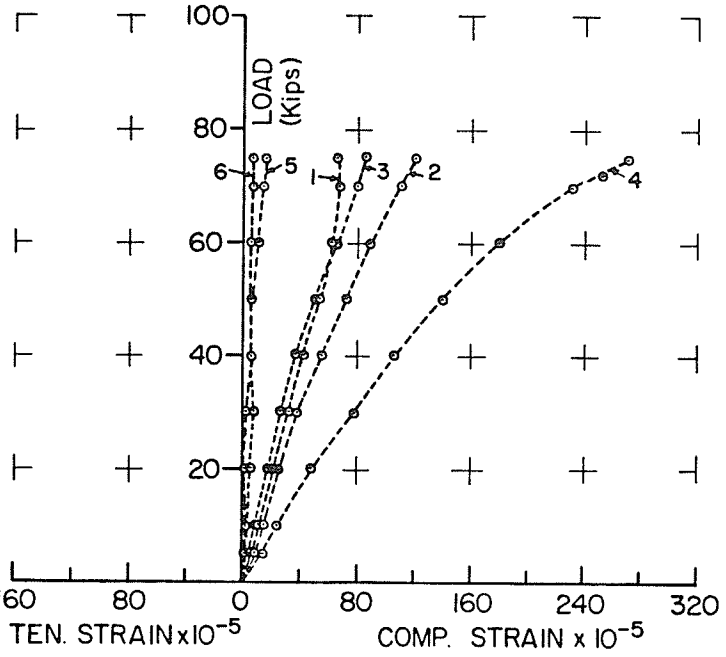

Figure 4.34 Load-strain curve for Sample #14, Side A.

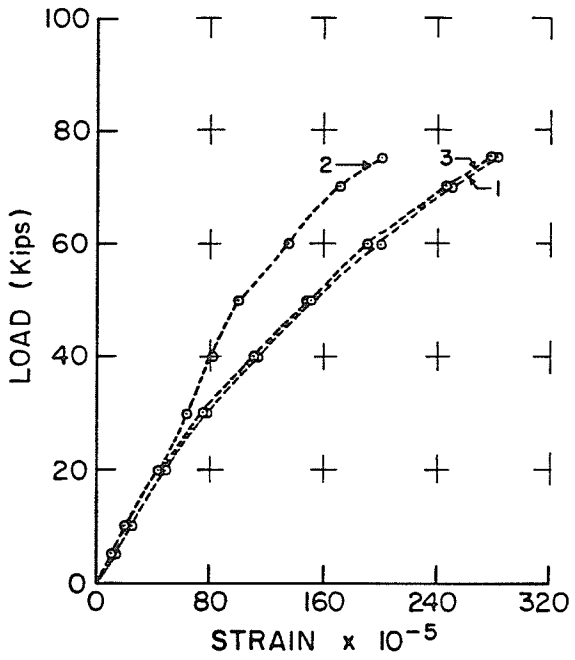

Figure 4.35 Load-strain curve for Sample #14, Side B.

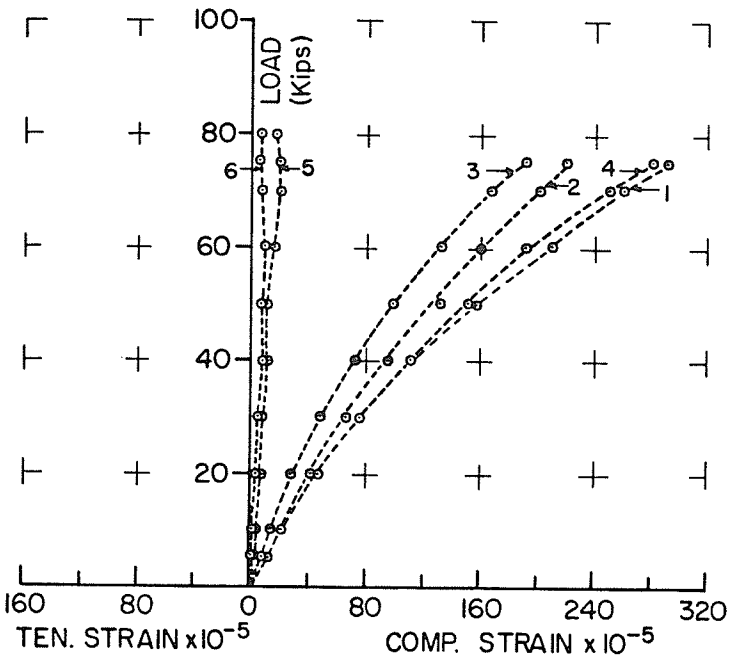

Figure 4.36 Load-strain curve for Sample #14, Side C.

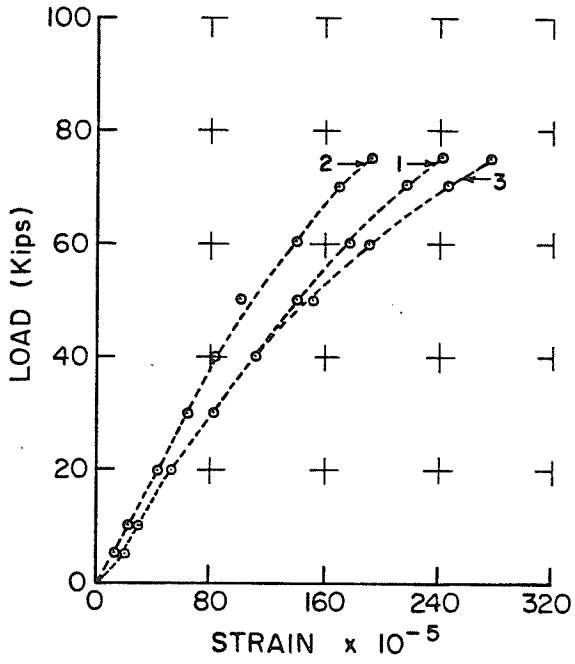

Figure 4.37 Load-strain curve for Sample #14, Side D.

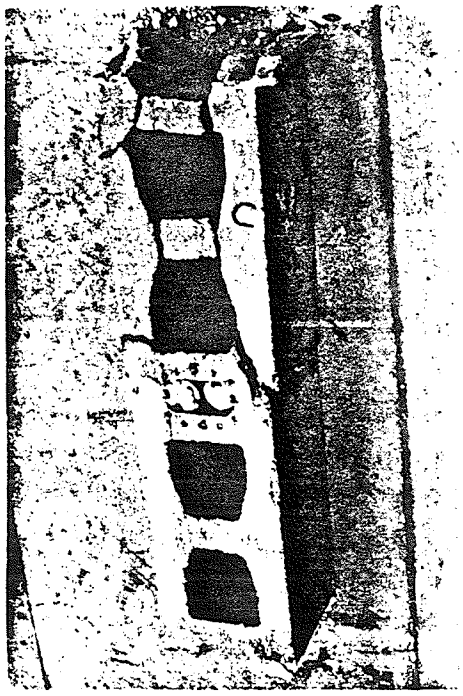

Plate 4.20 Typical mode of failure for the unfilled two-block prism axially loaded with PIN/FIX end conditions.

strength is higher (see Table 4.1). However, in both modes, the crushing occurred first, followed by outward lateral deflection of the block shell, with vertical cracks between the masonry and the concrete fill. The summary of the prisms' properties, failure load, and stresses is shown in Table 4.1.

Load-strain curves for prisms #3 and 4 are shown in Figure 4.38. (Note that the strains are the average readings of two 3-inch strain gauges placed at the center of sides B and D.) Load-strain curves for prisms #18, 11, and 12 are shown in Figures 4.39 to 4.48. (See Figure 2.17 for positions of electrical strain gauges and "Demec" points.) Plates 4.21 and 4.22 show typical failures for mode one and two respectively.

4.3.1.3 PARTIALLY FILLED TWO-BLOCK PRISMS ECCENTRICALLY LOADED WITH PIN/FIX END CONDITIONS

One specimen was tested under eccentric load with PIN/FIX end conditions. The mode of failure was by crushing and lateral deflection to the outside of the block shell at the mortar joint (see Plate 4.23). The specimen was originally tested to simulate the compression zone in the masonry beams, but the test results showed that there was a moment at the FIX end which resisted the applied moment; thus the prism acted as a PIN/FIX eccentrically loaded short column. A summary of the prism's properties and failure load is shown in Table 4.1.

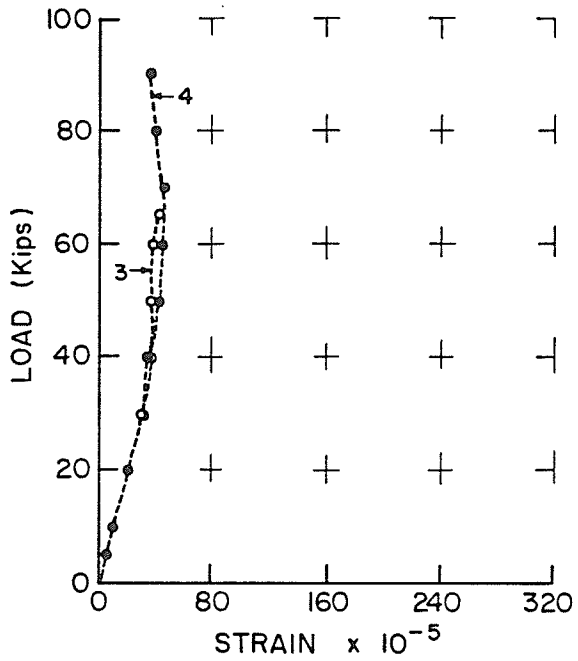

Figure 4.38 Load-strain curve for Samples #3 and #4.

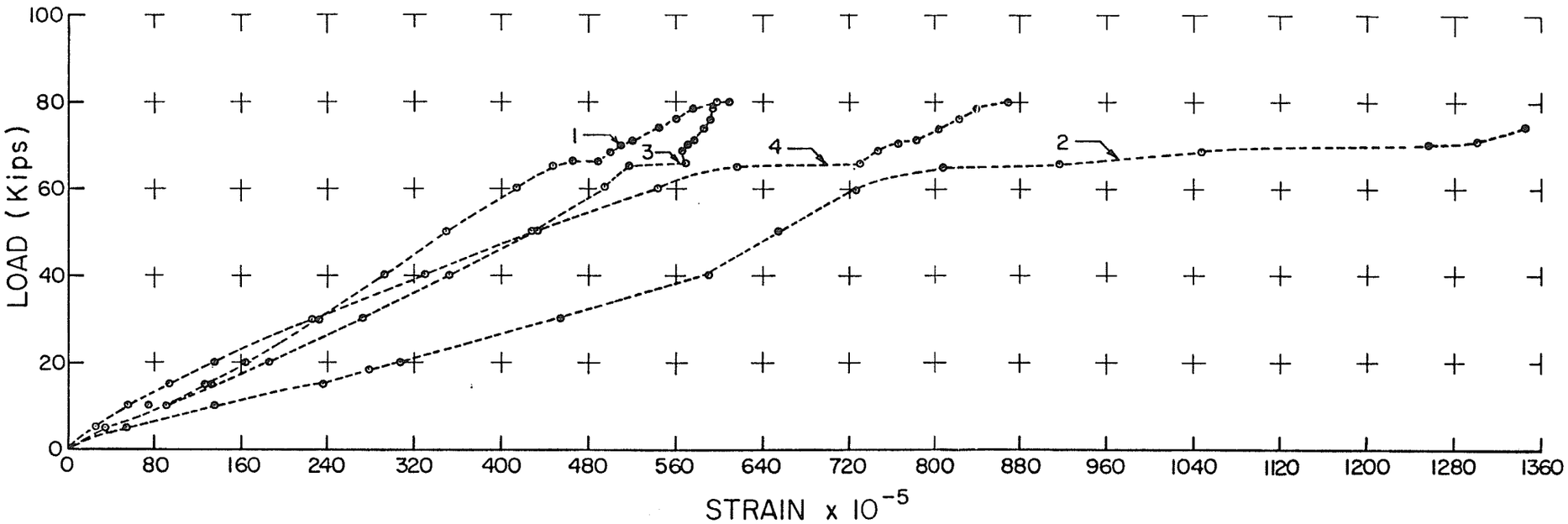

Figure 4.39 Load-strain curve for Sample #18, Side A.

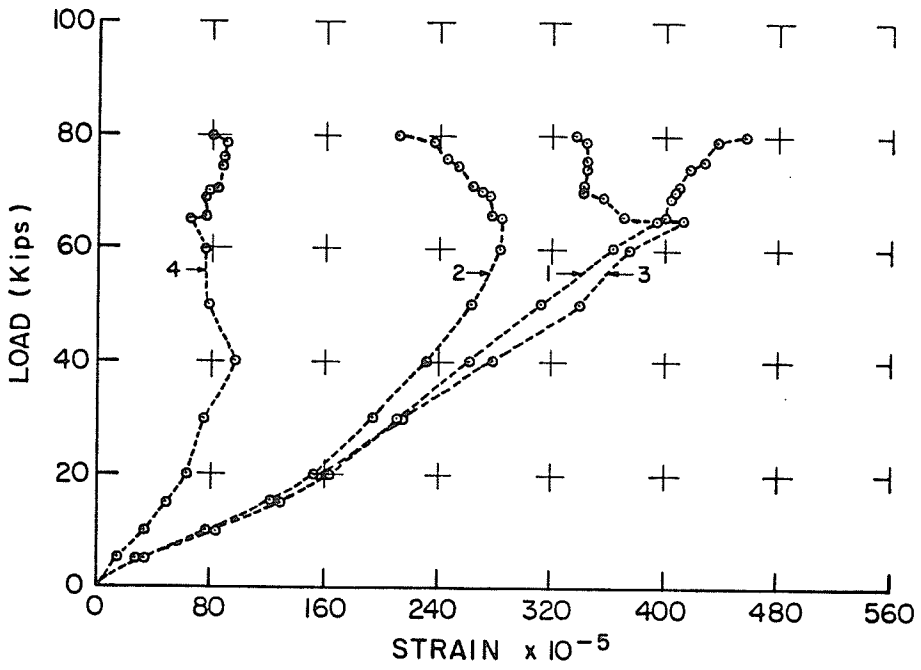

Figure 4.40 Load-strain curve for Sample #18, Side C.

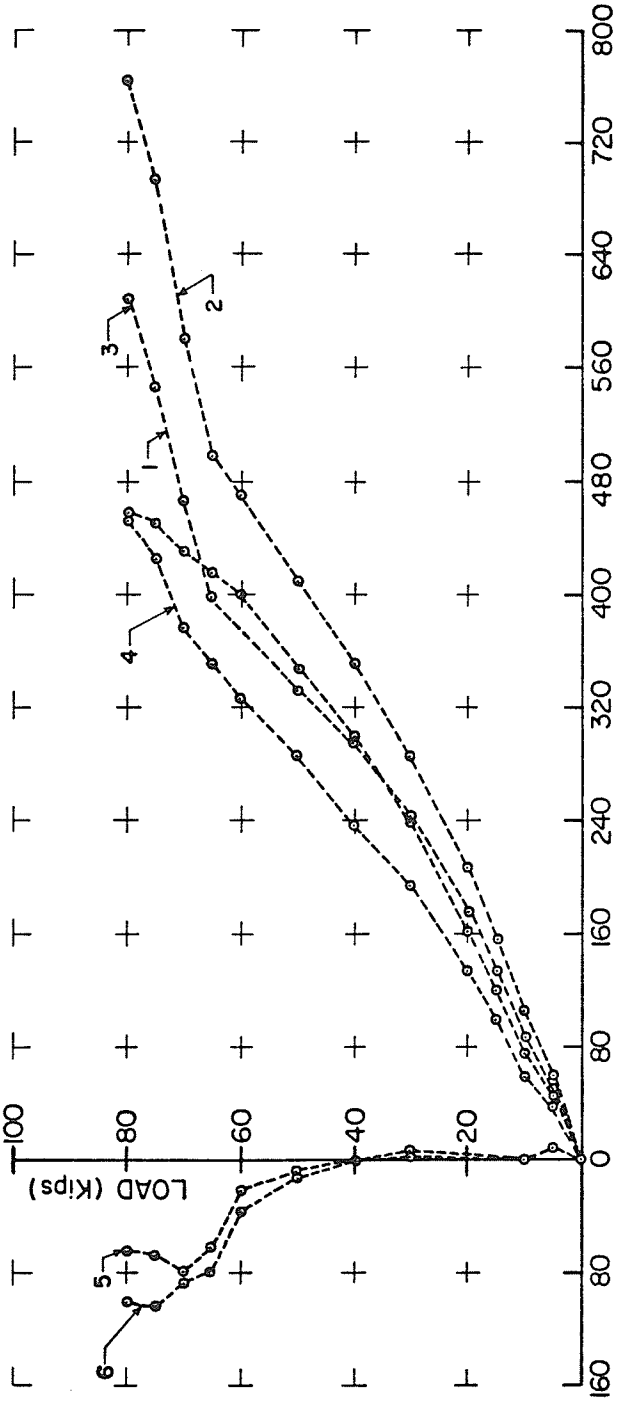

Figure 4.41 Load-strain curve for Sample #11, Side A.

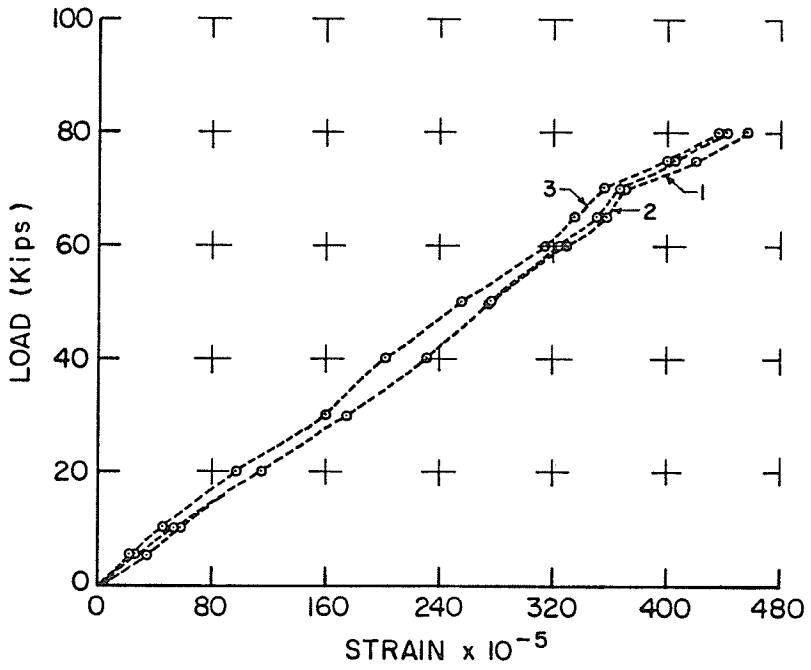

Figure 4.42 Load-strain curve for Sample #11, Side B.

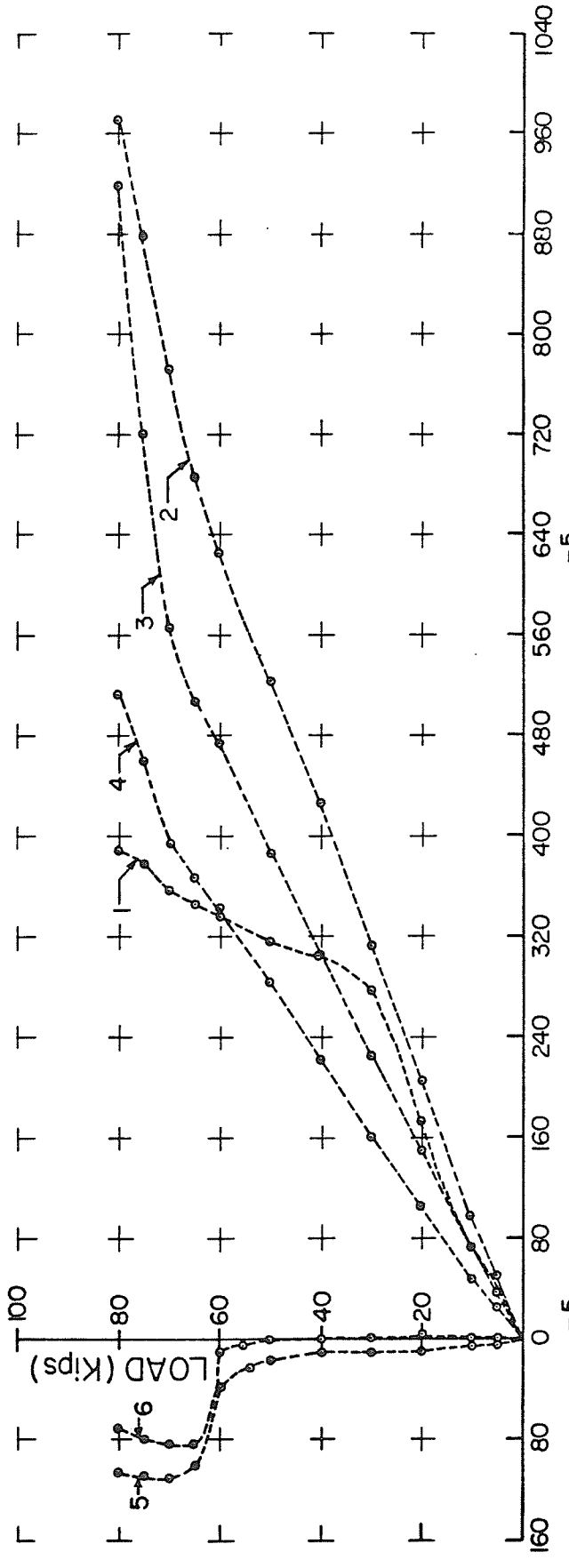

Figure 4.43 Load-strain curve for Sample #11, Side C.

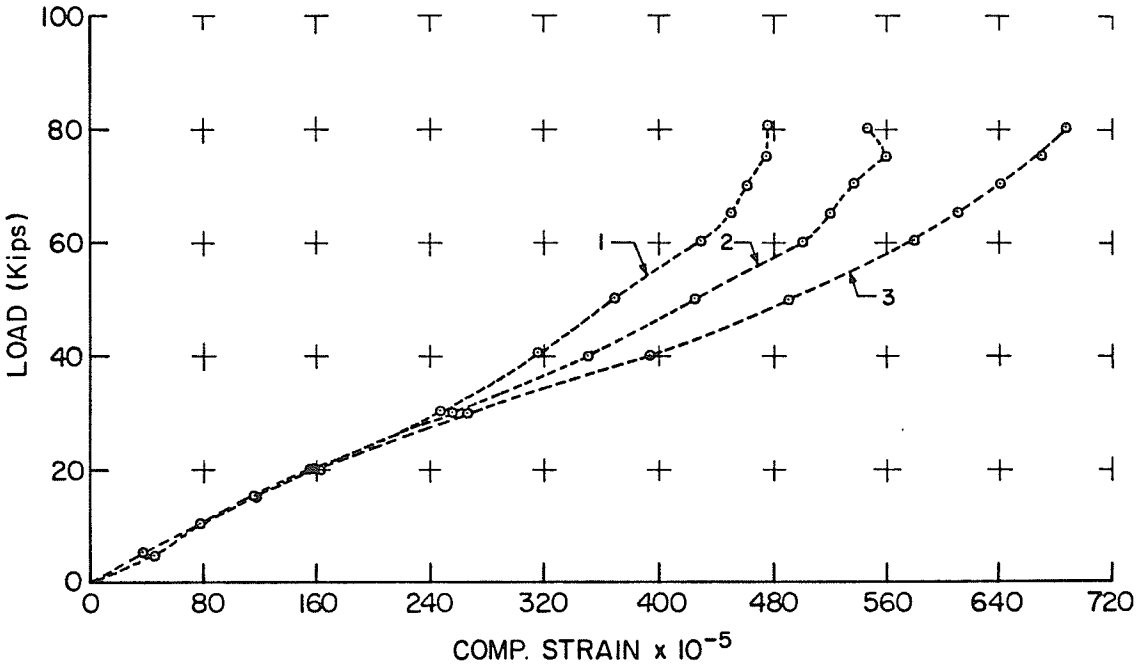

Figure 4.44 Load-strain curve for Sample #11, Side D.

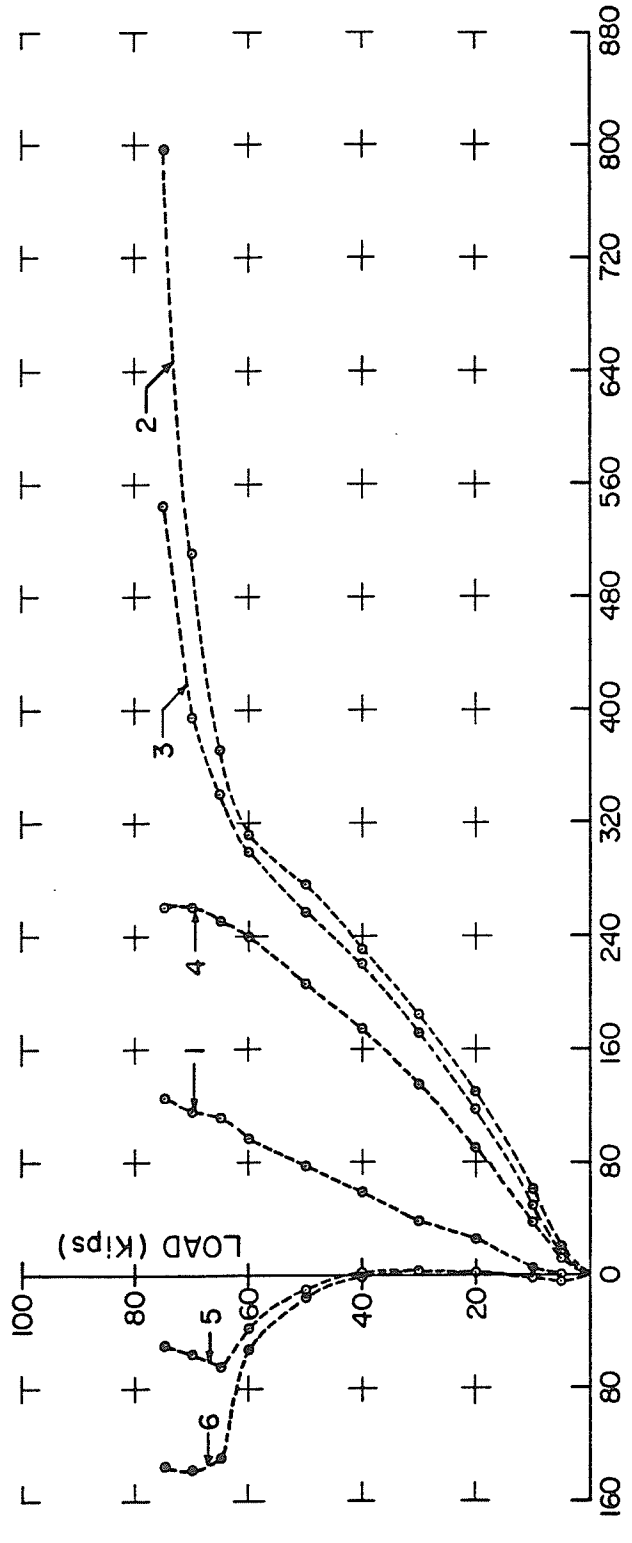

Figure 4.45 Load-strain curve for Sample #12, Side A.

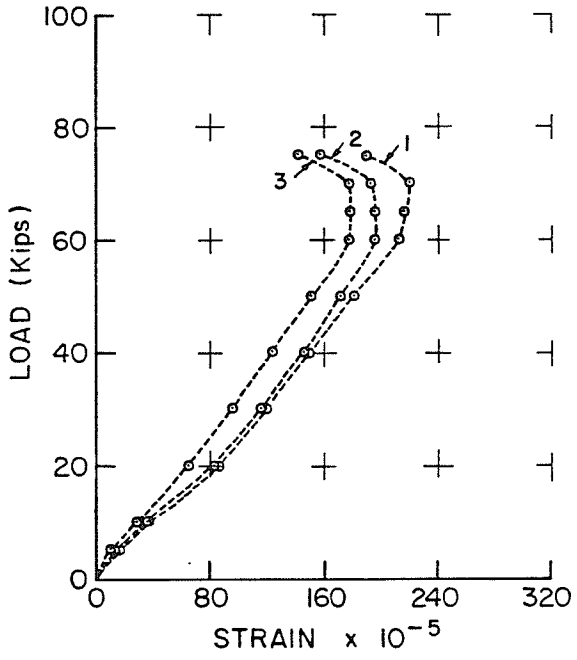

Figure 4.46 Load-strain curve for Sample #12, Side B.

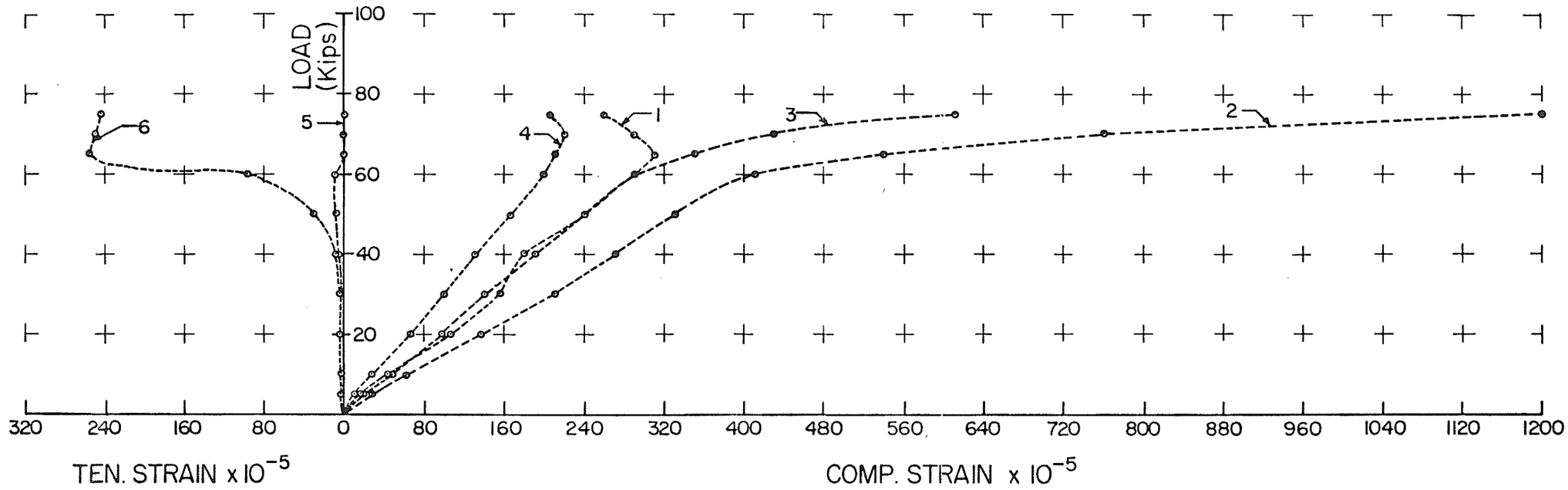

Figure 4.47 Load-strain curve for Sample #12, Side C.

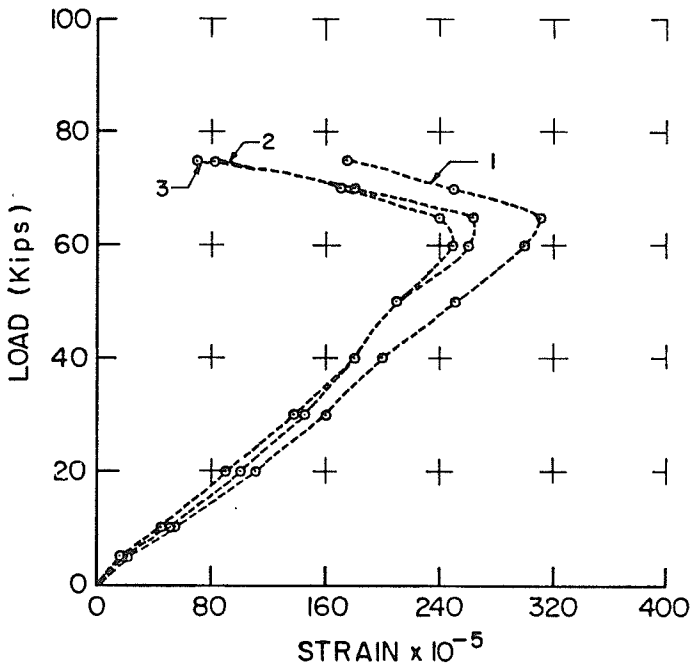

Figure 4.48 Load-strain curve for Sample #12, Side D.

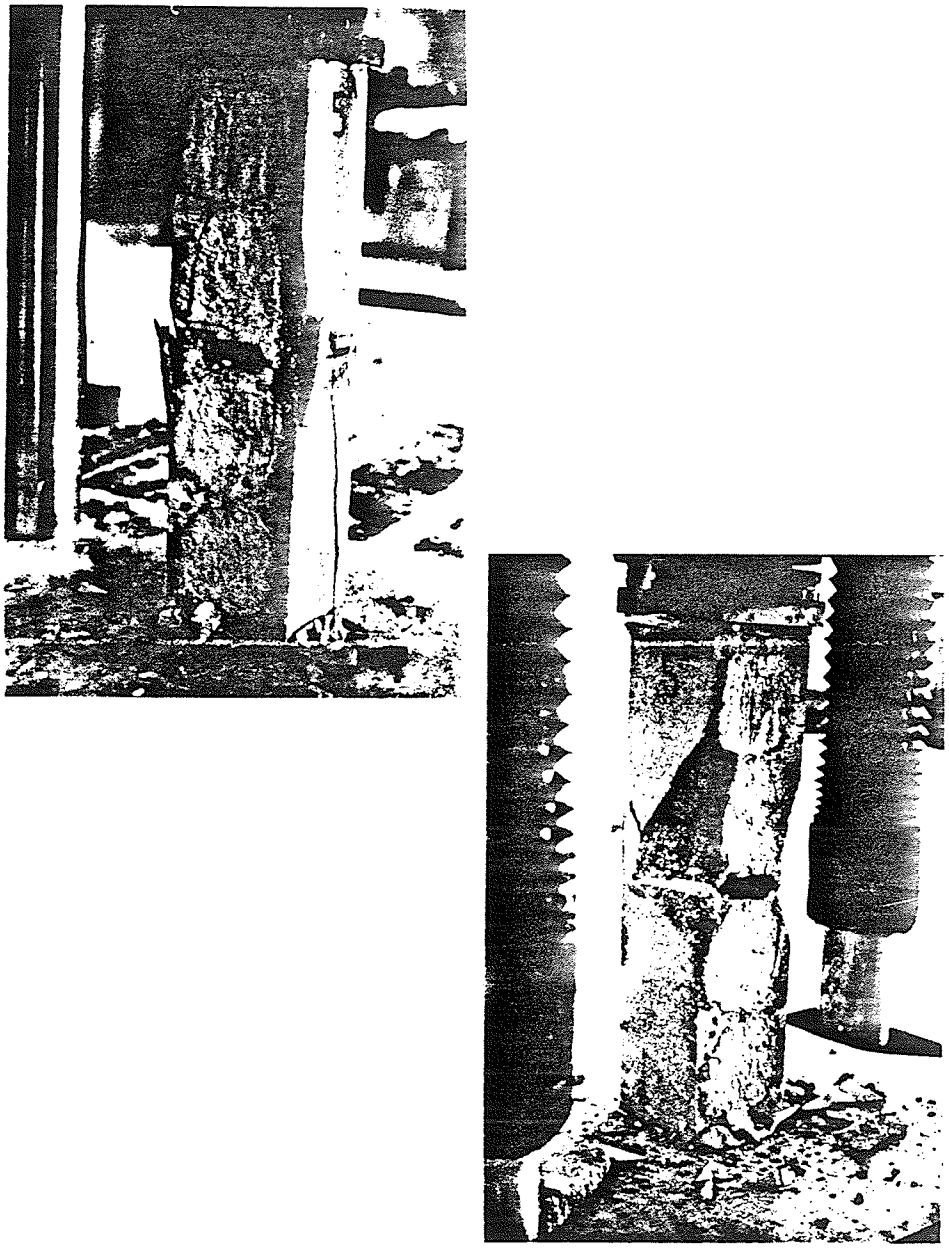

Plate 4.21 Typical Mode I failure by mortar crushing of the partially filled two-block prism axially loaded with PIN/FIX end conditions.

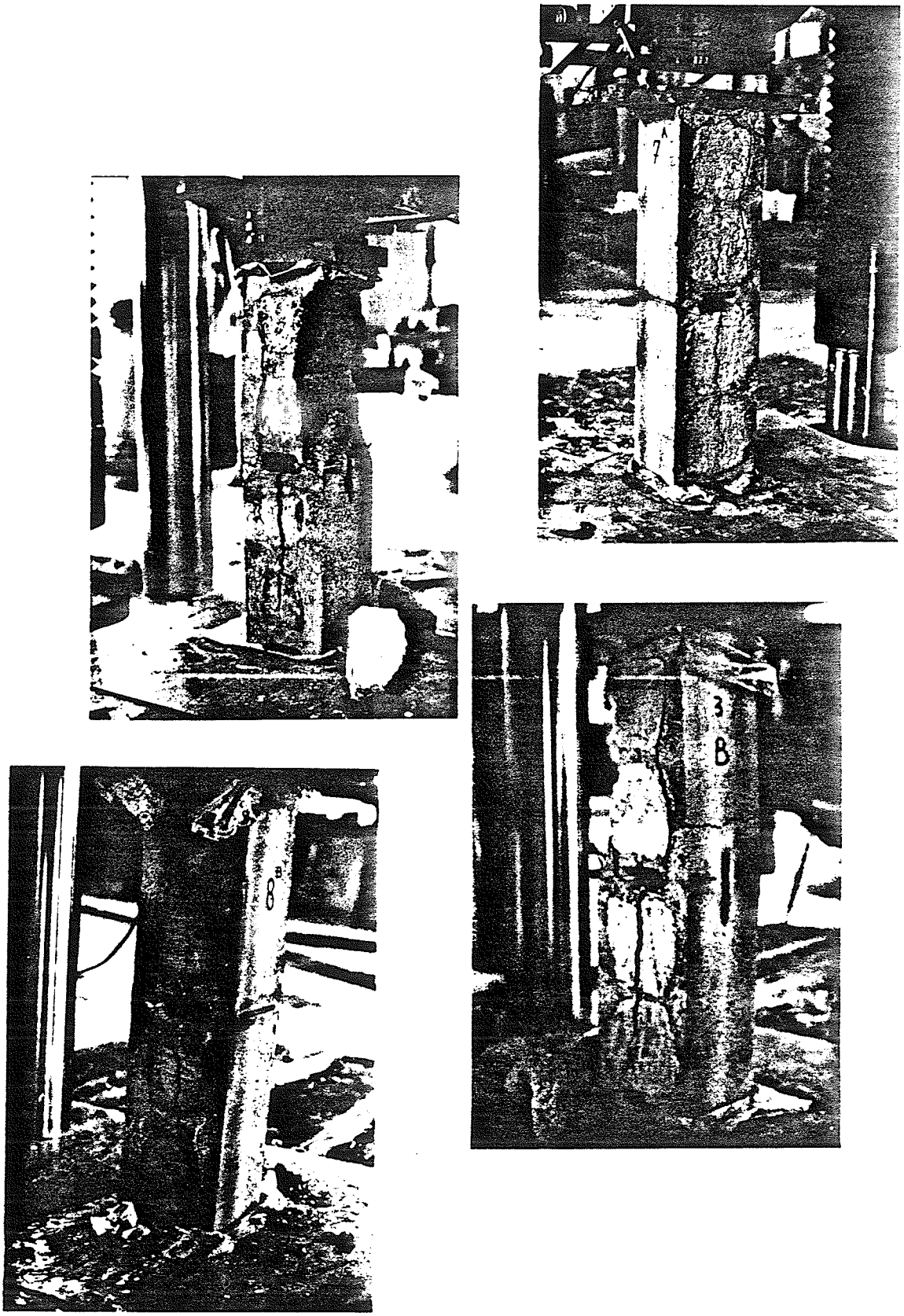

Plate 4.22 Typical Mode II failure by splitting and leg crushing of the partially filled two-block prism axially loaded with PIN/FIX end conditions.

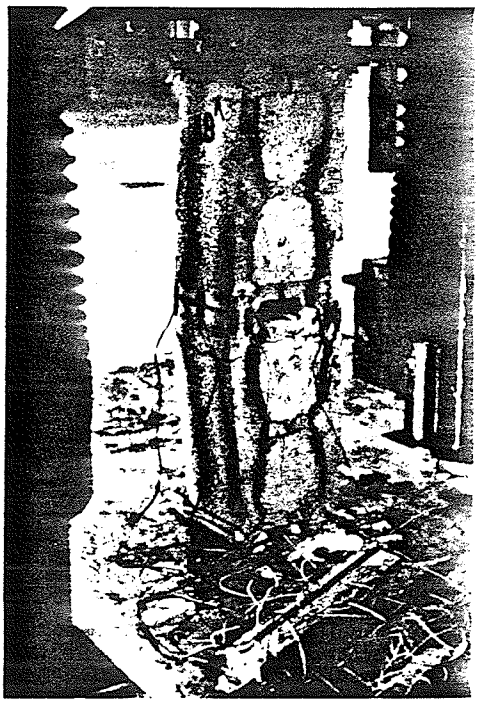

Plate 4.23 Typical mode of failure for the partially filled two-block prism eccentrically loaded with PIN/FIX end conditions.

4.3.1.4 PARTIALLY FILLED TWO-BLOCK PRISMS ECCENTRICALLY LOADED WITH PIN/PIN END CONDITIONS

Four specimens were tested under eccentric load with PIN/PIN end conditions. The modes of failure were essentially by crushing and lateral deflection of the block shell at the mortar joint. There was little evidence of tensile cracks at the center of the webs near the mortar joints. However, vertical cracks were observed between the masonry and the concrete fill. Horizontal cracks were observed at the tension side of the prism between the masonry and the mortar joints. A summary of the prisms' properties, failure loads, and stresses is shown in Table 4.1.

Load-strain curves for prisms #17 and 13 are shown in Figures 4.49 to 4.56 respectively. (See Figure 2.17 for positions of "Demec" points.) Plate 4.24 shows the typical mode of failure for these eccentrically loaded prisms.

4.3.1.5 COMPLETELY FILLED TWO-BLOCK PRISMS AXIALLY LOADED WITH PIN/FIX END CONDITIONS

Three specimens were tested under axial load with PIN/FIX end conditions. The mode of failure was essentially by crushing and lateral deflection of the block shell at the support points or the mortar joints. Vertical cracks were visible at the supports and between the masonry and the concrete fill. A summary of the prisms' properties, failure loads, and stresses are shown in Table 4.1

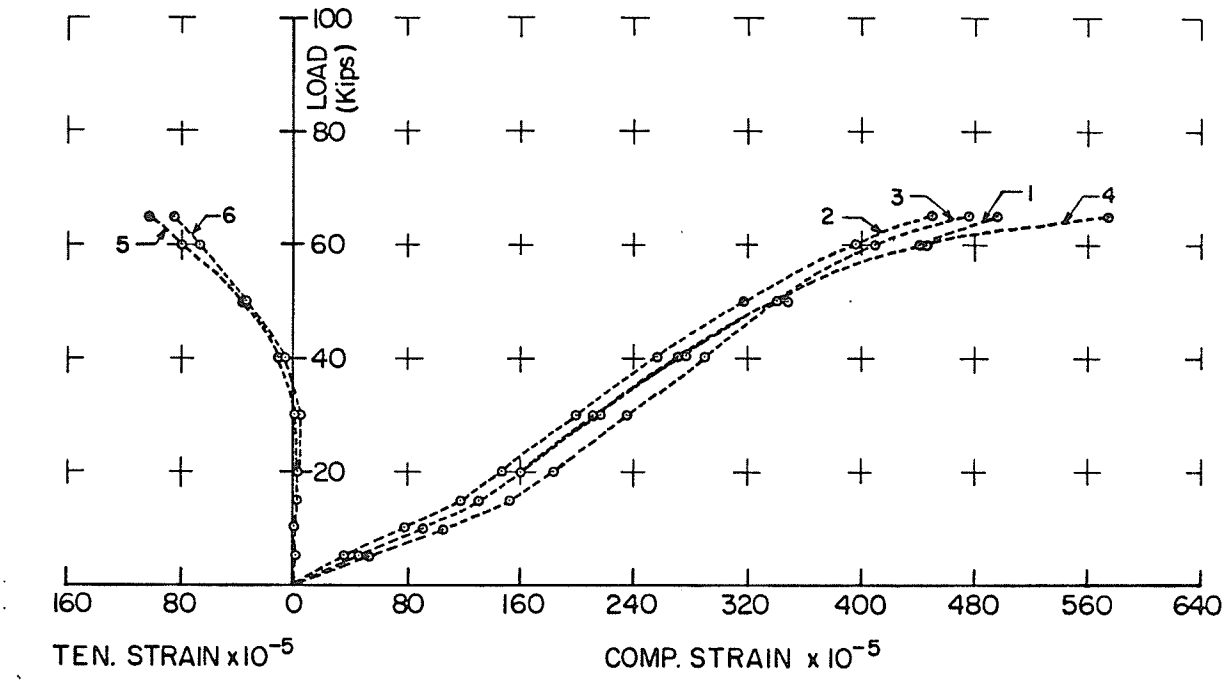

Figure 4.49 Load-strain curve for Sample #17, Side A.

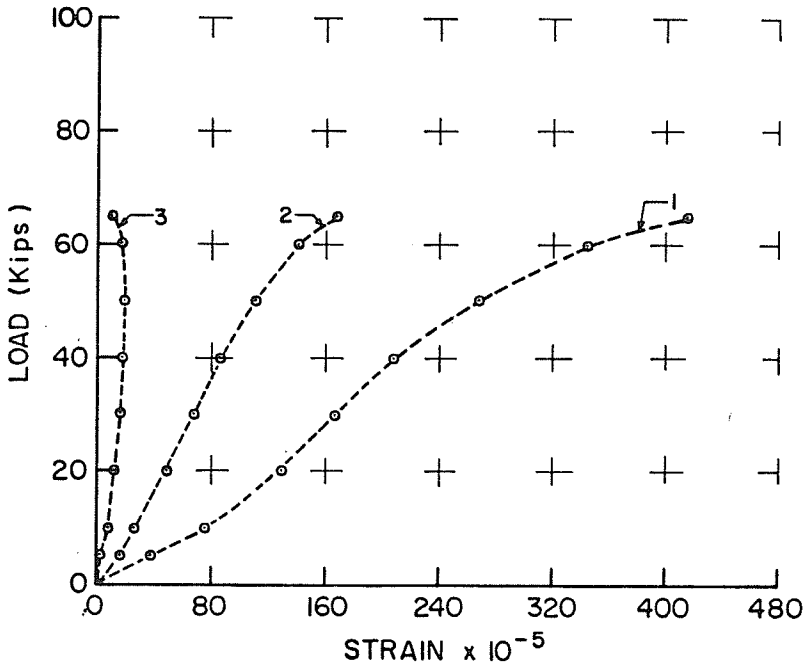

Figure 4.50 Load-strain curve for Sample #17, Side B.

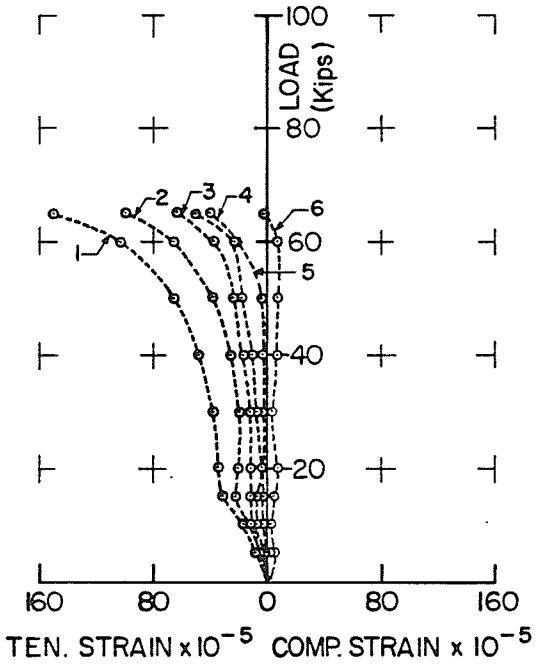

Figure 4.51 Load-strain curve for Sample #17, Side C.

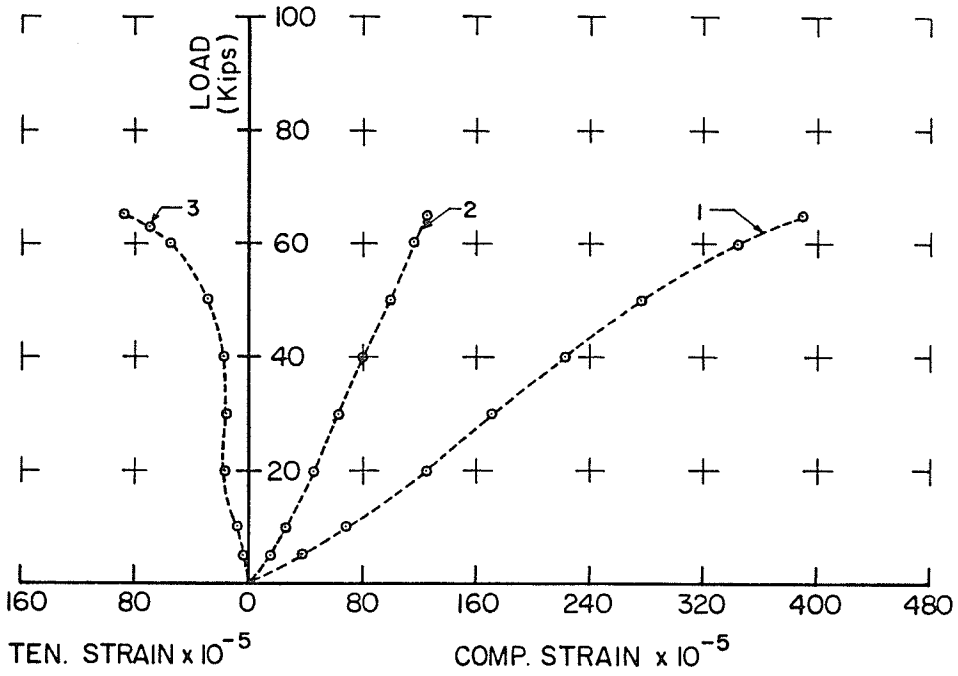

Figure 4.52 Load-strain curve for Sample #17, Side D.

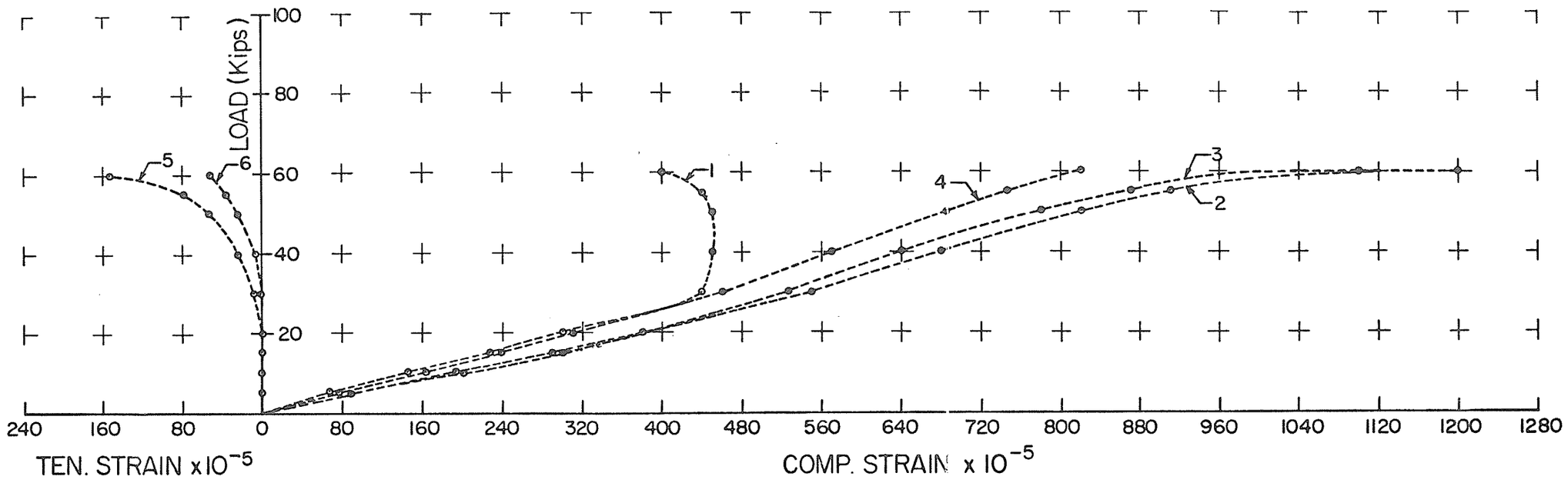

Figure 4.53 Load-strain curve for Sample #13, Side A.

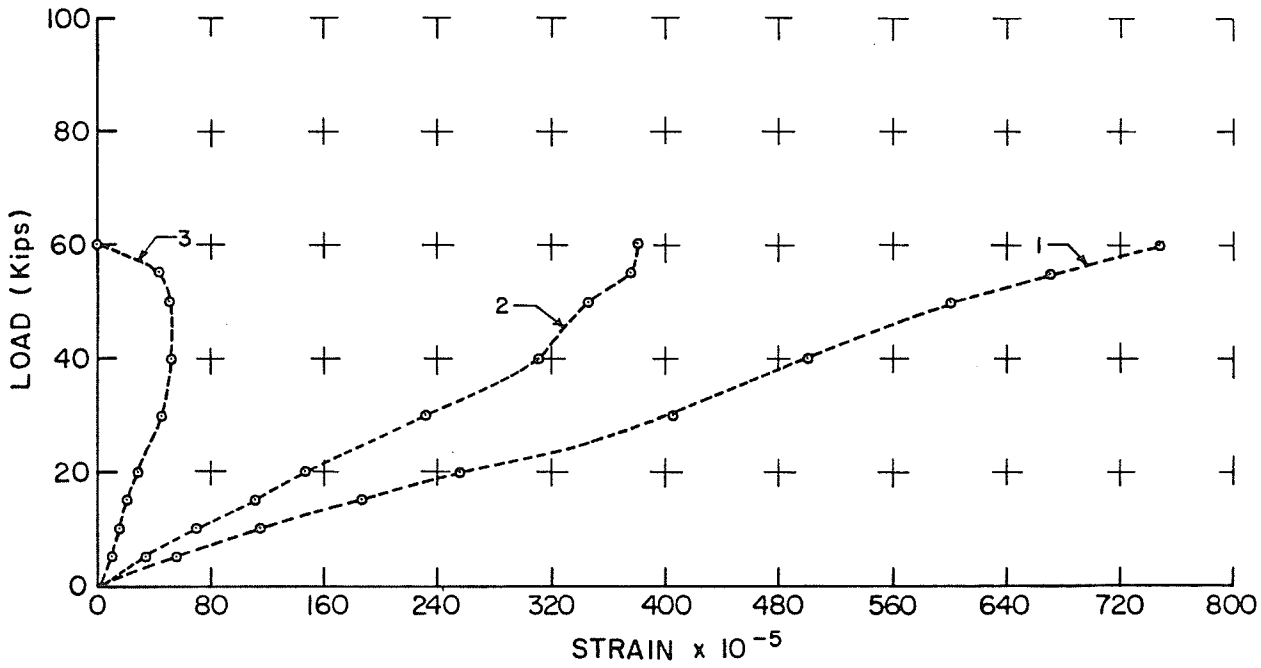

Figure 4.54 Load-strain curve for Sample #13, Side B.

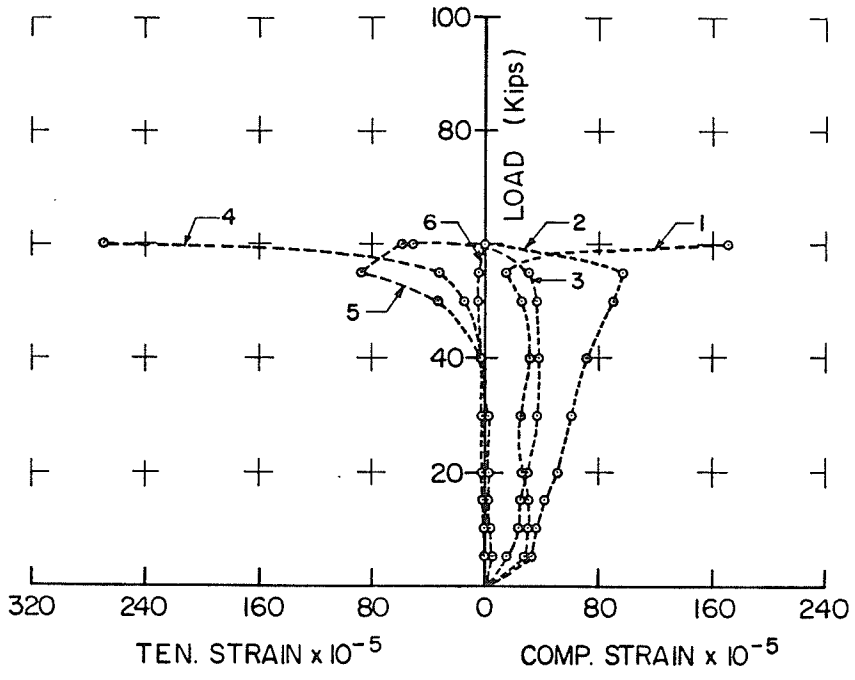

Figure 4.55 Load-strain curve for Sample #13, Side C.

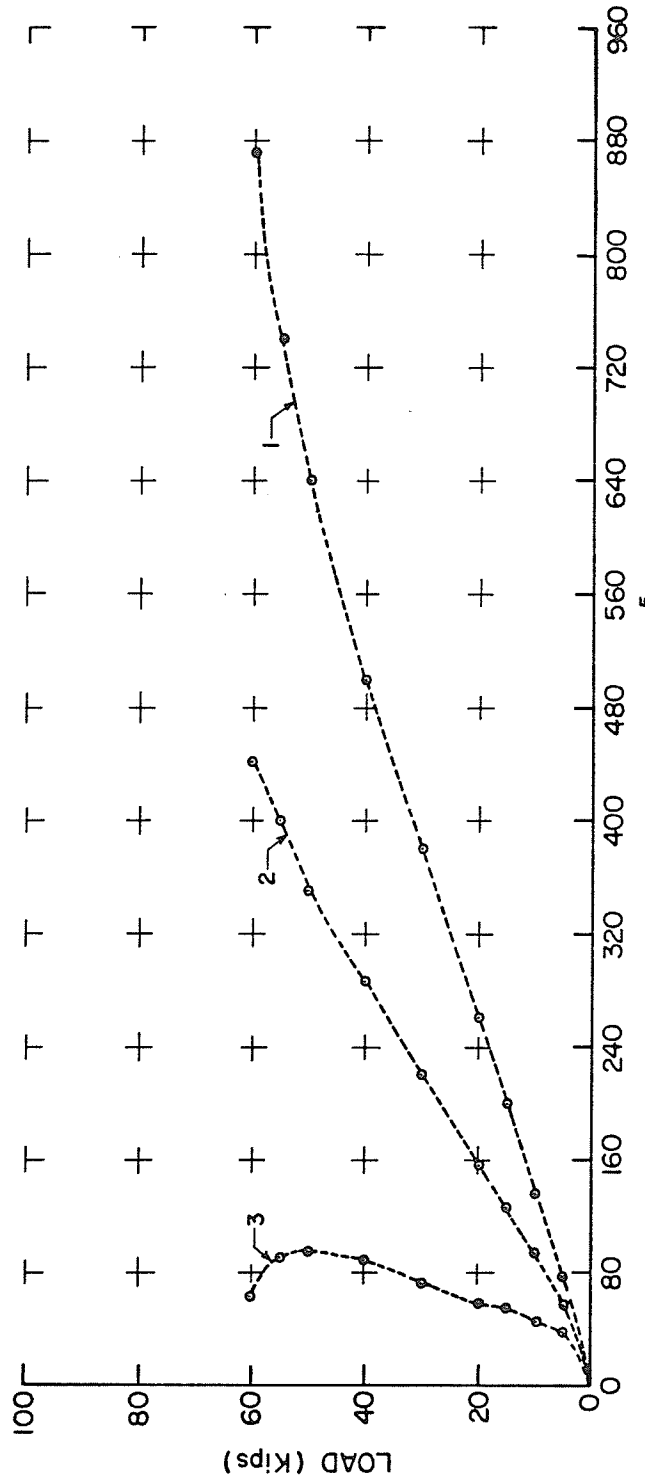

Figure 4.56 Load-strain curve for Sample #13, Side D.

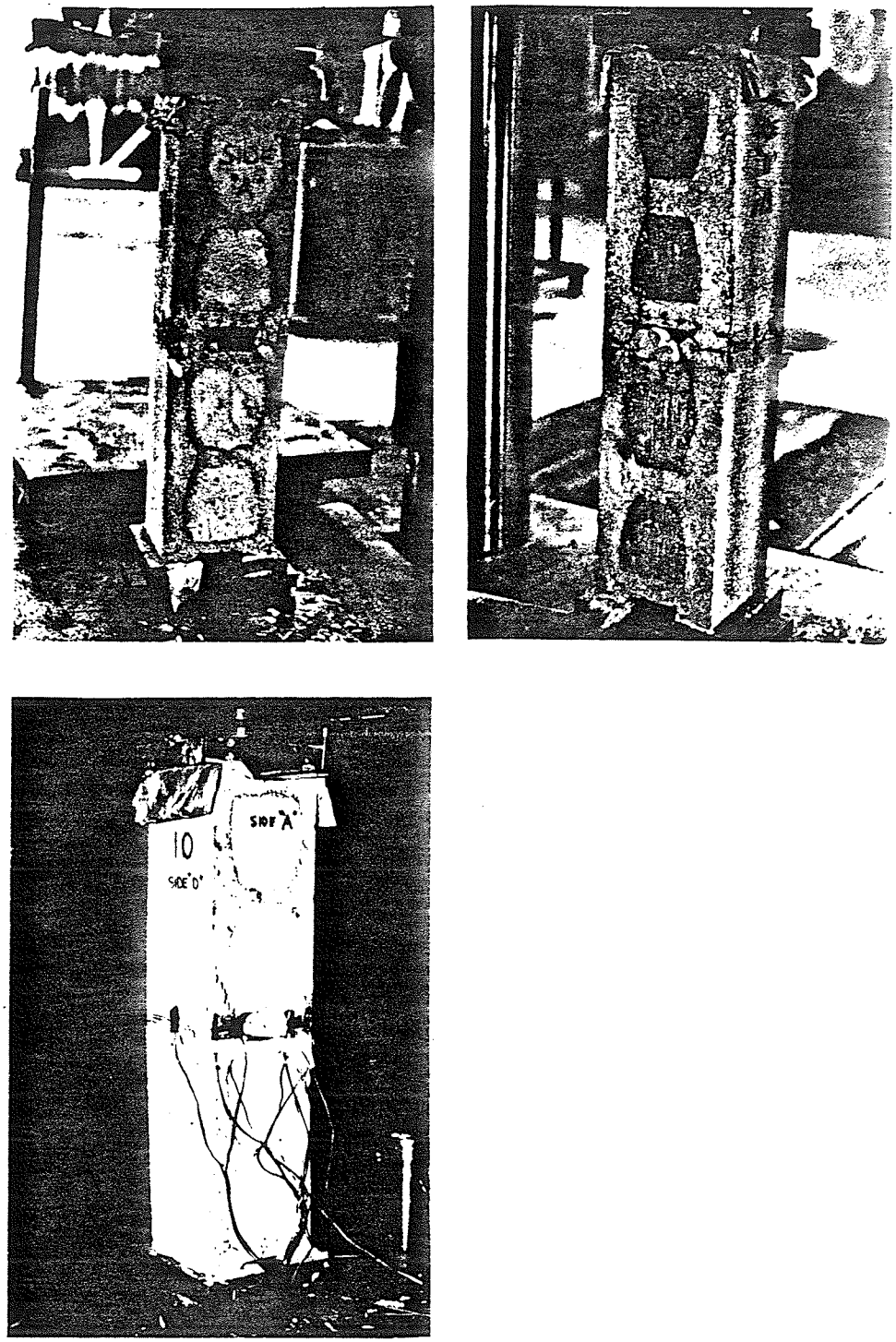

Plate 4.24 Typical mode of failure for the partially filled two-block prism eccentrically loaded with PIN/PIN end conditions.

Load-strain curves for prisms #19 and 22 are shown in Figures 4.57 to 4.64. (See Figure 2.17 for the positions of the "Demec" points.) Plate 4.25 shows a typical prism failure.

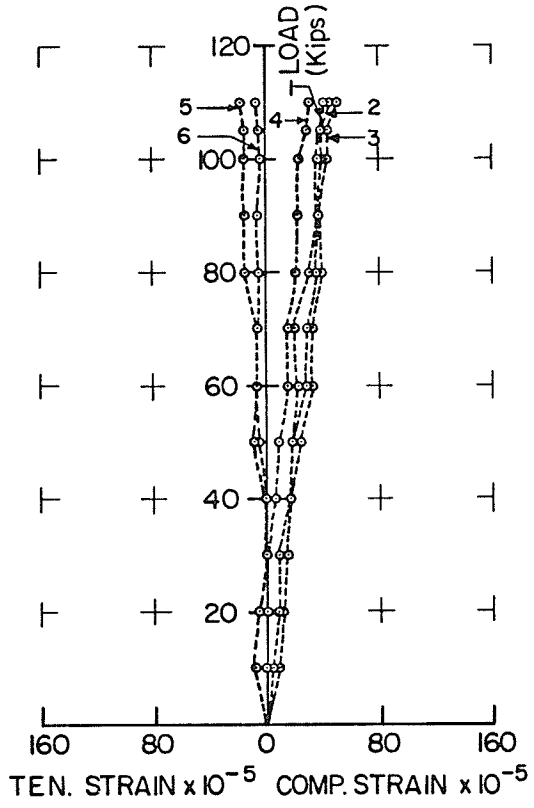

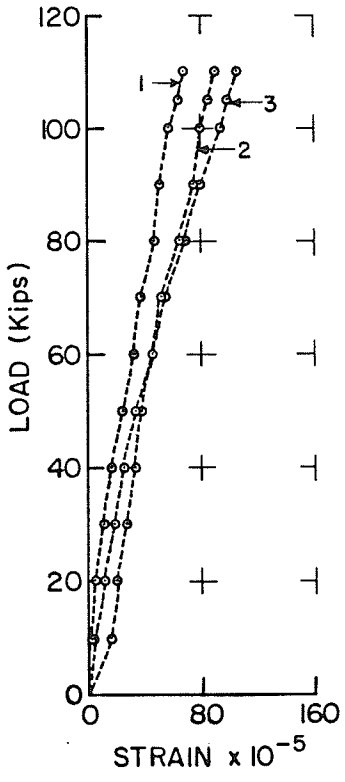

Figure 4.57 Load-strain curve for Sample #19, Side A.

Figure 4.58 Load-strain curve for Sample #19, Side B.

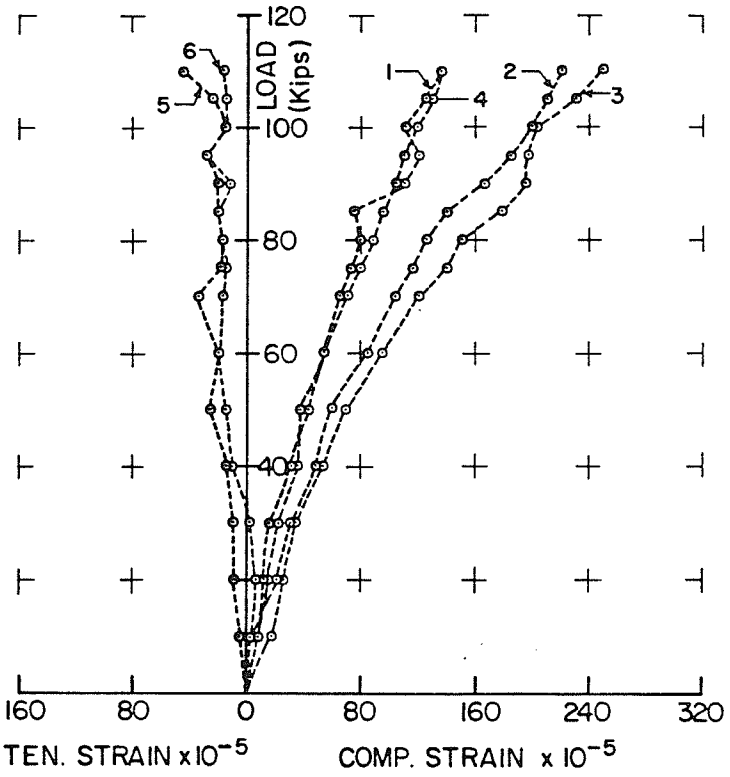

Figure 4.59 Load-strain curve for Sample #19, Side C.

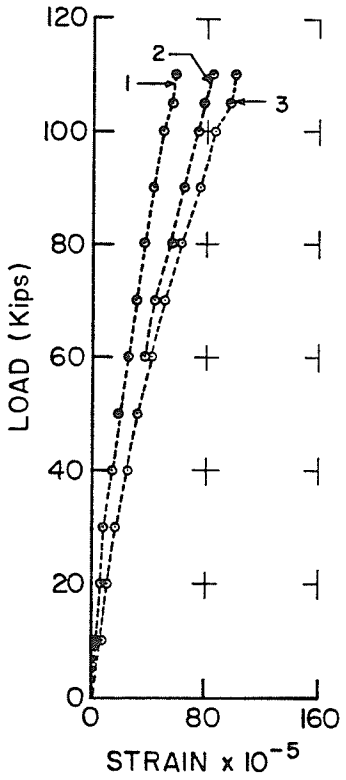

Figure 4.60 Load-strain curve for Sample #19, Side D.

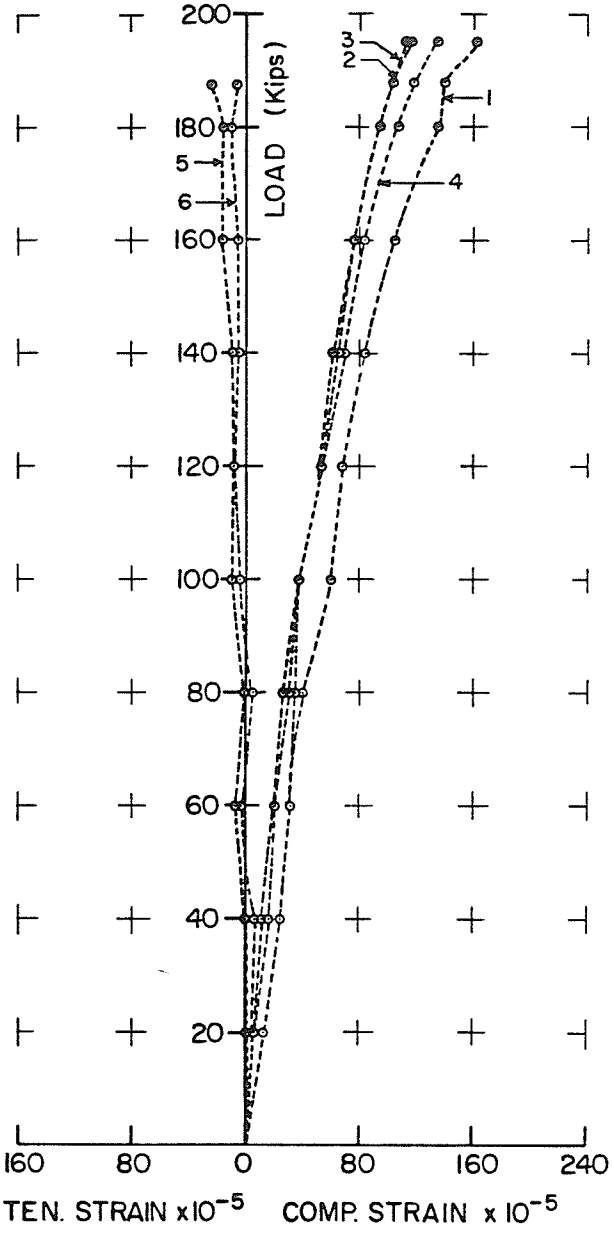

Figure 4.61 Load-strain curve for Sample #22, Side A.

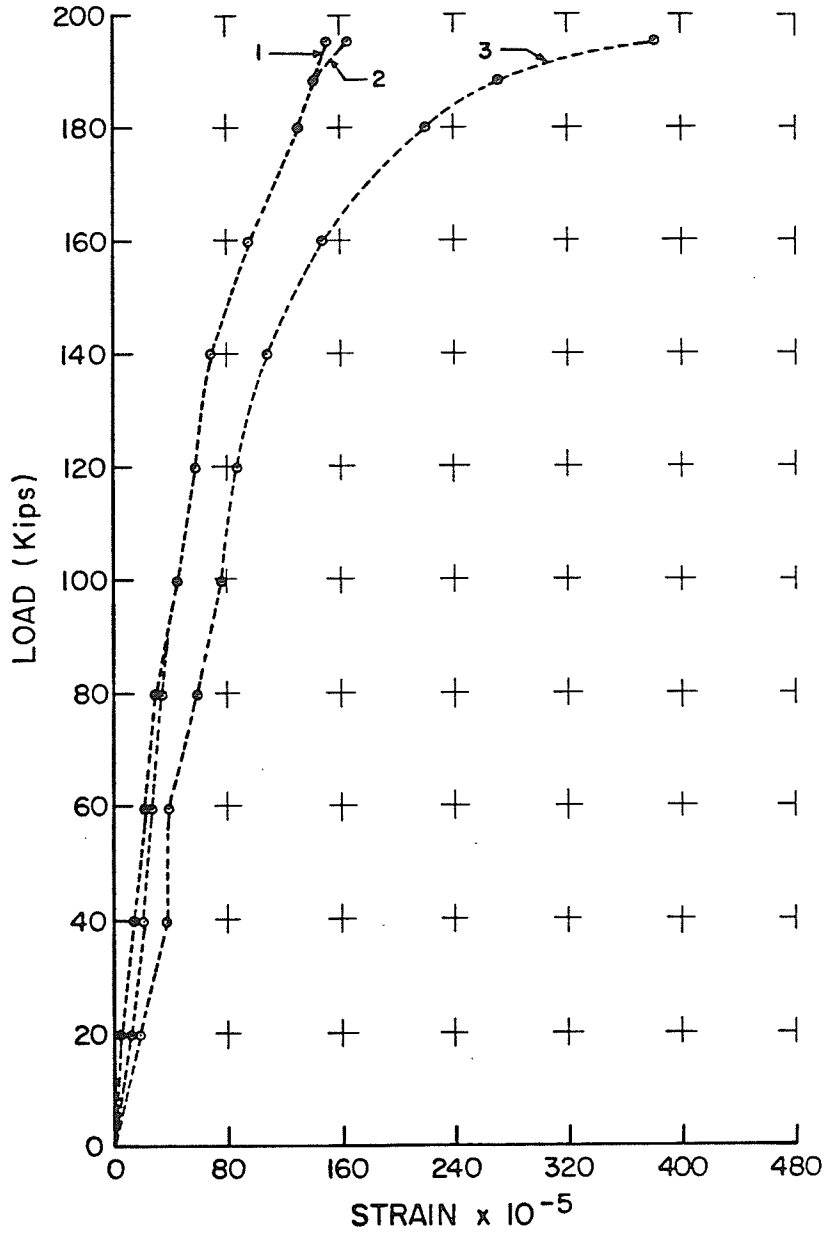

Figure 4.62 Load-strain curve for Sample #22, Side B.

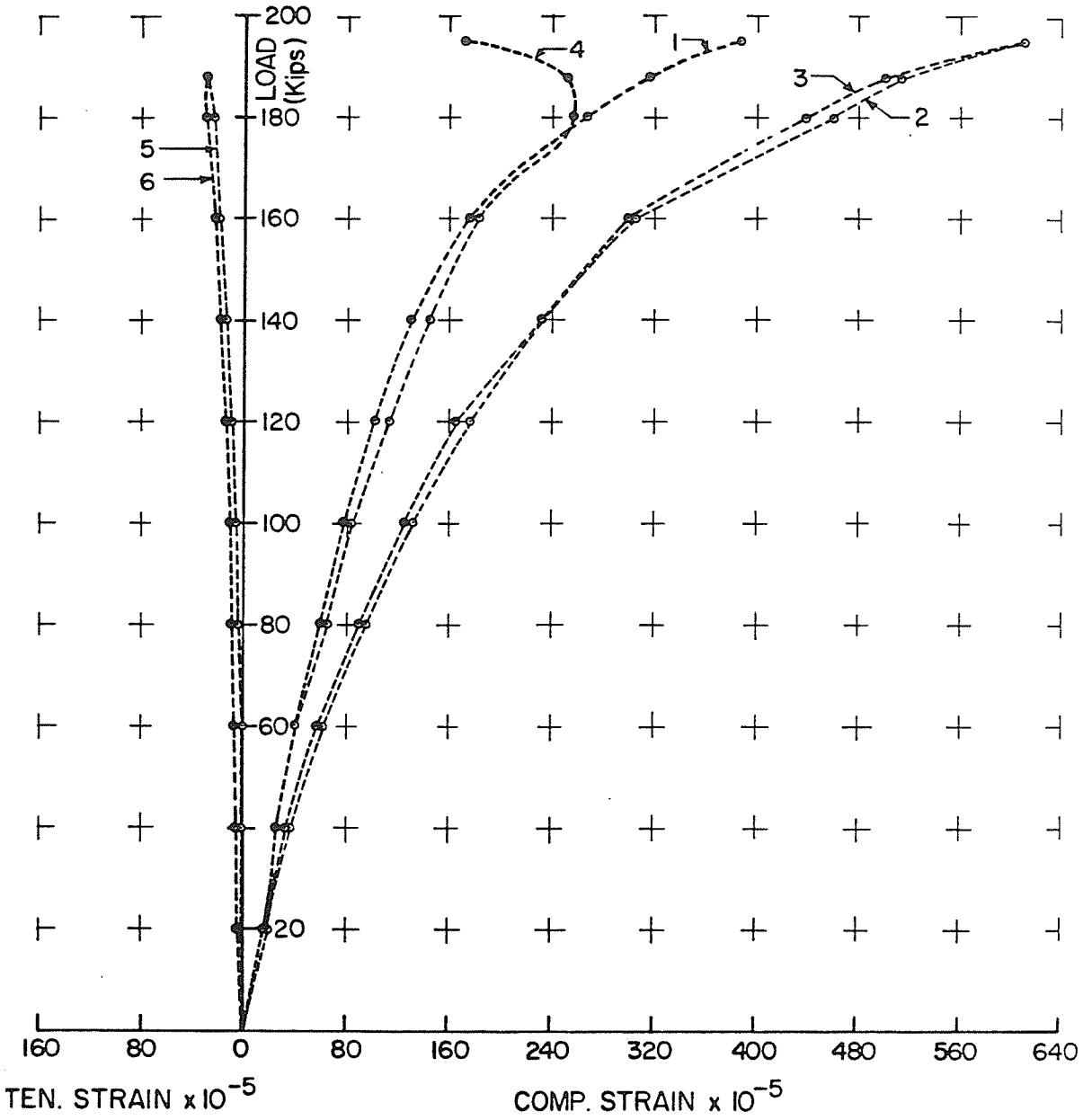

Figure 4.63 Load-strain curve for Sample #22, Side C.

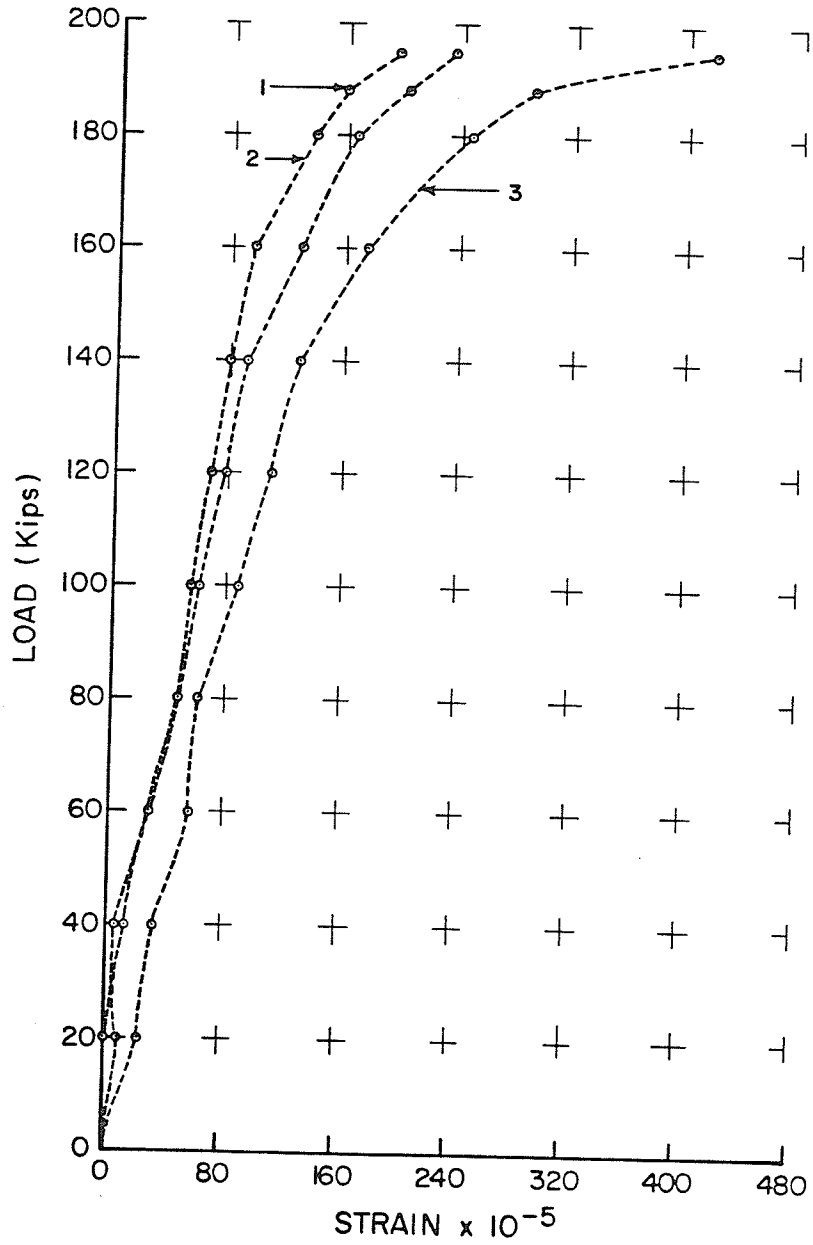

Figure 4.64 Load-strain curve for Sample #22, Side D.

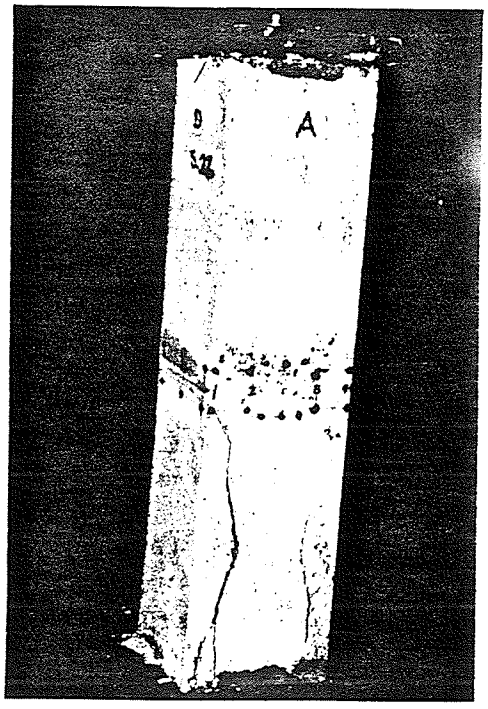

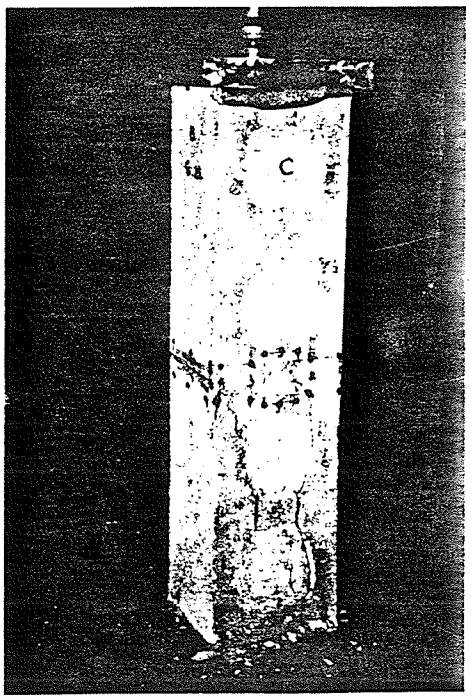

Plate 4.25 Typical mode of failure for the completely filled two-block prism axially loaded with PIN/FIX end conditions.

Table 4.1 Summary of the material properties and test data for the two-block prisms.

TWO-BLOCK PRISMS DESCRAPTION	SPECIMEN NO.	$P_{(ULT.)}$ (IBS.)	AREA USED	SPECIMEN COMP. STRENGTH (P.S.I)	f_G' GROUT AVERAGE (P.S.I)	f_M' MORTAR AVERAGE (P.S.I)	f_B' BLOCK AVERAGE (P.S.I)
UNFILLED AXIALLY LOADED	14	82600	NET	4128	___	4090	4411
	20	99400	NET	4967			
PARTIALLY FILLED AXIALLY LOADED M#1*	5	75300	NET	2724	4117	2584	4411
	6	76500	NET	2768			
	8	65750	NET	2379			
PARTIALLY FILLED AXIALLY LOADED M#2*	1	84000	NET	2754	3748	3367	4411
			GROSS	1445			
	2	92000	NET	3016			
			GROSS	1582			
	3	66000	NET	2164			
			GROSS	1135			
	4	89500	NET	2934			
			GROSS	1539			
	7	88800	NET	2911			
			GROSS	1527			
	11	87200	NET	2856			
			GROSS	1500			
	12	80600	NET	2643			
			GROSS	1386			
	15	92007	NET	3017			
			GROSS	1582			
	18	81200	NET	2662			
			GROSS	1397			
PARTIALLY FILLED AXIALLY LOADED PIN / FIX	9	71300	___	___	4117	2584	4411
PARTIALLY FILLED ECCENTRICALLY LOADED PIN / PIN	10	68679	NET	3380	4761	3286	4411
			GROSS	1773			
	13	65000	NET	3199			
			GROSS	1678			
	16	67395	NET	3317			
			GROSS	1740			
	17	69200	NET	3405			
			GROSS	1787			
COMPLETELY FILLED AXIALLY LOADED	19	147700	GROSS	2540	3996	4773	4411
	21	176100	GROSS	3029			
	22	195000	GROSS	3354			

* See Section 4.3.1.2.

CHAPTER 5

TEST RESULTS AND COMPUTER ANALYSIS EVALUATION

5.1 GENERAL

In this chapter, the results from testing and from the finite element analysis are discussed, and the strains obtained are used to explain the various phenomena of failure. Furthermore, the selection of a rational value of (f_m') to be used in Ultimate Strength Design is discussed.

Because the finite element analysis used assumes elastic behaviour, the stress distributions obtained are inappropriate at failure, yet the strains are more likely to be indicative of actual behaviour. Since the stresses in the elastic region are proportionally related to the strains, and the analysis used a constant modulus of elasticity for each material, then the stresses resulting from the analysis can be used to explain the observed mode of failure, and to understand the sequence of internal failures leading to final collapse.

The actual strain readings on the two-block prisms during load testing tend to confirm the applicability of strain patterns obtained from the F.E.M. even well past reasonable expectations of elastic behaviour.

In this chapter the test results and modes of failure are compared with the F.E.M. analysis elastic stresses, since the stresses are proportionally related to strains in the elastic region.

5.2 SINGLE-BLOCK SPECIMENS

Different types of single-block* specimens (unfilled, partially filled and completely filled) and models were tested under axial load and analyzed with different end conditions and material properties.

The material properties for the tested specimens along with the test results and the analysis results for the single-block specimens are listed in Table 5.1.

5.2.1 UNFILLED SINGLE-BLOCK SPECIMENS

The average compressive strength of five unfilled single-block specimens is listed in Table 5.1. This average compressive strength was used to determine the value of f_m' by using method B in the CAN3-S304. This code uses two methods, A and B. Method A relates to actual prism tests, whereas method B evaluates f_m' on the basis of the strength of the block unit and the type of mortar.

The average compressive strength of the specimens is 3353 p.s.i. On the other hand, the compressive strength of the block material was f_B' = 4411 p.s.i. This discrepancy can be explained by the finite element analysis results. The F.E.M. analysis results (see Figure A.1 and Table 5.1) show very high localized elastic vertical stresses occurring at the outer and inner faces of the

*The word "block" in this chapter means a standard hollow block.

block legs and openings respectively. These localized stresses are responsible for the reduction in the compressive strength of the specimens. The nonuniformity in the elastic vertical stresses was due to the shape of the standard concrete block where there is a tendency of the shell to deflect laterally. The analysis results also show high elastic tension and shear stresses (see Table 5.1) compared to the ultimate tensile and shear stresses given by the CSA Standard CAN3 - A 23.3 -1977 [5] which are:

$$f_t = 6\sqrt{f_B'} \quad \text{- - - - - - - - -} \quad (5.1)$$

$$v = 2\sqrt{f_B'} \quad \text{- - - - - - - - -} \quad (5.2)$$

where:

f_t = Ultimate tensile stresses in concrete (p.s.i.)

v = Ultimate shear stresses in concrete (p.s.i.)

f_B' = Block concrete compressive strength (p.s.i.)

The predicted mode of failure was that first there would be crushing at the outer face of the block legs followed by disintegration of the whole specimen; which, in fact, completely agrees with the actual mode of failure (see Plate 2.1(a)).

The F.E.M. analysis results for the PIN/PIN end condition model are shown in Table 5.1. This model represents an isolated block from the beams' top course, while the PIN/FIX model represents the tested unfilled single-block specimen. The stress results from the PIN/PIN model show

higher localized elastic vertical stresses at the outer face of the legs and the inner face of the openings. They also show a reduction in the tensile stresses and an increase in the shear stresses.

The tests were expected to show that a masonry beam, built with hollow blocks on the top course only, would have a very brittle failure caused by localized crushing. This would be followed by shearing and tensile failure in the compression zone.

5.2.2 PARTIALLY FILLED SINGLE-BLOCK SPECIMENS

The average compressive strength of five specimens was calculated by using the net and gross areas of the specimens (see Table 5.1). These values were used as the f_m' in the Ultimate Strength Design calculations. The F.E.M. analysis results are also shown in Table 5.1.

Test results show a reduction in the net average compressive strength of the specimens (2898 p.s.i.) compared to the material compressive strength (f_B' = 4411 p.s.i.). This reduction was due to the high localized vertical compression stresses to the inner face of the block legs and to the high shear stresses in the block legs, as can be seen from the F.E.M. analysis results (Figure A.3 (a,b,c) and Table 5.1 for PIN/FIX models). The high shear stresses and the nonuniformity in the vertical stresses were due to the shape of the partially filled single-block specimen

where there is a tendency of the shell to deflect laterally to the outside.

The predicted mode of failure was by crushing to the inner face of the block legs and shearing in the leg area followed by lateral deflection of the block shell. This completely agrees with the actual mode of failure (see Plate 2.1(b)).

The F.E.M. analysis results for the PIN/PIN end condition model show a reduction in the localized elastic vertical stresses. They also show a sharp increase in the tensile stresses and a reduction in the shear stresses compared to the PIN/FIX model (see Table 5.1 and Figure A.4 (a,b,c)).

The high tensile stresses resulting from the F.E.M. analysis for the PIN/PIN model explain the splitting at the center of the webs in the tested partially filled two-block prisms (see Plate 4.22). They also explain the horizontal crack at the center of Beam #3 (see Plate 4.8). The splitting forces in the masonry beams became very critical in the highly reinforced masonry beams. The confinement of the horizontal mortar joints was very helpful in preventing this type of splitting. For that reason, the use of the horizontal mortar joint reinforcements in the top course is not recommended because they will buckle during testing. This buckling would destroy the horizontal mortar confinement at the compression zone.

A reduction in the localized elastic vertical stresses and the shear stresses was predicted from the F.E.M. analysis of a model with lower concrete grout compressive strength (f_G = 500 p.s.i.) than the original model with (f_G = 3560) (see Table 5.1 and Figure A.5 (a,b,c)). This leads to the speculation that the ultimate compressive strength of the specimens was going to increase as the grout compressive strength decreased.

In summary, the reduction in the average compressive stress of the partially filled single block specimens was due to the high localized vertical and shear stresses.

5.2.3 COMPLETELY FILLED SINGLE-BLOCK SPECIMENS

The F.E.M. analysis results for the vertical elastic stresses are shown in Figure A.6. The reference uniformly distributed load used for this model was 525 p.s.i. which has the same total load as the uniformly distributed load 1000 p.s.i. which was applied on the unfilled and the partially filled single-block specimens.

According to the analysis, the elastic vertical stresses should be distributed uniformly in the specimen. This leads to the prediction that there is no reduction in the compressive strength of the tested specimens due to high localized vertical stresses, tensile stresses and shear stresses. Therefore, the ideal beam is the completely filled beam; but, as explained earlier (see Section 2.1.1),

Table 5.1 Test and analysis results for the single-block specimens.

	TEST RESULTS						ANALYSIS RESULTS				CSA STANDARD*	
SPECIMEN DESCRIPTION	AVERAGE ULTIMATE LOAD IBS.	AREA USED	SPECIMEN AVERAGE COMPRESSIVE STRENGTH (P.S.I)	f_G' (AVG.) GROUT COMPRESSIVE STRENGTH (P.S.I)	f_M' (AVG.) MORTAR COMPRESSIVE STRENGTH (P.S.I)	f_B' (AVG.) BLOCK COMPRESSIVE STRENGTH (P.S.I)	END CONDITIONS AND MATERIAL PROPERTIES	F_1 (AVG.) PRINCIPLE STRESS (P.S.I)	F_c (AVG.) MAX. HORIZ. COMPRESSIVE STRESS (P.S.I)	F_t (AVG.) MAX. HORIZ. TENSILE STRESS (P.S.I)	F_v (AVG.) MAX. SHEAR STRESS (P.S.I)	$f_t=6\sqrt{f_B'}$ ULTIMATE TENSILE STRESS (P.S.I)	$v=2\sqrt{f_B'}$ ULTIMATE SHEAR STRESS (P.S.I)
UNFILLED SINGLE BLOCK	67120	NET	3353	—	—	4411	PIN / FIX	4532	251	920	575	398	133
							PIN / PIN	6014	179	339	827		
PARTIALLY FILLED SINGLE BLOCK	88389	NET GROSS	2898 1521	3560	—	4411	PIN / FIX	4057	719	238	814	398	133
							PIN / PIN	3304	237	1055	507		
							PIN / FIX $f_G'=500$	3564	722	281	513		

* CSA Standard A 23.3 - 1977.

it is unlikely that the voids between the blocks will be filled normally.

5.3 TWO-BLOCK PRISMS

Different types of two-block prisms and models (unfilled, partially filled and completely filled) were tested under axial and eccentrical loads and analyzed with different end conditions and material properties.

The material property results, test results, and analysis results for the two-block prisms are listed in Tables 4.1 and 5.2.

5.3.1 UNFILLED TWO-BLOCK PRISMS

Test results for the load-strain curves (Figures 4.34 to 4.37) show a higher strain at the outer face of the mortar joints (curves 1 and 4) than the inner face (curves 2 and 3). This was due to the deflected shape of the tested specimens (see Figure A.7).

Horizontal tensile stresses were recorded at the center of the masonry webs near the mortar joints (curves 5 and 6).

The F.E.M. analysis results tend to confirm the test results, where higher elastic vertical stresses are shown at the outer face of the mortar joints than the inner face (see Figure A.8). The analysis shows also high tensile and shear stresses compared to the ultimate stresses given by the CAN3 - A23.3-77 code.[5]

Confinement stresses at the mortar joints were shown by the analysis results (Table 5.2). The confinement stresses were perhaps due to the difference between the material properties of the mortar and the masonry. Hilsdorf,[12] Hatzinikolas[11], and Thomas [19] investigated the behaviour of axially loaded masonry prisms and walls, and proved that the mortar joints are confined because of the presence of tensile stresses in the masonry.

The predicted mode of failure was by crushing at the outer face of the mortar joints followed by total disintegration of the prism, which is in complete agreement with the test mode of failure (see Plate 4.20).

A similarity in the failure modes between the single-block specimen and the two-block prism existed, but there was a difference in the specimen's average compressive strengths. This difference may be due to the plastic properties of the mortar which allows it to absorb more energy.

The analysis results for the PIN/PIN end conditions model show a sharp increase in the elastic vertical stresses at the outer face of the mortar joints and also show an increase in the shear stresses and a decrease in the tensile stresses compared to the PIN/FIX model (see Table 5.2 and Figure A.9).

Testing unfilled single-block specimens was sufficient to gather the data required for the design of the unfilled beam; because of the already proven similarity between the unfilled single-block specimens and the two-block prisms.

5.3.2 PARTIALLY FILLED TWO-BLOCK PRISMS

Test results for the load-strain curves (Figures 4.39 to 4.48) show higher strain readings at the inner face of the mortar joints (curves 2 and 3) than the outer face (curves 1 and 4). This was due to the deflected shape of the tested specimens (see Figure A.10).

Horizontal tensile stresses were recorded at the center of the masonry webs near the mortar joints (curves 5 and 6).

Samples #5,6 and 8 failed by crushing at the mortar joints (see Plate 4.21). This was due to lower mortar compressive strength compared to the compressive strength of partially filled single-block specimens (compare Table 4.1 and 5.1). This mode of failure was not evident in the masonry beams due to the higher mortar compressive strength. The second mode of failure was by crushing of the inner face of the mortar joints followed by lateral deflection of the block shell. There were also very high splitting forces in the center of the webs (see Plate 4.22). The second mode of failure indicates a higher compressive strength of the prism than the first mode (see Table 4.1).

Load - strain curves for prisms #3 and 4 show very strange behaviour; i.e., the curves tend to become vertical after passing the elastic region. This behaviour is due to the lateral deflection of the block shell after the crushing of the inner face of the mortar joint.

Yielding and redistribution phenomena were shown at the higher load levels in the load-strain curves for sample #9. This was due to the plastic properties of mortar. Page[15], in his study, demonstrates that an extensive stress redistribution will occur at the higher stress levels. This redistribution is caused by non-linear material behaviour (predominantly in the mortar joints). The Finite Element Method, being based on linear elasticity, is not applicable in this case.

All the tested prisms show very high strain readings. The highest strain reading recorded was (0.01464 in/in), which is very high compared to the ultimate strain (ε_u = 0.003) given by the CSA Standard CAN3 - A23.3 - M77.[5]

Test results showed a reduction in the average net compressive strength of the partially filled two-block prisms (2773 p.s.i) compared to the compressive strength of the concrete block material (f_B' = 4411 p.s.i.) This reduction was due to the high localized vertical stresses, tensile stresses and shear stresses, as given by the F.E.M. analysis (see Table 5.2 and Figure A.11 (a,b,c). The analysis also confirms the prism test results, where high elastic vertical stresses were shown at the inner face of the mortar joints rather than the outer face.

Confinement stresses at the mortar joints similar to the unfilled two-block prism were shown in (Table 5.1 and Figure A.11(b)).

The predicted mode of failure was by crushing and shearing at the inner face of the mortar joints, followed

by lateral deflection of the block shell, which matches the test mode of failure (see Plate 4.22).

There is a similarity between the failure modes of the partially filled single-block specimens and the partially filled two-block prisms (compare the plates and the analysis figures for the two specimens). The resulting compressive strength of these two specimens is also similar (see Table 4.1 and Table 5.1).

The analysis results for the PIN/PIN end conditions model show a sharp increase in the tensile stresses at the center of the webs near the mortar joints. They also show a decrease in the shear stresses, while the localized vertical stresses and the mortar confinement stresses remain the same compared to the PIN/FIX model (see Table 5.2 and Figure A.12 (a,b,c)).

The average strain profile results across the mortar joint for the axially loaded partially filled two-block prisms with PIN/FIX end conditions are shown in Figure 5.1. The Figure shows great differences between the test and the analysis results for the strain at the mortar joint. There are several possible reasons for this: (1) the F.E.M. is an idealized method which does not consider the microcracks resulting from testing (see the dashed area in Figure 5.1), (2) the mortar in the cubes is stressed differently than the mortar in the joints, and, in addition, (3) the mortar thickness is different in each case. This affects the strength and, therefore, the performance of the mortar as demonstrated by Hatzinikolas[11] and Hilsdorf[12] in their work.

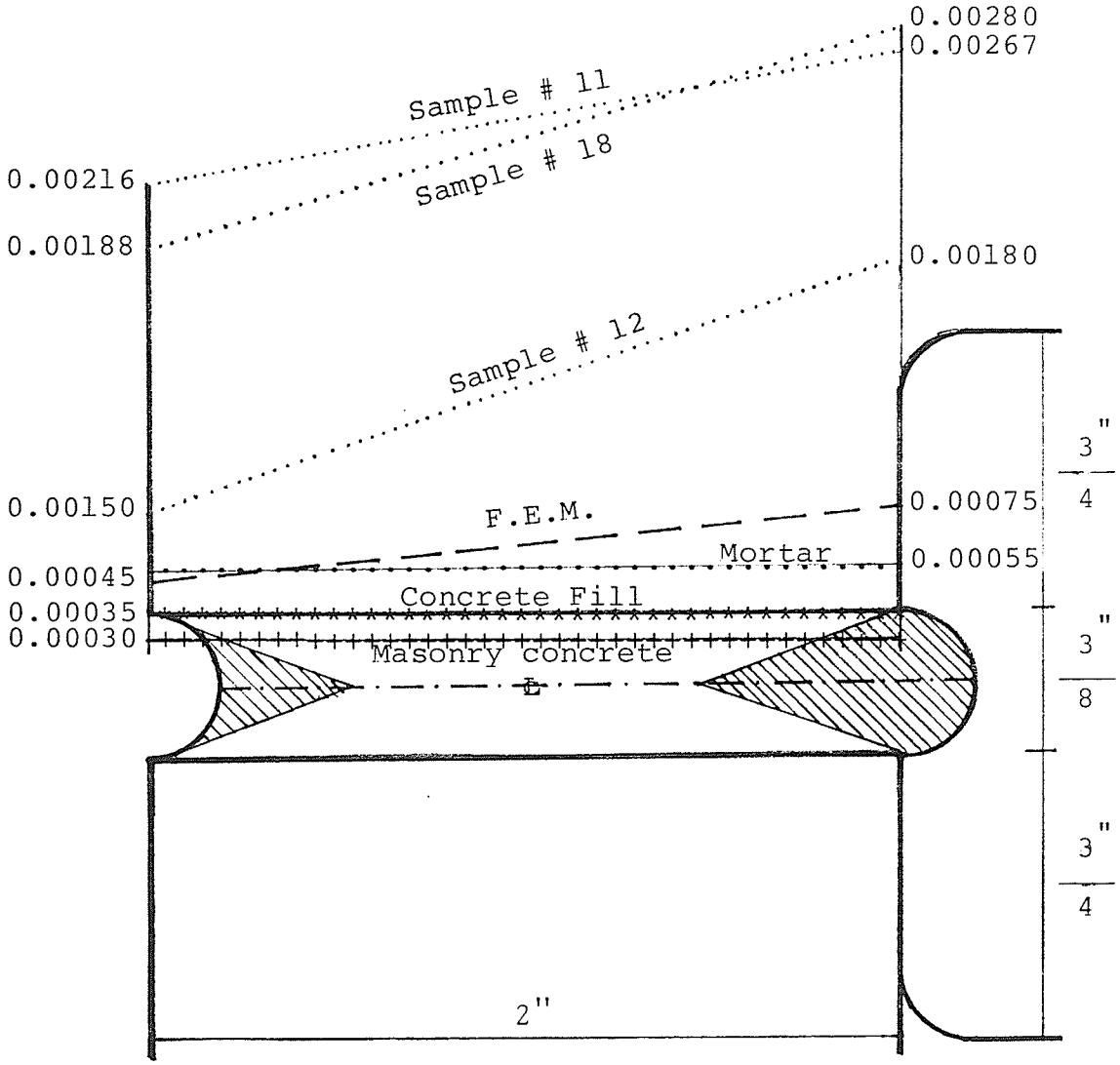

- Area where the microcracks initiated at early stages of loading due to the tendancy of the mortar to deflect to the outside.

Figure 5.1 Average strain profile across the mortar joint for the axially loaded partially filled two-block prism with PIN / FIX end conditions.

To obtain the data to design the partially filled beam, it was only necessary to test partially filled single-block specimens. This conclusion was due to the similarity between the partially filled single-block specimens and the two-block prisms.

5.3.3 PARTIALLY FILLED TWO-BLOCK PRISMS ECCENTRICALLY LOADED WITH PIN/PIN END CONDITIONS

The load-strain curves on the compression side of the eccentrically loaded partially filled two-block prisms (Figures 4.49 to 4.56) show higher strain readings at the inner face of the mortar joints (curves 2 and 3) than the outer face (curves 1 and 4). This was due to the deflected shape of the specimens. The test results also show horizontal tensile stresses at the center of the masonry webs near the mortar joints.

The load-strain curves on the tension side of the eccentrically loaded prisms show tensile strains in the vertical and the horizontal directions (curves 1,2,3,4,5 and 6). There was evidence of lateral deflections of the block shell where the load/strain curves progressed vertically or backwards at high load levels (see curve 1 in Figure 4.53).

All the tested prisms show very high strain readings. The highest strain reading recorded was (0.012 in 1 in/in).

The average net and gross compressive strengths were determined and used as the f_m' for the Ultimate Design

Theory (see Table 5.4). The three-dimensional F.E.M. analysis tends to confirm the test results, showing higher elastic vertical stresses at the inner face of the mortar joints rather than at the outer face (see Table 5.3 and Figures 3.17 (a,b, c)).

The analysis shows confinement stresses in the mortar joints similar to the analysis results for the axially loaded unfilled and partially filled two-block prisms (Table 5.3 and Figures A.18 (a,b,c) and A.19 (a,b,c)).

The predicted mode of failure was by crushing of the inner face of the mortar joints, followed by lateral deflection of the block shell, which completely agrees with the test mode of failure (see Plate 4.24).

The test and the analysis results for both the eccentrically and the axially loaded partially filled prisms show tensile stresses at the center of the webs near the mortar joints. However, these tensile stresses do not have such serious implications in the eccentrically loaded prisms. This has been demonstrated by a comparison of the heavily and lightly reinforced beams. In the first case, the compression zone acts as it would in an axially loaded prism, causing dangerous splitting in the center of the beam (see Plate 4.8). In the second case, the compression zone acts as it would in an eccentrically loaded prism, which also causes splitting in the center of the beam; but in this case, it is not serious (see Beam #1 and 2). The

confinement of the horizontal mortar joints under the top course, as discussed earlier in Section 5.2.2, helps to reduce this type of splitting in either case.

5.3.4 COMPLETELY FILLED TWO-BLOCK PRISMS

Test results for the load-strain curves (Figures 4.57 to 4.64) show higher strain readings at the inner face of the mortar joints (curves 2 and 3) than the outer face (curves 1 and 2). This was probably due to the incomplete filling of the voids between the two blocks.

Horizontal tensile stresses were recorded at the center of the masonry webs near the mortar joints (curves 5 and 6).

All the tested prisms show lower strain readings compared to the partially filled two-block prisms. The highest strain reading recorded was (.0061 in/in).

The average gross compressive strength was used as the f_m' for the Ultimate Design Theory (see Table 5.4).

A reduction in the average gross compressive strength of the tested prisms (2974 p.s.i.) was seen in comparison with the compressive strength of the block and the grout materials (f_B' = 4411 p.s.i., f_G' = 3996 p.s.i.). This reduction was due to the localized vertical stresses and shear stresses.

The F.E.M. analysis shows almost uniformly distributed elastic vertical stresses (see Figure A.15). It also shows

very low tensile and shear stresses compared to the other tested specimen models (see Table 5.2).

The test and the analysis results show that the ideal case was the completely filled beam; but, as explained before (see section 2.1.1), filling the voids between the blocks usually does not happen.

Table 5.2 Test and analysis results for the two-block prisms using the two-dimensional F.E.M. analysis.

	TEST RESULTS						ANALYSIS RESULTS				CSA STANDARD*	
SPECIMEN DESCRIPTION	AVERAGE ULTIMATE LOAD IBS.	AREA USED	SPECIMEN AVERAGE COMPRESSIVE STRENGTH (P.S.I)	f_G' (AVG.) GROUT COMPRESSIVE STRENGTH (P.S.I)	f_M' (AVG.) MORTAR COMPRESSIVE STRENGTH (P.S.I)	f_B' (AVG.) BLOCK COMPRESSIVE STRENGTH (P.S.I)	END CONDITIONS AND MATERIAL PROPERTIES	F_1 (AVG.) PRINCIPLE STRESS (P.S.I)	F_c (AVG.) MAX. HORIZ. COMPRESSIVE STRESS (P.S.I)	F_t (AVG.) MAX. HORIZ. TENSILE STRESS (P.S.I)	F_v (AVG.) MAX. SHEAR STRESS (P.S.I)	$f_t=6/\sqrt{f_B'}$ ULTIMATE TENSILE STRESS (P.S.I)	$v=2/\sqrt{f_B'}$ ULTIMATE SHEAR STRESS (P.S.I)
UNFILLWD TWO-BLOCK	91900	NET	4547	---	4090	4411	PIN / FIX	7757	650	1232	862	398	133
							PIN / PIN	8354	635	501	1137		
PARTIALLY FILLED TWO-BLOCK MODE # 1	72517	NET	2624	4117	2584	4411	PIN / FIX	3710	364	723	668	398	133
							PIN / PIN	3710	364	866	564		
							PIN / FIX $f_G'=500$	3265	409	476	599		
							PIN / FIX $f_M'=500$	3662	544	732	668		
PARTIALLY FILLED TWO-BLOCK MODE # 2	84578	BLOCK LEGS GROSS	2773 1455	3748	3367	4411	PIN / FIX	4326	424	843	779	398	133
							PIN / PIN	4326	424	1009	657		
							PIN / FIX $f_G'=500$	3807	477	555	699		
							PIN / FIX $f_M'=500$	4270	635	854	779		
COMPLETELY FILLED TWO-BLOCK	172933	GROSS	2974	3996	4773	4411	PIN / FIX	4819	487	108	538	398	133

* CSA Standard A 23.3 - 1977.

Table 5.3 Test and analysis results for the two-block prisms using the three-dimensional F.E.M. analysis.

	TEST RESULTS						ANALYSIS RESULTS				CSA STANDARD*	
SPECIMEN DESCRIPTION	AVERAGE ULTIMATE LOAD IBS.	AREA USED	SPECIMEN AVERAGE COMPRESSIVE STRENGTH (P.S.I)	f_G' (AVG.) GROUT COMPRESSIVE STRENGTH (P.S.I)	f_M' (AVG.) MORTAR COMPRESSIVE STRENGTH (P.S.I)	f_B' (AVG.) BLOCK COMPRESSIVE STRENGTH (P.S.I)	END CONDITIONS AND MATERIAL PROPERTIES	F_l (AVG.) PRINCIPLE STRESS (P.S.I)	F_c (AVG.) MAX. HORIZ. COMPRESSIVE STRESS (P.S.I)	F_t (AVG.) MAX. HORIZ. TENSILY STRESS (P.S.I)	F_v (AVG.) MAX. SHEAR STRESS (P.S.I)	$f_t=6\sqrt{f_B'}$ ULTIMATE TENSILY STRESS (P.S.I)	$v=2\sqrt{f_B'}$ ULTIMATE SHEAR STRESS (P.S.I)
PARTIALLY FILLED TWO-BLOCK ECCENTRICALLY LOADED	67568	NET GROSS	3325 1744	4761	3286	4411	PIN / PIN	7266	983	638	——	398	133

* CSA Standard A 23.3 - 1977.

5.4 MASONRY BEAMS

A summary of the single-block specimens and two-block prisms; and beam properties is given in Tables 5.4 and 5.5 respectively.

In calculating the anticipated failure load for a beam (i.e., its resisting moment), not only is the yield strength of the reinforcement required, but also a suitable value of f_m', the masonry compressive strength, and its associated area. The CSA Standard CAN3-S304 [6] is somewhat incomplete in its recommendations for values of f_m' to use for bending, basing its recommended value on the results of axial load tests on materials acting as walls; and, in any case, the rather special case of voids between filled blocks is not specifically covered. In determining f_m' for the purpose of design, the results from the single and two-block specimens were used to calculate the anticipated failure load. The CSA Standard S304 was followed in some cases to check its validity in determining (f_m') for the design of these special beams. In the present investigation, failure loads were calculated for each beam using eight different interpretations of f_m' (see Table 5.4). The results of these estimates of failure load are shown in Table 5.6 as a ratio $P_{(test)}/P_{(cal.)}$. The average value of $P_{(test)}/P_{(cal.)}$ for all beams was 1.07, 1.00, 1.12. 1.00. 1.13. 1.08, 1.08 and 1.00 for each of the eight interpretations of f_m'.

These eight interpretations of f_m' are listed in Table 5.4, which also lists the methods of deriving f_m'. The CSA Standard CAN3 - S304 uses two methods, A and B. Method A relates to actual prism tests, whereas method B evaluates f_m' on the basis of the strength of the block unit and the type of mortar.

The mortar compressive strength was not used in design due to the less evident mortar crushing in the tested beams. It is the author's opinion that the mortar compressive strength should not be used as the f_m' in the calculation because it dose not accurately represent the type of failure.

Table 5.6 shows the failure loads for the various beams obtained by test and by calculation using the eight values of f_m' and using the actual gross widths (7 5/8") and the net leg widths (4") of the block. Also given in Table 5.6 is the ratio of tested failure load : calculated failure load (shown as $P_{(test)}/P_{(cal.)}$). Although cases 2,4, and 8 on the average (see bottom row of Table 5.6) give an excellent evaluation of anticipated failure, some of the individual beams failed at loads up to 17 - 18% below predictions. Cases 3 and 5, based on the gross area of the specimens (see Table 5.4), resulted in a very high margin of safety (i.e., 12 - 13% higher than predicted). On the other hand, case 1, using the code method B derived from block unit strength and mortar

Table 5.4 Summary of compressive strength and material properties for the single and the two-block specimens.

Case	Test Specimens	Avg. Comp. Strength (p.s.i.)	Area used	f_m'[1] (p.s.i.)	CSA[2] Method used	f_m' (mortar) (p.s.i.)	f_G' (Grout) (p.s.i.)	f_B' (Block) (p.s.i.)
1	Standard Empty Block	3353	Net	1806	B	-	-	4411
2	Standard Partially Filled Block	2898	Net	2898	Non	-	3560	4411
3		1521	Gross	1521	Non			
4	Axially Loaded, Partially Filled Two-Block Prism	2773	Net	2773	Non	3367	3748	4411
5		1455	Gross	1455	A			
6	Eccentrically Loaded, Partially Filled Two-Block Prism	3325	Net	3325	Non	3286	4761	4411
7		1744	Gross	1744	Non			
8	Axially Loaded Completely Filled Two-Block Prism	2974	Gross	2974	A	4773	3996	4411

1. Masonry compressive strength.

2. CSA Standard S304-1977 "Masonry Desing and Construction for Buildings".

Table 5.5 Summary of beam properties.

	Beam Dimensions			Longitudinal Steel			Web Steel				Grout	Mortar	Block Concrete
Beam	No. of courses	b (ins.)	d (ins.)	Tension reinforcement bars	As (in^2)	fy (psi)	stirrup bars	As (in^2)	fy (psi)	spacing S (ins)	f_G' (psi)	f_m' (psi)	f_B' (psi)
1	4	7.625	28.75	1/15M	0.31	70,163	24/10M	0.155/ bar	51,855	8	3113	4117	4411
2	4	7.625	29	1/25M	0.775	74,851	24/10M	0.155/ bar	49,435	8	3344	4057	4411
3	4	7.625	27.25	2/25M	1.55	74,271	24/10M	0.155/ bar	54,678	8	4807	4192	4411
4	4	7.625	26.75	3/25M	2.325	76,489	24/10M	0.155/ bar	54,678	8	3641	3895	4411
5	4	7.625	27.75	1/30M 1/25M	1.86	69,216 74,051	24/10M	0.155/ bar	54,678	8	3982	4417	4411
6	3	7.625	20.00	1/25M	0.775	74,871	24/10M	0.155/ bar	53,613	8	4646	3554	4411
7	3	7.625	20.00	2/20M	0.93	64,247	24/10M	0.155/ bar	51,855	8	4789	4054	4411
8	3	7.625	19.25	2/25M	1.55	74,845	24/10M	0.155/ bar	52,984	8	4678	4025	4411

Table 5.6 Summary of beam results.

Beam no.	$P_{(test)}$ (kips)	CASE 1 $P_{(cal)}$ (kips)	CASE 1 $P_{(test)}/P_{(cal)}$	CASE 2 $P_{(cal)}$ (kips)	CASE 2 $P_{(test)}/P_{(cal)}$	CASE 3 $P_{(cal)}$ (kips)	CASE 3 $P_{(test)}/P_{(cal)}$	CASE 4 $P_{(cal)}$ (kips)	CASE 4 $P_{(test)}/P_{(cal)}$	CASE 5 $P_{(cal)}$ (kips)	CASE 5 $P_{(test)}/P_{(cal)}$	CASE 6 $P_{(cal)}$ (kips)	CASE 6 $P_{(test)}/P_{(cal)}$	CASE 7 $P_{(cal)}$ (kips)	CASE 7 $P_{(test)}/P_{(cal)}$	CASE 8 $P_{(cal)}$ (kips)	CASE 8 $P_{(test)}/P_{(cal)}$
1	21.6	17.3	1.25	17.6	1.23	17.2	1.25	17.5	1.23	17.1	1.26	17.3	1.25	17.3	1.25	17.6	1.23
2	51.0	48 2	1.06	50.0	1.02	47.3	1.08	49.8	1.02	47.0	1.08	48.0	1.06	48.0	1.06	50.0	1.02
3	83.0	82.8	1.00	90.0	0.92	79.3	1.05	89.4	0.93	78.3	1.06	82.2	1.01	82.2	1.01	90.2	0.92
4	105.5	110.7	0.95	127.6	0.83	102.2	1.03	126.4	0.83	99.8	1.06	109.1	0.97	109.1	0.97	128.4	0.82
5	102.0	94.7	1.08	104.6	0.97	90.4	1.13	103.9	0.98	89.0	1.15	94.2	1.08	94.2	1.08	105.0	0.97
6	34.8	31.7	1.10	33.5	1.04	30.8	1.13	33.4	1.04	30.6	1.14	31.6	1.10	31.6	1.10	33.6	1.04
7	34.9	32.6	1.07	34.5	1.01	31.6	1.10	34.4	1.01	31.4	1.11	32.4	1.08	32.4	1.08	34.6	1.01
8	57.6	53.1	1.08	60.3	0.95	49.5	1.16	59.8	0.96	48.5	1.19	52.4	1.10	52.4	1.10	60.6	0.95
Average			1.07		1.00		1.12		1.00		1.13		1.08		1.08		1.00

Table 5.6 cont'd

Beam No.	Deflection at Ult. Load(ins)	Mode of Failure	Remark	$\frac{As}{As(bal)} \times 100\%$ based on case 1 b=7.625", f_m'=1806 psi
1	1.6	Flexure	Tension Failure	14
2	0.9	Flexure	Tension Failure	37
3	1.16	Flexure	Tension Failure	79
4	0.96	Flexure	Compression Failure	116
5	0.73	Flexure	Compression Failure	88
6	1.36	Flexure	Tension Failure	54
7	1.38	Flexure	Tension Failure	52
8	1.08	Flexure	Compression Failure	113

REMARK: values of (b) and (fm') used in calculation of $P_{(cal.)}$ (see Table 1).

Case 1 : b = 7.625 fm' = 1806 p.s.i.
Case 2 : b = 7.625 fm' = 2898 p.s.i.
Case 3 : b = 7.625 fm' = 1521 p.s.i.
Case 4 : b = 7.625 fm' = 2773 p.s.i.
Case 5 : b = 7.625 fm' = 1455 p.s.i.
Case 6 : b = 4 fm' = 3325 p.s.i.
Case 7 : b = 7.625 fm' = 1744 p.s.i.
Case 8 : b = 7.625 fm' = 2974 p.s.i.

type, yielded results with a reasonable margin of safety (7% higher than predicted). The results of case 1 are supported by the results from cases 6 and 7 for eccentrically loaded two-block prisms. The predicted failure load was calculated by ordinary Ultimate Strength Design techniques developed with reinforced concrete, only replacing f_c' by f_m'.

The overall performance of the beams tested agreed, in general, with reinforced concrete beams previously tested by Mattock [14] and also with the reinforced masonry beams tested by Edghill [9] and Baydak [4].

The $\frac{M}{bd^2}$ - strain curves for the tested beams are shown in Figure 5.2 (a,b). The crack moment in masonry beams was found to be lower than in concrete beams. This was due to the discontinuities in the concrete fill, and poor bond between concrete fill, mortar and block.

The CSA Standard CAN3 - S304 does not recommend any value for the modulus of rupture (f_{mr}) for masonry members in flexure. To find the most reasonable value for the modulus of rupture for the tested masonry beams (f_{mr}), three different cases for the masonry beam cross sections were studied to evaluate the gross moment of inertia to be used for (f_{mr}) calculations. These cross-sections are shown in detail in Figure 5.3 (a,b,c) which represent cases 1, 2, and 3, respectively. Table 5.7 lists the calculation results for the cracked section and the uncracked

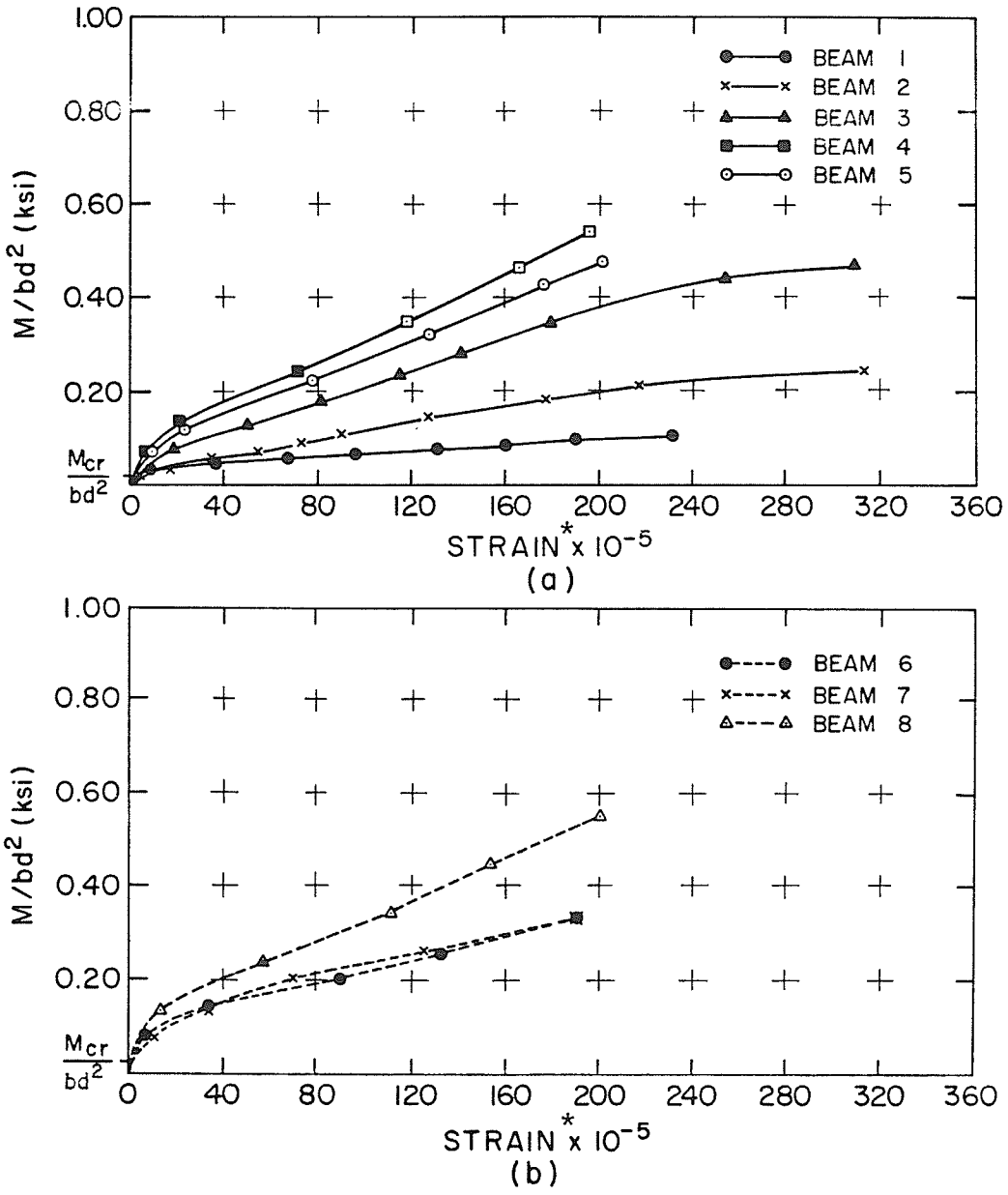

Figure 5.2 $\frac{M}{bd^2}$ - strain* curves (a) Beams 1,2,3,4 and 5
(b) Beams 6,7, and 8

---

* Strain at level of reinforcement.

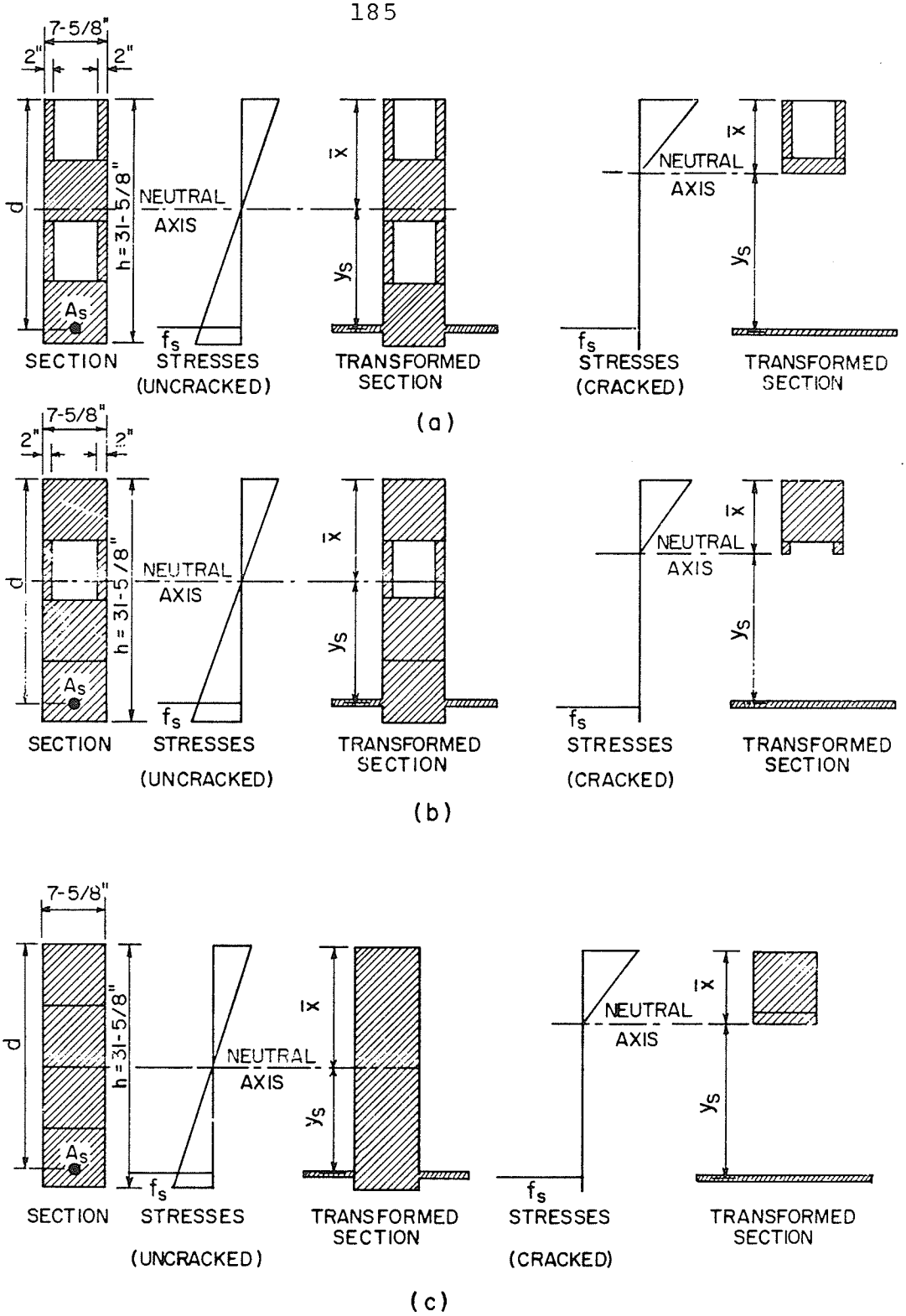

Figure 5.3 Three cross-section cases for tested masonry beams.(a) and (b) partially filled sections (c) completely filled section.

Table 5.7 Beam cross-section properties and modulus of rupture calculation.

BEAM NO.	CASE*	UNCRACKED SECTION $\bar{X}$ (IN)	y_t (IN)	I_4 (IN^4)	CRACKED SECTION $\bar{X}$ (IN)	jd (IN)	I_4 (IN^4)	M_{cr}** (K-IN)	AVERAGE f_{mr}** (P.S.I)	AVERAGE f_r*** (P.S.I)
	a	16.89	14.73	15084	7.32	26.31	2815			
1	b	15.83	15.79	19346	5.52	26.91	3121	148		
	c	16.06	15.56	20866	5.52	26.91	3121			
	a	17.34	14.28	16060	10.50	25.50	5823			
2	b	16.25	15.37	20460	8.26	26.25	6801	148		
	c	16.42	15.20	21489	8.25	26.25	6800			
	a	17.80	13.82	16679	12.72	23.01	8073		125	
3	b	16.71	14.90	21234	10.64	23.70	9906	148	106	319
	c	16.82	14.80	22889	10.48	23.76	9944		98	
	a	18.23	13.39	17318	14.20	22.02	9850			
4	b	17.14	14.48	22026	12.35	22.63	12389	148		
	c	17.20	14.42	23764	12.03	22.74	12536			
	a	18.10	13.52	17323	13.56	23.23	9453			
5	b	16.97	14.65	21979	11.60	23.88	11683	148		
	c	17.06	14.56	23683	11.35	23.97	11770			
	a	13.38	10.24	6339	8.47	17.18	2469			
6	b	12.03	11.59	8598	6.64	17.79	2971	82		
	c	12.31	11.31	9113	6.62	17.79	2971			
	a	13.47	10.15	6433	9.03	16.99	2784		128	
7	b	12.13	11.49	8738	7.12	17.63	3401	82	106	319
	c	12.40	11.22	9252	7.12	17.63	3401		98	
	a	13.73	9.9	6585	10.33	15.81	3463			
8	b	12.46	11.16	9013	8.66	16.36	4449	82		
	c	12.67	10.95	9524	8.42	16.44	4444			

* See Figure 5.3.

** See Figure 5.2 and Appendix C.

*** Modulus of rupture for concrete , see CSA Standard A23.3 - 77.

section, and gives the masonry modulus of rupture (f_{mr}) for the three different cross-sections. The results show that case 3 gives the smallest and the most appropriate value for the masonry modulus of rupture (f_{mr} = 98 p.s.i.), which is easy to calculate, because it's based on the completely filled cross-section.

Due to the lower tensile stresses in the masonry beams, it seems reasonable to retain the ρ minimum value ($\frac{80}{f_y}$) stipulated in CAN3 - S304 rather than be restricted by the higher values in CAN3 - A.23.3 for reinforced concrete.

The beam tests show also that the tensile cracks always appeared first at the mortar joint and progressed upward through the mortar joints and the blocks in a way similar to a reinforced concrete beam. The diagonal cracks usually developed midway between the end-bearing support and the loading point at 45^{o}. It was found that the presence of mortar joints did not affect the direction of this crack very much. All of this agreed with Edghill's test[9] which indicated that the existence of mortar joints did not constitute a weakness for the development of diagonal tension cracks.

The long-term cracking control was calculated for the tested beams and listed in Table 5.8. Long-term cracking control is governed by the quantity Z which limits the distribution of flexural reinforcement. The CAN3 - A.23.3-77[5] code limited the Z quantity by 175 Kip/in for

Table 5.8 Z quantity calculation for long-term cracking control

BEAM NO.	f_s (.60 f_y) (P.S.I)	d_c (IN)	A IN^2/BAR	Z* KIP/IN
1	42.1	2.87	43.84	211
2	44.7	2.62	40.03	211
3	44.6	4.37	33.36	234
4	45.9	4.87	24.78	227
5	43.0	3.87	29.55	209
6	44.9	3.62	55.28	263
7	38.5	3.62	27.64	179
8	44.9	4.37	33.36	236

* See Appendix C.

interior exposure and 145 Kip/in for exterior exposure of concrete faces. The calculation results show a higher value for Z than the code limits (see Table 5.8). This means that for the tested beam it is necessary to change the arrangement to a larger number of smaller diameter bars to reduce the effective tensile area (A) which will control the long term cracking.

Examination of the load/deflection curves (see Figure 5.4) shows that the reinforced masonry beams behave in a manner rather similar to reinforced concrete beams (i.e., beams with lower levels of steel are more ductile than those with higher values). In general, however, the reinforced masonry beams display lower ductility than similarly reinforced concrete beams. One divergence from anticipated behaviour can be seen from Figure 5.4 where a dip in the load/deflection curves can be seen following yielding of the steel (see the load-deflection for Beams 5 and 8). This effect is more noticeable in beams with heavy reinforcement. This particular effect is caused specifically by the stress concentrations introduced at the void between blocks. Local crushing takes place at this location, allowing a stress redistribution to take place. Therefore, the beam has suffered some local crushing, and perhaps some undesirable deflection and cracking; but it has not exhausted its load-carrying potential.

A comparison between the load-deflection curves of the masonry reinforced beams (see Figure 5.4) and the load deflection performance of some reinforced concrete beams having steel percentages ranging between $\rho_{minimum}$ to $\rho_{balanced}$ (see Figure 5.5) was done. The reinforced concrete beams show more ductility than the masonry beams (compare Figures 5.4 and 5.5).

The deflection for the tested beams was calculated using three different beam cross-section cases (see Figure 5.3 (a,b,c)) and two different methods of calculation. Method One calculated the approximate deflection based on the gross moment of inertia (I_g) for the uncracked cross-section (see Δ_1 in Table 5.9). Method Two was based on the effective moment of inertia (I_e) given in the CAN3 - A23.3 - 77 code (see Δ_2 in Table 5.9).

Strain readings taken across mortar joints in all tested types of prisms recorded values well in excess of (0.003) as failure approached. Thus, it appears reasonable to use the value of 0.003, as in reinforced concrete, in the application of flexure to reinforced masonry.

The strain readings for each beam were plotted and the overall results were satisfactory. In Beam #1, each individual column of "Demec" readings taken on the beam at five different specific load levels was plotted. Some deviation from linearity for each strain profile was observed. This non-linearity of the strain profile might be due to

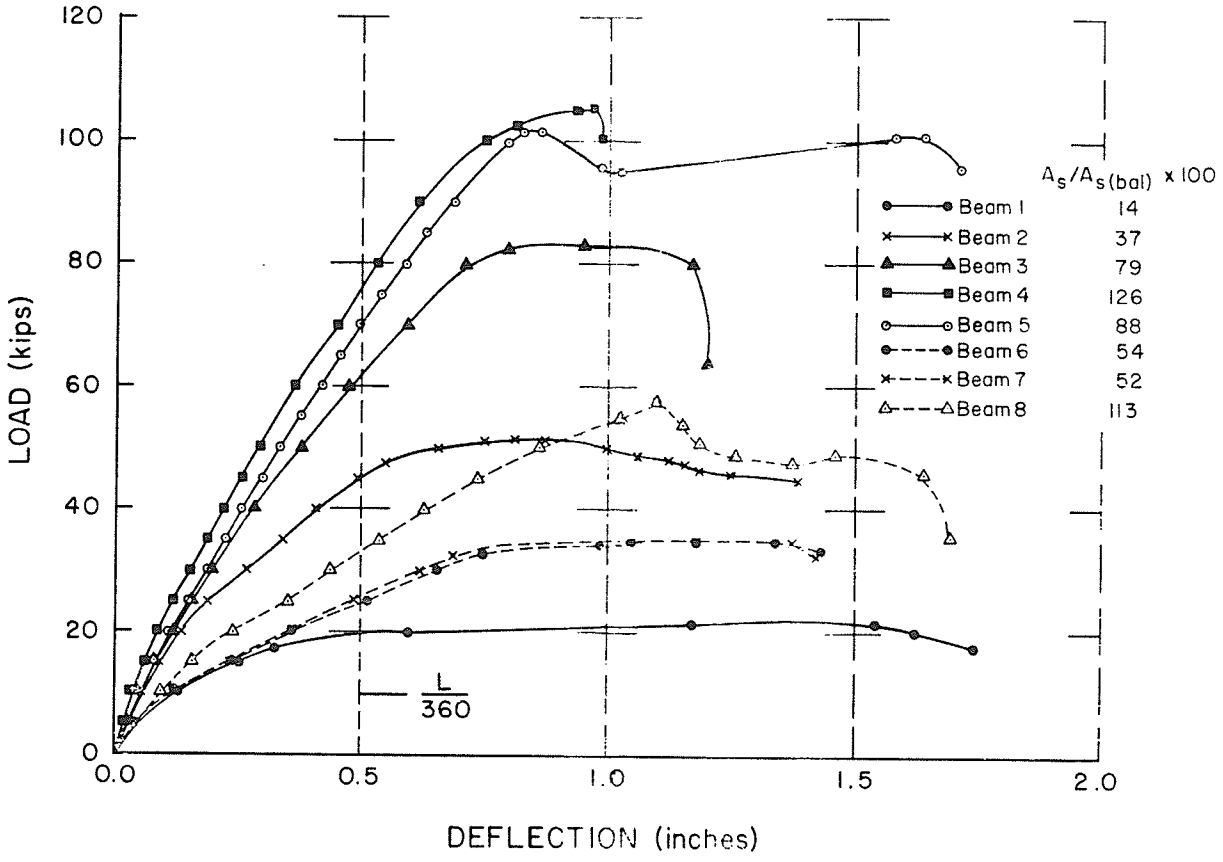

Figure 5.4 Load-deflection curves for the tested masonary beams.

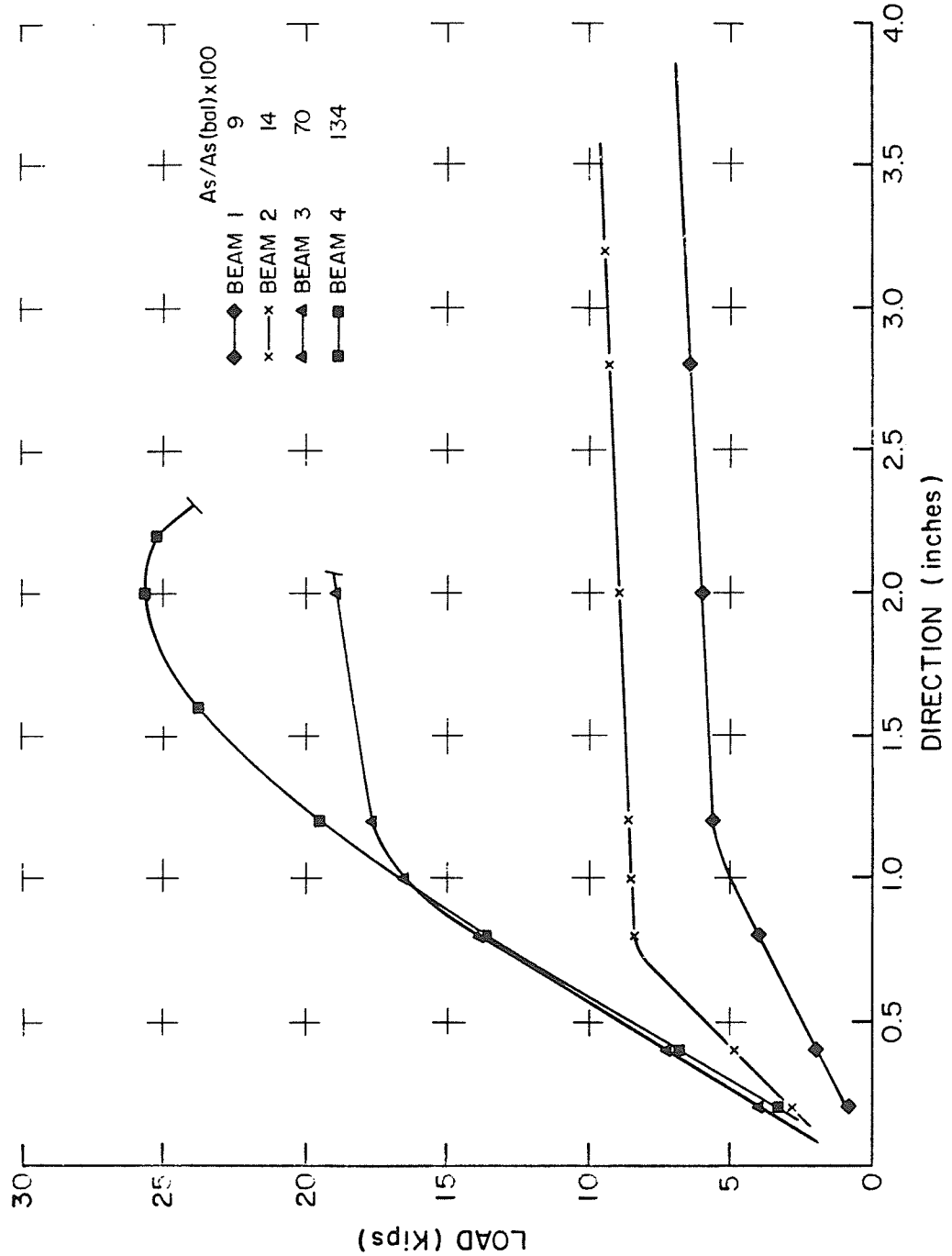

Figure 5.5 Load-deflection curves for reinforced concrete beams.

Table 5.9 Calculation of beam deflections

BEAM NO.	CASE	P (TEST) (KIPS)	M_a (APPLIED) (K-IN)	M_{cr} (CRACK) (K-IN)	I_e (IN^4)	Δ_1* (IN)	Δ_2* (IN)	Δ (ACTUAL) (IN)
	a				2916	.08	.42	
1	b	21.6	734	148	3254	.06	.38	1.60
	c				3266	.06	.38	
	a				5831	.18	.50	
2	b	51.0	1616	148	6811	.14	.43	.90
	c				6811	.14	.43	
	a				8073	.29	.59	
3	b	83.0	2576	148	9908	.22	.48	1.16
	c				9947	.21	.48	
	a				9851	.35	.62	
4	b	105.5	3251	148	12390	.28	.49	.96
	c				12537	.25	.48	
	a				9454	.34	.62	
5	b	102.0	3146	148	11684	.27	.50	.73
	c				11771	.25	.50	
	a				2470	.32	.81	
6	b	34.8	1108	82	2973	.23	.67	1.36
	c				2973	.22	.67	
	a				2785	.31	.72	
7	b	34.9	1111	82	3403	.23	.59	1.38
	c				3403	.22	.59	
	a				3463	.50	.96	
8	b	57.6	1792	82	4449	.37	.74	1.08
	c				4444	.35	.74	

* See Appendix C.

a crack developing within the gauge length in some parts of the beams and outside the gauge length in the other parts. An average of all six sets of "Demec" readings from both faces of the beam gives the best plot of the strain profile. The result showed a reasonable linear strain profile. For Beam #1 to Beam #8, only the average of the strain readings at each face, and the average of the strain readings at both faces are shown. From the average strain readings plotted for each beam, it was evident that the measured strain profiles for each beam were reasonably linear. It can be concluded that the assumption of plane sections remaining plane during bending is applicable to reinforced masonry beam design.

The longitudinal strain of the reinforcement was also plotted on the average strain diagram for Beam #1 and Beam #3. Beam #1 and Beam #2 showed that the measured concrete strains at the same depth as the longitudinal reinforcement agreed reasonably well with the measured longitudinal reinforcement strains. It was evident that a good bond had been achieved at the contact surface between the steel and the concrete fill. However, Beam #3 showed much higher strains on the longitudinal reinforcement compared to the measured concrete strains at the same level.

An inspection was carried out after testing found that flexural cracks had developed across the strain gauge which was attached to the reinforcement. A higher steel strain was developed at that location.

The typical movement of the neutral axis during loading was not as pronounced in some of the beams. This might be due to the small inaccuracies in individual strain measurements and small errors in the location of gauge lines. Nevertheless, the general behaviour was that the neutral axis was observed moving upward in the beam with small percentages of steel and moving downward in the beams with high percentages of steel. For beam #2 which had a small percentage of steel, there was a clear upward movement of the neutral axis with increasing load (see Figure 3.18). This behaviour agrees well with that of reinforced concrete beams.

From the actual test results, it was found that the maximum attainable shear stress as analyzed by CSA Standard S304 - 1977 [6] was quite conservative. The code limits the maximum allowable shear stresses for flexural members to 0.05 f_m' p.s.i. or 150 p.s.i., whichever is lower. However, Beam #4 experienced a shear stress of 280 p.s.i. with no sign of shear failure observed. Although this investigation was not addressed to the question of shear stress, it is apparent that the code limitations are conservative; and there is a need for further research in this area.

CHAPTER 6

CONCLUSIONS AND RECOMMENDATIONS

6.1 CONCLUSIONS

A number of problems are encountered in masonry beams, such as discontinuities in the concrete fill and poor bond between concrete fill, mortar and block. The effect of these on the behaviour of beams was part of this thesis program. This included studying the behaviour of masonry beams in flexure which also requires a deep understanding of how the compression zone is affected by the voids between the blocks.

Single-block specimens and two-block prisms were tested and analyzed using F.E.M. analysis. A suitable value of f_m' was determined and a study of the mode of failures was done.

Two series of reinforced concrete masonry beams, representing a total of eight beams, were built and tested. Each beam had a different percentage of tensile steel reinforcement. The Ultimate Strength Theory with an appropriate value for f_m' was used for the design of the masonry beams.

Based on test results and theoretical analysis of the specimens, prisms, and beams, the following main conclusions have been reached:

(1) Reinforced masonry beams can be safely designed using the Ultimate Strength Theory based on "CSA Standard CAN3 - A23.3 - 77 "Code for the Design of Concrete Structure for Buildings." [5] The maximum usable strain used for the design of masonry beams was 0.003 as stated in the code for concrete beams. However, a few minor adjustments to the theory had to be made with reference to the CSA Standard S304 - 1977 on "Masonry Design and Construction for Buildings."[6]

(2) The value of f_m' which should be used in the Ultimate Strength Theory instead of f_c' was obtained from the CSA Standard 304 - 1977 on "Masonry Design and Construction for Buildings," [6] with the unfilled block unit being loaded in the direction in which it will be stressed.

(3) The assumption of plane section before bending remaining plane after bending can be applied in the masonry beam design.

(4) The range of reinforcement that may be used in reinforced masonry appears to be similar to that for reinforced concrete. However, because of the reduced ductility in flexure, it is probably wise to restrict the steel ratio ρ to values below 0.6 $\rho_{balanced}$ compared to 0.75 $\rho_{balanced}$ for reinforced concrete. Furthermore, as

reinforced masonry has a lower tensile strength than reinforced concrete due to discontinuities, it seems reasonable to retain the minimum value stipulated in CAN3 - S304 rather than be restricted by the higher values in CAN3 - A23.3 for reinforced concrete.

(5) Using horizontal mortar joint reinforcement at the compression zone of the masonry beams is not recommended. The lateral buckling of this reinforcement during testing destroys the horizontal mortar joint and, therefore, its confinement which helped to prevent splitting in the center of the beam's top course.

(6) The finite element analysis is an excellent technique for depicting the stress and strain distributions in the tested specimens. After using both the two and three dimensional F.E.M. analysis, it was concluded that the two dimensional analysis is sufficient for analyzing single and two-block specimens, and masonry beams.

(7) Finally, it should be borne in mind that the beams tested were prepared in the laboratory under controlled, nearly ideal conditions, and that the quality of masonry work on the job site is not likely to be as good. This is probably more so for masonry than concrete. Consequently, the use of a performance factor as high as 0.9 seems inad-

visable. Performance factors varying from 0.90 to 0.75 as the steel ratio increases from the minimum to the maximum values would be more reasonable.

6.2 RECOMMENDATIONS AND SUGGESTED FUTURE RESEARCH

(1) CSA Standard S304 - 1977 [6] limits the maximum allowable shear stress for flexural members to 0.05 f_m' p.s.i. or 150 p.s.i., whichever is lower. The results of these tests show a much higher shear capacity than that allowed. It is recommended that a research project be undertaken to find a more rational allowable shear stress.

Eventually, an Ultimate Strength Design approach should be considered in evaluating shear as well as flexural capacity for reinforced masonry beams. Further investigation is required.

(2) Two-and three-dimensional finite element analysis needs to be developed for masonry beams, taking into account the plastic behaviour of the materials used for construction.

(3) Due to the low ductility of the singly reinforced masonry beams found in this project, masonry beams designed with both top and bottom steel may be more desirable. It is suggested that a research project on doubly reinforced

masonry beams be undertaken and the flexural capacity and ductility for the beams be evaluated.

(4) It is suggested that tests be carried out on reinforced masonry beams with similar dimensions and reinforcement, but changing the block type used. Shear capacity, flexural capacity and ductility of each beam type could then be compared and evaluated.

BIBLIOGRAPHY

(1) ACI Standard 318 - 1971, "Building Code Requirements for Reinforced Concrete". American Concrete Institute, Detroit, Michigan, 103 pp.

(2) Amrhein, J.E. 1978, "Reinforced Masonry Engineering Handbook". Masonry Institute of America, Los Angeles, Calif., 3rd ed., 445 pp.

(3) Bathe, K.J., Wilson, E.L. and Peterson, F.E. June 1973, "SAP IV, A Structural Analysis Program for Static and Dynamic Response of Linear Systems". Earthquake Engineering Research Center (Report No. EERC 73-11) College of Engineering, University of California, Berkeley, Calif., n.p.

(4) Baydack, Donald A. 1972, "An Investigation of Concrete Block - Formed Beams". Master's Thesis, University of Manitoba, Winnipeg, Manitoba; 129 pp.

(5) CSA Standard CAN3 - A23.3 - 77, "Code for the Design of Concrete Structures for Buildings". Canadian Standards Association, Rexdale, Ontario; 131 pp.

(6) CSA Standard CAN3 - S304 - 77, "Masonry Design and Construction for Buildings". Canadian Standards Association, Rexdale, Ontario; 91 pp.

(7) CSA Standard CAN3 - A179 - 75, "Mortar and Grout for Unit Masonry". Canadian Standard Association, Rexdale, Ontario; 20 pp.

(8) Doherity, W.P., Wilson, E.L and Taylor, R.L. Jan. 1969, "Stress Analysis of Axisymmetric Solids Utilizing Higher-order Quadrilateral Finite Elements". Structural Engineering Laboratory (Report No. S.E.S.M. 69-3), University of California, Berkeley, Calif., n.p.

(9) Edghill, Richard L. 1971, "An Investigation of Block-formed Structural Members". Master's Thesis, University of Manitoba, Winnipeg, Manitoba; 163 pp.

(10) Hamid, A.A. and Drysdale, R.G. 1980, "Concrete Masonry under Combined Shear and Compression along the Mortar Joints". ACI Journal, September - October 1980, No. 5, Proceedings V. 77, pp. 314 - 320.

(11) Hatzinikolas, M., Longworth, J. and Warwaruk, J. 1980, "Failure Modes for Eccentrically Loaded Concrete Block Masonry Walls". ACI Journal, July - August 1980, No. 4, Proceedings V.77, pp. 258 - 263.

(12) Hilsdorf, H.K. 1967, "Investigation into the Failure Mechanisms of Brick Masonry Loaded in Axial Compression". International Conference on Masonry Structural Systems, University of Texas at Austin; pp. 34 - 41.

(13) Hilsdorf, H.K. 1972, "Masonry Materials and Their Physical Properties". Proceedings, ASCE - IABSE International Conference on Planning and Design of Tall Buildings, V. III, Bethlehem; pp. 981 - 999.

(14) Mattock, Alan H. 1965, "Flexural Mechanics of Reinforced Concrete". Proceedings of the International Symposium on Flexural Mechanics of Reinforced Concrete, Miami, Fla., Nov. 10 - 12, 1964. American Society of Civil Engineers; pp. 143 - 181.

(15) Page, A.W. 1978, "Finite Element Model for Masonry." ASCE Journal, August 1978, V. 104, No. ST8; pp. 1267 - 1285.

(16) Park, R. and Paulay, T. 1975, "Reinforced Concrete Structures". John Wiley & Sons, New York, 769 pp.

(17) Plewes, Gordon W. 1978, "Masonry Bibliography 1900 - 1977". International Masonry Institute, Washington, D.C., 345 pp.

(18) Rathbone, A.J. 1980, "The Behaviour of Single - Course Reinforced Concrete Blockwork Beams". Proceedings Second Canadian Masonry Symposium, Ottawa, Canada, pp. 259 - 274.

(19) Thomas, F.G. 1953, "The Strength of Brickwork". The Structural Engineer, London, V. 31, No. 2, 35 pp.

APPENDIX A

F.E.M. ANALYSIS RESULTS

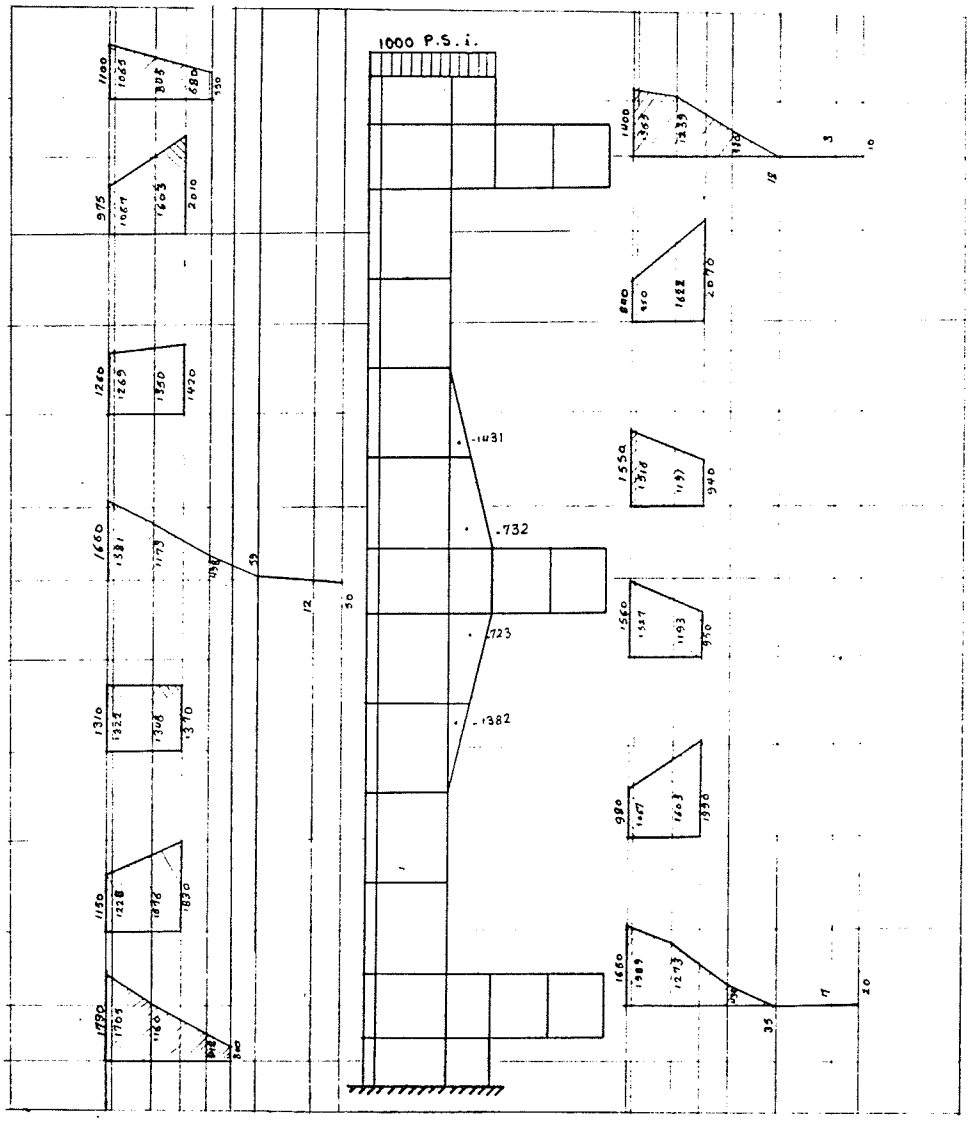

Figure A.1 Direct vertical stresses for the unfilled single-block specimen with PIN/FIX end conditions.

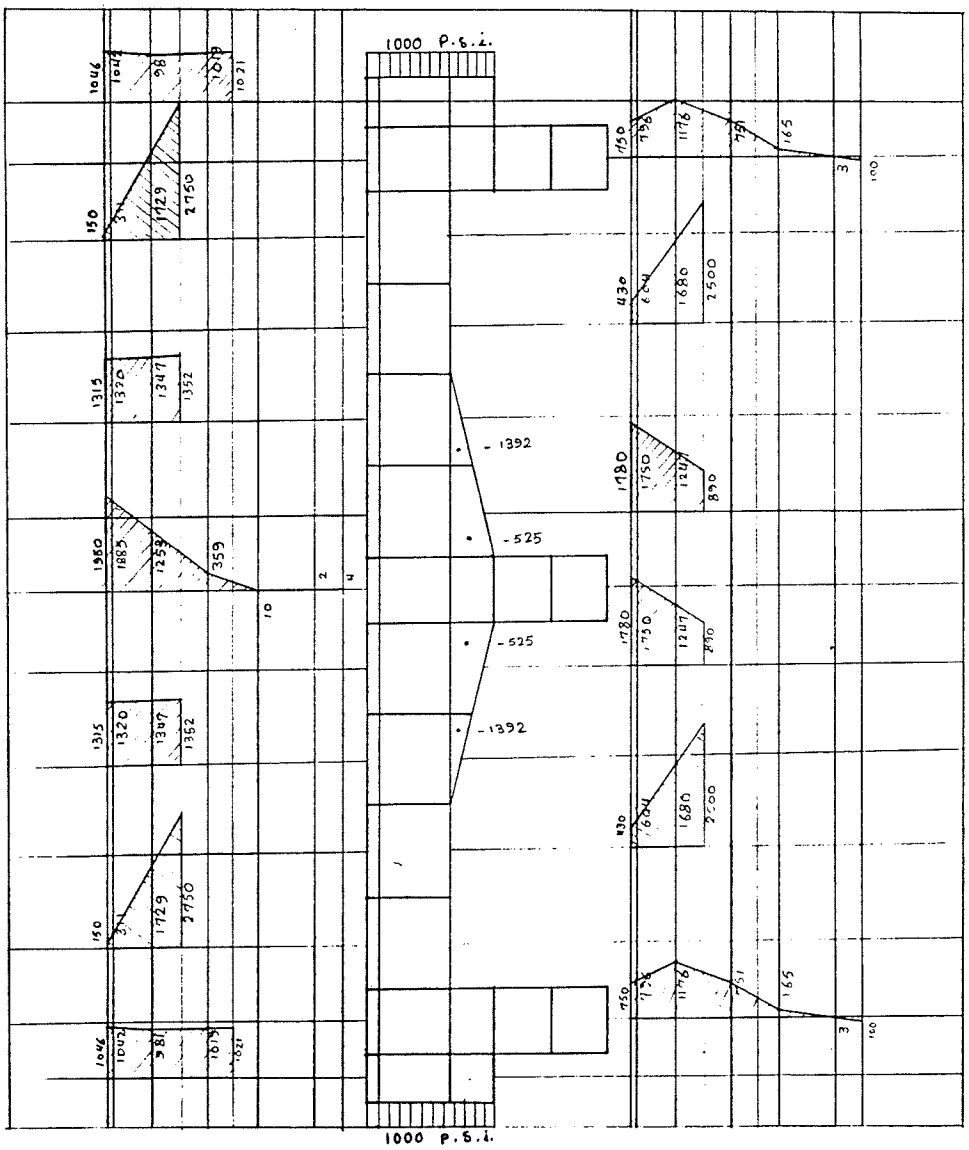

Figure A.2 Direct vertical stresses for the unfilled single-block specimen with PIN/PIN end conditions.

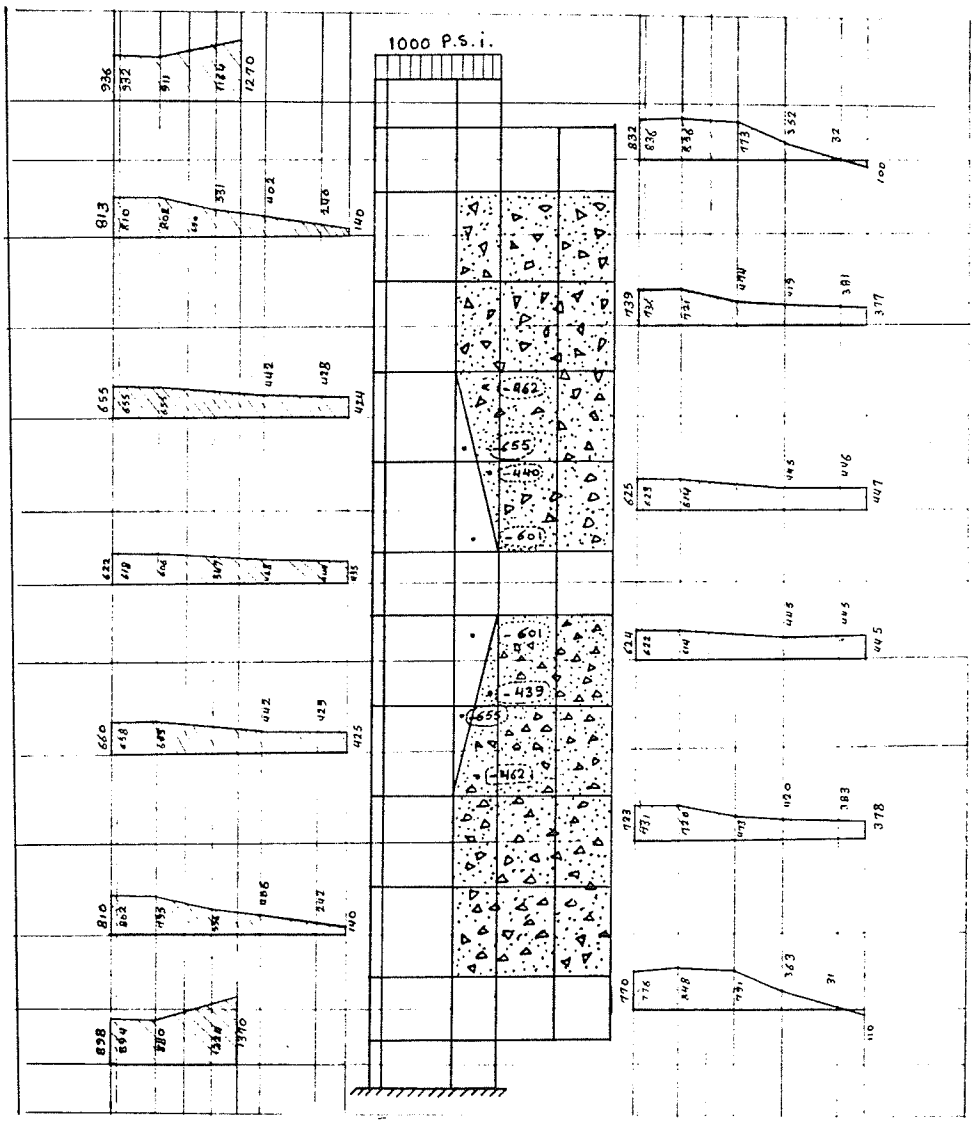

(a)

Figure A.3 Stresses for the partially filled single-block specimen with PIN/FIX end conditions (a) Direct vertical stresses (b) Direct horizontal stresses (c) Shear stresses

Figure A.3 continued

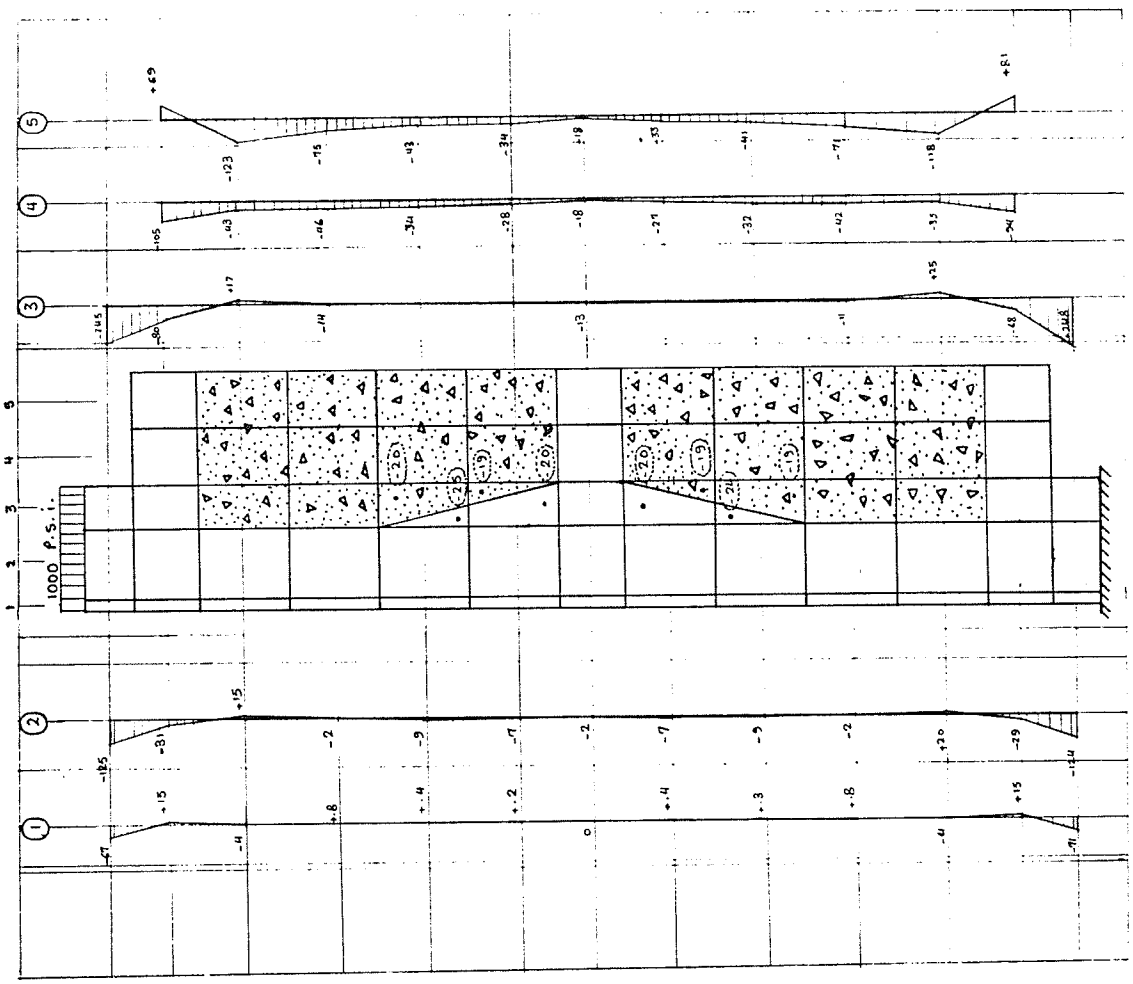

(b)

(c)

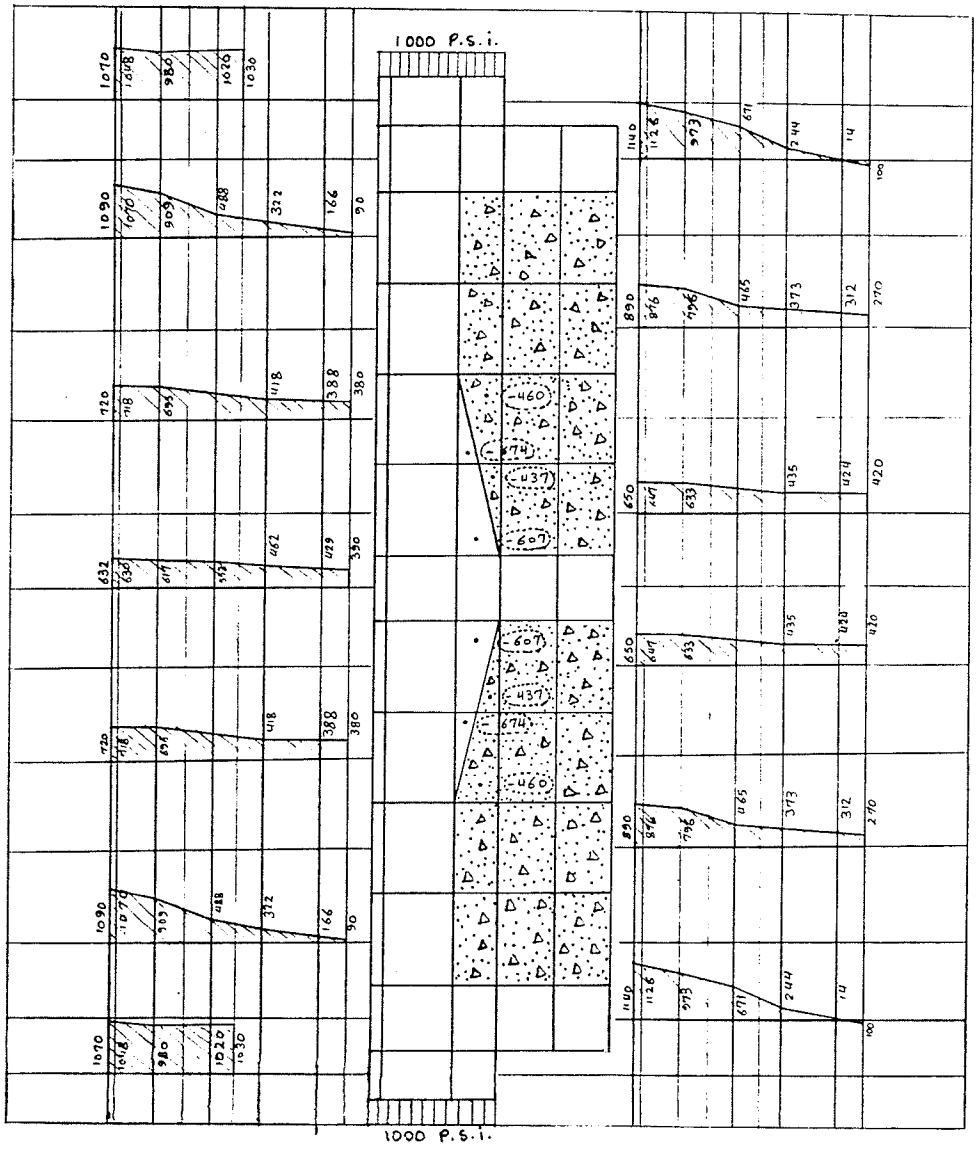

(a)

Figure A.4 Stresses for the partially filled single-block specimen with PIN/PIN end conditions (a) Direct vertical stresses (b) Direct horizontal stresses (c) Shear stresses

Figure A.4 continued

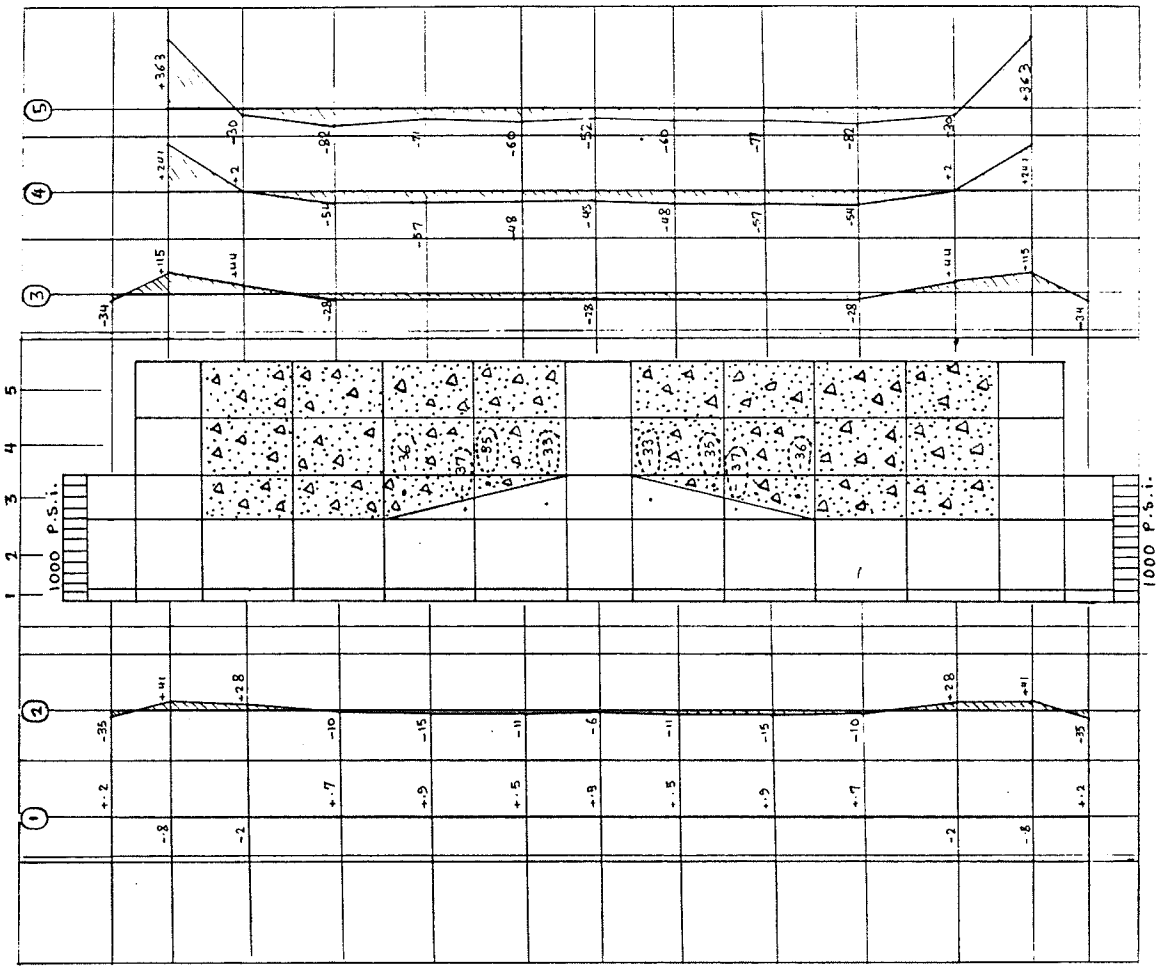

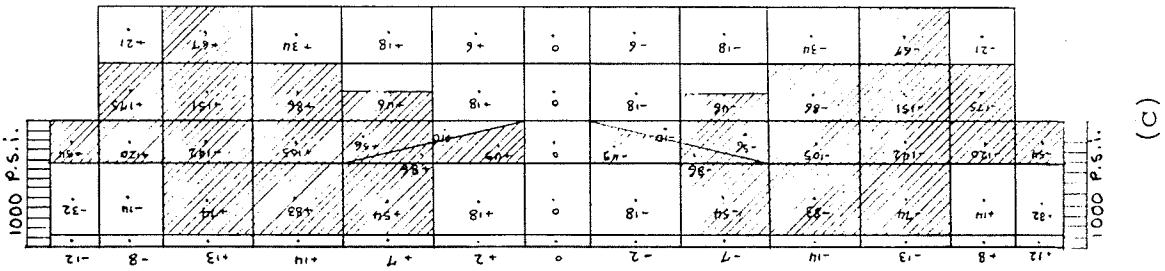

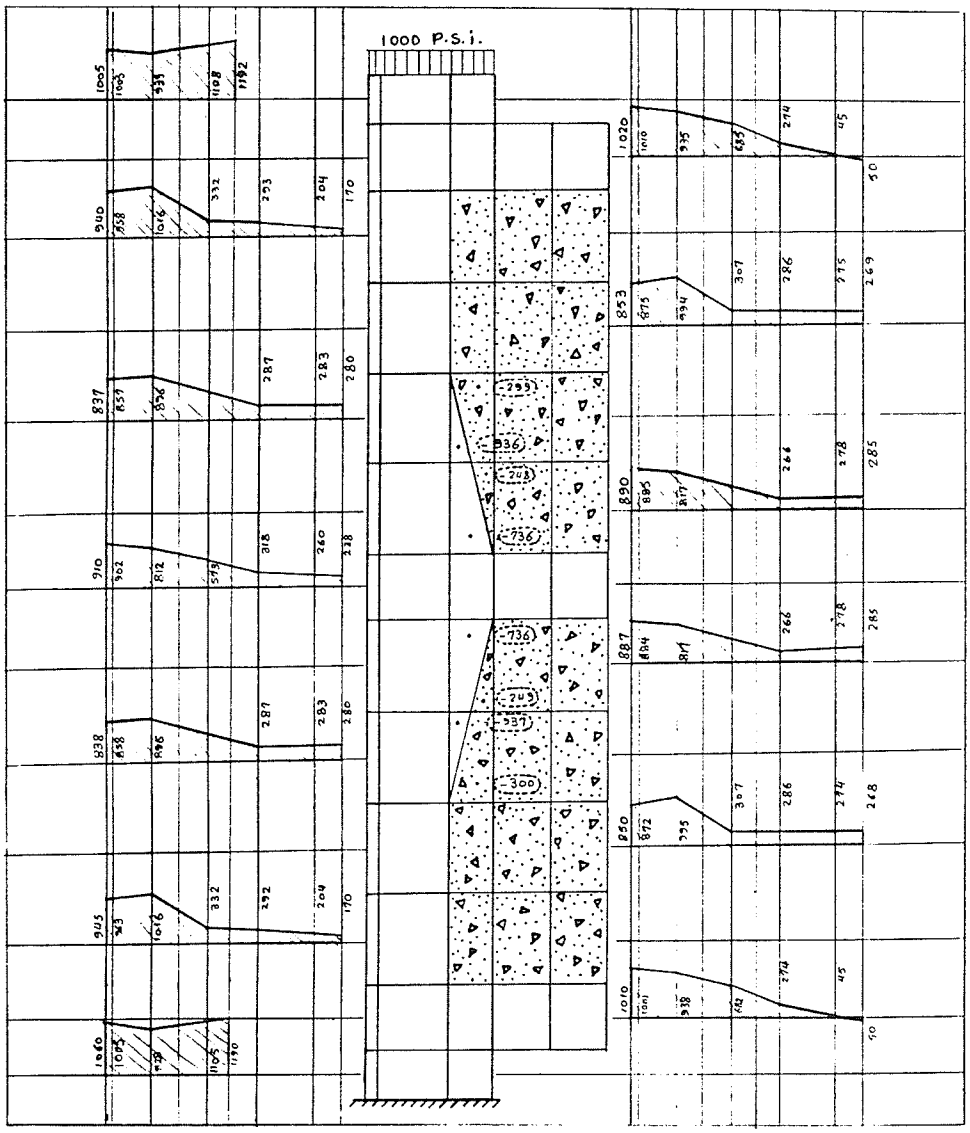

(a)

Figure A.5 Stresses for the partially filled single-block specimen with PIN/FIX end conditions and f_c' = 500 p.s.i.
(a) Direct vertical stresses
(b) Direct horizontal stresses
(c) Shear stresses

Figure A.5 continued

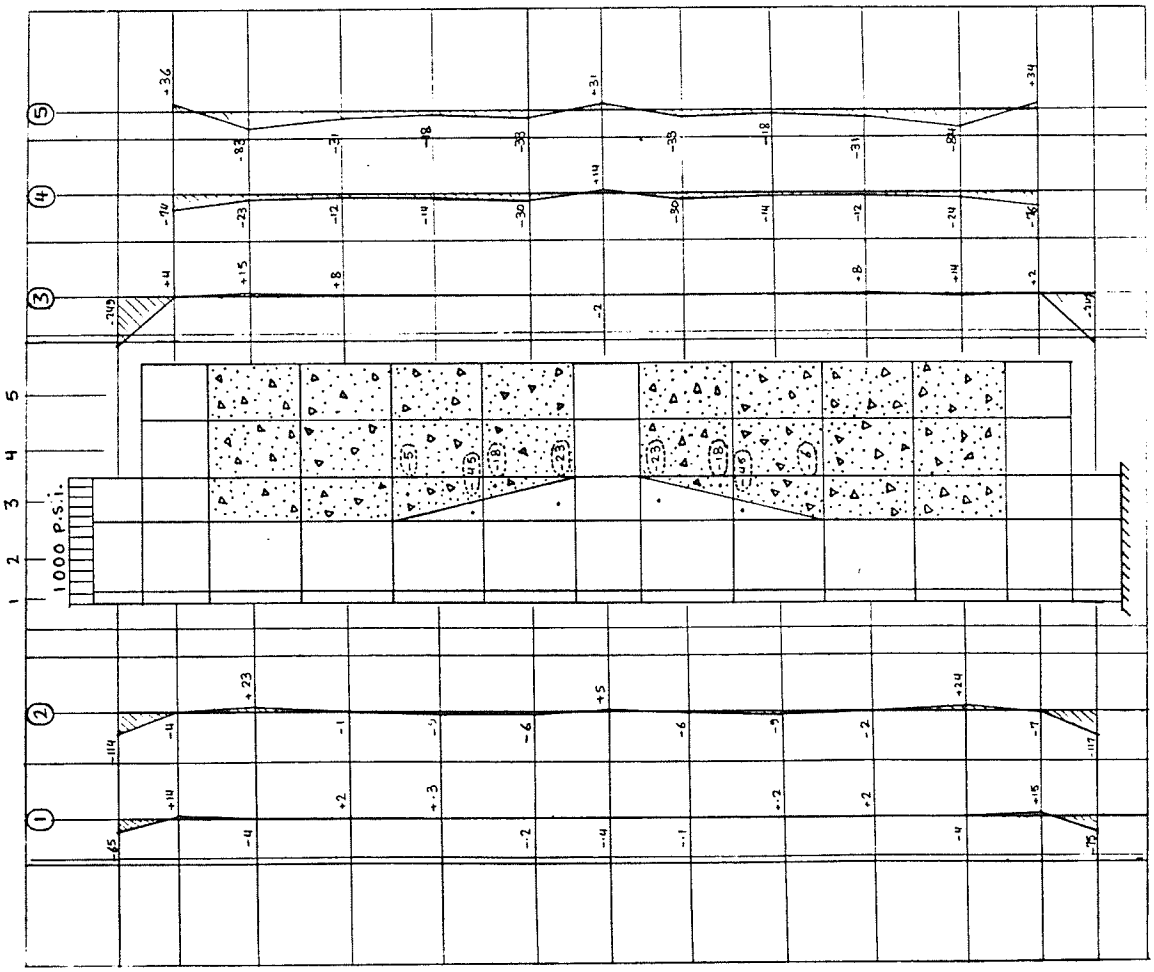

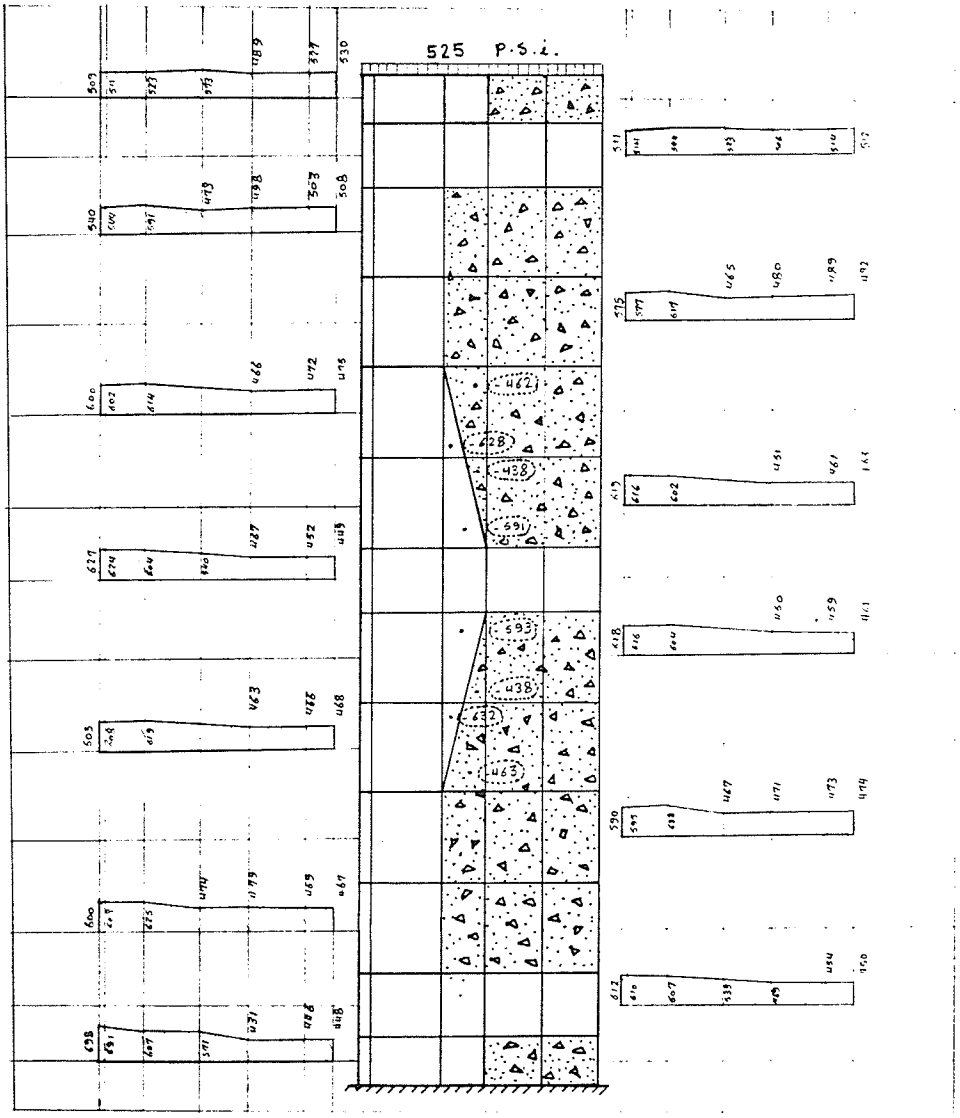

Figure A.6 Direct vertical stresses for the completely filled single-block specimen with PIN/FIX end conditions.

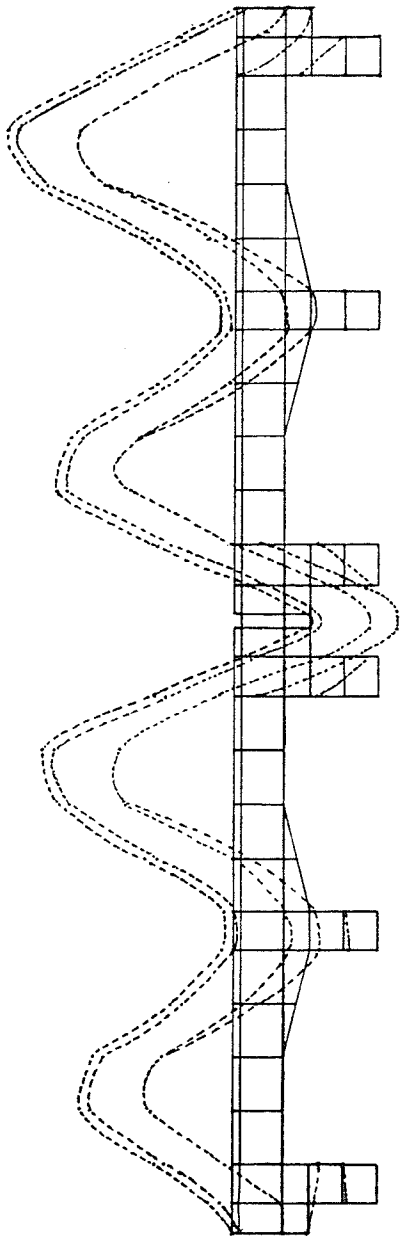

Figure A.7 Magnified lateral deflection for the unfilled two-block prism.

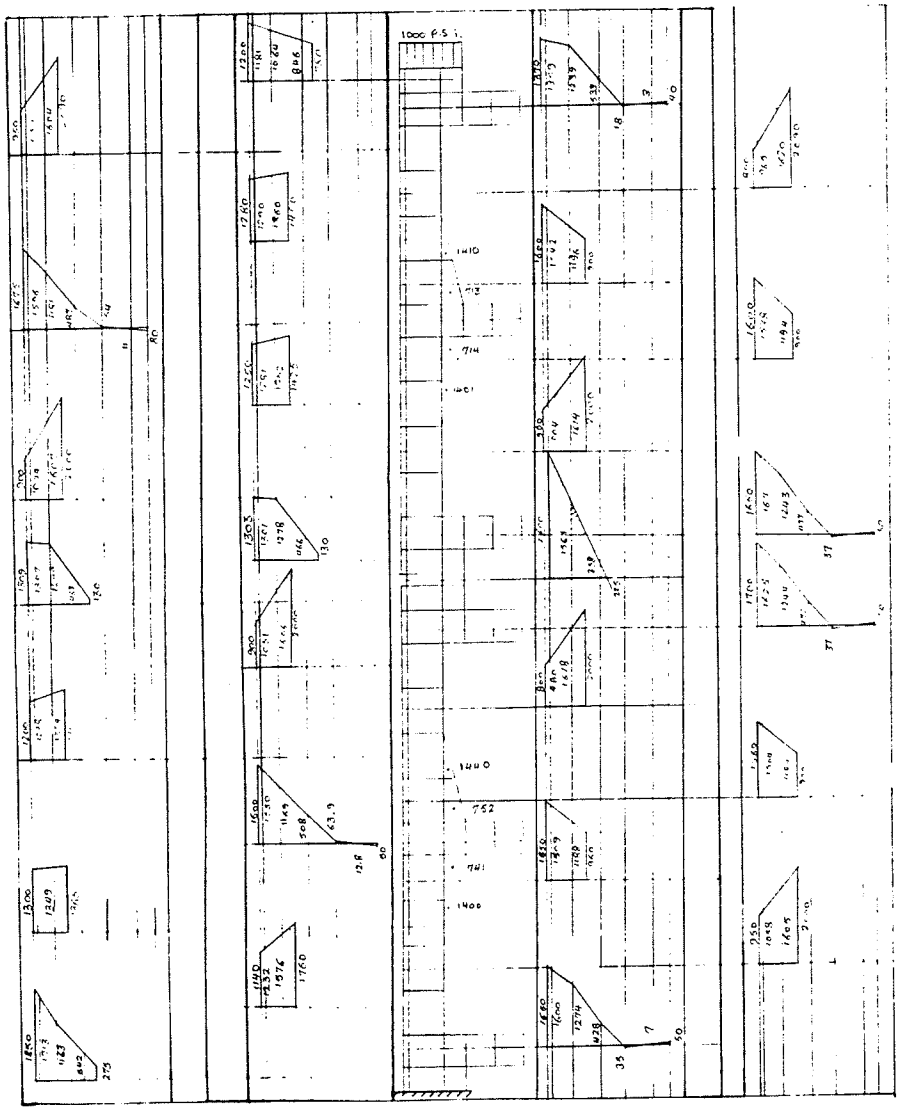

Figure A.8 Direct vertical stresses for the unfilled two-block prism with PIN/FIX end conditions.

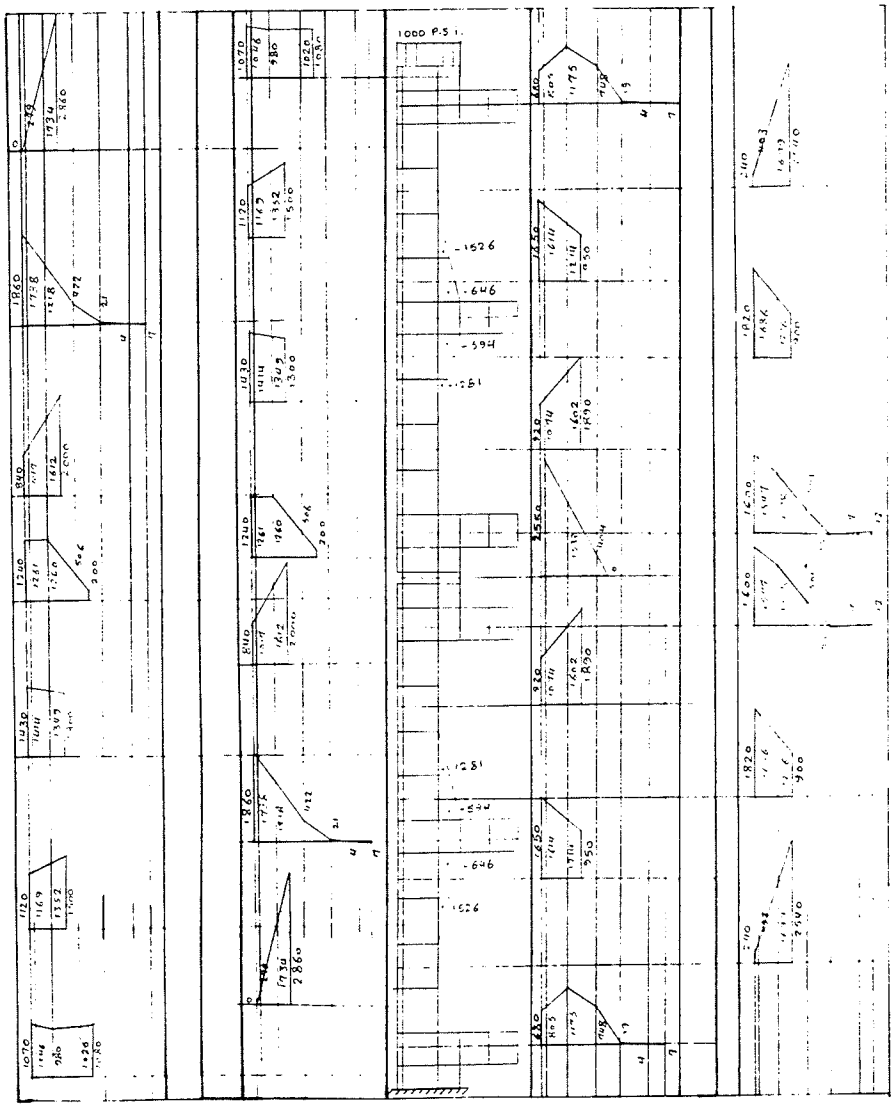

Figure A.9 Direct vertical stresses for the unfilled two-block prism with PIN/PIN end conditions.

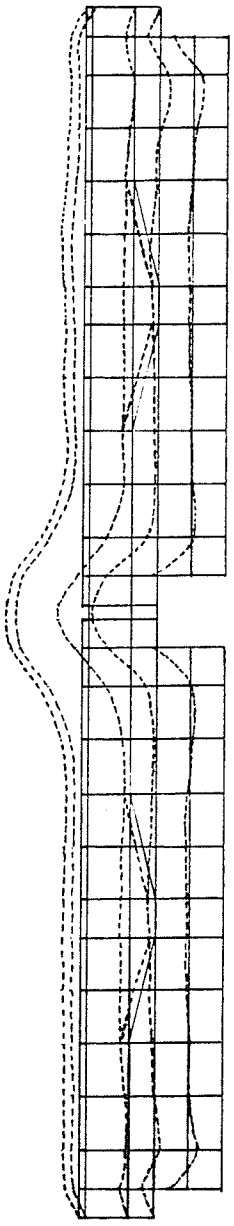

Figure A.10 Magnified lateral deflection for the partially filled two-block prism.

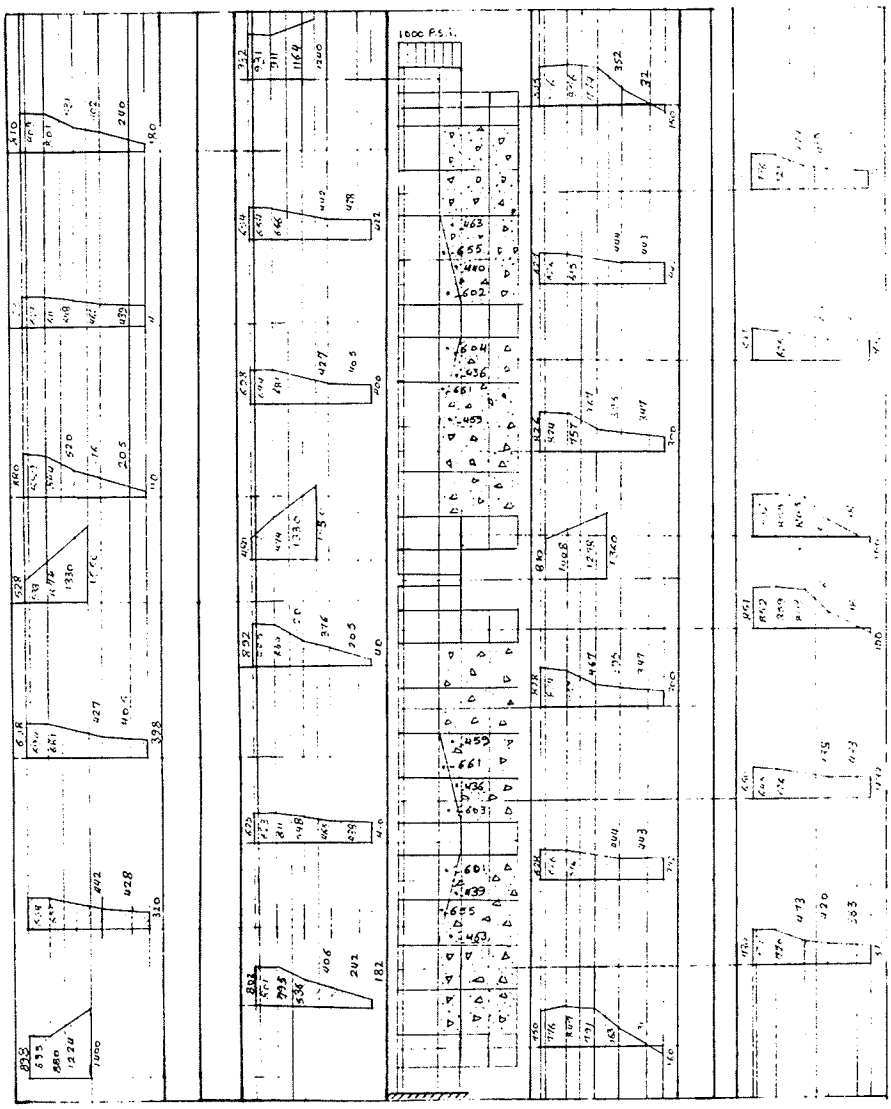

(a)

Figure A.11 Stresses for the partially filled two-block prism with PIN/FIX end conditions (a) Direct vertical stresses (b) Direct horizontal stresses (c) Shear stresses

Figure A.11 continued

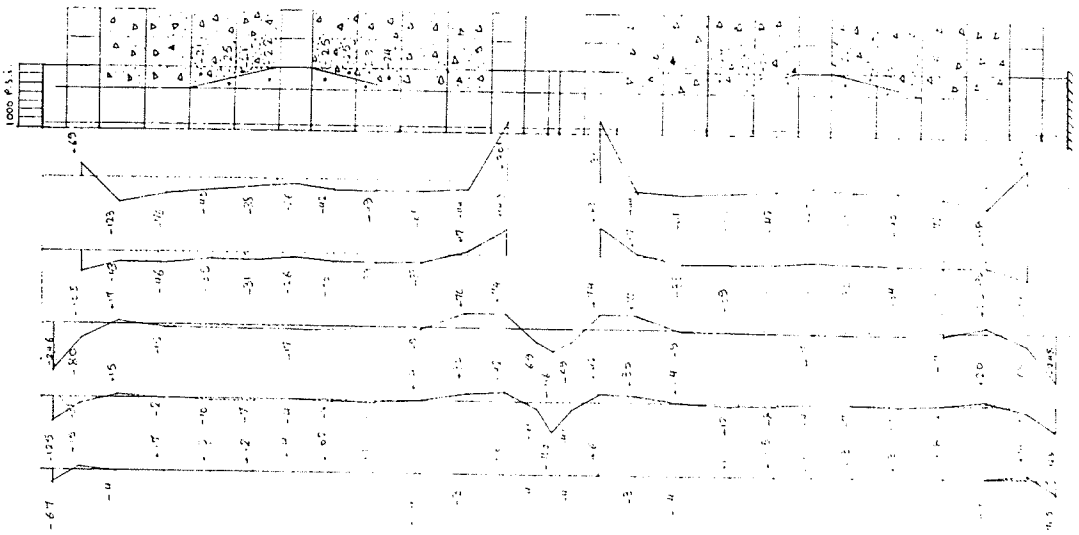

(b)

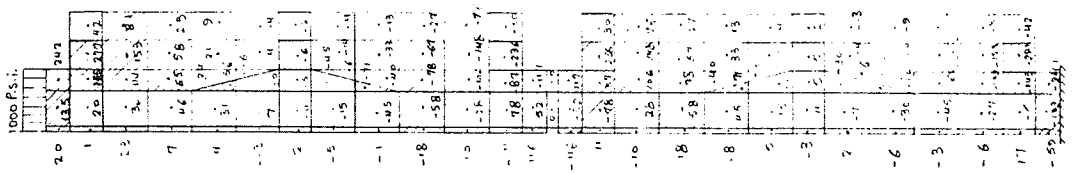

(c)

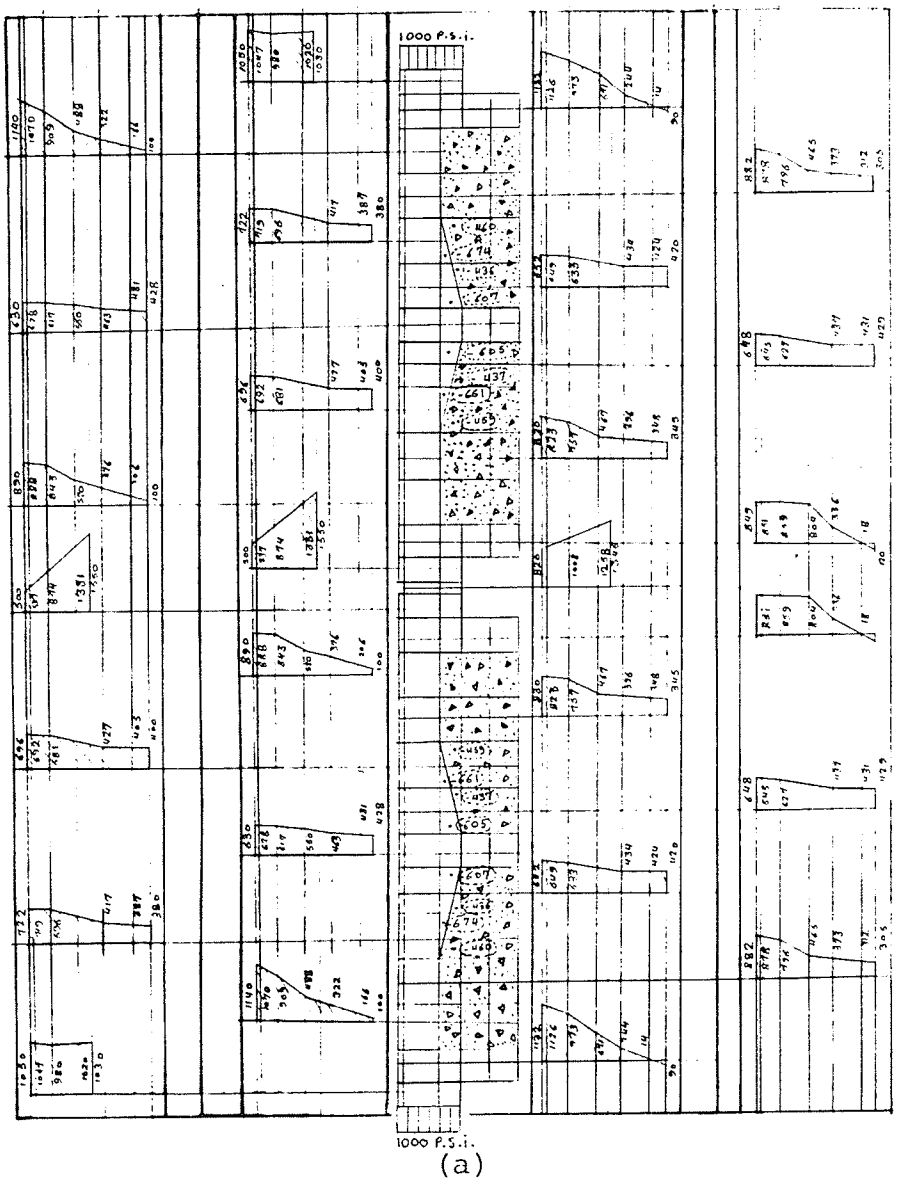

(a)

Figure A.12 Stresses for the partially filled two-block prism with PIN/PIN end conditions (a) Direct vertical stresses (b) Direct horizontal stresses (c) Shear stresses

Figure A.12 continued

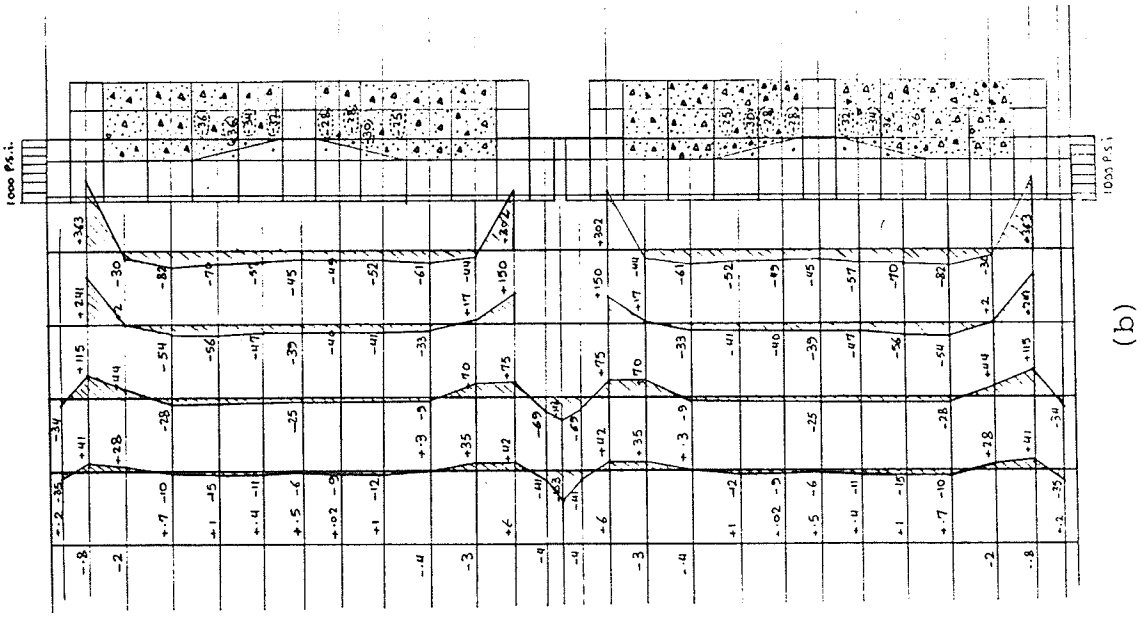

(b)

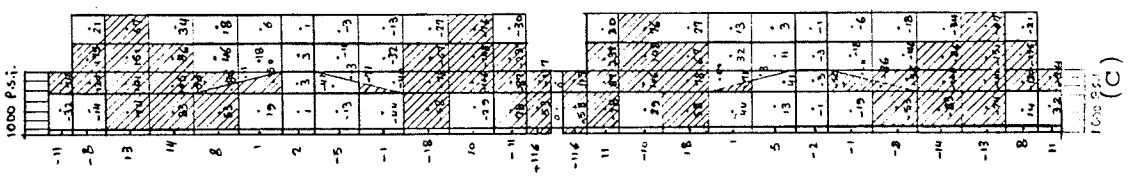

(c)

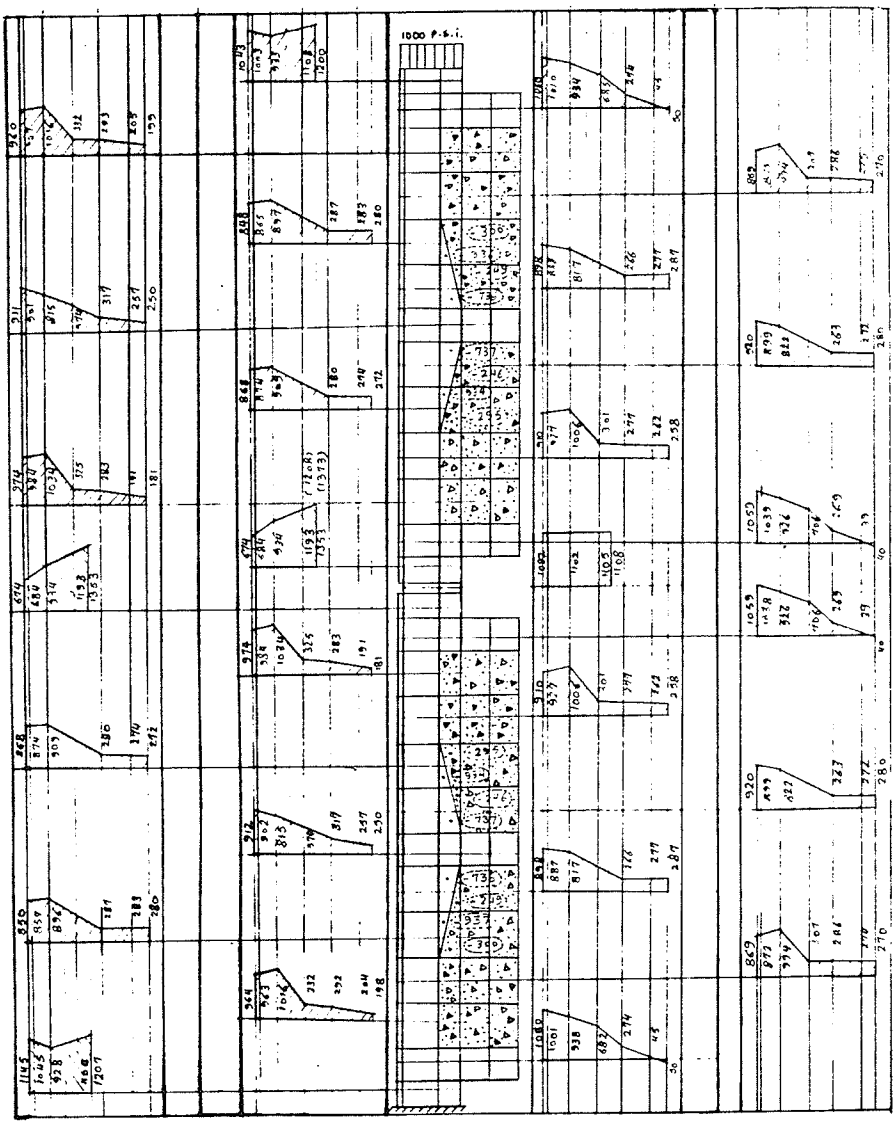

(a)

Figure A.13 Stresses for the partially filled two-block prism with PIN/FIX end conditions and f_G' = 500 p.s.i.
(a) Direct vertical stresses
(b) Direct horizontal stresses
(c) Shear stresses

Figure A.13 continued

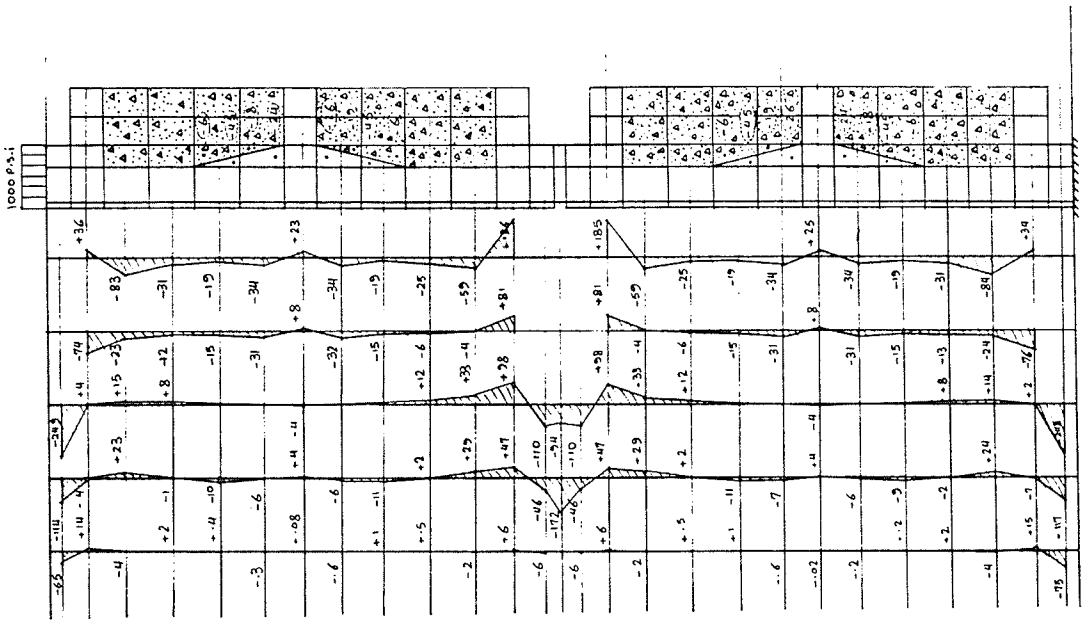

(b)

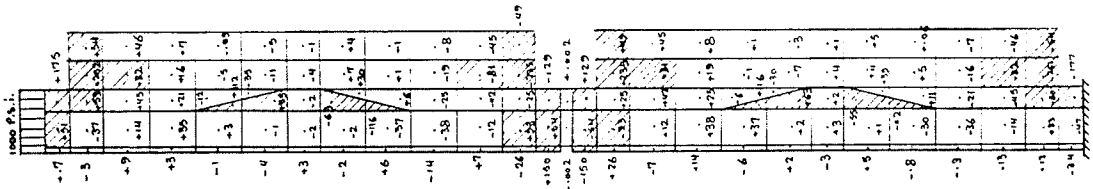

(c)

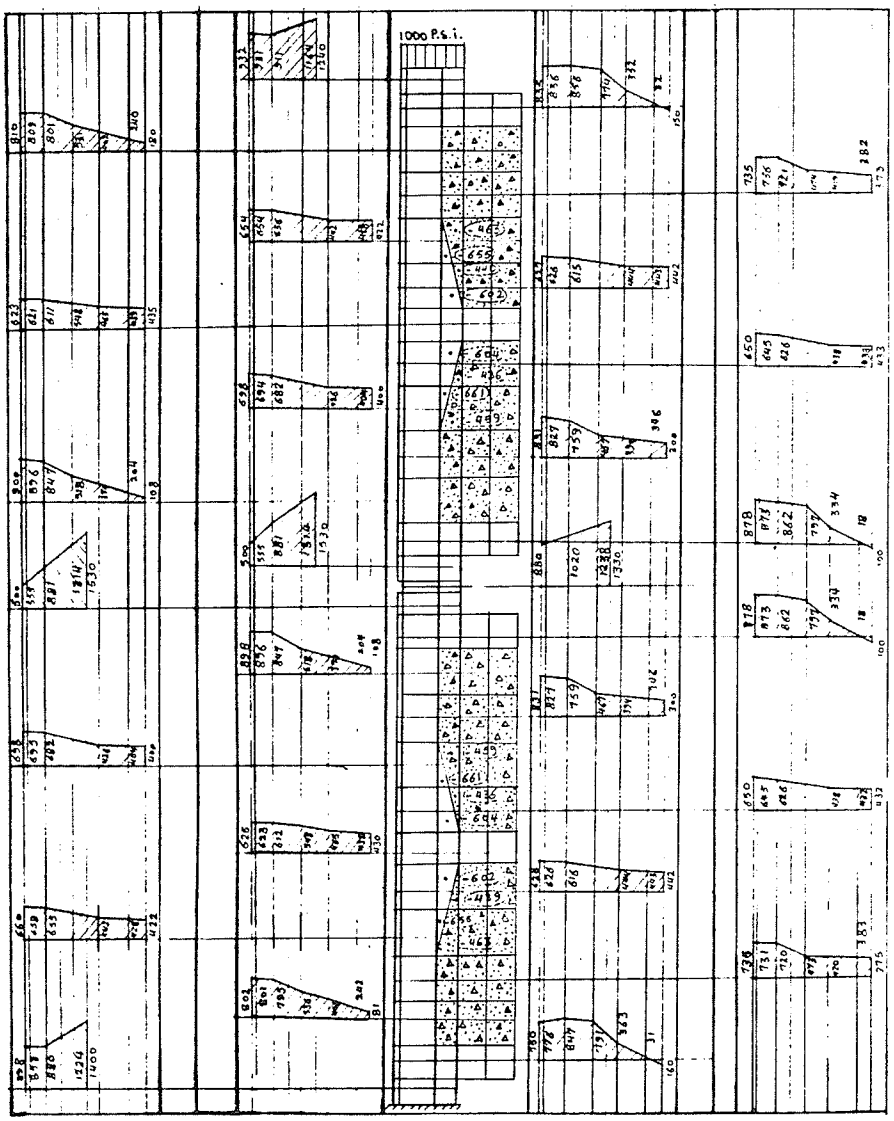

(a)

Figure A.14 Stresses for the partially filled two-block prism with PIN/FIX end conditions and f_M' = 500 p.s.i.
(a) Direct vertical stresses
(b) Direct horizontal stresses
(c) Shear stresses

Figure A.14 continued

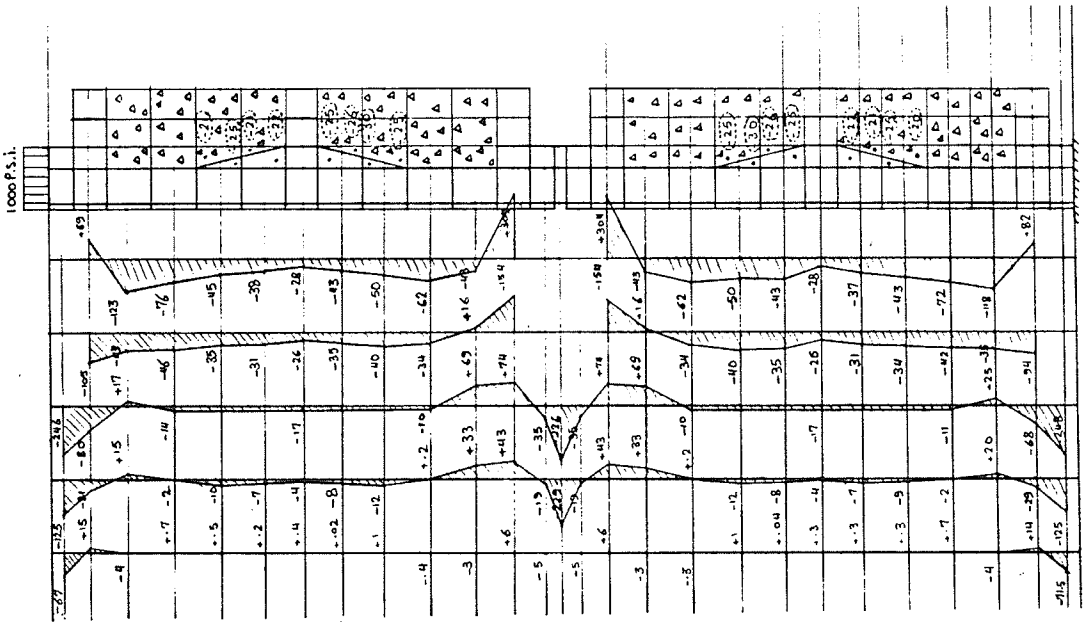

(b)

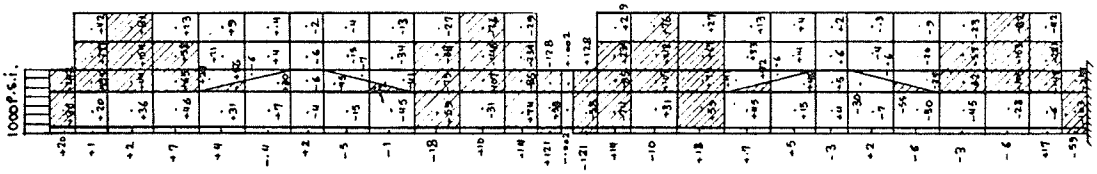

(c)

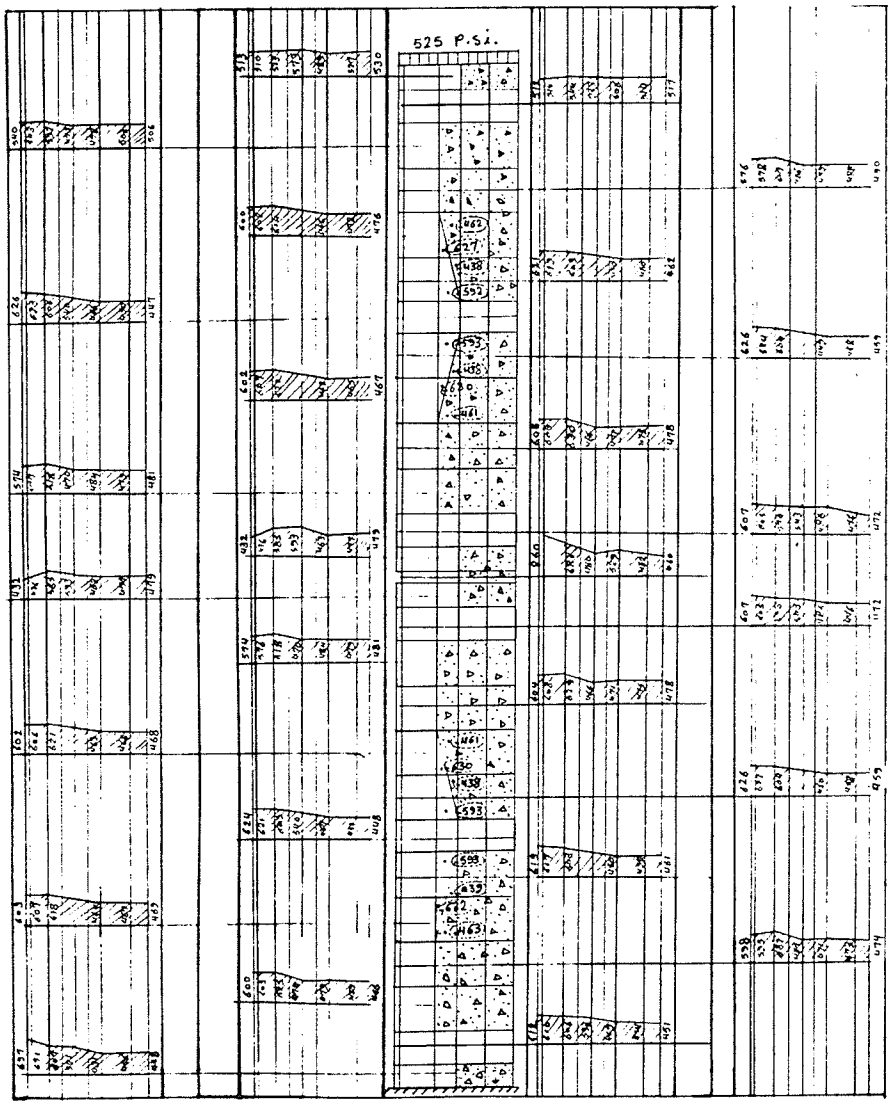

Figure A.15 Direct vertical stresses for the completely filled two-block prism with PIN/FIX end conditions.

(a)

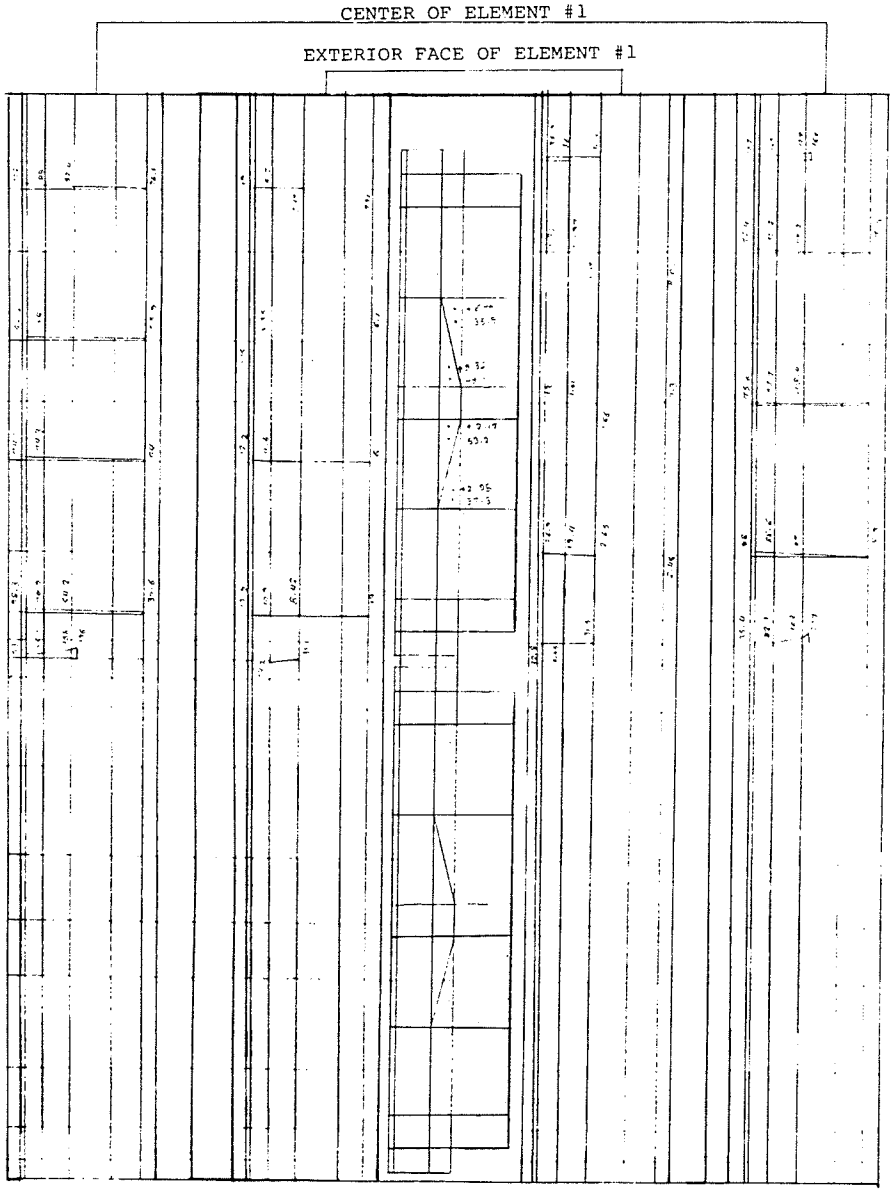

Figure A.16 Direct vertical stresses at six different sections for the partially filled two-block prism eccentrically loaded with PIN/PIN end conditions.

Figure A.16 continued

(b)

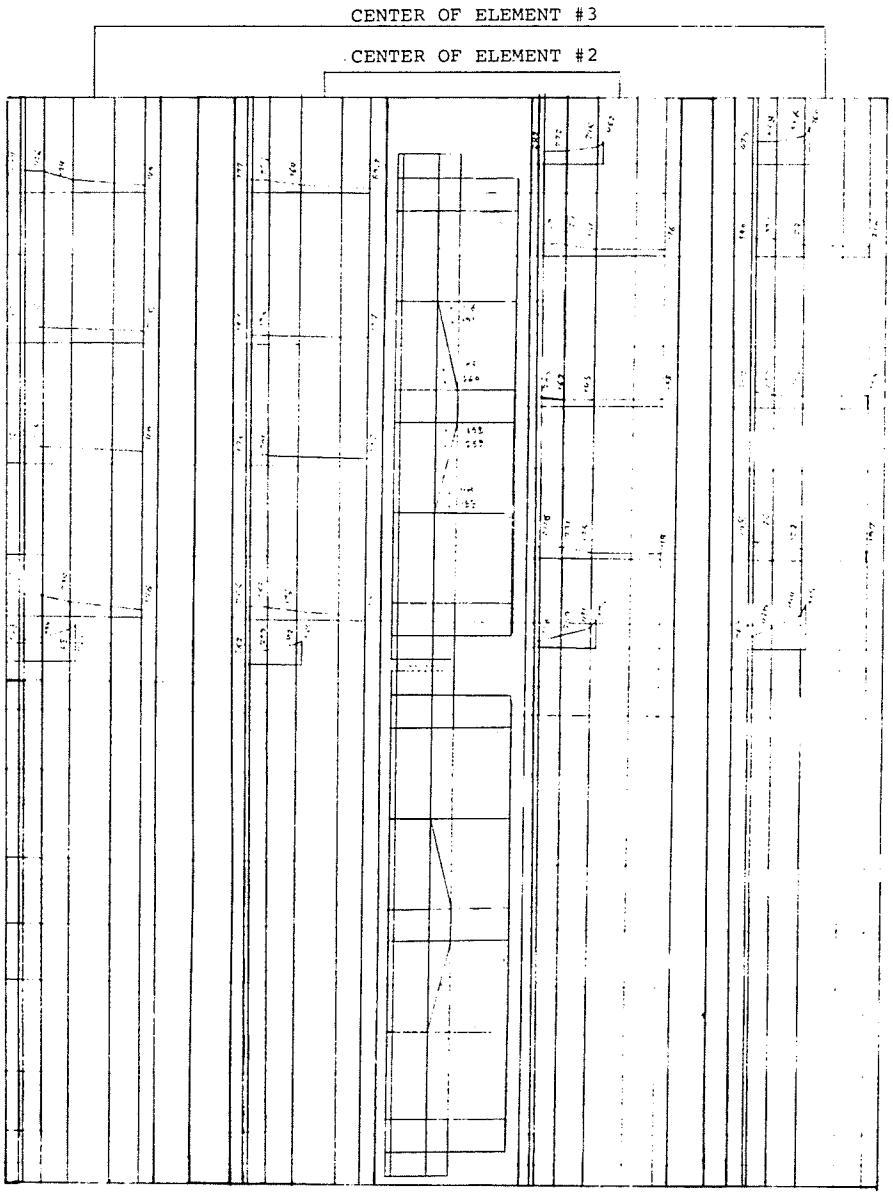

Figure A.16 continued

(c)

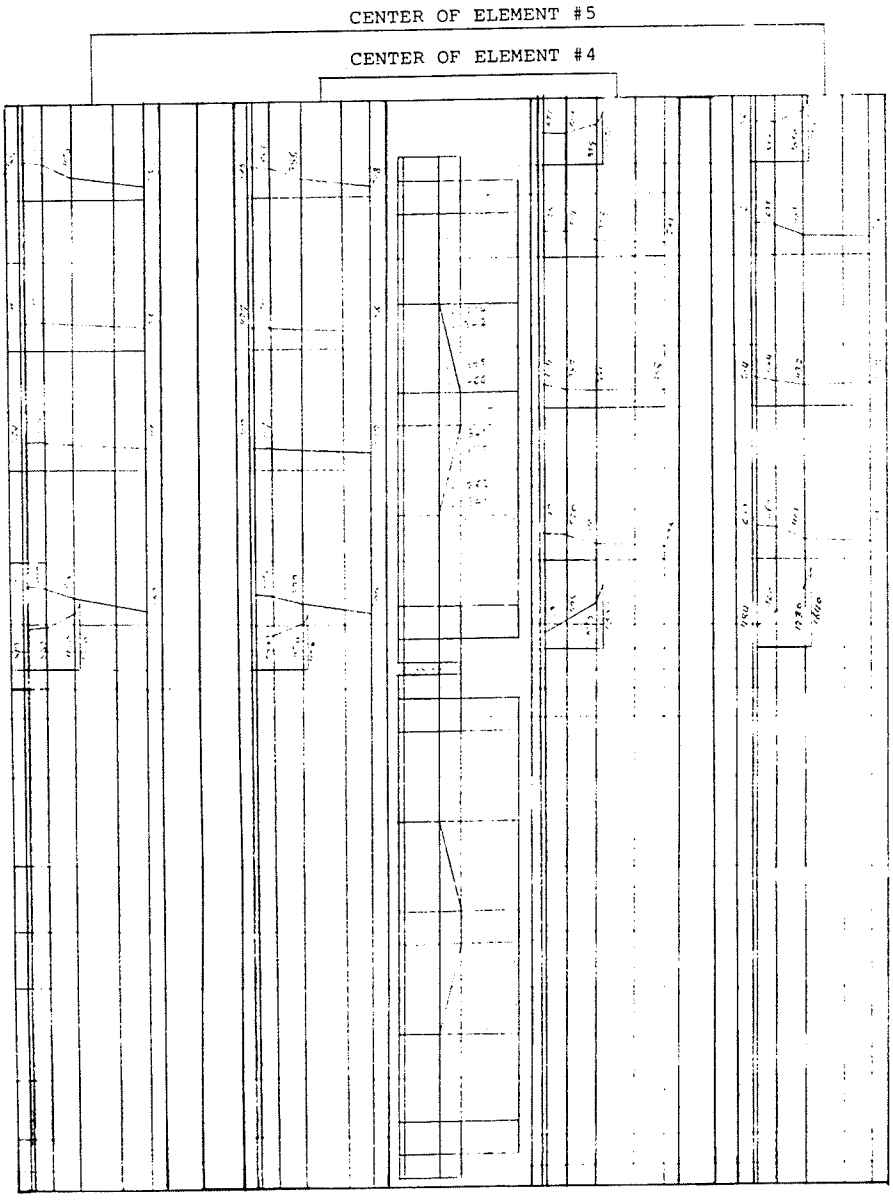

(a)

x-direction*

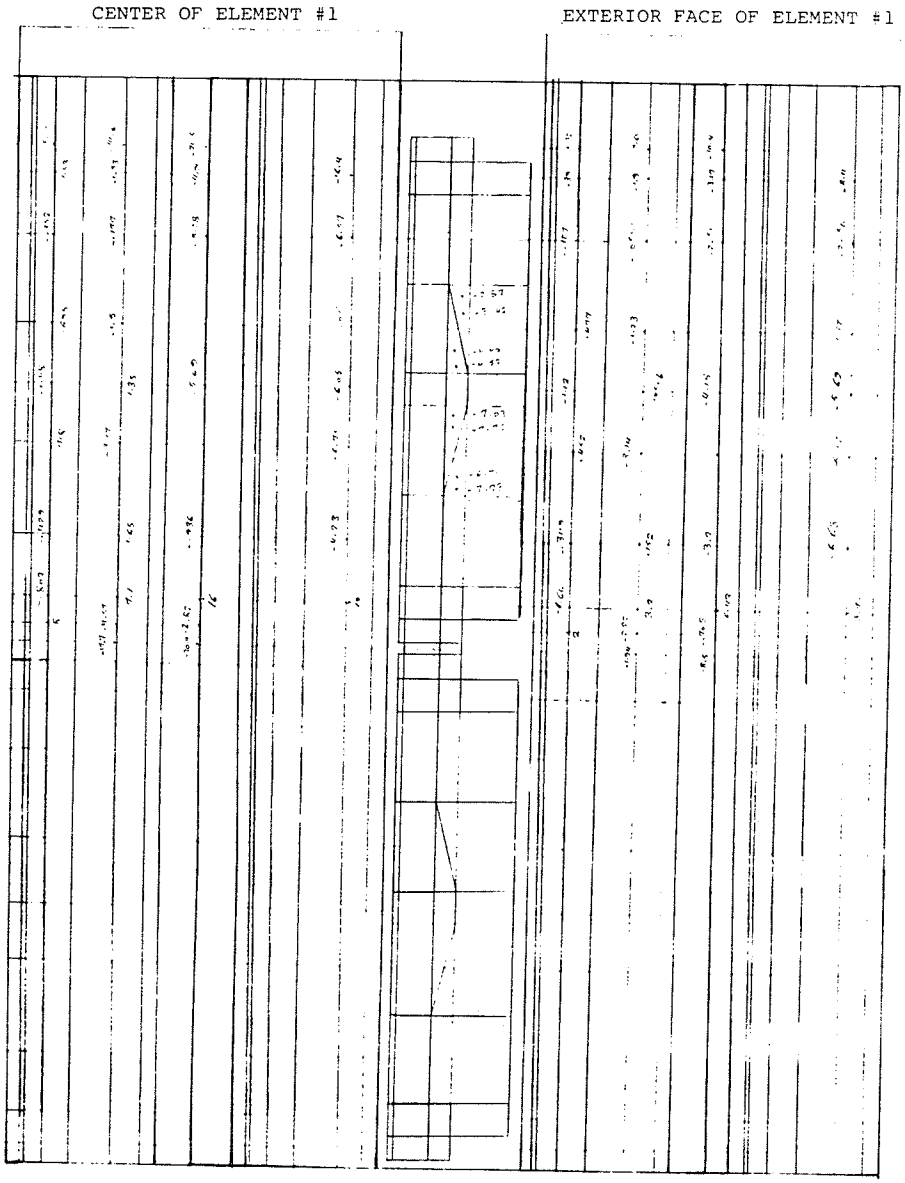

Figure A.17 Direct horizontal stresses at six different sections for the partially filled two-block prism eccentrically loaded with PIN/PIN end conditions.

*See Figure 3.3

Figure A.17 continued

(b)

x-direction

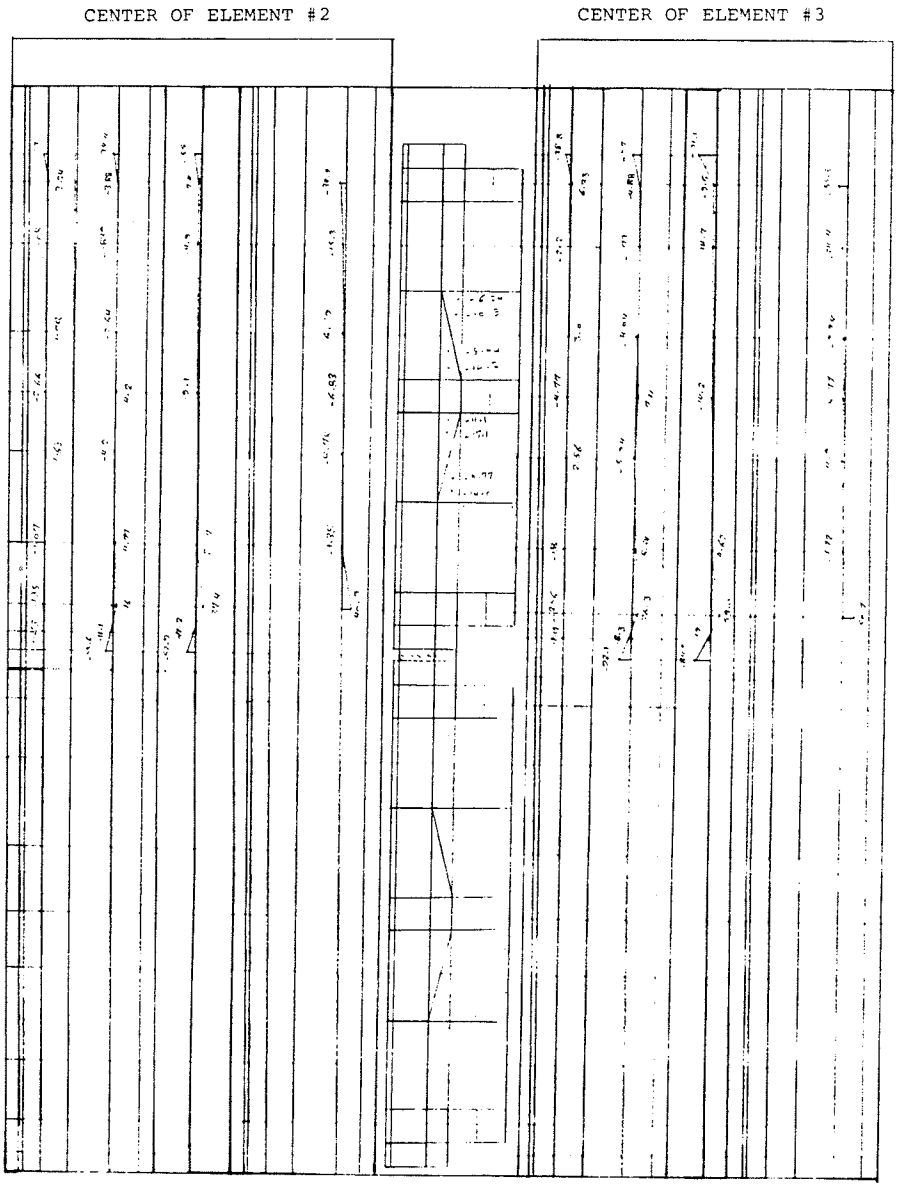

Figure A.17 continued

(c)

x-direction

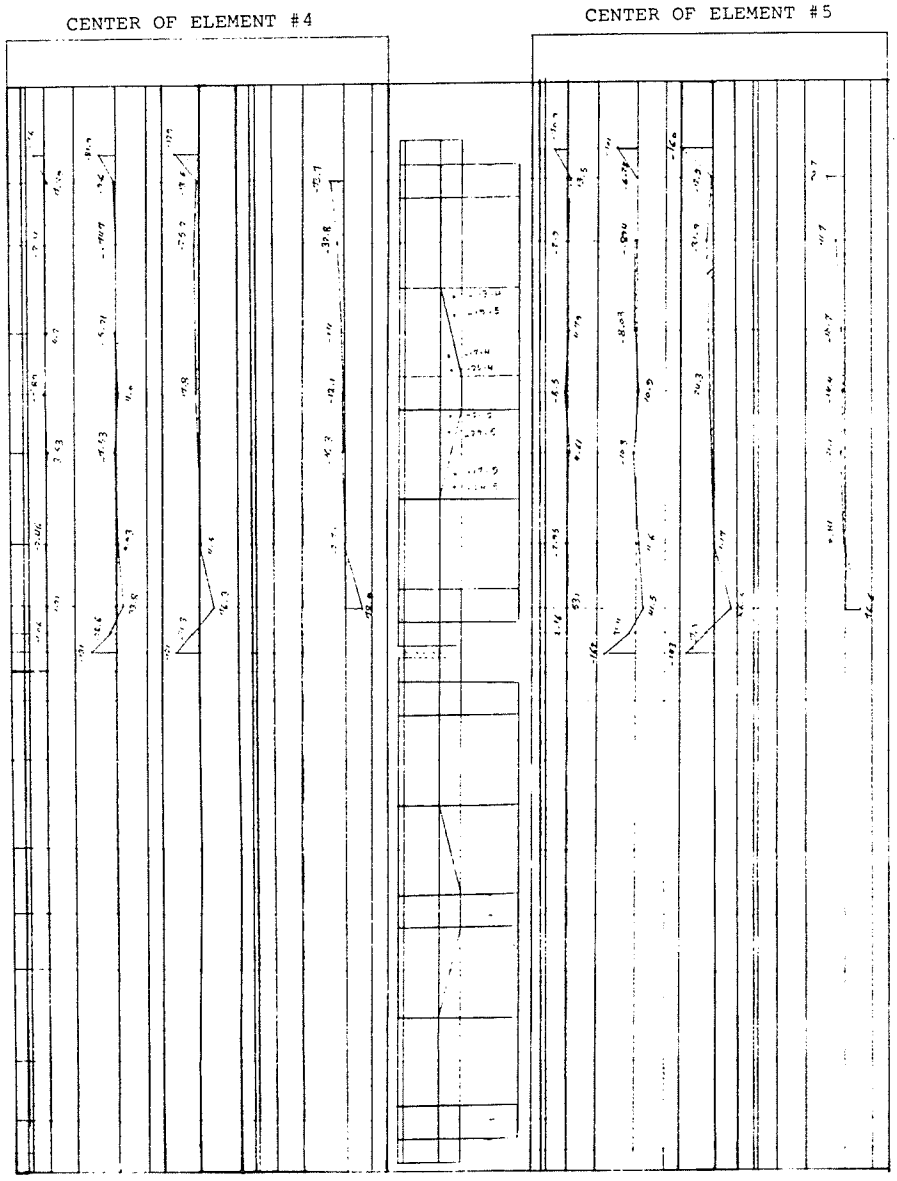

(a)

y-direction*

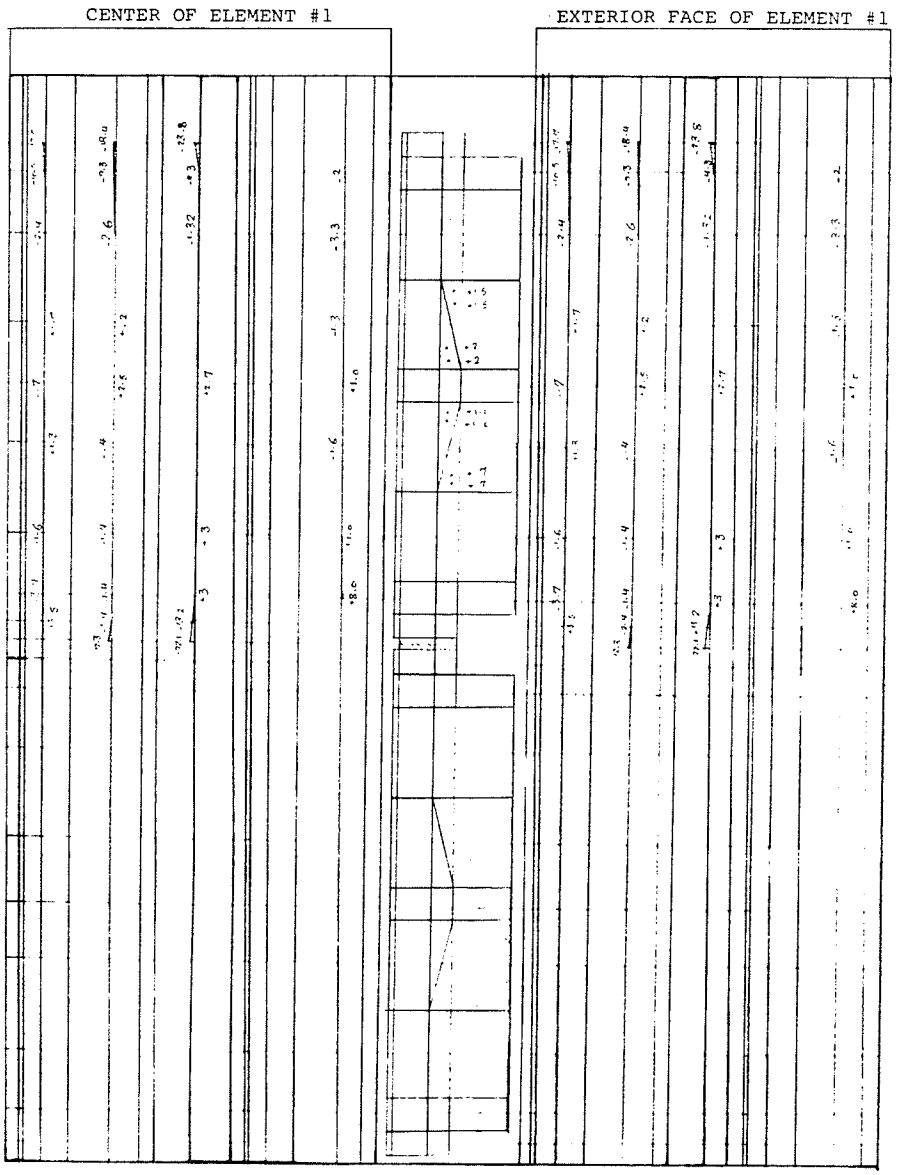

Figure A.18 Direct horizontal stresses at six different sections for the partially filled two-block prism eccentrically loaded with PIN/PIN end conditions.

*See Figure 3.3

Figure A.18 continued

(b)

y-direction

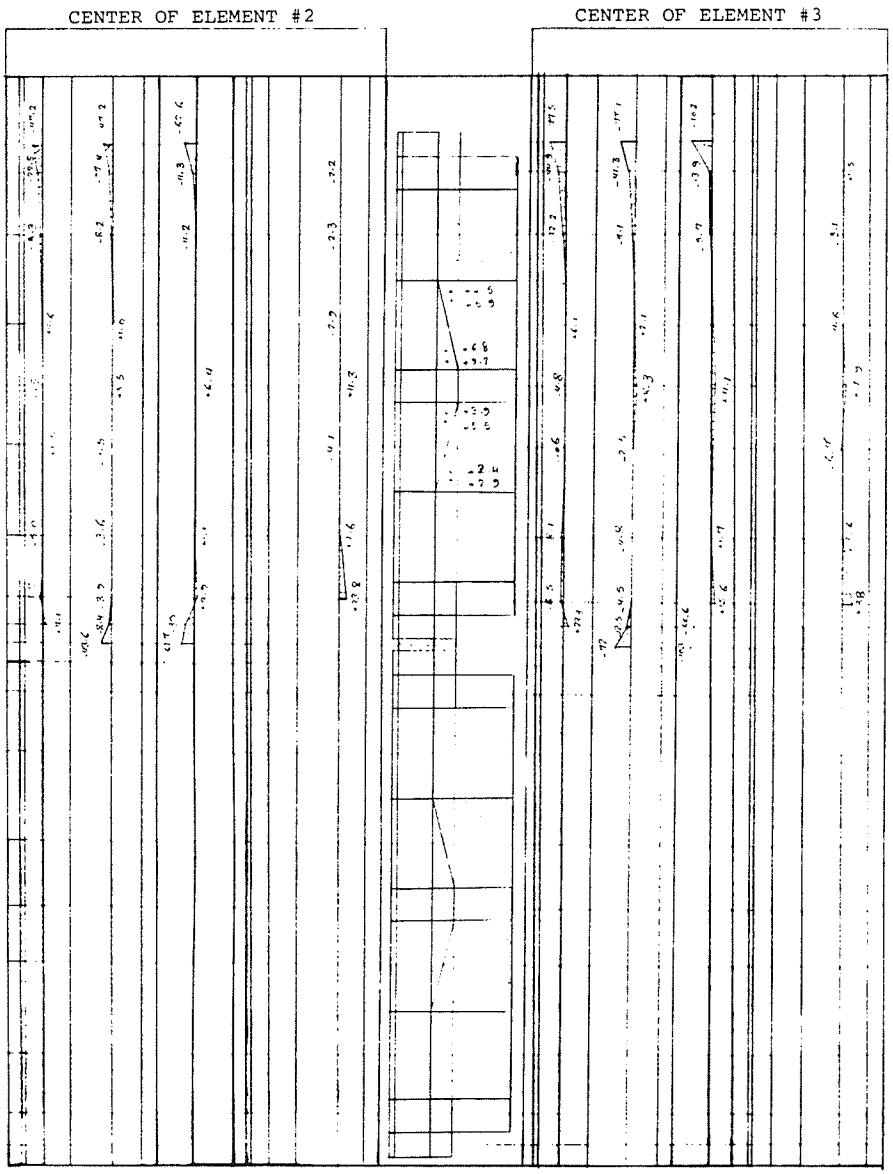

Figure A.18 continued

(c)

y-direction

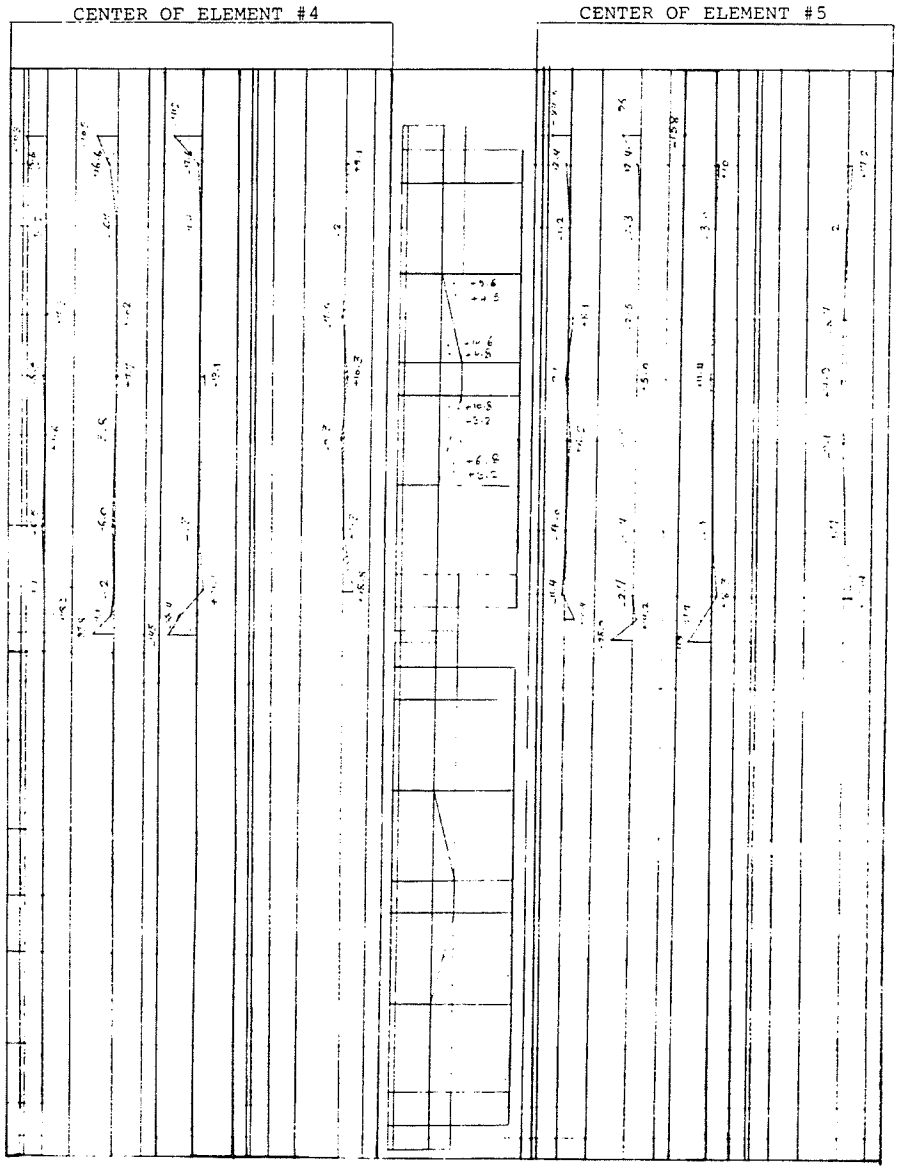

APPENDIX B

STRAIN READINGS

TABLE B.1

Beam #1 Strain readings for side "A"

NO	LOAD (KIPS)				
	4	10	13	16	18
1	-.00007	-.00029	-.00040	-.00048	-.00059
2	-.00004	-.00014	-.00020	-.00024	-.00029
3	-.00006	-.00024	-.00033	-.00041	-.00048
Average for 1,2,3	-.00006	-.00022	-.00031	-.00038	-.00045
4	-.00001	-.00004	-.00005	-.00003	-.00001
5	-.00003	.00002	-.00000	-.00002	-.00001
6	-.00003	-.00005	-.00005	-.00006	-.00007
Average for 4,5,6	-.00002	-.00003	-.00003	-.00004	-.00003
7	.00002	.00028	.00047	.00071	.00091
8	-.00004	.00033	.00045	.00054	.00063
9	.00003	.00006	.00007	.00007	.00007
Average for 7,8,9	.00000	.00022	.00033	.00044	.00054
10	.00009	.00072	.00104	.00138	.00169
11	.00001	.00065	.00090	.00112	.00132
12	.00007	.00050	.00061	.00074	.00085
Average for 10,11,12	.00006	.00062	.00085	.00108	.00128
13	.00011	.00092	.00131	.00172	.00206
14	.00009	.00089	.00133	.00152	.00192
15	.00006	.00089	.00119	.00142	.00183
Average for 13,14,15	.00009	.00089	.00127	.00159	.00194

TABLE B.2

Beam #1 Strain reading for side "B"

NO	LOAD (KIPS)				
	4	10	13	16	18
1	-.00005	-.00022	-.00029	-.00035	-.00039
2	-.00004	-.00012	-.00015	-.00019	-.00022
3	-.00006	-.00027	-.00034	-.00040	-.00046
Average for 1,2,3	-.00005	-.00020	-.00026	-.00031	-.00049
Average for A & B	-.00006	-.00021	-.00029	-.00035	-.00047
4	-.00003	-.00002	-.00002	-.00002	-.00002
5	-.00001	-.00002	.00004	.00005	.00006
6	-.00003	-.00003	.00003	.00008	.00013
Average for 4,5,6	-.00002	-.00002	.00002	.00004	.00006
Average for A & B	-.00002	-.00003	-.00001	.00000	.00002
7	-.00002	.00003	-.00004	.00004	.00004
8	-.00001	.00035	.00047	.00124	.00069
9	-.00007	.00035	.00066	.00091	.00113
Average for 7,8,9	-.00003	.00025	.00039	.00073	.00062
Average for A & B	-.00002	.00024	.00036	.00059	.00058
10	.00007	.00032	.00044	.00056	.00065
11	.00001	.00073	.00100	.00120	.00141
12	.00015	.00093	.00139	.00182	.00216
Average for 10,11,12	.00008	.00066	.00094	.00119	.00141
Average for A & B	.00007	.00064	.00090	.00114	.00135
13	.00000	.00063	.00098	.00126	.00153
14	.00014	.00112	.00144	.00181	.00246
15	.00005	.00106	.00163	.00207	.00243
Average for 13,14,15	.00006	.00093	.00135	.00172	.00214
Average for A & B	.00007	.00091	.00131	.00165	.00200

TABLE B.3

Beam #1 Longitudinal steel strain readings

LOAD(KIPS)	1	2	3	4	5	6	7	8	9	10
STRAIN	.00001	.00003	.00005	.00009	.00023	.00036	.00052	.00067	.00079	.00096

LOAD (KIPS)	11	12	13	14	15	16	17	18
STRAIN	.00111	.00131	.00145	.00160	.00179	.00188	.00211	.00231

TABLE B.4

Beam #2 Strain readings for side "A"

NO	LOAD (KIPS)				
	12	24	36	44	48
1	-.00031	-.00053	-.00084	-.00106	-.00117
2	-.00015	-.00033	-.00044	-.00057	-.00068
3	-.00028	-.00054	-.00081	-.00107	-.00145
Average for 1,2,3	-.00025	-.00047	-.00069	-.00090	-.00111
4	-.00013	-.00021	-.00034	-.00040	-.00051
5	-.00008	-.00014	-.00032	-.00031	-.00045
6	-.00014	-.00022	-.00038	-.00046	-.00055
Average for 4,5,6	-.00012	-.00019	-.00035	-.00039	-.00050
7	.00013	.00027	.00048	.00070	.00101
8	-.00001	-.00001	-.00005	-.00006	.00012
9	.00005	.00011	.00022	.00033	.00057
Average for 7,8,9	.00006	.00012	.00022	.00032	.00049
10	-.00035	.00034	.00095	.00163	.00221
11	-.00002	-.00002	-.00008	-.00002	-.00001
12	.00040	.00066	.00109	.00145	.00229
Average for 10,11,12	.00001	.00033	.00065	.00102	.00150
13	.00011	.00028	.00046	.00062	.00076
14	.00095	.00180	.00288	.00357	.00445
15	.00047	.00093	.00168	.00230	.00383
Average for 13,14,15	.00051	.00100	.00167	.00216	.00301

TABLE B.5

Beam #2 Strain readings for side "B"

NO	LOAD (KIPS)				
	12	24	36	44	48
1	-.00025	-.00038	-.00057	-.00080	-.00096
2	-.00010	-.00020	-.00043	-.00043	-.00061
3	-.00026	-.00048	-.00073	-.00097	-.00115
Average for 1,2,3	-.00020	-.00035	-.00058	-.00073	-.00091
Average for A & B	-.00022	-.00041	-.00064	-.00081	-.00101
4	-.00009	-.00016	-.00019	-.00024	-.00033
5	-.00004	-.00008	-.00012	-.00019	-.00023
6	-.00009	-.00013	-.00018	-.00023	-.00025
Average for 4,5,6	-.00007	-.00012	-.00016	-.00022	-.00027
Average for A & B	-.00010	-.00016	-.00025	-.00030	-.00032
7	.00011	.00020	.00037	.00054	.00096
8	-.00001	.00005	.00005	.00002	.00001
9	.00019	.00034	.00072	.00087	.00124
Average for 7,8,9	.00010	.00019	.00038	.00048	.00074
Average for A & B	.00008	.00015	.00030	.00040	.00061
10	.00045	.00074	.00118	.00168	.00265
11	.00003	.00004	.00003	.00005	.00003
12	.00072	.00144	.00214	.00278	.00340
Average for 10,11,12	.00040	.00074	.00112	.00150	.00203
Average for A & B	.00021	.00053	.00089	.00126	.00177
13	.00055	.00104	.00190	.00267	.00427
14	.00093	.00173	.00270	.00365	.00455
15	.00019	.00044	.00061	.00073	.00086
Average for 13,14,15	.00056	.00107	.00174	.00235	.00323
Average for A & B	.00054	.00103	.00170	.00226	.00312

TABLE B.6

Beam #2 Longitudinalsteel strain readings

LOAD (KIPS)	2	4	6	8	10	12	14	16	18	20
STRAIN	.00005	.00017	.00024	.00035	.00043	.00055	.00064	.00073	.00081	.00090

LOAD (KIPS)	22	24	26	28	30	32	34	36	38	40
STRAIN	.00097	.00105	.00114	.00126	.00138	.00150	.00162	.00177	.00190	.00201

LOAD (KIPS)	42	44	46	48	50
STRAIN	.00216	.00232	.00254	.00351	.00363

TABLE B.7

Beam #3 Strain readings for side "A"

NO	LOAD (KIPS)				
	20	40	60	71	80
1	-.00034	-.00073	-.00120	-.00152	-.00189
2	-.00013	-.00038	-.00052	-.00063	-.00071
3	-.00046	-.00090	-.00145	-.00184	-.00223
Average for 1,2,3	-.00031	-.00067	-.00106	-.00133	-.00161
4	-.00018	-.00033	-.00052	-.00067	-.00082
5	-.00013	-.00025	-.00043	-.00055	-.00069
6	-.00026	-.00044	-.00069	-.00087	-.00111
Average for 4,5,6	-.00018	-.00034	-.00055	-.00069	-.00087
7	-.00000	.00022	.00031	.00036	.00036
8	-.00003	-.00007	-.00013	-.00016	-.00023
9	.00006	.00021	.00031	.00036	.00029
Average for 7,8,9	-.00001	.00012	.00016	.00019	.00014
10	.00032	.00098	.00130	.00145	.00159
11	.00002	.00009	.00032	.00049	.00063
12	.00044	.00106	.00155	.00184	.00196
Average for 10,11,12	.00026	.00071	.00106	.00126	.00139
13	.00013	.00106	.00167	.00207	.00240
14	.00052	.00096	.00147	.00179	.00206
15	.00036	.00109	.00176	.00215	.00259
Average for 12,13,14	.00034	.00103	.00163	.00200	.00235

TABLE B.8

Beam #3 Strain readings for side "B"

NO	LOAD (KIPS)				
	20	40	60	71	80
1	-.00036	-.00068	-.00106	-.00131	-.00141
2	-.00013	-.00034	-.00058	-.00074	-.00097
3	-.00027	-.00061	-.00099	-.00127	-.00154
Average for 1,2,3	-.00025	-.00054	-.00088	-.00111	-.00131
Average for A & B	-.00028	-.00061	-.00097	-.00122	-.00146
4	-.00016	-.00033	-.00054	-.00069	-.00084
5	-.00005	-.00015	-.00029	-.00045	-.00046
6	-.00012	-.00026	-.00044	-.00055	-.00067
Average for 4,5,6	-.00011	-.00025	-.00042	-.00057	-.00066
Average for A & B	-.00015	-.00030	-.00049	-.00063	-.00077
7	.00009	.00028	.00039	.00043	.00032
8	.00002	.00003	.00004	-.00003	-.00003
9	.00009	.00031	.00046	.00051	.00064
Average for 7,8,9	.00007	.00018	.00027	.00030	.00031
Average for A & B	.00002	.00015	.00022	.00025	.00023
10	.00051	.00117	.00169	.00197	.00205
11	-.00004	.00011	.00041	.00063	.00082
12	.00047	.00093	.00134	.00152	.00172
Average for 10,11,12	.00031	.00074	.00115	.00137	.00152
Average for A & B	.00029	.00072	.00111	.00132	.00148
13	.00043	.00111	.00173	.00211	.00246
14	.00044	.00100	.00151	.00189	.00222
15	.00042	.00101	.00170	.00205	.00242
Average for 13,14,15	.00043	.00104	.00165	.00201	.00237
Average for A & B	.00039	.00104	.00164	.00201	.00236

TABLE B.9

Beam #3 Longitudinal steel strain readings

LOAD (KIPS)	5	10	15	20	25	30	35	40	45	50
STRAIN		.00019	.00037	.00050	.00064	.00081	.00098	.00115	.00131	.00141

LOAD (KIPS)	55	60	65	71	75	80	82	84
STRAIN	.00163	.00179	.00196	.00217	.00233	.00254	.00275	.00308

TABLE B.10

Beam #4 Strain readings for side "A"

NO	LOAD (KIPS)				
	20	40	60	80	95
1	-.00020	-.00049	-.00081	-.00119	-.00152
2	-.00012	-.00026	-.00042	-.00057	-.00067
3	-.00026	-.00061	-.00098	-.00141	-.00175
Average for 1,2,3	-.00019	-.00045	-.00073	-.00107	-.00131
4	-.00012	-.00026	-.00042	-.00058	-.00075
5	-.00015	-.00026	-.00035	-.00051	-.00065
6	-.00014	-.00029	-.00046	-.00065	-.00083
Average for 4,5,6	-.00014	-.00027	-.00041	-.00058	-.00074
7	-.00004	.00002	.00005	.00006	.00003
8	-.00004	-.00006	-.00010	-.00013	-.00016
9	.00000	.00010	.00014	.00018	.00008
Average for 7,8,9	-.00003	.00002	.00003	.00004	-.00002
10	.00016	.00052	.00071	.00089	.00102
11	-.00001	.00003	.00022	.00041	.00052
12	.00027	.00071	.00105	.00130	.00129
Average for 10,11,12	.00014	.00042	.00066	.00087	.00094
13	.00018	.00070	.00124	.00172	.00208
14	.00031	.00055	.00088	.00124	.00143
15	.00017	.00079	.00130	.00178	.00211
Average for 13,14,15	.00022	.00068	.00114	.00158	.00187

TABLE B.11

Beam #4 Strain readings for side "B"

NO	LOAD (KIPS)				
	20	40	60	80	95
1	-.00024	-.00051	-.00079	-.00108	-.00139
2	-.00011	-.00015	-.00033	-.00047	-.00057
3	-.00018	-.00043	-.00069	-.00099	-.00127
Average for 2,3	-.00018	-.00036	-.00060	-.00085	-.00108
Average for A & B	-.00019	-.00041	-.00067	-.00096	-.00120
4	-.00010	-.00019	-.00030	-.00044	-.00059
5	-.00009	-.00016	-.00026	-.00036	-.00047
6	-.00009	-.00018	-.00027	-.00039	-.00052
Average for 4,5,6	-.00009	-.00018	-.00028	-.00040	-.00053
Average for A & B	-.00012	-.00023	-.00035	-.00049	-.00064
7	.00002	.00019	.00031	.00037	.00030
8	.00001	.00005	.00003	.00004	-.00006
9	.00000	.00011	.00019	.00028	.00026
Average for 7,8,9	.00000	.00010	.00018	.00023	.00017
Average for A & B	-.00002	.00006	.00011	.00014	.00008
10	.00030	.00081	.00121	.00154	.00153
11	.00001	.00013	.00042	.00065	.00080
12	.00021	.00057	.00075	.00100	.00113
Average for 10,11,12	.00017	.00050	.00079	.00106	.00115
Average for A & B	.00016	.00046	.00073	.00097	.00105
13	.00020	.00087	.00144	.00198	.00235
14	.00032	.00064	.00107	.00145	.00175
15	.00011	.00069	.00114	.00163	.00195
Average for 13,14,15	.00021	.00073	.00122	.00169	.00202
Average for A & B	.00022	.00071	.00118	.00164	.00195

TABLE B.12

Beam #5 Strain readings for side "A"

NO	LOAD (KIPS)				
	20	40	60	80	90
1	-.00022	-.00047	-.00072	-.00100	-.00116
2	-.00012	-.00029	-.00049	-.00071	-.00083
3	-.00023	-.00052	-.00080	-.00111	-.00128
Average for 1,2,3	-.00019	-.00043	-.00067	-.00094	-.00109
4	-.00012	-.00025	-.00038	-.00054	-.00064
5	-.00009	-.00017	-.00029	-.00042	-.00050
6	-.00012	-.00023	-.00037	-.00048	-.00060
Average for 4,5,6	-.00011	-.00022	-.00035	-.00048	-.00058
7	-.00004	.00004	.00012	.00014	.00017
8	-.00003	.00000	.00003	.00003	.00002
9	.00000	.00014	.00020	.00026	.00028
Average for 7,8,9	-.00002	.00006	.00012	.00014	.00016
10	.00016	.00049	.00076	.00105	.00120
11	.00000	.00021	.00050	.00072	.00084
12	.00027	.00066	.00089	.00120	.00134
Average for 10,11,12	.00014	.00045	.00072	.00099	.00113
13	.00010	.00079	.00128	.00179	.00208
14	.00034	.00075	.00122	.00164	.00186
15	.00028	.00079	.00130	.00183	.00210
Average for 13,14,15	.00024	.00078	.00127	.00175	.00201

TABLE B.13

Beam #5 Strain readings for side "B"

NO	LOAD (KIPS)				
	20	40	60	80	90
1	-.00025	-.00053	-.00080	-.00108	-.00127
2	-.00015	-.00027	-.00046	-.00070	-.00081
3	-.00024	-.00051	-.00079	-.00106	-.00128
Average for 1,2,3	-.00021	-.00044	-.00068	-.00095	-.00109
Average for A & B	-.00020	-.00044	-.00068	-.00095	-.00100
4	-.00011	-.00023	-.00034	-.00046	-.00053
5	-.00008	-.00018	-.00029	-.00042	-.00050
6	-.00014	-.00027	-.00041	-.00056	-.00065
Average for 4,5,6	-.00011	-.00023	-.00035	-.00048	-.00056
Average for A & B	-.00011	-.00023	-.00035	-.00048	-.00057
7	.00000	.00016	.00023	.00030	.00034
8	-.00002	-.00004	.00001	.00002	.00002
9	.00002	.00010	.00016	.00022	.00025
Average for 7,8,9	.00000	.00007	.00013	.00018	.00020
Average for A & B	-.00001	.00007	.00013	.00016	.00018
10	.00028	.00073	.00092	.00121	.00134
11	.00000	.00016	.00050	.00076	.00089
12	.00024	.00055	.00083	.00115	.00129
Average for 10,11,12	.00017	.00048	.00075	.00104	.00117
Average for A & B	.00016	.00047	.00074	.00102	.00115
13	.00025	.00086	.00135	.00187	.00212
14	.00027	.00068	.00119	.00167	.00189
15	.00031	.00086	.00139	.00192	.00222
Average for 13,14,15	.00028	.00080	.00131	.00182	.00208
Average for A & B	.00026	.00079	.00129	.00179	.00205

TABLE B.14

Beam #6 Strain readings for side "A"

NO	LOAD (KIPS)				
	6	12	18	24	32
1	-.00007	-.00018	-.00030	-.00050	-.00078
2	-.00020	-.00046	-.00082	-.00114	-.00166
3	-.00007	-.00018	-.00031	-.00044	-.00069
Average for 1,2,3	-.00011	-.00027	-.00048	-.00069	-.00104
4	-.00005	-.00006	-.00008	-.00011	-.00017
5	-.00005	-.00012	-.00012	-.00014	-.00018
6	-.00003	-.00005	-.00006	-.00010	-.00014
Average for 4,5,6	-.00004	-.00008	-.00009	-.00012	-.00016
7	.00002	.00004	.00005	.00032	-.00055
8	.00003	.00025	.00068	.00104	-.00143
9	.00003	.00004	.00005	.00009	-.00020
Average for 7,8,9	.00003	.00011	.00026	.00048	.00073
10	.00003	.00005	.00003	.00083	.00147
11	.00026	.00092	.00188	.00233	.00309
12	.00002	.00003	.00017	.00060	.00110
Average for 10,11,12	.00010	.00033	.00069	.00125	.00189

TABLE B.15

Beam #6 Strain readings for side "B"

NO	LOAD (KIPS)				
	6	12	18	24	32
1	-.00004	-.00016	-.00030	-.00049	-.00075
2	-.00019	-.00042	-.00074	-.00108	-.00159
3	-.00007	-.00019	-.00032	-.00054	-.00078
Average for 1,2,3	-.00010	-.00026	-.00045	-.00070	-.00104
Average for A & B	-.00010	-.00027	-.00047	-.00070	-.00104
4	-.00005	-.00009	-.00011	-.00017	-.00026
5	-.00006	-.00011	-.00011	-.00017	-.00026
6	-.00004	-.00006	-.00009	-.00013	-.00018
Average for 4,5,6	-.00005	-.00009	-.00010	-.00014	-.00021
Average for A & B	-.00005	-.00009	-.00010	-.00013	-.00019
7	.00004	.00004	.00003	.00003	.00005
8	.00005	.00029	.00074	.00111	.00156
9	.00002	.00003	.00003	.00028	.00050
Average for 7,8,9	.00004	.00012	.00027	.00047	.00070
Average for A & B	.00004	.00012	.00027	.00048	.00072
10	.00001	-.00001	-.00001	.00019	.00063
11	.00030	.00098	.00209	.00262	.00340
12	.00000	.00003	.00002	.00084	.00156
Average for 10,11,12	.00010	.00033	.00069	.00122	.00186
Average for A & B	.00010	.00033	.00069	.00125	.00188

TABLE B.16

Beam #7 Strain readings for side "A"

NO	LOAD (KIPS)				
	6	12	18	24	32
1	-.00004	-.00016	-.00029	-.00040	-.00058
2	-.00017	-.00054	-.00103	-.00146	-.00209
3	-.00007	-.00015	-.00029	-.00042	-.00061
Average for 1,2,3	-.00009	-.00028	-.00054	-.00076	-.00109
4	-.00004	-.00012	-.00011	-.00017	-.00024
5	-.00005	-.00016	-.00025	-.00036	-.00050
6	-.00002	-.00007	-.00010	-.00014	-.00022
Average for 4,5,6	-.00004	-.00012	-.00015	-.00022	-.00032
7	.00003	.00002	.00013	.00029	.00048
8	.00003	.00023	.00055	.00071	.00097
9	.00003	.00002	.00020	.00029	.00040
Average for 7,8,9	.00003	.00011	.00029	.00034	.00062
10	.00006	.00009	.00070	.00115	.00175
11	.00018	.00083	.00136	.00182	.00252
12	.00004	.00009	.00058	.00099	.00139
Average for 10,11,12	.00009	.00034	.00088	.00132	.00189

TABLE B.17

Beam #7 Strain readings for side "B"

NO	LOAD (KIPS)				
	6	12	18	24	32
1	-.00004	-.00015	-.00034	-.00047	-.00068
2	-.00016	-.00052	-.00094	-.00131	-.00186
3	-.00006	-.00015	-.00027	-.00040	-.00060
Average for 1,2,3	-.00009	-.00027	-.00052	-.00088	-.00105
Average for A & B	-.00009	-.00028	-.00053	-.00082	-.00107
4	-.00004	-.00007	-.00011	-.00015	-.00022
5	-.00007	-.00017	-.00023	-.00030	-.00041
6	-.00003	-.00005	-.00009	-.00012	-.00017
Average for 4,5,6	-.00005	-.00010	-.00015	-.00019	-.00027
Average for A & B	-.00008	-.00011	-.00015	-.00021	-.00030
7	.00003	.00002	.00015	.00025	.00038
8	.00003	.00026	.00060	.00081	.00109
9	-.00002	-.00002	.00009	.00025	.00044
Average for 7,8,9	.00001	.00009	.00028	.00044	.00064
Average for A & B	.00002	.00010	.00029	.00039	.00063
10	.00001	.00007	.00057	.00087	.00123
11	.00015	.00082	.00142	.00194	.00274
12	.00000	.00006	.00067	.00115	.00176
Average for 10,11,12	.00005	.00032	.00089	.00132	.00191
Average for A & B	.00007	.00033	.00089	.00132	.00191

TABLE B.18

Beam #8 Strain readings for side "A"

NO	LOAD (KIPS)				
	10	20	30	40	50
1	-.00012	-.00030	-.00056	-.00081	-.00107
2	-.00028	-.00064	-.00103	-.00152	-.00022
3	-.00011	-.00027	-.00048	-.00071	-.00097
Average for 1,2,3	-.00017	-.00040	-.00069	-.00101	-.00142
4	-.00008	-.00012	-.00021	-.00032	-.00051
5	-.00011	-.00023	-.00030	-.00045	-.00067
6	-.00008	-.00032	-.00020	-.00029	-.00046
Average for 4,5,6	-.00009	-.00022	-.00024	-.00035	-.00055
7	-.00001	.00015	.00030	.00040	.00044
8	.00003	.00023	.00042	.00059	.00071
9	.00003	.00019	.00033	.00042	.00049
Average for 7,8,9	.00002	.00019	.00035	.00047	.00055
10	.00005	.00036	.00096	.00138	.00186
11	.00033	.00087	.00137	.00192	.00248
12	.00004	.00049	.00089	.00129	.00162
Average for 10,11,12	.00014	.00057	.00111	.00153	.00199

TABLE B.19

Beam #8 Strain readings for side "B"

NO	LOAD (KIPS)				
	10	20	30	40	50
1	-.00010	-.00027	-.00053	-.00070	-.00093
2	-.00023	-.00056	-.00095	-.00138	-.00200
3	-.00011	-.00028	-.00058	-.00073	-.00098
Average for 1,2,3	-.00015	-.00037	-.00069	-.00094	-.00130
Average for A & B	-.00016	-.00039	-.00069	-.00098	-.00136
4	-.00007	-.00010	-.00020	-.00027	-.00040
5	-.00009	-.00015	-.00023	-.00043	-.00052
6	-.00007	-.00011	-.00019	-.00029	-.00060
Average for 4,5,6	-.00008	-.00012	-.00021	-.00033	-.00051
Average for A & B	-.00009	-.00017	-.00023	-.00034	-.00053
7	.00003	.00018	.00033	.00044	.00053
8	.00005	.00027	.00051	.00072	.00093
9	.00004	.00014	.00033	.00044	.00045
Average for 7,8,9	.00004	.00020	.00039	.00053	.00064
Average for A & B	.00003	.00020	.00037	.00050	.00060
10	.00004	.00046	.00094	.00127	.00161
11	.00038	.00112	.00165	.00237	..00310
12	.00004	.00028	.00080	.00114	.00149
Average for 10,11,12	.00015	.00077	.00113	.00159	.00207
Average for A & B	.00015	.00067	.00112	.00156	.00203

APPENDIX C

DESIGN AND ANALYSIS

DESIGN AND ANALYSIS

The masonry beams were designed and analyzed using the Ultimate Strength method for reinforced concrete in accordance with CSA Standard CAN3 - A23.3 - M77 "Code for the Design of Concrete Structures for Buildings." (5) A few minor adjustments to the theory were made with reference to the CSA Standard CAN3 - S304 - M77 on "Masonry Design and Construction for Buildings." (6)

Typical masonry beam details are shown in Figure 2.2. A typical beam cross-section is shown in Figure C.1

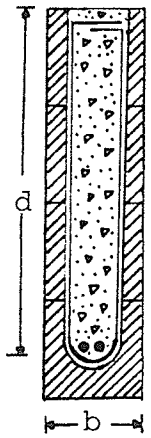

C.1 Typical beam cross-section

The load, shear and moment relationships for the beams are shown in Figure 2.19.

LONGITUDINAL REINFORCEMENT PERCENTAGES

The minimum percentage of longitudinal reinforcement was governed by the CSA Standard CAN3 - S304 - 1977 code[6] where

$$\rho_{min} \geq \frac{80}{f_y} \qquad \text{(c.1)}$$

The maximum percentage of longitudinal reinforcement was governed by the CSA Standard CAN3 - A23.3 - 77 code[5] where

$$\rho_{(balance)} \leq .85\,\beta_1\,\frac{f_m'}{f_y}\,\frac{.003}{.003 + \frac{f_y}{29\times10^6}} \qquad \text{(c.2)}$$

where

ρ = percentage of longitudinal reinforcement (A_s/bd)

f_y = reinforcement yield strength (p.s.i.)

f_m' = Masonry unit ultimate compressive strength (p.s.i.)

β_1 = 0.85

FLEXURAL COMPUTATIONS

$$M_u = \frac{A_s f_y}{12}\left(d - \frac{a}{2}\right) \qquad \text{(c.3)}$$

$$a = \frac{A_s f_y}{.85 f_m' b} \qquad \text{(c.4)}$$

$$P_u = \frac{M_u - M_c}{5} \qquad \text{(c.5)}$$

Flexural Computations continued:

$$M_c = \frac{W_c L^2}{8} \qquad (c.6)$$

$$P_{(cal.)} = 2P_u \qquad (c.7)$$

where

M_u = Ultimate moment (K - ft)

A_s = Area of longitudinal steel (in^2)

d = Effective depth (from compression face to the centroid of longitudinal reinforcement (in).

a = Depth of equivalent rectangular stress block

b = Breadth of beam (in)

P_u = Maximum third point load at ultimate flexural capacity (Kips)

M_c = Moment created by self weight of the beam (K - ft)

W_c = Weight per longitudinal foot of the beam (assume concrete and masonry blocks all have the same density which is equal to 150 p.c.f.)

L = Length of clear span (ft)

$P_{(cal.)}$ = Maximum calculated applied load (Kips)

SHEAR

The shear capacity of the beams without shear reinforcements was calculated according to the CSA Standard CAN3 - S304 - 1977 [6]

where

$$v_m = 0.02\, f_m' \leq 50 \text{ p.s.i.} \qquad \text{(c.8)}$$

$$V_u = P_u + \left(\frac{W_c L}{2} - W_c\right) \qquad \text{(c.9)}$$

$$v_u = \frac{V_{u(1000)}}{bd} \qquad \text{(c.10)}$$

v_m = Maximum allowable shear stress for a flexural member without shear reinforcement (p.s.i.)

V_u = Maximum shearing force in the beam at ultimate applied load (Kips)

v_u = Shearing stress carried by the beam at ultimate load (p.s.i.)

The CSA Standard CAN3 - S304 stated the need for web reinforcement if the value of the calculated shear (v_u) exceeds the allowable shear stresses permitted on masonry without web reinforcement (v_m). Web reinforcement provided to carry all the shear stresses was calculated by:

$$A_v = \frac{v_u S}{f_y b} \qquad \text{(c.11)}$$

where

A_v = Web reinforcement cross-sectional area (in^2)

S = Spacing of vertical shear reinforcement (in)

MODULUS OF RUPTURE

The CSA Standard CAN3 - S304 doesnot recommend any value for the modulus of rupture (f_{mr}) for masonry members in flexure. Based on the test results, a reasonable value for modulus of rupture would be:

$$f_{mr} = 2.3 \sqrt{f_m'} \qquad \text{(c.12)}$$

where

f_{mr} = Masonry modulus of rupture (p.s.i.)

f_m' = Masonry unit ultimate compressive strength (p.s.i.)

The crack moment for masonry beams then becomes

$$M_{cr} = \frac{f_{mr} I_g}{y_t} \qquad \text{(c.13)}$$

where

M_{cr} = Moment at first cracking (K - in)

I_g = Moment of inertia of the gross uncracked section (in^4)

y_t = Distance from centroidal axis of gross section to the extreme tension fiber

LONG-TERM CRACKING CONTROL

Long-term cracking control is governed by the quantity Z which limits the distribution of flexural reinforcement. The CSA Standard CAN3 - A23.3 - 77 code formula and Z limits are given by

$$Z = f_s \sqrt[3]{d_c A} \leq 175 \text{ Kip/in for interior exposure} \quad \text{(c.14)}$$

$$Z = f_s \sqrt[3]{d_c A} \leq 145 \text{ Kip/in for exterior exposure} \quad \text{(c.15)}$$

where

Z = A quantity limiting distribution of flexural reinforcement (Kip/in)

d_c = Thickness of concrete cover measured from the extreme tension fiber to the center of the bar located closest thereto (in).

A = Effective tension area of concrete surrounding the main tension reinforcing bars and having the same centroid as that reinforcement divided by the number of bars (in^2)

DEFLECTION

The approximate calculation of deflection for the third - point loading was calculated by

$$\Delta_1 = \frac{23}{1296} \frac{wl^3}{E_m I_g} \quad \text{(c.16)}$$

where

Δ_1 = Approximate mid-point deflection (in)

w = Test applied load (lbs.)

l = Beam clear span (in)

E_m = Concrete masonry modulus of elasticity (p.s.i.) equal 1000 f_m' but not to exceed 3,000,000 (p.s.i.)

I_g = Moment of inertia of the gross uncracked section (in^4)

The CSA Standard CAN3 - A23.3 - 77 code suggests using an effective moment of inertia instead of the gross

moment of inertia.

$$I_e = \left(\frac{M_{cr}}{M_a}\right)^3 I_g + \left[1 - \left(\frac{M_{cr}}{M_a}\right)^3\right] I_{cr} \qquad \text{(c.17)}$$

where

I_e = Effective moment of inertia (in^4)

M_{cr} = Moment at first cracking (K - in)

M_a = Applied moment (K - in)

I_g = Moment of inertia of the gross uncracked section (in^4)

I_{cr} = Moment of inertia of the cracked section (in^4)